Development of Novel Magnetic Resonance Imaging Techniques to Evaluate Plasticity in the Injured Human Cervical Spinal Cord

by

David W. Cadotte

A thesis submitted in conformity with the requirements
for the degree of Doctor of Philosophy

Institute of Medical Science
University of Toronto

Development of Novel Magnetic Resonance Imaging Techniques to Evaluate Plasticity in the Injured Human Cervical Spinal Cord

David W. Cadotte

Doctor of Philosophy

Institute of Medical Science
University of Toronto

2014

Abstract

Traumatic injury to the human spinal cord is a devastating condition that results in motor and sensory impairment. The goal of this thesis is to develop magnetic resonance imaging techniques as a biomarker to evaluate the human spinal cord after injury. The specific aims are: 1a) to characterize the standard T_1 and T_2-weighted intramedullary spinal cord signal characteristics first used by clinicians treating spinal cord injury in order to classify patients along a spectrum of injury severity; 1b) to calculate the sensitivity and specificity of MRI biomarkers to determine neurological function and 1c) to determine whether standard T_1 and T_2-weighted imaging biomarkers offer an advantage over clinical examination to predict neurological outcomes. 2) To determine whether spinal functional MRI can be used to distinguish spinal cord injury patients from healthy controls by 2a) determining whether there is an abnormal neuro-vascular response to afferent stimulation in dermatomes of normal sensation, above the level of injury, in spinal cord injury (SCI) patients 2b) to determine whether the neuro-vascular response to afferent stimulation in dermatomes of altered sensory perception, below the level of injury, is correlated to the degree of sensory loss and 2c) to determine the functional connectivity between regions of the spinal cord that process an afferent stimulus and other regions of the brainstem-spinal cord axis. 3) To outline the diversity of segmental anatomy of the human spinal cord across a cohort

of individuals by 3a) measuring the position of vertebral bodies and spinal cord segments relative to the ponto-medullary junction; 3b) to calculate the relative positions of vertebral bodies and spinal cord segments; and 3c) to predict the position of spinal cord segments. Results indicate that 1) standard T_1 and T_2-weighted intramedullary spinal cord signal characteristics offer no advantage over clinical examination to predict prognosis. 2) Spinal fMRI can be utilized to provide evidence of spinal cord plasticity after traumatic injury and 3) there is natural diversity of the position of vertebral and spinal cord segments relative to the ponto-medullary junction that should be taken into account for advanced imaging studies. Collectively, the new knowledge presented herein contributes to the advancement of imaging techniques to investigate the human spinal cord.

Acknowledgments

To begin, I would like to thank my family and friends for providing a pilar of support during the arduous training of both neurosurgery and the concomitant pursuit of PhD studies. I am privileged to point out that there are simply too many close friends and family to mention in these pages. With great sadness, my father, Wayne Cadotte, died in October of 2010, after suffering for many years from the debilitating consequences of a bleeding cavernous malformation. During this difficult time I learned the importance of patience and communication for those with neurological deficits – a lesson that will carry with me throughout my career in neurosurgery. I am particularly grateful to Eleanor Shin, my best friend and now fiancé, for being by my side during the very long post-graduate medical education years. Despite facing her own challenges with recovering from a traumatic brain injury, she has always supported me in my academic persuits.

As my supervisor, I am grateful to Dr. Michael Fehlings for supporting me through five years of intense training in the field of spinal cord injury. It was on a cold winters morning in 2008 when Dr. Fehlings and I discussed the need to improve the use of imaging biomarkers for use in spinal cord injury patients. Over the ensuing months we planned an approach to study emerging advanced imaging methods and how to best integrate such methods to benefit our patients. Dr. Fehlings introduced me to several experts in the field including Dr. Pat Stroman and Dr. Julien Cohen-Adad; both of which provided their own unique guidance toward the projects outlined in this thesis. I am most grateful to Dr. Fehlings for his insistence on me applying for various grants and awards, submitting my work for publication at numerous national and international meetings and getting involved with organized neurosurgery to appreciate how institutional organizations can help advance the cause for a specific disease process. Dr. Fehlings has given me numerous skill sets that I will carry throughout my entire career and, most importantly, he has instilled in me the confidence I need to be a successful clinician scientist. Equally significant, Dr. Fehlings has taught me the importance of patient care and to always consider the role a physician plays in advocating for those marginalized by their disease process. On a practical level, Dr. Fehlings has taught me about leadership and time management – he always answers his phone when I call and responds to my (many!) email messages regardless of where he might be around the globe. He instilled in me the notion of dividing time into ‘10 minute blocks’ so as to stay productive even

in times of a hectic clinical schedule. As I said to him personally as my training drew to a close, “I could not have imagined such a successful and encompassing learning experience when I embarked on this portion of my career just a few short years ago – for all these many lessons, I will always be thankful”.

I am grateful to the members of my program advisory committee: Dr. Karen Davis, Dr. David Mikulis and Dr. Michael Salter. It is a daunting task for a student such as myself to present ideas and research data to such esteemed professionals in their respective disciplines. I am grateful for the knowledge you provided me during my training, the skepticism with which you thought through my research projects and the stimulating questions you asked at each of the program advisory committee meetings. I am particularly grateful for Dr. Mikulis introducing me to the American Society for Functional Neuroradiology – a remarkable society that brings together radiologists and clinicians and surgeons to communicate the most advanced imaging techniques that have potential to improve the care of our patients. I am equally grateful to Dr. Karen Davis for her enthusiasm for the scientific method and her exquisite attention to detail. Dr. Davis introduced me to the Organization for Human Brain Mapping, a truly global collection of minds focusing on advancing imaging to improve our understanding of the human central nervous system. Both Dr. Davis and Dr. Michael Salter taught me ‘Somatosensory Neuroscience’, a graduate course in the winter term of 2011. Having been through many undergraduate and graduate courses at multiple Universities in Canada – I can honestly say this was one of the most intellectually stimulating courses I have taken in my life. By reviewing the most important historical papers that collectively comprise our current understanding of somatosensory anatomy and physiology – this is just as much a course in critical thinking and communication as it is in somatosensory neuroscience. Along this line, I am grateful to Dr. Michael Salter for listening to each of my presentations and always seeming to ask the most ‘simple’ questions that highlight the work at hand. It was these seemingly simple questions that most stimulated my drive to understand the topic at a deeper level.

I am fortunate to have been successful at receiving several research grants and awards for the work contained within this thesis. I am grateful to each of the organizations that took the time to recognize either my results or potential to carry out a research project, these organizations include: the Ontario Neurotrauma Foundation, Rick Hansen Institute, Congress of Neurological Surgeons, American Association of Neurological Surgeons (Codman Neurotrauma Award),

Cervical Spine Research Society, Canadian Institutes for Health Research, Craig H. Neilsen Foundation, University of Toronto Department of Surgery and the Gerald and Tootsie Halbert Chair in Neural Repair and Regeneration at the University of Toronto.

I would also like to thank Keith Ta and Eugen Hlasny for their assistance with MRI data collection and Diana Kryski of Kryski Biomedia for providing a few of the illustrations contained in Chapter 5.

I would like to thank Dr. David Fleet (Professor of Computer Science, University of Toronto), his PhD student, Micha Livne and my brother, Adam Cadotte, now a second year medical student at the University of Toronto enrolled in the CREMS program, for each of their respective roles in the work contained within Chapter 5 of this thesis. Chapter 5 contains a novel approach to segmenting and performing measurements of the human cervical spinal cord – the computer vision techniques and computer programming aspects of this chapter would not have been possible without the collaboration of these three individuals.

Lastly, I would like to acknowledge the Neurosurgery program and the Surgeon Scientist Program at the University of Toronto. Each of these programs is visionary in scope and has the potential to continuously improve how surgery is performed in an ever-changing world. Specifically, I would like to thank Drs. Jim Rutka (former Chairman) and Chris Wallace (former program director) for admitting me into the Neurosurgery training program in 2006 and Drs. Andres Lozano (current Chairman) and Abhaya Kulkarni (current program director) for tolerating my absence from the program to pursue my PhD studies.

Table of Contents

List of Tables

List of Figures

List of Abbreviations

20-HETE	20-hydroxyeicosatetraenoic acid
ABC	Airway, Breathing, Circulation
AIS	American Spinal Injury Association Impairment Scale
ASA	Anterior spinal artery
ASIA	American Spinal Injury Association
ATLS	Advanced Trauma Life Support
ATP	Adenosine triphosphate
BBB	Blood brain barrier
BOLD	Blood oxygen level dependent
CBF	Cerebral blood flow
$CMRO_2$	Cerebral metabolic rate of oxygen consumption
CNS	Central Nervous System
CT	Computed tomography
DTI	Diffusion tensor imaging
DVT	Deep vein thrombosis
EEG	Electroencephalography
EET	Epoxyeisoatrienoic acid
EPI	Echo planar imaging
FA	Fast adapting
FAST	Focused Assessment with Sonography for Trauma
fMRI	Functional Magnetic Resonance Imaging
FOV	Field of view
GE	Gradient echo; General Electric
GLM	General linear model
GW	Gestational week(s)
ICCP	International Campaign for Cures of SCI Paralysis
ICU	Intensive Care Unit
IL	Interleukin
LOS	Length of Stay
MABP	Mean arterial blood pressure
MRC	Medical Research Council
MEG	Magnetoencephalography
MRI	Magnetic Resonance Imaging
MT	Magnetization transfer
NEP	Neuro-epithelial cells
NMDA	n-Methyl-D-aspartate
NASCIS	National Acute Spinal Cord Injury Study
PD	Proton Density
PET	Positron Emission Tomography
PSA	Posterior spinal artery
RF	Radio Frequency
SA	Slow adapting
SCBF	Spinal cord blood flow
SCI	Spinal Cord Injury

SE	Spin echo
SEEP	Signal enhancement of extravascular protons
SEM	Standard error of the mean
SNR	Signal-to-noise ratio
SPM	Statistical parametric map
STASCIS	Surgical Timing in Acute Spinal Cord Injury Study
STIR	Short T_1 Inversion Recovery
SV-OCT	Speckle variance optical coherence tomography
TNF	Tumor necrosis factor
TE	Echo time
TR	Repetition time
TRP	Transient receptor potential
TRPA	ankyrin transmembrane protein channel
TRPM	melastatin or long TRP channel
TRPV	vanilloid TRP channel
USD	United States Dollar
ZPP	Zone of Partial Preservation

Chapter 1
Introduction and General Aims

This chapter is modified from the following:

Cadotte DW, Fehlings MG. Will imaging biomarkers transform spinal cord injury trials? Lancet Neurol. 2013 Sep;12(9):843-4. doi: 10.1016/S1474-4422(13)70157-1. Epub 2013 Jul 2.

Cadotte DW, Fehlings MG. Visualizing plasticity and repair in the injured CNS. Nature Reviews Neurology. 2013. Advanced Online Publication.

1.1 Preamble

Traumatic spinal cord injury (SCI) is a devastating event in a person's life, and can lead to loss of independence for activities of daily living.[1] One challenge of translating novel therapeutics into clinical practice is measurement of a treatment effect from the natural history of recovery after SCI. Natural history varies between individuals due to the heterogeneity that exists both in terms of how individuals are injured (primary injury), and the resulting downstream biological effects of that initial trauma (secondary injury). As an illustration of such heterogeneity, up to 20% of severely injured individuals who would typically not be expected to recover show improvement, in the absence of any intervention, on standard neurological testing defined by the American Spinal Injury Association (ASIA) in what has become the gold standard for the assessment of SCI.[2,3] Neurological assessment can be summarized as motor testing of five key muscle groups in the upper extremity, five key muscle groups in the lower extremity and recording of perceived sensation in C2 through S5 dermatomes. The American Spinal Injury Association Impairment Scale (AIS) summarizes motor and sensory testing and divides patients into 5 classes, 'A' though 'E', where 'A' represents the most severely damaged spinal cord and 'E' represents a full neurologic recovery.[3] Despite its somewhat subjective nature, it is easy to use and easy to communicate information between treating physicians. Unfortunately, the ASIA classification system does not incorporate advances in our understanding of SCI nor does it recognize the heterogeneity of SCI. Both primary and secondary injury mechanisms result in heterogeneity within an AIS class and this heterogeneity, in turn, is reflected by an apparent spontaneous recovery from an AIS class indicating a severe injury (ASIA A) to one of more motor and sensory function (for example, ASIA C). The consequence of using this classification scheme is that large clinical trials are needed to distinguish a treatment effect from natural history.

Since its adoption into clinical medicine in the early 1980's, magnetic resonance imaging (MRI) has been used to directly visualize the human central nervous system. Clinicians and surgeons treating traumatic spinal cord injury patients have embraced this technology to better characterize lesions of the spinal cord that were previously inferred based on clinical examination and disrupted bony elements observed with standard x-ray equipment or computed tomography. While MRI had an almost immediate effect on improving surgical planning, use of this technology in combination with other efforts to improve outcome for spinal cord injury

patients has been slower coming. Given that novel strategies to improve outcome after traumatic spinal cord injury will be initially tested within the context of clinical trials, it follows that advanced imaging techniques should be used to improve the design and conduct of such studies. Through the development of imaging biomarkers to characterize residual structure and function after traumatic injury, one could expect to use these biomarkers as a means of refining inclusion and exclusion criteria to reduce heterogeneity within a given treatment group. Imaging biomarkers can potentially be utilized at any stage of SCI from acute to subacute to chronic depending on the intended target of the therapeutic intervention. Also, they are capable of targeting a multitude of substrates within the central nervous system (CNS) from motor to sensory to autonomic pathways. Such surrogate markers could serve as the endpoint for stratified block randomization trials, reported as a percentage change from baseline. When the interpretation of any given biomarker is called into question, the use of animal models through a reverse-translation approach will certainly be useful.

If this strategy is to be successful, it will be important to establish whether or not an imaging biomarker is capable of detecting subclinical changes to the CNS and ultimately whether or not such subclinical changes provide a favorable conduit to improved clinical function. As discussed by many leading authors in the field, a single therapeutic strategy is unlikely to serve as the magic bullet for restoring function after injury. Rather, a combination of strategies at different time points is likely required.[4] For example, the use of neuroprotective strategies during the acute phase followed by neuroregenerative therapies in later stages of recovery after hostile, secondary injury mechanisms, have subsided. By adopting this approach, the next generation of clinical trials will effectively personalize the care of SCI patients.

The ultimate outcome after SCI must be measured in terms of clinical function. The effectiveness of a novel therapeutic intervention however can potentially be streamlined by more accurately characterizing spinal cord injury (and therefore reducing heterogeneity within a treatment group) and measuring changes to the CNS (surrogate outcomes) in a more efficient, less expensive way through use of noninvasive imaging biomarkers. By characterizing residual structure and function of the spinal cord the opportunity exists to refine the diagnosis of traumatic SCI and more closely follow the effect of novel therapeutic interventions.

1.2 General Aims

Given this broad framework for the implementation of MRI based biomarkers to aid in the characterization of spinal cord injury and measuring the effect of novel therapeutic interventions, this thesis will address the following general aims:

1. To characterize the T_1 and T_2-weighted intramedullary spinal cord signal characteristics first used by clinicians treating spinal cord injury in order to classify patients along a spectrum of injury severity
2. To determine whether spinal functional MRI can distinguish spinal cord injury subjects from healthy controls based on the integrity of ascending pathways of the spinal cord
3. To determine the population variation in human cervical spinal cord anatomy

This thesis represents a total of 8 published works as follows: 2 peer-reviewed editorials that formulate the preamble of Chapter 1; 2 book chapters and 1 peer-reviewed review paper that make up the literature review of Chapter 2; 2 peer-reviewed primary research papers that make up each of Chapter 4 and 5 (chapter 6 has been submitted for peer review, publication is pending); and 1 peer-reviewed review paper contained within chapter 7.

Chapter 2
Literature Review

This chapter is modified from the following:

David W. Cadotte and Michael G. Fehlings. Spinal Cord Injury. Principles of Neurological Surgery, Third edition. Eds. Ellenbogen, Abdulrauf and Sekhar. April 26, 2012. ISBN-10: 1437707017.

D.W. Cadotte, D. Mikulis and M.G. Fehlings. Imaging of the injured Cervical Spine and Spinal Cord. In: The Cervical Spine 5th edition, edited by Dr. Edward C. Benzel. Lippincott Williams and Wilkins. August 29, 2012. ISBN-10 1605477524 | ISBN-13: 978-1605477527.

David W. Cadotte, Patrick W. Stroman, David Mikulis and Michael G. Fehlings. A systematic review of spinal fMRI research: outlining the elements of experimental design. Journal of Neurosurgery *Spine (Suppl) 17:102-118, 2012*. Accepted May 7, 2012. Published September 2012.

2 Literature Review

2.1 An overview of traumatic spinal cord injury

Traumatic injury to the spinal cord usually occurs due to an unforeseen event such as a motor vehicle accident or falling from a height. This causes damage to the cellular constituents and functional circuits that transmit motor, sensory and autonomic signals between the periphery and the brain. Dysfunction of the human spinal cord can also arise from a penetrating assault, chronic progressive disorders such as cervical spondylotic myelopathy, autoimmune or inflammatory conditions and primary and secondary tumors. This thesis is concerned with traumatic injury to the spinal cord and therefore, other mechanisms that cause dysfunction of the spinal cord will not be discussed further.

2.1.1 Epidemiology, clinical management, and spinal cord syndromes

Spinal cord injury has been studied at a population level in order to understand the incidence, prevalence and economic costs of this devastating event. Such studies tend to come from developed countries that have the financial resources to conduct this research but spinal cord injury certainly does not respect borders. In fact, neurotrauma in the developing world is estimated to be higher than the developed world for reasons such as poor quality of roads, unsafe driving practices, old vehicles without seatbelts or airbags, and a greater portion of relatively inexpensive transportation such as small motorcycles. Nonetheless, the estimated incidence of spinal cord injuries in the developed world is approximately 11.5 - 53.4 per million.[5] However, the actual incidence may be higher as an unknown number of patients suffering spinal cord injury die at the scene of the accident without ever being examined or treated in a hospital.[6] Another study in the 1970s estimated that approximately 48 – 79 % of individuals die either at the scene of the accident or on arrival to hospital.[7] The number of patients who die is likely less today, mainly as a result of an improved understanding of the cardio-respiratory complications that can arise following injury and advanced intensive care units that are well versed in managing these complications.

One way to comprehend the costs involved in treating a person with spinal cord injury is to imagine that a 25-year-old sustains an injury and becomes completely dependent on family and the health care system from this point forward in life. One study estimated financial total costs to

be in the range of 3 million dollars (USD)[8], not to mention the impact of this event on the person's family and peers. The average age of a spinal cord injured patient is the late 20's and early 30's is more common in males. Thus, since spinal cord injuries affects people as they are starting their careers and families, a lack of income combined with insurmountable medical costs translates into financial and emotional hardship. Depression and forms of psychological distress are common in this patient group. In well-developed health care systems support networks exist to aid patients and families through the life that they could not have imagined. In third world countries, patients and families are left to their own devices.

Clinical management

A patient who sustains a spinal cord injury has often sustained concomitant injuries and may be medically unstable; in fact, the treating physician may not recognize the presence of spinal cord injury immediately. Adherence to Advanced Trauma Life Support (ATLS) protocol is essential. Airway, breathing and circulation (ABC's) are of paramount importance to be followed by the treatment of any immediate life-threatening condition. If there is concern that any one of these domains is unstable, it should be re-visited before moving on to assess neurological function. Hypotension, in particular, must be avoided as it can exacerbate secondary spinal cord injury (this topic is expanded on below). Following stabilization of the patient, the treating physician should then proceed with the neurological examination. This comes in the form of testing for motor power, sensory impairment and reflexes including rectal tone. This examination should be documented on the standard American Spinal Injury Association forms (available at http://www.asia-spinalinjury.org/publications/2006_Classif_worksheet.pdf). Following a detailed clinical examination, and assuming the presence of a neurological deficit, imaging of the spinal column with either x-ray or CT scan and imaging of the spinal cord and surrounding soft-tissues with MRI should follow in short order. Concurrently, the astute clinician should be aware of the following concepts that are essential for proper care of the SCI patient: spinal shock and neurogenic shock.

Spinal shock

Spinal shock is a term used to describe depressed spinal reflexes caudal to the injury site following spinal cord injury. This is an important concept to understand as the initial neurological examination may not be an accurate reflection of disrupted neuronal circuits,

including those that control motor and sensory pathways. Normally, these reflex pathways receive continuous input from the brain. When this tonic input is disrupted, the normal reflex pattern is disrupted and can vary from areflexic through to hyperreflexic depending on the time since the original injury. Clinically, this translates into the potential for a misleading representation of deficits if spinal reflexes are absent following injury. It is therefore recommended that patients not only be examined on presentation to the treating physician but also at the 72-hour mark following injury.

Neurogenic shock

Neurogenic shock is a potentially life threatening condition and must be managed as such. Without a clear understanding of this condition, inappropriate management of a trauma patient who often suffers concomitant hemodynamic instability could be fatal. Neurogenic shock is defined as disruption of the sympathetic nervous system with preserved parasympathetic activity. This typically occurs with patients suffering a severe spinal cord injury at the level of T6 or higher. Disruption of the sympathetic division of the autonomic nervous system has three effects on the cardiovascular system: coronary blood flow, cardiac contractility and heart rate. With preserved parasympathetic activity this translates clinically into bradycardia (and possibly other cardiac arrhythmias) in the setting of profound hypotension. A prudent clinician must look for these characteristics in combination, as many trauma patients are hypotensive as a result of blood loss or intravascular hypovolemia but will mount an appropriate tachycardia response.

The treatment of neurogenic shock is therefore quite difficult. While it is theoretically possible to distinguish between hypovolemic and neurogenic shock, this is not so clinically. In fact, acute trauma patients sustaining a high cervical spinal cord injury may suffer from both conditions. It has therefore been recommended by the Consortium for Spinal Cord Medicine to rule out other causes of shock before assuming a diagnosis of neurogenic shock. The practical treatment of these patients rests on initially restoring intravascular volume and if symptoms of neurogenic shock persist, vasopressors (such as dopamine) should be used. The goal of treatment in the first week after sustaining a spinal cord injury is to maintain a mean arterial blood pressure of 85 mmHg.

Spinal cord syndromes

Terminology used to describe deficits and identify different spinal cord syndromes in an order to localize the lesion to a particular area of the spinal cord and a particular segmental level is as follows. Paresis describes weakness or partial paralysis. For example, hemiparesis describes weakness on one side of the body. In contrast both paralysis and the suffix plegia refer to no movement. For example hemiplegia refers to no movement on one side of the body. When a select region of the spinal cord is damaged a predictable pattern of neurological deficit is encountered. These syndromes are expanded on in the paragraphs that follow and depicted in

Figure 2-1. , along with a description of the ASIA impairment scale.

ASIA Impairment Scale		
ASIA Grade	Complete or Incomplete	Description
A	Complete	No motor or sensory function is preserved in the sacral segments S4-S5
B	Incomplete	Sensory but not motor function is preserved below the neurological level and includes the sacral segments S4-S5
C	Incomplete	Motor function is preserved below the neurological level, and more than half of key muscles below the neurological level have a muscle grade less than 3
D	Incomplete	Motor function is preserved below the neurological level, and at least half of key muscles below the neurological level have a muscle grade of 3or more
E	Incomplete	Motor and sensory function are normal

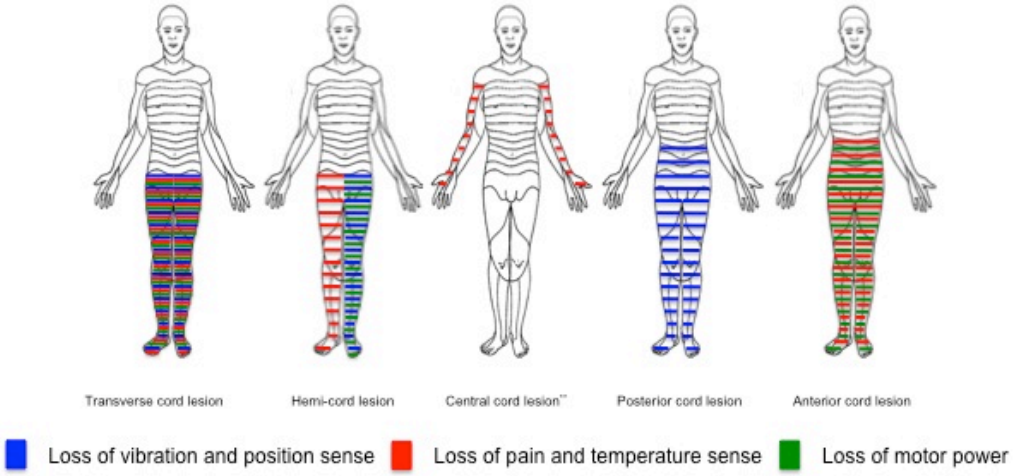

Figure 2-1. ASIA Impairment Scale and Spinal cord syndromes. Central cord syndrome** is representative of a small lesion. If the central cord lesion were large, one would expect involvement of the motor and vibration/position sense systems (see text for further explanation). Motor power is graded according to the following scale: 0 = total paralysis, 1 = palpable or visible contraction, 2 = active movement, full range of motion, gravity eliminated, 3 = active movement, full range of motion, against gravity, 4 = active movement, full range of motion, against gravity and provides some resistance, 5 = active movement, full range of motion, against gravity and provides normal resistance, NT = not testable – the patient is unable to reliably exert effort or the is muscle unavailable for testing due to factors such as immobilization, pain on effort or contracture. Sensory testing is graded according to the following scale: 0 = absent, 1 = impaired, 2 = normal and NT = not testable. Reproduced from Principles of Neurological Surgery, Third edition. Eds. Ellenbogen, Abdulrauf and Sekhar with permission from Elsevier.

Transverse spinal cord lesions disrupt all motor and sensory pathways at and below the level of the lesion. There is a sensory level that corresponds to the level of the lesion. Hemi-section of the spinal cord, commonly referred to as Brown-Séquard syndrome, is characterized by damage to one-half of the spinal cord and all motor and sensory pathways at that level and neurological deficits at and below that level. This results in ipsilateral upper-motor neuron weakness and ipsilateral loss of vibration and position sense at and below the level of lesion. There is contralateral loss of pain and temperature sensation below the level of the lesion. There may also be ipsilateral loss of pain and temperature at the level of the lesion for one or two spinal segments if the lesion has damaged posterior horn cells before fibers have crossed to the other side.

Central cord syndrome is commonly caused by a traumatic spinal cord contusion, posttraumatic syringomyelia or a medullary spinal tumor. This lesion tends to affect pathways that are in the immediate vicinity of the central portion of the spinal cord and the symptoms differ depending on the size of the lesion. Small lesions affect spinothalamic fibers that cross in the ventral commissure and cause bilateral regions of suspended sensory loss to pain and temperature. If the lesion is larger, anterior (ventral) horn cells, corticospinal tracts and Dorsal columns may be affected. Loss of these pathways respectively results in lower motor neuron deficits at the level of the lesion, upper motor neuron signs below the level of the lesion and loss of vibration and position sense below the level of the lesion. In addition to suspended pain and temperature loss with small lesions, larger lesions can result is complete loss of pain and temperature below the level of the lesion if the anterolateral pathways are compressed from a medial aspect. Given the spinal cord laminations, sacral sparing is observed.

Posterior cord syndrome involves bilateral loss of vibration and position sense below the level of the lesion as a result of disruption of the Dorsal columns. If the lesion is large enough, one may observe upper motor neuron signs below the level of the lesion indicating involvement of the lateral corticospinal tracts. In addition to traumatic injury, vitamin B12 deficiency or tertiary syphilis can cause isolated involvement of the posterior columns.

Anterior cord syndrome results in loss of pain and temperature sensation below the level of the lesion (spinothalamic pathways), lower motor neuron signs at the level of the lesion (anterior horn cell damage) and upper motor neuron signs below the level of the lesion (lateral

corticospinal tracts). In addition, urinary incontinence is common because of the ventral location of the descending pathways controlling sphincter function. Common causes of this syndrome include trauma and anterior spinal artery infarct.

At this point in the clinical management of traumatic SCI, the treating physician has typically made a diagnosis based on both clinical examination and imaging evidence and has adequately managed changes in blood pressure. Several treatment options exist that are available in most institutions that offer neurosurgical care. Broadly speaking, treatment options during the acute phase of injury are generally considered to be 'neuroprotective' in nature, which aim to mitigate ongoing damage to the spinal cord as a result of secondary injury mechanisms. Prior to discussing these treatment options, the pathophysiology of spinal cord injury is reviewed.

2.1.2 Pathophysiology: primary and secondary injury

In a true reductionist fashion to delineate the precise cause of neurological dysfunction after traumatic injury, researchers have divided the temporal sequence of destructive events into primary and secondary injury. Primary injury refers to the destructive forces that directly damage the neural structures such as the sheer force tearing an axon or a direct compressive force occluding a blood vessel resulting in ischemia. These destructive primary mechanisms not only result in instantaneous damage to neurons and blood vessels but also initiate a cascade of cellular mechanisms that result in ongoing damage to the neural structures, termed secondary injury. For example in the setting of a fracture dislocation where the bony spinal column is displaced and physically pushed up against the spinal cord, these cellular mechanisms are thought to be locked in the 'on' position until such physical forces are removed either by closed reduction or surgically. Secondary injury may persist from hours to weeks to years following primary injury. A great deal of work has gone into the detailed understanding of these cellular cascades and along with this work has come an appreciation for the destructive effects of the mechanisms and the role of potential therapeutics to halt these cascades. In the remainder of this section the most important secondary mechanisms of injury will be reviewed followed by an overview of translational research therapeutic targets that resulted from these basic science discoveries.

Secondary injury stems from any aberrant physiological or physical force and results in further tissue damage and potential exacerbation of primary injury. Two of the easiest physiological parameters to recognize are hypotension and hypoxia. Both of these conditions are relatively

common in trauma patients who often sustain concomitant injuries and blood loss. Both are also amenable to medical management shortly after the patient arrives at hospital. Both global hypotension and hypoxia add to the overall effect of hypoperfusion to the damaged area of the spinal cord. Several other mechanisms add to hypoperfusion including disruption of the microvasculature, loss of normal autoregulatory mechanisms and increased interstitial pressure.[9-11] The effects of this ischemic insult are cytotoxic cell swelling of both neurons and glial cells; as a downstream effect of this, blockade of action potentials has been demonstrated as a result of axonal swelling.[12]

Ionic dysregulation and excitotoxicity are closely linked events that contribute to tissue damage. Calcium dysregulation in particular has been widely linked to cell death through a number of different processes including calpain activation, mitochondrial dysfunction and free radical production.[13] Whether calcium dysregulation or disruption of other ionic gradients, loss of ionic homeostasis is central to both necrotic and apoptotic cellular death. Excitotoxicity results from activation of glutamate receptors via the influx of both sodium and calcium ions. As cell death occurs, either through the process of necrosis or apoptosis, extracellular glutamate levels rise presumably due to the failure of energy dependent transporters such as the Na^+ K^+ ATPase membrane transporter.[14] In the section below we will discuss how antagonists of NMDA receptors are potential targets of translations research in order to minimize cellular death.

Free radical mediated secondary injury occurs through the process of lipid peroxidation that ultimately results in disruption of axons and death of both neurons and glial cells. Considering the mechanism of free radical damage, peroxynitrite and other reactive oxygen species, act through a chain reaction that ultimately destroys cellular membranes and leads to cell lysis, organelle dysfunction and calcium dysregulation.[15] This, in turn, adds to the ionic dysregulation described in the above paragraph. Free radicals have been measured in the damaged tissue of experimental models and are found to be elevated for approximately 1 week following injury returning to pre-injury baseline only after 4-5 weeks.[16] Examples of these free radicals include hydrogen peroxide, hydroxyl radical, nitric oxide and the superoxide radical. Specific radicals, such as peroxynitrite have been directly liked to the activation of apoptotic cascades in rat SCI models.[17] As with NMDA receptors above, free radical oxygen species become a potential target of translations research. One concept is that the degree of secondary damage that occurs following spinal cord injury may be preventable if one could manage the level of these free

radicals (see translational research section below).

Tight junctions between endothelial cells act as an interface between the systemic circulation and the central nervous system including the spinal cord. Known as the blood brain barrier (BBB), its function it also acts as a selective barrier to solutes such as glucose while maintaining impermeability to macromolecules and infectious agents such as bacteria. Endothelial cells and astrocytes are normally bridged by tight junctions and are interspersed with very selective transmembrane proteins to allow the passage of vital molecules and ions. With the destructive forces that accompany SCI, comes the destruction of the BBB. This can results from either direct mechanical destruction, such as damaged blood vessels and spinal cord parenchyma or from destruction at a cellular level. The latter is best understood as result of the effects of numerous inflammatory mediators on the endothelial cells that disrupt the normally impermeable barrier. One way researches have studied this effect is through the use of a compound called horseradish peroxidase. When injected into the peripheral circulation of a normal animal, this compound does not cross the fortress of the BBB and remains in the systemic tissues. When injected into animal models of SCI, the compound was found to permeate into the CNS at a peak time of 24 hours following injury. Such permeability was persistent for up to 2 weeks following injury.[18] A number of compounds have been identified that are thought to contribute to this ongoing permeability following injury, each of which members of the secondary mechanisms of spinal cord injury. Inflammatory mediators affecting vascular permeability include tumor-necrosis-factor-alpha (TNFα) and interleukin-one-beta (IL-1β) and both have been shown to be unregulated following SCI.[19,20] Other compounds that play a role include matrix metalloproteinases, histamine and reactive oxygen species including nitric oxide.[16]

The inflammatory reaction following SCI has received a renewed interest in recent years largely because of what is thought of as the dual nature of the immune response. Inflammatory mediators are thought to be responsible for the ongoing destruction of tissue but also seem to be clearing cellular debris and optimizing the environment for regenerative growth. Several non-cellular mediators are involved in the cascade of events, the most prominent of which are TNFα, interferons and interleukins.[21] Cellular mediators following SCI include both resident microglia and peripheral inflammatory cells. A few of the well characterized examples, mainly from studies in the rodent population, include astrocytes, T cells, neutrophils and invading monocytes.[22] An example of this dual nature of protection and destruction is that TNFα is

significantly upregulated following SCI.[23] Subsequent studies that applied neutralizing antibodies to TNFα following experimental injury resulted in improved neurological function.[24] However, TNFα-deficient mice have more apoptotic cells, increased lesion size and worse function following SCI compared to wild type mice.[25] This demonstrates the complexity of the inflammatory cascade in SCI and that many players are acting in a complex pattern, some of which may aid in optimizing function and others may result in ongoing destruction. Further research in this field will tease out these details and provide specific targets for translational research to optimize the potential for recovery.

Cellular death via the apoptotic pathway is thought to play little role in the fate of neurons[26] but a considerable role in the fate of oligodendrocytes[27] following SCI. While it may be difficult to demonstrate the apoptotic mechanism of neuronal death in human SCI, there is some evidence for its role in animal models.[28] In contrast, the apoptotic mechanism of oligodendrocyte death is at least partially elucidated. Following SCI, microglia are activated within the first 2 – 48 hours and express the Fas ligand.[29] This ligand has a receptor largely expressed on the oligodendrocyte and communication occurs via the p75 neurotrophin receptor.[30] The interaction of the Fas ligand and its receptor initiate apoptosis by way of the caspase cascade that ultimately results in proteolysis, DNA cleavage and cell death.

In contrast, cell death via the necrotic pathway has been demonstrated in both neuronal and non-neuronal cells. Several of the secondary mechanisms of injury discussed above, such as hypoperfusion and excitotoxicity, culminate in the necrotic death of neurons. Oligodendrocytes are also susceptible to this death pathway and the loss of this cell type results in axonal demyelination. This demyelination, in combination with other insults on the neuronal processes such as lipid peroxidation and ischemic swelling, results in death of the associated neuronal cell bodies.[31] Animal studies have provided evidence that preserved axons represent a critical therapeutic target in order to regain neurological function.[32] In stark contrast to this, post mortem human studies have failed to identify demyelinated axons[33] and may represent an important disconnect between animal and human pathology following SCI.

Primary and secondary injuries are conceptual frameworks that divide the temporal sequence of events following SCI. This framework provides a basis for research into the complex pathways that are activated in response to trauma, some of which may result in optimizing the local

environment for neurological recovery and others that have deleterious side effects. The pathological processes that occur at the cellular level include ischemia, vasospasm, ion-mediated cellular damage, excitotoxicity, oxidative cellular damage, neuroinflammation, and cellular death. Each of these processes involves complex cascades of events that are potential targets for intervention. In the paragraphs that follow, select targets will be highlighted that may eventually prove to be beneficial in treating persons that sustain a SCI.

2.1.3 Neuroprotection through medical and decompressive strategies

Recent advances in the treatment of SCI stem from an improved understanding of secondary injury cascades, the development of neuroprotective strategies and the testing of therapies through clinical trials. Broadly speaking, neuroprotective strategies are thought to have a maximal effect if implemented as close to the time of injury as possible and may take the form of either a medical therapy or a decompression strategy (either open surgical decompression or closed reduction through the application of traction). The last few decades has seen advances in both medical and decompressive approaches.

Three different medical therapies have been studied in the context of a human clinical trial with the aim of improving neurological outcomes after spinal cord injury.[34-39] The neuroprotective agents studied include methylprednisolone,[34-37] GM-1 (Sygen),[38] and gacyclidine (GK-11).[39] Of these, only methylprednisolone demonstrated a statistically significant result of improved patient outcomes when given within 8 hours of injury; however its widespread adoption into clinical use has been called into question due to adverse effects.[40] Nonetheless, each of these studies contributed to our improved understanding of traumatic spinal cord injury. A panel of experts supported by the International Campaign for Cures of SCI Paralysis (ICCP) reviewed these and other works with the aim of establishing guidelines for the conduct of clinical trials in SCI.[2,3,41,42] These guidelines are a valuable asset for clinicians and researchers dedicated to the improvement of SCI trials and ultimately, patient outcomes. Of particular interest is the natural history of SCI where the authors describe the rapid rate of recovery during the first three months after injury that continues to approximately one year and tends to plateau at this time point. This has practical implications for the study of SCI insofar that larger trials are needed if the intervention in question is implemented closer to the time of injury whereby a higher degree of spontaneous recovery necessitates larger intervention and control groups. Along the same lines of reasoning,

the authors warn against the prognostic value of the ASIA examination at time points of less than 72 hours as spinal shock may confound early assessments. In short, clinical trials have taught us much more than the effectiveness, or lack thereof, of one particular therapeutic agent. Choosing an endpoint, selection of trial participants, stratification of subjects and the coordination of protocols across distant centers of excellence each have their challenges and advantages for a given study.

Evidence for methylprednisolone therapy

The use of methylprednisolone as a neuroprotective agent to mitigate the deleterious effects of secondary injury is still controversial. It has been shown to offer modest benefit in terms of neurological outcome following SCI.[43] The National Acute Spinal Cord Injury Study (NASCIS) aimed to investigate whether patients would benefit from its administration.

NASCIS was designed as a multicenter trial and was completed as three separate trials: NASCIS I, NASCIS II and NASCIS III. The first study compared low and high-dose methylprednisolone (no placebo), the second trial was randomized and controlled with a placebo and the third trial compared the effects of 24 versus 48-hour treatment. NASCIS I randomized SCI patients into two cohorts: a 100 mg loading dose of methylprednisolone followed by 25 mg every 6 hours for 10 days group, and a 1000 mg loading dose of methylprednisolone followed by 250 mg every 6 hours for 10 days group. [44] There were no differences in neurological outcome between the two groups at one year after injury. NASCIS II investigated a 30 mg/kg bolus of methylprednisolone over one hour followed by 5.4 mg/kg/hr over the following 23 hours and included a placebo group and naloxone administration group. The reason for the higher doses (in comparison to NASCIS I) involved the analysis of animal research that suggested a therapeutic benefit only above a certain threshold. Results from the overall group showed no significant differences in neurological outcome at 6 months; a subgroup analysis demonstrated improved motor and sensory outcomes in patients receiving methyprednisolone within 8 hours of injury.[35] NASCIS III examined outcomes in acute SCI patients receiving 30mg/kg bolus of methypredniosolone followed by 5.4mg/kg/hr for either 23 hours or 47 hours. Patients treated with methylprednisolone for 48 hours had better neurological outcomes in comparison to the other treatment groups if therapy was initiated within 3-8 hours of injury, however the 48-hour regimen was associated with increased risk of sepsis and pneumonia.[36] Following the completion

of each of these studies, Bracken conducted a reviewed along with two other independent trails and concluded that high-dose therapy was safe and afforded a modest benefit in terms of neurological outcome.[45]

Clearly the results were not overwhelmingly in favor of methylprednisolone administration and there is still considerable debate as to whether or not it should be used. Furthermore, if a practicing physician decides to use this therapy, there is debate as to which administration protocol should be used. Independent experts in the field have published protocols for administering methylprednisolone following acute SCI based on the timing of administration.[43] According to one such protocol, patients with acute non-penetrating SCI should receive methylprednisolone as per the NASCIS II protocol if started less than 3 hours after injury. If started between three to eight hours after injury, then the NASCIS III 48 hour protocol should be applied. If therapy cannot be administered within 8 hours of injury, or there is a penetrating SCI, then methylprednisolone should not be administered for neuroprotection. The decision to administer methylprednisolone must account for patient medical co-morbidities. For example, the risks of administration may outweigh the benefits in a patient with diabetes mellitus and a complete thoracic SCI injury. Blood glucose levels must be carefully monitored during the course of methylprednisolone therapy, and hyperglycemia aggressively managed with an insulin infusion. Due to the high complication rate, the most recent guidelines put forth by the Joint Section on Spine and Peripheral Nerves of the American Association of Neurological Surgeons and Congress of Neurological Surgeons state that methylprednisolone should not be used due to the high rate of complications.[40] The use of steroids in SCI patients remains a subject of debate. Given that SCI is a heterogeneous condition, and that recent data from the STASCIS trial focused on cervical SCI, it appears that complications in this patient group are lower than previously reported studies, perhaps due to a more homogenous sample.

In addition to the completion of the above-mentioned medical trials, evidence has continued to mount for early decompression of the spinal cord. Current clinical management can take the form of either closed reduction in the cervical spine, as is often performed in the setting of bilateral locked facets with progressive neurological deterioration, or of surgical decompression. Early decompression is supported by ample evidence in pre-clinical animal models.[46] Concerns of perioperative hemodynamic changes causing decreased spinal cord perfusion and therefore exacerbating the original injury have largely been overcome by studies designed to test for safety

of the procedure.[47,48] Recently, the Surgical Timing in Acute Spinal Cord Injury Study (STASCIS) demonstrated that early surgery (<24 hrs) after spinal cord injury was associated with better neurologic recovery at 6 months as defined by a 2-grade improvement in the American Spinal Injury Association impairment scale with no difference in complication rate between those undergoing early or late surgery.[49] These treatment options and evidence for each of these approaches will be reviewed here.

Evidence for early closed reduction of bilateral locked facets

Imaging of the spinal column with a CT scan and the spinal cord and soft tissues with MRI should follow clinical examination. These imaging modalities provide essential information that determines subsequent steps in management. In the setting of severe flexion injuries, disruption of the anterior, middle and posterior columns along with the ligamentous joint capsules can occur. This is an extreme example on the spectrum of flexion injuries and usually results in a quadriplegia. CT imaging reveals the inferior articular facets from one vertebral body to be dislocated anteriorly with respect to the superior facets of the adjacent vertebra. MRI is necessary to investigate the degree of neural element involvement and the degree of ligamentous compromise. Treatment of this injury usually begins with closed reduction of the facet dislocation; whether or not one investigates the cervical spine with MRI prior to this maneuver is a controversial issue. An important qualifying factor in this situation is that the patient must be awake, alert and able to participate in repeated neurological examinations. This notion rests in the dictum of 'do no harm to your patients'. Early closed reduction of bilateral locked facets aims to relieve severe spinal cord compression in the setting of significant ligamentous damage by restoring normal bony alignment. The technique should be performed in a monitored setting and involves applying either Gardner-Wells tongs or a Halo-crown as a rigid fixation device to the skull and applying a traction force. Increasing weight is added over time while neurological status is monitored for stability and lateral x-rays are used to follow the bony anatomy. The goal is to obtain reduction of the cervical facets. A post-reduction MRI should be obtained to rule out disc herniation. This maneuver should only be performed in specialty centers with surgeons experienced in its application. Under no circumstances should this maneuver delay operative management. The evidence for this technique was recently reviewed and consisted of a number of class II and III studies, with retrospective and prospective designs.[48] The results of these studies varied from neurological deterioration to no neurological change to neurological

improvement. In order to further distill the controversy, several authors reported that the method is safe and that neurological decline is often transient and improves with removal of added weight. Furthermore, a number of studies report neurological improvement, which led to the recommendation of early closed reduction as a clinical guideline in patients with bilateral locked facets and an incomplete tetraplegia or in those with deteriorating neurological status.

Evidence for early surgical decompression

The concept of surgical decompression for spinal cord injury has received a great deal of attention in the past two decades largely because of the concepts of secondary injury. It is important to consider the indications for surgery following traumatic SCI. The first and foremost is spinal instability caused by torn ligaments and bony fracture. There is little controversy over the need for surgical stabilization in this setting. The other, and focus of this section, is surgical decompression that aims to improve neurological outcome without a strong indication for the treatment of spinal column instability. Physical compression of the spinal cord is responsible for triggering an ongoing series of deleterious cascades and surgical decompression aims to relieve this compression. Evidence is mounting for improved outcomes in this setting.

One of the parameters to consider when studying the effect of surgical decompression after SCI is the timing of this decompression. There is no definition of this timing although most authors and spinal surgeons consider early surgery to be performed within 24 hours of initial injury. A great deal of the pre-clinical animal literature focuses on timing of surgical decompression at much earlier times following injury – in the range of 8 – 24 hours. These animal studies consistently report improved neurological outcomes with early decompression. There have been many systematic literature reviews that address previous pre-clinical and clinical research.[48,50,51]

Clinical evidence of improved neurological function in response to surgical decompression established through human clinical trials is less extensive. The quality of evidence is divided into three levels: Level I evidence is based on at least one properly designed randomized controlled trial; level II evidence stems from either a well designed controlled study without randomization or via a cohort or case-control study and level III evidence is based on expert opinion or the advice of an expert panel. Methodological quality was assessed by the same means outlined in section 2.3.2. No level I evidence exists to guide clinicians with regard to the timing of surgical decompression following SCI. All of the studies to date represent either level II or III evidence.

Two level II studies have been published.[52,53] Vaccaro *et al*. studied 62 patients who presented with an SCI between C3 and T1.[53] They defined early surgery as treatment within 72 hours and late surgery as treatment after 5 days. The authors found no difference between the groups with regard to length of stay (LOS) in the intensive care unit (ICU) or inpatient rehabilitation, or in American Spinal Injury Association (ASIA) motor scores. In contrast, Cengiz *et al*. studied 27 patients who sustained a traumatic SCI from T8 to L2.[52] They defined early and late surgery as occurring within 8 hours of injury and late surgery as occurring 3–15 days after injury. There were several differences between the groups at follow-up. The early surgery group demonstrated greater improvements on the ASIA impairment scale, no complications in hospital, and a shorter hospital and ICU LOSs. Four patients in the later surgery group experienced complications: three cases of lung failure and one case of sepsis. The authors concluded that there are statistically significant differences between patients treated early and those treated late, both with regard to neurologic improvement and overall morbidity. There were no mortalities in either group.

Most clinical studies that have attempted to address the question of timing of decompression following traumatic SCI represent level III evidence. The following sections provide an overview of investigations that outline the effect of early surgery on the following: Hospital LOS, Medical complications following SCI and Neurologic outcomes.

Length of stay

When attempting to study the effect of early surgery on SCI, a relatively easy metric to follow is the length of time a patient spends in the ICU or inpatient unit. This measurement considers not only the severity of the injury, but also the accessibility of the medical system in terms of stabilizing the patient and allowing him or her to proceed with rehabilitation. Of the 22 clinical studies identified in this review, nine level III studies measured LOS.[54-62] Early surgical decompression offered a statistically significant shorter hospital LOS in all nine studies (although Guest *et al*.[57] reported no *p* values), and shorter ICU LOS in one study.[62] A subset of studies further subdivided overall LOS into duration of stay in the ICU, and found that this time point was also shorter in patients receiving early decompressive surgery.[55-58] Only one study that measured these values found no correlation between the timing of surgical decompression and ICU LOS.[58] An obvious extension of this metric is the rate at which patients are readmitted to

hospital. This was measured in only one study, in which there was no difference between the early and late surgical intervention groups.[60]

Medical complications

The following complications of SCI were recorded in eight of the 22 studies: respiratory complications, wound infections, decubitus ulcers, cardiac complications, urinary tract infections, gastrointestinal hemorrhage, deep vein thrombosis (DVT), and death. Four studies showed no difference in the rate of medical complications between early and late surgical groups,[54,59,63,64] whereas four studies showed fewer complications overall in those receiving early surgical decompression.[55,56,60,61] Specifically, the following results were reported: Mirza *et al*.[61] reported significantly fewer complications in persons receiving surgery within 72 hours of injury; Croce *et al*.[56] reported lower rates of pneumonia and DVT in persons receiving surgery within 24 hours; Chipman *et al*.[55] reported a lower frequency of all complications in patients with an Injury Severity Score above 15 receiving surgery within 72 hours of injury (although this same group reported an equal number of medical complications in persons with an Injury Severity Score <15, regardless of the time of decompression); McKinley *et al*.[60] report higher rates of pneumonia in the late surgery group (>72 hours after injury), but equal rates of other complications (i.e., DVT, pulmonary embolism, ulcers) in the early and late groups.

Neurologic outcomes

Thirteen of 20 studies were powered for and directly reported on the recovery of neurologic function after surgical intervention. The remainder of the studies, 7 of the 20 level III studies, were powered to investigate other aspects of acute spine trauma such as time to reach the hospital, feasibility of early surgery and inpatient complications. Early surgical decompression was associated with better neurologic outcomes in four studies: Clohisy *et al*.[65] reported that surgical decompression within 48 hours was associated with significant improvements on the modified Frankel scale; McLain and Benson[64] reported better neurologic improvement (no *p* value reported) with surgical decompression within 24 hours; Mirza *et al*.[61] found that surgery within 72 hours, but not after this time, was associated with significant improvements in the ASIA motor score; Papadopoulos *et al*.[66] found that patients who received surgical decompression within 12 hours (±1.3 hours) of injury experienced significantly greater neurologic improvements than those with surgery outside this time window.

Seven studies with the same level of evidence reported no neurologic benefit to early surgical decompression.[56,57,59,60,67-69] Two studies showed equivocal results.[63,70]

The last few decades of both pre-clinical and clinical research have been grounded in the notion that secondary injury cascades result in ongoing damage to the spinal cord after the primary injury has occurred. Researchers and clinicians alike agree that if these secondary injury mechanisms can be expeditiously mitigated, outcomes after SCI are likely to improve. A partial list of potential neuroprotective agents is provided in Table 2-1 along with strategies aimed at influencing plasticity and select cellular and bioengineering strategies. The translation of pre-clinical work into the clinical realm has been accomplished with clinical trials exploring the use of medical neuroprotective agents and both closed and open reduction techniques to alleviate ongoing compression of the spinal cord after injury. These advances represent a truly remarkable achievement over the developments that occurred prior to this modern era of treatment practice. One of the many lessons learned from conducting such trials is the heterogeneity that exists within a cohort of traumatic spinal cord injury patients and the implications this has for evaluating the efficacy of a treatment strategy. Advanced imaging techniques stand to improve this aspect of clinical trials by characterizing residual anatomy and therefore reducing the heterogeneity of a group of individuals under study.

Table 2-1 Neuroprotective, regenerative and cellular strategies that are emerging from pre-clinical work into the realm of translational research for potential use in humans.

Selected neuroprotective approaches, in early phase clinical trials, with a potential role for improving outcomes in SCI.	
	Riluzole
	Minocycline
	Polyethylene glycol/magnesium
	Hypothermia
Selected molecular/pharmaceutical strategies with a potential role for improving outcomes in SCI by influencing regeneration or plasticity.	
	Nogo-A monoclonal antibody (ATI-335)
	Cethrin
	Rolipram
	Lithium Carbonate
	Chondroitinase ABC
Cellular strategies either in Phase I clinical trials or destined for Phase I clinical trials	
	Neural stem cells
	Oligodendroglial precursor cells
	Schwann cells
	Olfactory ensheathing cells
Bioengineered strategies in late stage pre-clinical trials or early Phase I studies	
	Cethrin
	Transcriptional factors to up-regulate VEGF (ZFP-VEGF)

2.1.4 Plasticity of the Human Spinal Cord after Traumatic Injury

Plasticity, when used in the context of describing changes to the CNS, is a concept that describes many potential changes. In the most recent *Handbook of Clinical Neurology,* neuroplasticity has been defined as "the tendency of neural circuits to undergo physiological and / or structural changes in response to changes in patterns of use that are brought about by injury or environmental influences".[71] The result of injury to a particular segment of the spinal cord renders caudal segments isolated from the brain with devastating consequences. Functional changes that occur after traumatic SCI are likely the result of several distinct mechanisms. Axonal segments isolated from the neuronal cell body undergo Wallerian degeneration while the proximal segment typically survives.[72] Injured axons encounter a number of inhibitory signals that prevent regeneration. Modification of these signals has been extensively studied in hopes of promoting axonal regeneration and ultimately the reconnection of damaged axons with appropriate targets to restore function. Neutralization of myelin inhibitors and degradation of inhibitory components of the glial scar are two approaches that have been used with success in animal models to limit the inhibitory environment of the spinal cord and promote plasticity after injury.[73-76] Dendritic remodeling is not as well studied in the spinal cord as it is in the brain but similar principles are thought to apply insofar that a loss of input to a postsynaptic neuron induces a pruning or loss of dendritic spines and atrophy of the postsynaptic neuron. Mechanisms underlying this loss of dendritic spines are poorly understood; perhaps the most studied observations involve changes in intracellular calcium signaling that is thought to regulate protein synthesis mediated by clusters of polyribosomes assocated with the base of dendritic spines.[77,78]

The administration of growth promoting factors to the injured spinal cord has also demonstrated success.[79-83] Cellular transplantation including genetically modified fibroblasts, Schwann cells, olfactory ensheathing cells and stem cells have each been used with varying degrees of success in animal models.[80,84-87]

Axonal regeneration is not solely responsible for functional improvements after injury. Plasticity of spared spinal cord and brainstem circuits likely contribute to functional recovery. This has

been demonstrated in lesioning experiements whereby initial recovery of motor function was abolished by lesioning the sensorimotor cortex.[74] Also, the distance that central axons can regenerate is, for the most part, limited to less than 2 spinal cord segments in rodents suggesting a limited capacity to form connections with supraspinal circuits.[73-75] Whether or not the human spinal cord is capable of axonal regeneration of 2 or more spinal cord segments, an absolute distance of > 20 mm, is unknown but would require an increase in distance traversed some ten times longer than rodents. Plasticity of spinal cord circuits has been demonstrated in the absence of directed therapies. For example, using a hemi-section SCI model, severed axons of the cortico-spinal tract that would normally innervate lumbar segments were demonstrated to re-organize and sprout onto propriospinal neurons of the cervical spinal cord.[88] In some cases these connections were made on long propriospinal neurons that circumvented the injury and led to a novel indirect motor pathway to lumbar motor circuits. These novel connections were also studied with electrophysiology that demonstrated anatomical evidence of trans-synaptic connectivity that coincided with restoration with hindlimb motor function.

Plasticity of the spinal cord has also been demonstrated in response to experimental treatments that target the inhibitory components of CNS myelin. Collateral sprouting of the unlesioned cortico-spinal tract into the denervated spinal cord has been demonstrated following unilateral pyramidotomy and treatment with an agent called IN-1, an antibody that neurtralizes the inhibitory myelin-assocaited protein Nogo-A; collateral sprouting was accompanied by recovery of forelimb motor behaviors.[89,90] This and several other studies indicate that manipualation of myelin inhibitors after injury can unmask the capacity of the adult CNS for re-organization. Targeting of both myelin and chondroitin sulfate proteoglycan inhibitors are now being considered as a combinatorial strategy for maximizing the potential for sprouting and other forms of plasticity after injury.[91]

Spinal cord injury not only results in the degeneration of severed or damaged axons but can also result in the demyelination of intact axons.[92,93] Moreover, functional impairment has been correlated to the degree of demyelination.[94] The delivery of neurotrophic factors that promote the integrity of oligodendrocytes demonstrates that demyelination can be reversed; this strategy is an appealing target for future development.[95]

Limiting the extent of secondary damage after spinal cord injury is another approach that is under investigation for promoting functional recovery. Cavitary formation, extension and a relatively slow penumbra of cell death spreading from the injury epicenter in both a rostral and caudal direction contribute to limit functional recovery after injury.[96-99] Targeting the inflammatory reaction or ongoing spinal cord compression after injury are two strategies that have been used to mitigate ongoing functional loss.[100-102]

2.1.5 Neurological outcomes of SCI patients

The endpoint of clinical trials, whether focusing on a pharmacological treatment or surgical decompression, is based on the recovery of motor and sensory function where motor recovery is typically used as a primary endpoint and sensory function a secondary endpoint.[1,49,103] The American Spinal Injury Association (ASIA) has put forth a standardized approach to evaluate and describe the segmental level and extent of injury based on a systematic examination of motor function and sensory perception. The ASIA standard was constructed based on the concept of a dermatome, defined as "the area of the skin innervated by the sensory axons within each segmental nerve root", and a myotome, defined as a "collection of muscle fibers innervated by the motor axons within each segmental nerve root". The sensory score is assessed bilaterally using pin-prick and light-touch modalities where the total score is obtained by testing 28 dermatomes from C2 to S5 on each side of the body; a score of 0-2 is given for each dermatome where 0 represents no sensation, 1 represents impaired sensation and 2 represents normal sensation. Thus, the total sensory score can range from 0 to 224 with higher scores indicating greater sensory function. The motor score is generated by summing a six-grade evaluation (a minimum of 0 and a maximum of 5) of 10 key muscle groups from upper and lower limbs on both the right and left side of the body such that the total score ranges from 0 to 100, with higher scores indicating greater motor function. The 6-point assessment of muscle strength is based on the Medical Research Council scale, where each muscle of interest is rated from '0' indicating total paralysis to '5' indicating normal strength; the scale is outlined in greater detail in Table 2-2. After performing this clinical assessment, motor and sensory ratings are recorded on the ASIA clinical assessment form as illustrated in Figure 2-2.

Table 2-2. Medical Research Council (MRC) scale for muscle strength.

Muscle function grading	
0	total paralysis
1	palpable or visible contraction
2	active movement, full range of motion (ROM) with gravity eliminated
3	active movement, full ROM against gravity
4	active movement, full ROM against gravity and moderate resistance in a muscle specific position.
5	(normal) active movement, full ROM against gravity and full resistance in a muscle specific position expected from an otherwise unimpaired person.
NT	not testable (i.e. due to immobilization, severe pain such that the patient cannot be graded, amputation of limb, or contracture of >50% of the range of motion).

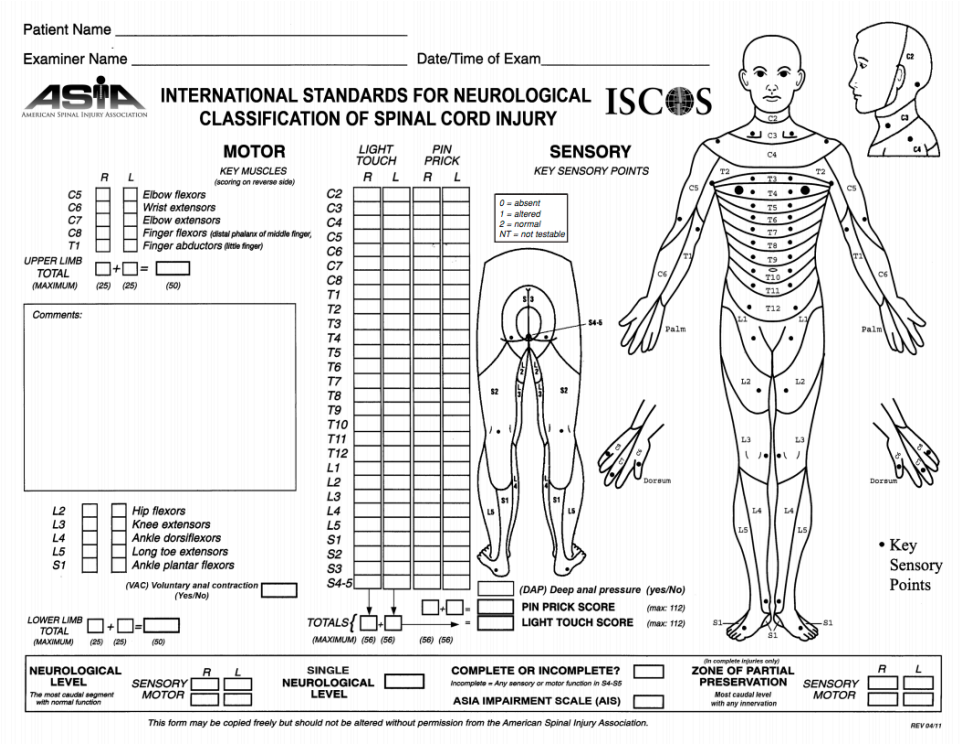

Figure 2-2. American Spinal Injury Association (ASIA) clinical assessment form. Source: http://asia-spinalinjury.org/elearning/ISNCSCI.php (accessed January 2014, available for free download)

Based on the motor and sensory scores obtained from clinical assessment described above, the ASIA standards provide discriminative information on spinal cord injured individuals by completeness of injury and by segmental level. Completeness of injury is described as: complete motor and sensory SCI, complete motor and incomplete sensory SCI and incomplete motor and sensory SCI. Level of injury refers to the last segmental spinal level of normal function. This discriminative information is outlined in Table 2-3. To further illustrate the use of the ASIA classification system, a clinical example is provided in the following paragraph.

Clinical Scenario to illustrate the use of the ASIA classification system: An otherwise healthy 27-year-old male is involved in a motor-vehicle accident as a front seat passenger. He is initially trapped in the car but extricated by the emergency response team over a twenty-minute period. He is brought to a trauma center within one hour of the initial injury and the following report is given: "Vital signs: blood pressure: 75/55, heart rate: 110, respiratory rate: 22, O_2 saturation: 95%; Glasgow coma scale 15; extensive scalp laceration with significant blood loss, not moving lower extremities and minimally moving upper extremities". Initial assessment by the trauma team confirmed the above vital signs. In addition, FAST scan was negative (Focused Assessment with Sonography for Trauma) ruling out any large intra-abdominal blood or fluid collection, there were no obvious long bone fractures and chest x-ray was clear. The scalp wound was closed in the trauma room. Neurological examination reveals evidence of spinal cord impairment as follows: Grade 5 deltoid and biceps bilaterally, grade 3 wrist extensors, grade 2 elbow extension, grade 1 finger flexors, grade 0 interossei and no movement in the lower extremities. Sensation (pin prick and soft touch) was intact to the level of C8 and absent below this level. Rectal tone was diminished but present. Perianal pinprick sensation was preserved. Urgent CT scan of the cervical spine was obtained by the trauma team revealing bilateral locked-facets at the level of C6 / C7.

Based on the clinical information presented in this scenario, the American Spinal Injury Association (ASIA) grade would be B. The motor and sensory levels are the most caudal segment of the spinal cord with normal sensory and motor function on both sides of the body. The motor level is defined in the ASIA classification system as that level with at least Grade 3 power. The cephalad muscle groups must have grade 5 strength. Upper extremity muscle groups tested are: C5 elbow flexors, C6 wrist extensors, C7 elbow extensors, C8 finger flexors and T1

finger abductors (interossei). The motor level in this case is C6: the deltoid and biceps (C5) are Grade 5 and the wrist extensors (C6) are Grade 3, the next motor level (triceps: C7) has Grade 2 power.

In order to distinguish complete versus incomplete injury one must look for preservation of neurological function distally. This includes sacral sparing (perineal sensation). Due to the fact that this fictitious patient has preserved peri-anal sensation, the injury would be classified as sensory-incomplete. Thus, the classification could be summarized as ASIA B (motor-complete, sensory-incomplete) with a motor level of C6 and a sensory level of C8.

Table 2-3. An overview of the American Spinal Injury Association classification scale.

ASIA Classification	
A	Complete: No motor or sensory function is preserved in the sacral segments S4-S5.
B	Incomplete: Sensory but not motor function is preserved below the neurological level and includes the sacral segments S4-S5.
C	Incomplete: Motor function is preserved below the neurological level, and more than half of key muscles below the neurological level have a muscle grade less than 3.
D	Incomplete: Motor function is preserved below the neurological level, and at least half of key muscles below the neurological level have a muscle grade of 3 or more.
E	Normal: motor and sensory function are normal.

A recent systematic review examining the psychometric properties of the ASIA standards in assessing motor and sensory function of individual with acute traumatic SCI was conducted to assess the appropriateness of this evaluation to discriminate and evaluate patients with SCI in a longitudinal manner.[103] Based on an extensive literature review that captured 69 unique studies of ASIA standards, the authors concluded that the ASIA standards represent an appropriate instrument to discriminate and evaluate SCI patients in a longitudinal fashion with the following caveats: 1) ASIA standards do not reliably assess children less than 4 years of age 2) the use of ASIA upper and lower extremity motor sub-scores instead of a single ASIA motor score is recommended, 3) the notion of a minimally clinically important difference of ASIA standards requires further investigation and 4) the threshold of a functionally meaningful change in ASIA score to document the benefit of a novel therapeutic intervention varies according to the level and severity of SCI.

2.2 Standard Imaging Evaluation of the SCI Patient

Imaging of the injured cervical spine can be broken down into imaging of the soft tissues, imaging of the vasculature, imaging of the bones and imaging of the spinal cord itself. There is an armamentarium of imaging tools that enables evaluation of each of these domains. The main purpose of imaging the injured cervical spine and spinal cord is to establish an accurate diagnosis and guide treatment directed towards maintaining spinal alignment with preservation of neurological function.

2.2.1 Detailed radiographic assessment of the cervical spine

Initial evaluation of the cervical spine following trauma

In the event of traumatic injury to the cervical spine the initial means of investigation is usually a plain x-ray or a CT scan.

Plain Radiography

The use of plain radiographs of the cervical spine occupies an important niche in the evaluation of the trauma patient both in terms of initial evaluation and for follow up. However, several authors have demonstrated fractures undetected on plain film later revealed by CT scan.[104,105] The standard views are Anterior-posterior (AP), lateral and open-mouth odontoid; a lateral

swimmers view may also be obtained to examine the cervico-thoracic junction if C7 and T1 are not adequately assessed on the true lateral projection. Dynamic flexion-extension views have limited role in the acute setting as muscle spasm and other distracting injuries often preclude an adequate examination.[106] This dynamic study is of value during the follow up period to assess potential ligamentous instability during recovery from injury.

The AP radiograph of the normal cervical spine should reveal the midline spinous processes at each level. The uncovertebral joints (C3-C6) should be symmetric and vertically aligned at all levels. The vertebral bodies should be of equal height and have a smooth cortical surface.

In evaluating the lateral radiograph one should systematically proceed through the following checklist: 1) the radiograph should display the occiput through the level T1. 2) The lines connecting the anterior and posterior margins of the vertebral bodies and the spinolaminar line (the anterior margin of the junction of the spinous process and lamina) should form a gentle convex curve with no steps or discontinuities. 3) The laminar space (the distance from the posterior aspect of the articular pillars to the spinolaminar line) should be uniform throughout the cervical spine. 4) The prevertebral soft tissues should be examined for increased opacity indicating swelling and possible ligamentous injury. 5) The intralaminar spaces (the space between the laminar arches) should not be widened. 6) The lateral atlanto-dental interval can be visualized.

The open-mouth odontoid view reveals the atlanto-axial articulation. One must examine for the lateral masses of C1, the dens, and the superior facets of C2. The occipital condyles may also be visualized. There should be no offsets between the occipital condyles, lateral masses of C1 and the lateral masses of C2.

Computed Tomography (CT)

While plain radiographs provide a fast means of surveying the regional anatomy in the initial evaluation of cervical spine trauma, especially in low-income countries where other modalities may not be readily accessible, CT scan has become the most common method of evaluation in most institutions and certainly in larger trauma centers. Some advantages of CT over plain x-rays are improved visualization of the cranio-cervical junction and the cervico-thoracic junction, improved rate of fracture detection and the ability to re-format images for improved fracture

detection and surgical planning in three dimensions. Reformatted images enable detection of fractures in the plane of section of acquired CT slices.

When considering the cost of CT over plain films many factors must be considered including the time required to complete the study, the technologist's time, film viewing stations and perhaps most important the accuracy of the diagnosis and its resultant costs both in terms of individual patient care and economic costs of misdiagnosis.[107,108] Several studies have attempted to gauge the cost of CT versus plain films with CT showing greater efficacy.[109]

CT protocol should be performed with 1mm slices to enable reformatting. Sagittal and coronal reformats are then reviewed just as the plain radiographs. The axial images are then reviewed individually using both bone and soft tissue settings to assess fractures and soft tissue injury including extradural hematoma and herniated discs.

MRI should be used to further evaluate patients with either evidence of bony or soft tissue injury (plain films or CT) or with neurological deficit (myelopathy or radiculopathy). MRI has superior soft tissue screening capability and is the only modality that can accurately assess injury to the spinal cord itself. The addition of pulse sequences such as STIR and fat-suppressed images have led to more sensitive evaluation of ligament damage.

2.2.2 Introduction to MR Imaging: important definitions and contrast mechanisms

Magnetic resonance imaging takes advantage of the different magnetic properties of body tissue types and involves acquiring digital signals and reconstructing these signals into an image. The magnetic properties of human tissue, generation of the MR signal, encoding of this signal, formation of an image and various contrast mechanisms are outlined in the following sub-sections. Fundamental MR principles are extensively detailed in a number of texts; the information contained herein was largely obtained from the following references.[110,111]

2.2.2.1 Magnetic properties of human tissue

The most abundant atomic nucleus in the human body is hydrogen (^{1}H) consisting of a single positively charged proton and present in the predominant tissue types including lipids and

proteins and, of course, water that is estimated to make up approximately 60% of body weight. The single proton that makes up the hydrogen nucleus has a large magnetic moment, a property that arises from the spin of the proton about its own axis. In the absence of an external magnetic field, protons have a random orientation. In the presence of an external magnetic field, protons experience torque causing each proton to precess or wobble around the axis of the external field; this fundamental observation of protons in an external magnetic field has been likened to a child's spinning top – it both spins to remain upright on a flat surface and wobbles about a different axis. In an external magnetic field a proton's spin can exist in only one of two quantized states described as either parallel (a low energy state) or anti-parallel (a high energy state). As one increases the strength of the external magnetic field a higher proportion of spins will take the lower energy state, producing a correspondingly larger net magnetization parallel to the external field, termed longitudinal magnetization. Higher magnetic fields also cause the spins to precess faster, a phenomenon that is described by the Larmor Equation:

$$\omega = \gamma\beta$$

Where ω is the Larmor frequency (also termed the precession or resonant frequency), γ is the gyromagnetic ratio, a fundamental property of each nucleus (for ^{1}H this ratio is 42.58 MHz/T) and β is the external magnetic field strength. Spins in a low energy state can absorb energy from oscillating magnetic fields and be forced into a high-energy state, termed excitation; the caveat here is that the energy delivered to the spin system must occur at the resonant frequency, as governed by the Larmor equation.

For typical magnetic field strengths the resonant frequencies are in the radio-frequency (RF) range.

When an RF pulse, an electromagnetic wave, is transmitted along the x-axis (perpendicular to the axis of the external magnetic field, B_0) protons that were previously precessing along the axis of the external magnetic field in the z direction will now begin to precess about the x-axis, the axis of the new RF-induced magnetic field, B_1. Because the magnetic field strength of B_1 is much weaker than the magnetic field strength of the external magnetic field B_0, the precessional frequency of spins around the B_1 axis is much slower.

In order to transfer energy to the spin system by applying a second magnetic field, the frequency of the RF pulse must match the frequency of precession of the protons; in this situation, resonance occurs and the spin system absorbs energy. If the RF excitation is applied continuously over time, the phases of the individual spins will align and an increasing number of spins will absorb energy, converting from the lower to the higher-energy state. RF excitation can be applied until there are, for example, an equal number of spins in each energy state, also meaning that there is no net longitudinal magnetization; in this case the original longitudinal magnetization vector has been completely converted into a transverse (orthogonal) magnetization vector. This is known as a 90° RF excitation pulse. If the RF pulse is twice as long it is termed a 180° RF excitation pulse and twice as many low-energy spins will convert to a high-energy state. In this way, RF excitation pulses can be applied to elicit any flip angle between 0° and 180°. After the RF excitation pulse is finished, spin excitation stops and the system starts returning to equilibrium. Of note, the RF pulse can be altered in terms of its strength and duration such that a very strong RF pulse applied over a short period of time or a weak RF pulse applied over a long period of time could both achieve the same flip angle.

Only the transverse component of the magnetization vector is measured; because the net transverse magnetization, M(t), precesses at the resonant Larmor frequency, ω, after the RF pulse, this causes the magnetic flux density to change over time in the receiver coil. For any given receiver coil, the size of the induced electromotive force will be proportional to both M(t) and ω. Both of these parameters increase linearly with magnetic field strength (B).

2.2.2.2 Generating and measuring the MR signal

A coil, in general, is an electrical device composed of multiple loops of wire that can either generate a magnetic field (gradient coil) or detect a changing (oscillating) magnetic field as an electric current induced in the wire (an RF coil). RF excitation is applied through transmitter coils and MR signals are measured through receiver coils. In most cases the same coil is used to both transmit and receive information. A gradient coil allows one to modify the strength of the external magnetic field in order to precisely determine a point in space, termed spatial encoding. This will be expanded on below, but briefly a slice-select gradient, a phase-encoding gradient and a frequency encoding gradient allows for determining spatial information in the z, y and x directions, respectively.

The purpose of an RF pulse is to flip the longitudinal magnetization induced by the static magnetic field. This is accomplished by causing the protons to precess *in phase* about the axis of the external magnetic field as well as causing them to precess about the axis of the induced RF field. The result is a spiral motion of spins toward the x-y plane; the flip angle is a function of the RF strength (B_1) and its duration and could be 180°, 90° or a fraction thereof.

After delivery of the RF excitation pulse, the entire spin system is in a relatively high-energy state, with more high-energy spins than were present at baseline. In a natural propensity to restore thermal equilibrium, the high-energy spins revert back to the low-energy state, releasing the same amount of energy as it took to become excited in the first place. In doing so, this decreases the transverse magnetization and restores the longitudinal magnetization, recalling that T_1 and T_2 relaxation occur by different phenomena. This process is referred to as decay of the MR signal or relaxation. Due to the fact that different tissues have different relaxation properties, one is able to distinguish tissue types. Alternatively, one can measure the same tissue over time, termed functional imaging.

The recovery of longitudinal magnetization is called T_1 relaxation, or spin-lattice relaxation, as the electromagnetic energy is converted into thermal energy and ultimately dissipated as heat in the surrounding tissue lattice. At the same time, the net transverse magnetization decays as individual spins become out of phase with each other. Due to the fact that each spin has a small magnetic moment and individual spins within the system interact with one another, spin-spin interactions cause some to precess slightly faster and some slightly slower than others. The net effect of these spin-spin interactions over time is that they begin to precess out of phase, which cancels out the net transverse magnetization, this is termed T_2 relaxation. Recovery of magnetization along the z-axis (longitudinal magnetization) and the decay of magnetization within the x-y plane (transverse magnetization) are two independent processes occurring at two different rates. T_2 decay occurs 5-10 times more rapidly than T_1 recovery.

Since the precession frequency of each spin is determined by local magnetic field strength, spin de-phasing can also occur from spatially dependent magnetic field inhomogeneities. The combined effects of spin-spin interactions and local field inhomogeneities, collectively referred to as T_2* relaxation, produce a greater and more rapid loss of phase coherence than T_2 relaxation

alone. T_2* weighted signals are widely used in functional imaging as will be further discussed if following sections.

Different tissue types have unique relaxation properties that depend on how fast longitudinal magnetization is regained through spin-lattice interactions and how fast phase coherence is lost through spin-spin interactions and field inhomogeneities. Tissue specific relaxation times are illustrated in Table 2-4. Measuring the MR signal during the relaxation period (after the RF pulse but before all of the signal is gone) provides image contrast because different amounts of signal will be measured from each tissue. By changing image parameters, images can be weighted to reflect one type of relaxation more than another. In doing so, images are said to be T_1-weighted or T_2-weighted.

Table 2-4 Approximate T_1 and T_2 relaxation times for central nervous system tissue at 3T.

Tissue type (frontal lobe)	**T1 (ms)**	**T2 (ms)**
Gray matter	1209	88
White matter	699	69
CSF	4300	1442

A forth type of contrast (other than T_1, T_2 and T_2*) is called proton density or PD-weighting. This results from acquiring images quickly after each widely spaced RF pulse. By allowing the longitudinal relaxation to fully recover while at the same time not allowing very much transverse magnetization decay, the images indicate the relative water concentration in different tissue types.

The time interval between RF pulses is called the repetition time, TR. The amount of time between the RF pulse and the MR signal measurement is called the echo time (TE). The TE affects the amount of net transverse magnetization in the following way: if the signal is measured quickly and the spins have little or no time to dephase then the transverse magnetization will be maximal. However, if the signal is measured at a longer echo time such that the transverse magnetization is out of phase, the signal is said to be T_2 or T_2* weighted depending on whether

or not local field inhomogeneities are accounted for (discussed further below; briefly this is done by using spin-echo or gradient-echo pulse sequences). Tissue contrast is achieved by optimizing T_1 and T_2 weighting. A long TR reduces the T_1 effect and a short TE reduces the T_2 effect (the opposite is also true).

The T_2 characteristics of a tissue are determined by the rate at which protons contained within that tissue dephase: dephasing rapidly equates with a short T_2 (dark on image), dephasing slowly equates with a longer T_2 (bright on image). For example the T_2 of water is long compared to the T_2 of fat or other proteinaceous material; this is because spin-spin interactions among the hydrogen protons of water is minimal which results in dephasing occurring at a much slower rate than fat tissue where the molecular structure is such that dephasing occurs more rapidly. Solid tissues dephase even more rapidly than fatty tissues and therefore have a shorter T_2.

The T_1 characteristics of a tissue are determined by the rate at which protons are able to give off their energy to the surrounding lattice. For water, the energy transfer is not efficient resulting in a long T_1. Solids have a very short T_1. Both the Larmor frequency and the natural motional frequencies of protons in water is much greater than the difference between the Larmor frequency and the motional frequencies of hydrogen protons in solid tissue resulting in a longer T_1 for water. The macromolecular structure of proteinaceous tissues allows for the natural motional frequencies of the surrounding water molecules to get closer to the Larmor frequency, thus yielding a more efficient energy transfer. Thus, proteinaceuos substances have a short T_1 and are brighter than water on T_1 weighted images.

By adjusting the TR and TE one can optimize the T_1 or T_2 weighted characteristics. By choosing a short TR and a short TE the acquisition is T_1 weighted. A long TR with a short TE results in a proton density weighted image. A long TR and a long TE yields a T_2 weighted image.

2.2.2.3 Spatial encoding and generation of an MR image

Capturing small current fluctuations in the receiver coil is only the starting point of reconstructing an image that reflects human anatomy. The challenge with image reconstruction is knowing what signal came from what three dimensional point in the body. To do this, one magnetic field gradient is required in each of the x, y and z directions to obtain spatial information. As mentioned above these are referred to as the slice-select gradient, the frequency

encoding gradient and the phase encoding gradient, respectively. In choosing the slice, recall that spins can only be exited with RF pulses oscillating at the same frequency. Altering either the bandwidth of the transmitted RF pulse or the slope of the gradient can vary the slice thickness. For example, the slice thickness can be decreased by either decreasing the bandwidth of the RF pulse or increasing the slice-select gradient. This will spatially encode the resonant frequencies of the spins where the RF energy necessary to produce transverse magnetization is absorbed and therefore produces an MR signal. Determining the remaining two-dimensional values within a given slice is accomplished by using two additional gradients: a frequency encoding and a phase encoding gradient. The frequency encoding gradient is the same strength for each echo and is applied during the reception of the echo altering the Larmor frequency along the x-axis. This provides specific information along the x-axis. The phase encoding gradient is applied in increments between the RF pulse and each echo, introducing a phase shift and provides spatial information along the y direction. By taking many measurements of the MR signal within each slice (across many frequency and phase encoding steps), the resulting data matrix, called 'k-space', contains many discretely sampled signals. By convention, each row of k-space (termed the k_x direction) spans the full range of the frequency encoding direction (-x to x) while each column of k-space (termed the k_y direction) spans the full range of the phase encoding direction (-y to y) so that the central point of k-space has neither frequency nor phase encoding information.

There are two fundamentally different kinds of pulse sequences, each with their own set of advantages and disadvantages, which can be used to acquire k-space. These are called spin-echoes (SE) or gradient-echoes (GE). Recall that the echo time (TE) for the image is defined as the amount of time between the RF excitation pulse and the largest signal echo, which always occurs at the central point in k-space. Since each image would take longer to acquire if only one row (phase-encoding step) were acquired per RF pulse, SE and GE methods have been developed to allow multiple phase-encoding lines of k-space to be acquired from a single RF pulse. This has been termed 'single shot' methods, and it is now common to use such techniques to fill all of k-space with only one RF excitation.

Following the initial excitation pulse, spin echo methods use a series of 180° RF pulses to flip the longitudinal magnetization and reverse the phase of each spin's precession. Therefore, T_1 and T_2 relaxation will occur normally but the dephasing effects of consistent magnetic field

inhomogeneities (T_2* relaxation) will be cancelled out at the center of the echo. This results in higher a signal-to-noise ratio (SNR) and better image quality close to air-tissue and bone-tissue interfaces but can take longer to acquire and lead to high doses of electromagnetic radiation being deposited in tissues relative to GE methods. Unlike SE parameters, GE pulse sequences do not use 180° RF pulses. Instead, as their name implies, they rely solely on magnetic field gradients to traverse k-space after the initial RF excitation pulse. The lack of 180° RF pulses allows spin dephasing from field inhomogeneities to accumulate, causing T_2* instead of T_2 weighting and poor image quality close to air-tissue and bone-tissue interfaces. A GE sequence also allows images to be acquired very quickly and with much lower doses of RF energy relative to SE methods.

K-space contains all of the raw MR signals with different amounts of phase- and frequency-encoding. To convert this data into a spatially encoded image, a two-dimensional Fourier transform is carried out. Due to the fact that each point in k-space is actually a spatial frequency component of the whole image, every point in k-space encodes information about the entire image. Data points close to the center of k-space encode the lower spatial frequencies such as gross anatomical features and image contrast while the outer points encode higher spatial frequencies such as edges and fine details. The central point in k-space, acquired at TE, encodes the global signal intensity of the entire image. Along this line of reasoning, reconstructing images from smaller portions of k-space does not result in a smaller field-of-view (FOV). This is due to the fact that there is an inverse relationship between k-space and image space in terms of the sampling density (also termed spatial resolution) and FOV. Increasing the sampling density in k-space produces images with larger FOVs whereas increasing the sampling range of k-space leads to higher image resolution. One last important point about k-space deserves mentioning: in addition to filling k-space line-by-line in a left to right and top to bottom trajectory, data can be acquired with different k-space trajectories. These are encoded using different combinations of gradients than with the traditional spatial encoding as used in SE or GE pulse sequences. Therefore, to accurately describe a pulse sequence, it must be designated as SE or GE and the k-space trajectory must be specified. For example, echo-planar imaging (EPI) has become one of the most popular ways to fill k-space. EPI uses a serpentine pattern with both high efficiency and speed to fill k-space; therefore pulse sequences could be designated as SE-EPI or GE-EPI to differentiate them from traditional k-space sampling methods.

2.2.2.4 Functional imaging

How signal intensity changes over time within a specific tissue (ie., adding the fourth dimension of time) allows one to use MR imaging to measure signal fluctuations that are related to metabolic and hemodynamic changes and is termed functional magnetic resonance imaging (fMRI). Compared to other functional neuroimaging methods such as positron emission tomography (PET), electroencepalography (EEG) or magnetoencephalography (MEG), fMRI is the only method that allows function to be mapped non-invasively throughout the entire central nervous system. However, each modality has its advantages and disadvantages that should be considered within the context of the scientific question at hand. fMRI signal results from bulk changes to CNS tissue associated with neurometabolic and blood flow events that are often related to underlying neuronal activity. The concepts associated with neurovascular coupling and functional hyperemia are extensively discussed in section 2.5.3. Because the single spinal fMRI study contained within this thesis relies on the contrast mechanism termed 'signal enhancement by extravascular water protons' or SEEP, this is reviewed here followed by a general introduction in time-series fMRI data analysis and the general linear model, as utilized in the spinal fMRI study presented in Chapter 6.

The traditional fMRI contrast mechanism utilized in brain imaging is termed blood oxygen level-dependent (BOLD) contrast. The BOLD signal is usually captured with T_2*-weighted gradient-echo pulse sequences with echo-planar imaging readouts, although BOLD responses can also be measured with T_2-weighted spin-echo sequences but with approximately 3.5 times less sensitivity at a given TE and about 2 times less sensitivity at the optimal TEs for BOLD contrast.[112] However, T_2-weighted signal changes have been shown to deviate from the accepted BOLD model where two important concepts have been demonstrated: 1) there is little-to-no signal reduction in spinal cord fMRI between GE and SE methods and 2) at very short echo times, there is a reduced dependence of the BOLD signal on TE.[113-115] These two findings led to the proposal of a second, non-BOLD component of endogenous neurovascular coupling / functional hyperemia response that is based on regional changes in proton density. The effect was termed 'signal enhancement of extravascular protons' (SEEP) and has been attributed to increased tissue water content in regions of neuronal activity.[115,116] The ability to utilize PD-weighted, spin echo imaging sequences rather than gradient echo sequences has a number of advantages for imaging the spinal cord. First, the SEEP signal is largely independent of field

strength such that imaging can be conducted at both lower field strength (0.2 T – 1.5 T) and higher field strength (3.0 T and higher). Second, because proton-density changes can be detected with spin echo sequences, image artifacts can be drastically reduced (relative to gradient echo imaging) in regions of air-tissue and bone-tissue interfaces, both of which are abundant around the spinal cord. Thus, the SEEP contrast mechanism offers significant advantages when imaging the spinal cord where BOLD imaging is often not possible due to magnetic susceptibility artifacts and is even more limited in the presence of titanium implants, a fact that is increasingly common in SCI patients treated for spinal instability. Nonetheless, the SEEP contrast mechanism has not gained widespread acceptance in the neuroimaging community. The evidence for and against these approaches is outlined in a recent review paper, although the contents of this narrative review do reflect the bias of the authors toward SEEP-based imaging.[117]

After collecting a time-series of images, fMRI data is subjected to a rigorous pipeline of data analysis techniques to generate a statistical parametric map (SPM): a probability map that shows regions of temporally correlated signal changes that are related to the task or stimulation paradigm. This is usually achieved by performing a voxel-wise general linear model (GLM) analysis to estimate the coefficients or beta-values (β_x) of various model parameters or 'basis functions' (p_x) of the anticipated signal change, as well as the residual error of the entire basis set. Mathematically, this takes the form of $\Delta S = \beta_1 p_1 + \beta_2 p_2 + \beta_3 p_3 + \ldots + \beta_n p_n + \text{error}$; where ΔS is the measured signal and β_x are the maximum likelihood estimates of each corresponding model parameter, p_x. Model parameters include the task paradigm and other modeled confounds such as scanner drift or other linear trends such as cardiac activity. Including such modeled confounds can reduce the error estimates considerably. Once the beta-values and the error estimates have been determined for each voxel, the probability that the measured signal corresponds to the task paradigm can be calculated by comparing the modeled component of interest to the residual error. This is done by dividing the estimated response magnitude (β_1) in each voxel by the estimated standard error of the mean (SEM) to give a t-statistic. The SPM is then displayed by building a t-map of the fMRI data and plotting the areas that exceed a certain user defined statistical threshold.

2.2.2.5 Spinal fMRI

This section explores several pertinent issues relevent to the application of spinal fMRI to investigate the human spinal cord; these include a review of the BOLD vs SEEP hemodynamic response function, motion artefacts and the use of a connectivty analysis for data interpretation.

2.2.2.5.1 BOLD vs SEEP response function in the human cervical spinal cord

There is a significant body of literature examining the BOLD hemodynamic response function and it has become well accepted that both the magnitude and time course of BOLD signals vary across individual subjects (for reasons such as age, differences in vascular anatomy including arteriole supply, capillary perfusion and venous drainage, blood hematocrit or the presence of vasoactive substances such as caffeine or alcohol)[118-123] and across brain regions.[124,125]

T_2*-weighted BOLD fMRI responses have been characterized in the human cervical spinal cord during blocks of a bulb-squeezing motor task.[126] Using a deconvolution approach, the optimal BOLD response in the spinal cord was estimated to have time-to-peak (TTP) of 9 seconds and a full-width at half-maximum (FWHM) of 10.5 or 8 seconds, depending on whether the data were modeled with or without a post-stimulus undershoot respectively.[126] This data suggests that the time course of the BOLD signal in the human cervical spinal cord is slower and wider than is observed in the brain. Using a series of event-related spinal fMRI experiements with proton-density weighted imaging (as used in Chapter 5 of this thesis), the SEEP hemodynamic response function in response to afferent thermal stimulation was measured as a time-to-peak of 7 seconds and a full-width at half-maximum of 5 seconds.[127] Thus, the SEEP response in the spinal cord is faster and narrower compared to BOLD signal changes.

2.2.2.5.2 Motion artifacts

Motion of the human cervical spinal cord, as it pertains to advanced imaging studies, has been characterized in great detail, including the generation of motion correction strategies.[128] The magnitude of spinal cord motion has been found to vary considerably across subjects in both the anterior-posterior (AP) and right-left (RL) directions; some subjects have been found to have greater motion than others, consistent with canine studies.[129,130] Cervical spinal cord motion has been found to oscillate in a predictable manner relative to the cardiac cylce in both the AP and

RL directions as follows: 0.6 +/- 0.34 mm in the anterior-posterior direction and 0.17 +/- 0.09 mm in the right-left direction.[131] This study also suggests that magnitude of motion correltes with spinal curvature.

2.2.2.5.3 Connectivity analysis

Functional connectivity is, in general terms, defined as the temporal correlation between spatially remote neurophysiological events. This is expressed as a deviation from statistical independence across such events. Functional connectivity can refer to correlations across subjects, across different trials or time points. With the broad range of potential targets for a correlation analysis, the definition of functional connectivity can be confusing.[128] Functional connectivity in the resting state has taken on a meaning of its own.[132] Functional connectivity can also be applied to stimulus or task-based studies where inter-regional correlations can be linked to events that may be associated with the task such as underlying genetics or personality.[128] Inter-regional correlations have been applied in the setting of spinal cord injury whereby the number of inter-spinal connections (correlations between a seed region and other regions of the spinal cord; in this reference the seed region is the dorsal quadrant of the spinal segment of the dermatome stimulated) was associated with the underlying degree of injury (ASIA grade).[133]

Correlations of fMRI time series data between spatially distinct regions in the human brainstem and spinal cord can also be influenced by the fMRI data acquisition, pre-processing and processing steps. While a detailed review of each of these steps is beyond the scope of this work, a few of the most important concepts are highlighted here and other more in-depth references are listed.[128] Data acquisition can take the form of either a gradient echo, echo planar imaging (EPI) sequence (most commonly used for the brain), implying a reliance on the BOLD hemodynamic response function, a spin echo EPI sequence, implying a reliance on the BOLD effect or a regular spin echo sequence, implying the SEEP contrast mechanism.[128] It is important to recall that all imaging acquisition methods aim to capture the signal generated by a neurophysiological event. Advantages of the gradient echo EPI sequence include faster acquisition of the brainstem-spinal cord volume and high sensitivity to the BOLD contrast. However, they suffer from signal drop out and image distortions caused by susceptibility artifacts, which are particularly prominent in the spinal region due to the presence of multiple tissue structures with different magnetic susceptibilities (e.g., spinal cord, cerebrospinal fluid, bones, cartilaginous disks,

adipose tissue and muscles). Spin echo EPI sequences reduce signal drop-out while regular spin echo sequences reduce both drop out and distortions. Data pre-processing (identification of segmental spinal cord levels, motion correction, temporal filtering) and processing (statistical analysis) steps have the potential to greatly influence results.

Functional connectivity (FC) analyses utilize correlation to generate subject-specific functional connectivity maps.[128] The correlations are performed between regions, which can be either anatomically defined (regions of interest, ROI), or functionally defined using parcellation methods (e.g., k-means clustering, independent component analysis). These FC maps can then be subjected to second level analysis using univariate statistics to compare features of the map between disease states. Null hypothesis testing is used to determine which features of the map might be different between healthy individuals and those with neurological impairment. This type of analysis was used in Chapter 5 of this thesis to study differences in the spinal cord processing of thermal heat in healthy controls and chronic cervical SCI.[133] Specifically, it was demonstrated that chronic, incomplete SCI patients process thermal sensory information differently than healthy controls and that such differences in spinal cord functioning persist in patients who fully recover from their injury. To the best of our knowledge, this is the first evidence of spinal cord plasticity obtained with spinal fMRI techniques; the pertinent findings are summarized in Figure 5-5.

Two shortcomings of utilizing a second level analysis of functional connectivity data include 1) the notion that secondary univariate analysis ignore spatially distributed patterns of functional connectivity and 2) while null hypothesis testing may be used to categorize results, it does not provide a means for evaluating the predictive power of the results.

2.2.3 MRI evaluation of the cervical spine

Traumatic injury to the cervical spine can be theoretically divided into injury to supporting structures (bony spinal column including ligament damage) and that of neural elements. MRI is essential for investigating the ligamentous and neural element involvement. Given the clinical suspicion for such injuries, MRI should be performed as soon as possible following the traumatic event, preferably within hours of injury.

A typical traumatic spine MRI protocol is built around a standard weighted screening protocol

that includes sagittal T_1 and T_2 weighted images supplemented by an axial T_2 weighted sequence. This basic protocol is effective in assessing roughly 90% of all spinal injuries. It however lacks the necessary sensitivity for visualization of edema patterns associated with ligamentous injury and with fractures, particularly those that involve vertebral bodies. An additional T_2 weighted sagittal sequence is therefore added with the ability to eliminate the high signal from marrow fat and subcutaneous fat. With this fat signal removed, injured ligaments and edematous bone marrow becomes obvious. These fat suppressed images can be obtained using frequency selective saturation added to conventional T_2 weighted spin echo images. A limitation however occurs when the magnetic field generated by the magnet or by surface coils varies across the anatomical region of interest leading to off-resonance effects that make fat saturation ineffective. This is usually caused by improper coil selection or availability, or by neck stabilization appliances containing metal. The solution is to employ a short inversion time spin echo sequence with the inversion time selected to null fat signal. The only drawback of this "STIR" sequence is the possibility of elimination signal for methemoglobin in a hematoma. This occurs if the T_1 relaxation of the blood matches that of the fatty tissue. This loss of specificity can be regained through application of a gradient echo sequence sensitive to tissue iron. If marked signal loss in a fluid collection is observed, the presence of blood products in confirmed. This can also be very effective in detecting hemorrhage within the spinal cord itself. Finally, all acute trauma imaging in MRI should be monitored while the patient is within the MRI system. This offers the opportunity to eliminate ambiguities in diagnosis by adding addition sequences to reduce or eliminate diagnostic dilemmas for optimizing acute patient management.

Perhaps the greatest value of MRI in the acute setting of spinal cord injury is to identify potentially reversible causes of neurological impairment. These include extra-dural compressive forces such as disc herniation and epidural hematoma that would be amenable to surgical intervention. MRI signal abnormalities within the spinal cord can provide indications of prognosis. Each of these considerations will be expanded upon below. MRI also plays a valuable role in the examination of patients with pre-existing conditions such as rheumatoid arthritis or ankylosing spondylitis.

Extramedullary injuries on MRI

As mentioned previously, traumatic insults to the spinal ligaments or cervical discs are evident

by bright T_2 signal changes. While such injuries are more easily identified on MRI in comparison to x-ray or CT one must exert some caution as the specificity is relatively low. In fact, one study identified only 8 of 14 surgically proven ligamentous disruptions.[128] One must examine carefully for each of the anterior and posterior longitudinal ligaments, the interspinous ligament, the ligamentum nuchae, the ligamentum flavum, and the ligaments at the craniocervical junction: the tectorial membrane, the transverse ligament and the alar ligaments. Any disruption should then be correlated with bony imaging on CT to ensure that an occult fracture was not overlooked. Furthermore, bone edema (visualized on MRI) is an indicator of a fracture and this location should also be correlated with CT.

Intramedullary signal change on MRI

Several authors have carried out post-mortem analysis comparing intramedullary signal changes with gross and histopathological analysis[128] associating imaging findings with hemorrhage, edema, cavitation and transection. The standard MRI evolution of a hematoma is described in Table 2-5. It is often the case that hematomas in the spinal cord are not homogeneous and have mixed T_1 and T_2 signal changes. As discussed previously, special iron sequences can help with regard to such mixed signal. Intramedullary signal characteristics provide valuable information to the clinician as they not only explain neurological deficit (in the absence of extramedullary compressive lesions) but also offer information with regard to prognosis (this topic will be expanded upon below).

Table 2-5 T_1 and T_2 signal characteristics of the standard evolution of a hematoma.

Standard Evolution of a Hematoma		
	T1	T2
Acute (hours) (De-oxy Hb)	Dark – iso intense	Bright
Subacute (days) (Met Hg)	Bright	Dark if RBC intact Bright if RBC lysed
Chronic (weeks) (fluid filled cavity)	Dark	Bright

2.2.3.1 Quantitative measurements in SCI

As the use of both CT and MRI became more common in the evaluation of SCI, in the clinical and research setting, a quantitative means of evaluating and reporting spinal canal compromise and spinal cord compression was required. Fehlings *et al* approached this problem with a multi-center study and established the following criteria.[128]

Maximal Spinal Canal Compromise (MCC)

Using mid-sagittal CT reconstructions (or MRI images) and the respective axial slices, one should identify the level of maximum spinal canal compromise and compare this with the normal canal diameter at the mid-vertebral body level above and below the lesion. This is quantified using the formula shown in Figure 2-3 where D_i is the anteroposterior canal diameter at the level of maximum injury, D_a is the anteroposterior canal diameter at the nearest normal level above the level of injury, and D_b is the anteroposterior canal diameter at the nearest normal level below the level of injury.

$$\text{Maximum canal compromise (\%)} = \left(1 - \frac{D_i}{(D_a + D_b)/2}\right) \times 100\%$$

Figure 2-3. Mid-sagittal T2 MRI and equation outlining the calculation for Maximal Canal Compromise (MCC). D_i is the anteroposterior canal diameter at the level of maximum injury, D_a is the anteroposterior canal diameter at the nearest normal level above the level of injury, and D_b is the anteroposterior canal diameter at the nearest normal level below the level of injury. Reproduced with permission from: **D.W. Cadotte,** D. Mikulis and M.G. Fehlings. Imaging of the injured Cervical Spine and Spinal Cord. In: The Cervical Spine 5th edition, edited by Dr. Edward C. Benzel. Lippincott Williams and Wilkins. August 29, 2012. ISBN-10 1605477524 | ISBN-13: 978-1605477527.

Maximal Spinal Cord Compression (MSCC)

The anteroposterior cord diameter on midsagittal and axial T_2 MRI images at the level of maximum compression should be compared with the anteroposterior cord diameter at the normal levels immediately above and below the level of injury. If cord edema is present, measurements of normal anteroposterior cord diameter should be made at midvertebral body levels just beyond the rostral and caudal extent of the cord edema at the levels where the cord appears normal. These values are quantified using the formula depicted in Figure 2-4 where d_i is the anteroposterior cord diameter at the level of maximum injury, d_a is the anteroposterior cord diameter at the nearest normal level above the level of injury, and d_b is the anteroposterior cord diameter at the nearest normal level below the level of injury.

$$\text{Maximum cord compression (\%)} = \left(1 - \frac{d_i}{(d_a + d_b)/2}\right) \times 100\%$$

Figure 2-4. Mid-sagittal T2 MRI and equation outlining the calculation for the Maximum Spinal Cord Compression (MSCC). Where d_i is the anteroposterior cord diameter at the level of maximum injury, d_a is the anteroposterior cord diameter at the nearest normal level above the level of injury, and d_b is the anteroposterior cord diameter at the nearest normal level below the level of injury. Reproduced with permission from: **D.W. Cadotte,** D. Mikulis and M.G. Fehlings. Imaging of the injured Cervical Spine and Spinal Cord. In: The Cervical Spine 5th edition, edited by Dr. Edward C. Benzel. Lippincott Williams and Wilkins. August 29, 2012. ISBN-10 1605477524 | ISBN-13: 978-1605477527.

2.3 Imaging biomarkers

2.3.1 Characteristics of an Imaging Biomarker

Many clinicians and researchers have attempted to utilize MRI as a tool to capture metrics that serve as a biomarker to better categorize SCI patients and, in turn, hope to use this refined categorization to offer better prognostic information to patients. The success of this strategy using T_1 and T_2 weighted images is the focus of chapter 4 of this thesis. Chapter 5 and 6 of this thesis are aimed at improving the metrics captured with MRI: chapter 5 aims to study a specific functional pathway of the spinal cord and document metrics to describe how this pathway changes after traumatic injury and chapter 6 aims to improve the spatial specificity of interpreting data acquired from the human spinal cord. The overarching theme of biomarkers is described here.

The United States Federal Drug Administration has recognized the potential for surrogate end-points to aid in the development of treatment strategies for various disease states. Specifically, they have defined surrogate end-points as a potentially valuable tool in both pre-clinical and clinical trials as follows: "A laboratory measurement or physical sign used as a substitute for a clinically meaningful end-point that measures directly how a patient feels, functions, or survives. Changes induced by a therapy on a surrogate end point are expected to reflect changes on a clinically meaningful end-point".[134] Specific to the use of advanced imaging methods, an 'imaging biomarker' has been defined as "any anatomic, physiologic, biochemical, or molecular parameter detectable with one or more imaging methods used to help establish the presence and / or severity of a disease".[135] Imaging biomarkers can be applied at any point along the continuum of developing novel strategies to improve patient outcomes in a particular disease state. For example, biomarkers may allow for early safety and proof-of-concept determinations and perhaps even reduce the number of animals in pre-clinical trials. Alternatively, biomarkers could be used to identify promising novel treatment strategies more quickly or, on the other hand, demonstrate that certain strategies hold no promise. The use of imaging biomarkers provides a unique ability to validate in humans the results identified in successful animal models whereby important questions such as dose effectiveness and potential mechanisms of action can be

studied. Biomarkers may allow for a single patient to serve as his or her own control, addressing both technical and ethical concerns around the use of blinded, randomized clinical trials. Specific examples of such a strategy have been proposed for ischemic stroke research using both perfusion and diffusion MRI based biomarkers and more recently in spinal cord injury with the use of MRI based anatomical measurements.[128]

Imaging biomarkers, whether used in pre-clinical or clinical decision-making must be appropriately validated as surrogate outcome measures. A number of criteria have been put forth to establish such validation: the presence of an imaging biomarker should be closely linked to the disease or condition under investigation; the detection and or quantitative measurement of the imaging biomarker should be accurate, reproducible and feasible over time; the measured changes over time in the imaging biomarker are closely coupled or linked to the success or failure of the therapeutic intervention under study.[128] While such a validation strategy is paramount before imaging biomarkers gain widespread acceptance for use in clinical research, a great deal of investigation must go into studying what imaging metrics may be useful as surrogate end points and well as when and where they should be applied.

Visualizing the CNS in the context of SCI affords the potential opportunity to 1) categorize patients in order to more accurately define the extent of injury and 2) follow sub-clinical changes in CNS structure or function. Imaging biomarkers offer the opportunity to improve on current categorization schemes by refining the diagnosis of such patients to include various structural or functional imaging metrics. For example, while current ASIA standards rely on the subjective clinical examination to document motor and sensory function, an imaging categorization might include the degree of spinal cord atrophy, the degree of demyelination or the presence of a functional imaging signature of a specific functional circuit. By refining the categorization scheme in this way, it will be possible to create more homogeneous treatment groups for study within the context of a clinical trial and, by doing so, improving the efficiency and reducing the number of patients required to achieve statistically meaningful comparisons. Before imaging metrics will be able to fulfill this role in the management of SCI patients, one must appreciate the historical context of this initiative (chapter 4), how the anatomy of the spinal cord varies across individuals (chapter 5) and what metrics might be used to evaluate the integrity of specific functional circuits (chapter 6). There are many other aspects of imaging biomarkers that are very promising that are not included in this thesis, such as structural imaging that might examine for

spinal cord atrophy or other advanced techniques that might examine for the integrity of white matter pathology of the spinal cord including diffusion imaging or magnetization transfer imaging.

2.3.2 The role of imaging biomarkers in clinical trials

Current pre-clinical investigations tend to focus on one of three broad treatment strategies: neuro-protection, neuro-regeneration and bioengineering strategies.[128] Each of the therapies developed and tested in pre-clinical animal models has potential for translation into a human clinical trial. However, given the relatively low incidence of traumatic spinal cord injury and the necessity of coordinating large trials over multiple centers, the bar for pre-clinical evidence of efficacy is set high. When a promising therapeutic strategy is identified, a number of aspects of each of the therapeutic intervention, the clinical management of SCI patients and various aspects of clinical trial design must be carefully considered for proper evaluation.

The goal of any clinical trial is to distinguish a treatment effect from the natural history of SCI. The natural history of traumatic spinal cord injury is difficult to appreciate for two reasons: 1) the nature of primary injury across individual people is diverse; 2) the individual responses to injury, referred to as secondary mechanisms of spinal cord injury, are heterogeneous. Nonetheless, previously clinical trials have provided insight into how people recover after injury and how this should be considered when conducting future clinical trials.[2]

Outcome is typically assessed in one of two ways: neurological scoring or functional scoring. Neurological scoring typically makes use of the American Spinal Injury Association (ASIA) scoring system (as described in section 2.1.1) and the extension of this, the ASIA Impairment Scale (also outlined in section 2.1.1). Very similar older scoring systems also exist but will not be reviewed here. These scoring systems capture the following information: the segmental level of the injury (defined as the lowest neurologically functional spinal segment) and motor / sensory capabilities of spinal segments. Neurological scoring systems capture information about the underlying capacity of the spinal cord to perform specific muscle actions, such as contraction of the biceps muscle or perceived sensation in a particular dermatome. Functional assessments on the other hand, capture information about how a patient uses the underlying neurological capacity to perform meaningful activities in their life. Neurological outcomes tend to be primary outcome measures in clinical trials. This is especially the case for both phase 1 and phase 2 trials

that focus on safety and efficacy, respectively. Phase 3 trials are generally designed to confirm efficacy and should incorporate functional outcome measures, as this is ultimately what improves the lives of patients – the ability to perform activities of daily living and integrate meaningfully with society.

In general, patients with sensorimotor loss will achieve some neurological recovery, especially if they have retained some neurological function below the level of their injury. The zone of partial preservation (ZPP) refers to myotomes and dermatomes below the neurological level that retain partial motor or sensory function. The farther one is from the time of injury, the more accurate predictions become with regard to outcome. Understanding the nuances of this natural history is important to the design of clinical trials. The closer to the time of injury that one attempts to study the intervention of a particular therapeutic option, the larger the number of patients that are required. In patients with motor complete lesions (AIS A and B) one can usually expect partial recovery within the ZPP. It has also been observed that motor recovery is more likely to occur if sensation is preserved in that segment. The vast majority of recovery occurs within the first three months after injury but can continue for up to 18 months and rarely longer. Sensory recovery can occur after SCI and typically follows the same time course as motor recovery. Recovery in motor incomplete patients (AIS C and D) is both more substantial and highly variable. This fact implies that if a therapeutic trial targets incomplete SCI patients in the acute stage of injury, higher patient numbers will be required.

This brief introduction into clinical trials and the natural history of recovery after spinal cord injury highlights two important points: 1) defining specific inclusion and exclusion criteria are important considerations that impact the size of the trial and 2) outcome measures can reflect both neurological capacity and functional abilities and are usually established based on the goal(s) of the trial. A number of important advances in the treatment of spinal cord injury have been made through the use of clinical trials; these will be discussed next as the results of these efforts have a direct impact of patient care and this knowledge is in keeping with the theme of chapter 2. Following this, an overview of how advanced imaging techniques may offer opportunities to improve the efficiency of clinical trials by refining current approaches to both inclusion / exclusion criteria and the development of specific outcome measures will be discussed.

2.4 Development and structural anatomy of the human cervical spine

2.4.1 Embryological development of the spinal cord and vertebral column

Development of the segmental structure of the human spinal cord has implications for characterizing anatomy across groups of individuals, as is commonly done in neuroimaging studies. Embryological development is an orderly process that can be described based on morphological, cytological or maturational criteria and is a direct result of a number of developmental pathways that include neurogenesis, neuronal migration, axonal growth, dendritic development, synaptogenesis, transmitter maturation and myelogenesis. Using the technique of ^{3}H thymidine autoradiography in rats, it has been well established that such developmental pathways are precisely timed and sequentially ordered.[136] While not possible to conduct invasive experiments in humans, the results of such experiments in animals can be used to interpret the progression of morphological, cytological and maturational developments that are analyzed post-mortem in catalogued human tissue, the largest collection of which resides at the National Museum of Health and Medicine, Armed Forces Institute of Pathology, Washington, DC.[137] While a detailed review of embryological development is beyond the scope of this thesis, several important aspects are relevant to advanced imaging techniques that include morphological and cytological characteristics. Specifically, this section will address two focused questions: 1) *What are the gross morphological features of the human spinal cord and how do these relate to the development of surrounding mesodermal elements?* And 2) *What is the cellular composition of the human spinal cord and how are these cells organized?* Each of these considerations will be reviewed concurrently along the time course of maturational development from the third gestational week (3.0 GW) to adult life. A number of texts have documented this literature including ([128]); when appropriate, primary research articles have been cited below.

Closure of the neural tube occurs during the third gestational week (7-10 somite stage), beginning in the cervical region and progressing both rostrally and caudally culminating in closure of the anterior neuropore first and then the posterior neuropore (lumbosacral spinal cord) by the 25-somite stage (roughly 3.5 gestational weeks, GW). This process results in the formation of the primitive spinal canal. After closure of the neural tube at approximately 3.5 GW, the spinal cord undergoes rapid growth, mainly due to proliferation of neuro-epithelial cells

(NEPs), through to the 7.0 GW stage, preceding development of the brain. During the first trimester (GW 3-14), the cylindrical shaped primordial spinal cord is described as having a roof plate and floor plate in the midline and lateral plates on both sides. These neuroepithelial plates first proliferate resulting in increased numbers of NEP's; the earliest post-mitotic cells to differentiate from the NEP's are the ventral motor neurons at approximately 4.5 GW. After the 5.5 GW time period, there is rapid growth of the spinal cord: the cylindrical spinal cord becomes pear-shaped due to the concomitant increase in ventral horn motor neurons and a decrease in the number of NEP cells in this region, now called the basal plate; the dorsal neuroepithelium matures considerably forming the alar plate. Rapid development continues throughout the first trimester with expansion of the ventral spinal cord occurring slightly earlier than the dorsal spinal cord; by the end of GW 14 the embryonic spinal canal lined by NEP's has transformed into the fetal central canal lined by ependymal cells and the central gray matter assumes its characteristic adult pattern of a dorsal, intermediate and ventral horn. Of particular note during the first trimester is the progressive segregation of motor columns in the ventral horn and the distribution of branches of the dorsal root primary afferents in relation to body growth and skeletal-muscular development. Motor neurons progressively segregate in the cervical spinal cord corresponding to the successive innervation of muscle groups in a proximal-to-distal fashion. For example, at GW 4-5-5.0 motor neurons form an amorphous mass in the ventral horn whose axons come into contact with the segmental myotome of the body. During GW 5.5-6.0, motor neurons begin to segregate into medial and lateral compartments whose axons innervate axial and limb muscles, respectively. This process continues such that the lateral group further divides into ventral, dorsal and retrodorsal tiers. Retrodorsal motor neurons further segregate into inferior and superior columns. By GW 12, the ventral motor neurons are segregated in a medial-lateral and ventral-dorsal fashion according to the somatic muscles they innervate. In a similar fashion, fibers from the dorsal root ganglion reach the spinal cord at approximately GW 5.0 in a segmental fashion. Entering dorsal root axons bifurcate into ascending and descending branches and later undergo successive branching within the spinal cord; this is refereed to as the dorsal root bifurcation zone. Subsequent to this, collateral fibers reach the ventral horn. Growth of long ascending branches, forming the cuneate and gracile fasciculi, occur by 8.5 and 10 GW respectively. Thus, the spinal cord is organized in a segmental fashion with reference to both motor and sensory function: motor neuron pools form in longitudinal columns that span many spinal cord segments and are arranged in a medial-lateral, dorsal-ventral fashion corresponding

to the muscles innervated (axial versus proximal versus distal limb muscles) whereas dorsal root afferents penetrate the spinal cord, branch in both ascending and descending directions and provide input to both local, segmental spinal circuits and ascending longitudinal fiber tracts. The length of the spinal cord matches that of the vertebral column up to GW 11 but by GW 14 the length of the spine exceeds that of the spinal cord. The greater growth rate of the bony vertebrae relative to the spinal cord continues until adolescence.

By the second trimester (after GW 14), the gray matter is well developed with neurons undergoing a maturation process. The white matter is thin at this time point and the concentration of glial cells is small but increases during this time period. Glial cells are distinguished from reactive glial cells whereby the latter are associated with increasing myelin concentration. During the second and third trimesters, the human spinal cord undergoes a gradual expansion of the white matter relative to the gray matter. Associated with expansion of the white matter is a progressive myelination of axons that occurs in three successive steps: 1) an increase in glial concentration, 2) an increase in the concentration of reactive glial cells and 3) myelination of the nerve fibers. Myelination of white matter begins in the collateralization zone of the dorsal root and in the future propriospinal tract – these two tracts contain nerve fibers that compose the segmental and inter-segmental reflex circuits of the spinal cord. Myelination then continues with other ascending circuits followed by some descending paleospinal axons such as the tectospinal tract (fibers responsible for coordinating head and eye movements) that go on to exert supraspinal control over the spinal cord. By birth, only 2 regions of the spinal cord remain unmyelinated: Lissauer's tract (which remains unmyelinated, and contains centrally projecting axons carrying discriminative pain and temperature information) and the lateral and ventral corticospinal tracts, that exert a higher-level, supraspinal control over the spinal cord. It is not until many months after birth that the corticospinal pathways become fully myelinated, a process that is associated with gradual control over the motor system beginning with the ability to hold one's head upright.

This short review of spinal cord embryological development is intended to draw 3 conclusions relevant to advanced imaging of the human spinal cord: 1) the growth rate of the spinal cord and spinal column are under different influences; the spinal cord reaches its full length by the end of the first trimester but the vertebral column continues to grow into adult life. As such, one must be cautious when drawing parallels between the spinal cord and spinal column such as to infer

the position of specific spinal cord segments. 2) The ventral spinal cord motor neurons innervate the axial and appendicular skeletal musculature in segmental fashion that is subdivided into specific motor columns. 3) The dorsal root afferent fibers penetrate the spinal cord in a segmental fashion and provide afferent input to both the dorsal horn (in both ascending and descending short segment fibers) and longitudinal tracts that ascend to the brainstem and higher centers in the brain.

2.4.2 Structural anatomy of the adult human cervical spinal cord

The spinal cord is the caudal continuation of the medulla oblongata and in the adult normally weighs 30-35g and is 42 to 45 cm long.[138] It is a long cylindrical structure with a segmental arrangement that corresponds to the body dermatomes and myotomes. It is surrounded by meninges and contained within the vertebral canal. The spinal cord terminates at the conus medullaris, typically positioned adjacent to the L1-L2 vertebral levels. The filum terminale, a fibrous band that continues from the conus medullaris to insert into the coccyx, anchors the distal portion of the spinal cord to its surrounding bony structure. The spinal cord has 31 pairs of spinal nerves: 8 cervical, 12 thoracic, 5 lumbar, 5 sacral and 1 coccygeal. Each of the spinal nerves traverse the respective inter-vertebral foramen and transition into rootlets prior to joining the spinal cord as dorsal or ventral root filaments. The cervical enlargement, the focus of this review, is approximately 13-14 mm in transverse and 9 mm in anterior-posterior diameter.[138] Detailed anatomy of the thoracic, lumbar and sacral spinal cord will not be further discussed but is outlined in detail in several anatomy texts.[138,139]

The cervical spinal cord has a number of surface architectural features: anterior surface – the anterior median fissure penetrates the spinal cord for a depth of approximately 3 mm and contains an epipial fold with sulcal branches of the anterior spinal artery and vein; posterior surface – the shallow posterior median sulcus that is continuous with a delicate glial partition – the posterior median septum that extends into the cord and reaches the deep-lying gray matter; Lateral surface – two sulci associated with spinal roots: the posterolateral sulcus (into which filaments of the dorsal root enter) and the anterolateral sulcus (emergence of ventral root fibers). Dorsal roots occur at more regular intervals and in greater number than ventral roots. The posterior intermediate sulcus sits between the posterior median and posterolateral sulci. The cervical enlargement spans C5-T2 and the corresponding nerve roots form the brachial plexus.[138]

The cervical segments are characterized by a relatively larger size compared to other segments of the spinal cord owing to the large amounts of white matter. In the lower cervical segments (C5 and below) the dorsal horns are enlarged and the ventral horns extend into the lateral funiculi owing to the large amount of sensory and motor information that is processed from the upper extremities.

In a configuration opposite to the cerebral cortex, the spinal cord consists of central gray matter in a butterfly shape surrounded by surface white matter that consists of ascending and descending myelinated axons. The central gray matter consists of cells arranged in columns, some of which span the entire length of the spinal cord and vary depending on the segmental level. Low-power visualization of Nissl-stained spinal cord transverse sections of the human spinal cord reveals a cytoarchitectural organization that is remarkable similar to that originally described in the cat; these characteristics are outlined in Table 2-6.[140] Recent studies also include a description of the dendro-architecture, both of which can be visualized in a series of outstanding figures contained within a text book edited by Paxinos and Mai, referenced here.[128]

Table 2-6 A comparison of Rexed's original laminar description of the cat spinal cord and cytoarchitectural features of human spinal cord tissue.

Rexed original description in cats	**Characteristics of the human spinal cord**
Lamina I (dorsal)	Marginal neurons cuffing the dorsal horn
Lamina II	Substantia gelatinosa of Rolando
Lamina III	Transition zone between lamina II and IV
Lamina IV	The region of large neurons in the center of the dorsal horn
Lamina V	Neurons located at the base of the dorsal horn (cannot be distinguished from lamina VI in humans)
Lamina VI	Neurons located at the base of the dorsal horn (cannot be distinguished from lamina V in humans)
Lamina VII	Central portion of gray matter
Lamina VIII	The group of neurons located medially in the ventral horn
Lamina IX	Columns of motor neurons in ventral horn
Lamina X	Neurons surrounding the central canal

2.5 Functional anatomy of the human spinal cord

Functional activation of the spinal cord, related to sensory stimulation or motor activity, results in specific spatial-temporal patterns of neuronal activity within the spinal gray matter. In broad terms, afferent sensory information is processed in the dorsal horn and efferent motor activity arises from higher cortical and subcortical centers to motor neurons in the ventral horn. When one considers a specific afferent stimulus, such as mechanical stimulation of the skin, the spatial-temporal pattern becomes more refined whereby neuronal activity is largely concentrated in lamina III - V of the spinal gray matter and the temporal course of activation is dependent on the intensity and duration of the stimulus. Underlying the temporal course of neuronal activity is a constant perfusion of blood that can be fine-tuned to a changing macro-environment, such as blood pressure or blood pH, or to changes in the micro-environment, such as increased metabolic requirements associated with a specific neuronal response. Stimulus specific hemodynamic response functions have not been characterized in the spinal cord but presumably a stimulus resulting in a greater degree of neuronal activity would require a requisite blood flow response greater than that of baseline flow or in response to a mild stimulus. The spinal cord hemodynamic response is the basis for the spinal fMRI signal, whereby a number of studies have reported either blood oxygen level dependent (BOLD) or signal enhancement by extracellular protons (SEEP) signal changes coinciding with specific stimulation paradigms.[141] Whether or not diverse stimulation paradigms abide by a universal hemodynamic response function is uncertain but this dictum has formed the foundation of all human spinal fMRI research to date.

Extensive spinal cord electrophysiology data exists to support the notion that different sensory stimuli yield differential spinal cord activation patterns. Generally speaking, the stimulus type, intensity, duration and inter-stimulus-interval each affect the degree of neuronal activity elicited in the spinal cord. From distal to proximal each of the sensory receptor, afferent fibers, synaptic termination in the dorsal horn and dorsal horn interneuron respond to a sensory stimulus. Underlying specific electrophysiology response patterns to either afferent or efferent information is how the spinal cord (and central nervous system in general) responds to meet increased metabolic needs associated with the transmission of synaptic signals and the restoration of ionic gradients. Thus, the functional spinal cord is a collective process involving both

electrophysiological activity and a response of the structural vascular network to meet increased metabolic requirements during specific patterns of activity. Each of these topics will be reviewed in the following subsections.

2.5.1 Processing of afferent information in the spinal cord

Processing of sensory information in the spinal cord can be considered along the flow of information from the peripheral to the central nervous system:

A. Stimulus-specific activation of receptors in the skin
B. Primary afferent fibers carrying information from sensory receptors
C. The response of dorsal horn interneurons to afferent stimulation
D. Ascending tract cells
E. Descending tract cells that modulate the activity of spinal cord circuits

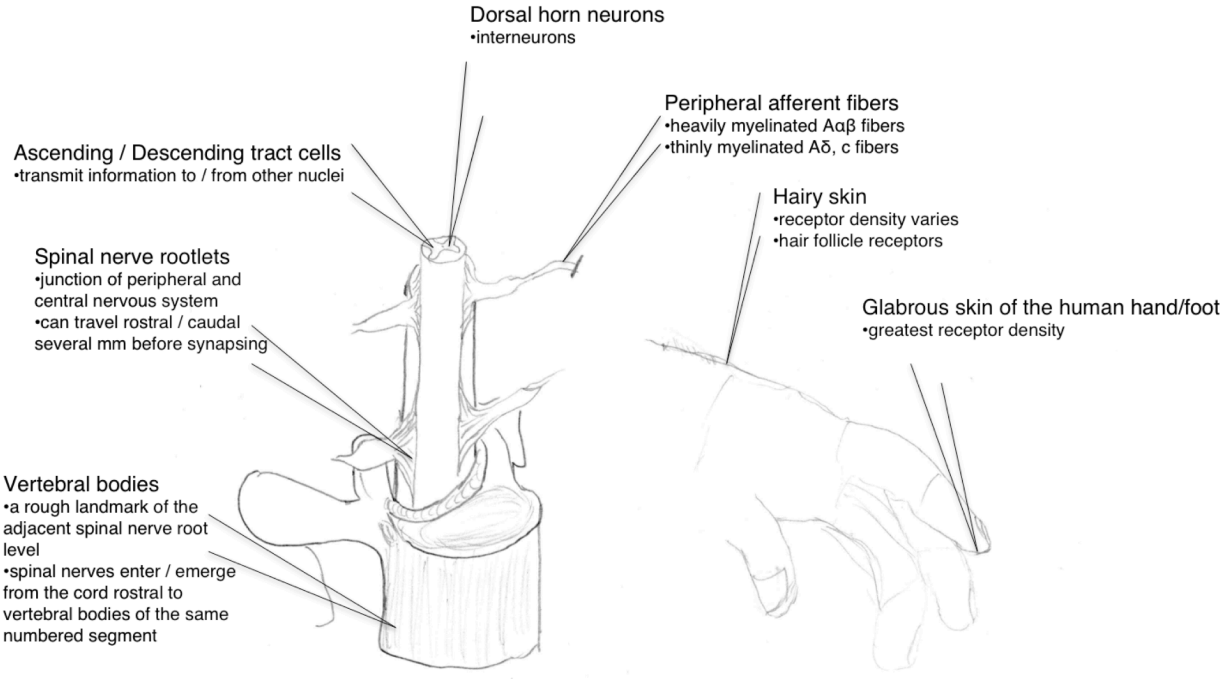

Figure 2-5. A diagrammatic representation of elements of the peripheral and spinal cord central nervous system that should be considered in the design of a spinal fMRI experiment. For example, receptor density of the human hand is considerably greater than receptor density of the proximal arm. (drawn by D. Cadotte for this thesis)

In the case of mechanical depression of the skin there is a relatively linear relationship between stimulus duration and electrophysiological activity, other sensory stimuli such as thermal heat result in unexpected electrophysiology characteristics and likely net metabolic activity; These emergent properties of the afferent fibers and spinal neurons are considered in detail below after a brief review of spinal cord neuronal composition and electrophysiology recording techniques.

2.5.1.1 Electrophysiological recording techniques and neuronal composition of the spinal cord

The relative composition of neuron type changes throughout the rostral-caudal and dorsal-ventral axis of the spinal cord, the most common neuron type, estimated to be as high as 97% at the S2 level in rats, is the propriospinal interneuron.[142] This is an important consideration when discussing electrophysiology recordings of the spinal cord, as it must be assumed that any extracellular or intracellular recording is from such an interneuron unless direct evidence is otherwise obtained; the exception would be if the location of the electrode is confirmed to be in lamina I or the ventral horn where interneuron populations are smaller. While the details of this characterization are beyond the scope of this work, several works are referenced that demonstrate features to distinguish interneurons from other neuron types.[128] While both intracellular and extracelluar recordings can be conducted *in vivo*, *in vitro* preparations provide the advantage of a lack of motion. In addition, the patch-clamp technique can be applied to spinal cord slice preparations and offer the ability to study excitatory and inhibitory postsynaptic currents.[128]

Extracellular, intracellular and whole-cell patch clamp recordings offer point-based measurements of individual neurons (or possibly many neighboring cells in the case of extracellular recordings) on a microsecond time scale. With carefully designed and executed experiments, these techniques are capable of recording the response of interneurons to peripheral nerve volleys. For example, Beall *et al* demonstrate that interneurons may respond with separate bursts of discharges to the Aβ and Aδ components of afferent input via electric stimulation of a peripheral nerve.[143] Provided sufficient stimulus strength, one may also be able to distinguish C fiber volleys that reach the spinal cord much later than either Aβ or Aδ volleys due to the differential degree of myelination of these peripheral fibers.[144]

Electrophysiological techniques can also be applied to study the population response of neurons, rather than point-based measurements as described above. This is accomplished by placing an electrode on the surface of the spinal cord or by placing a microelectrode within the spinal cord and these techniques are termed Cord Dorsum Potentials and Intraspinal Field Potentials respectively. Negative field potentials, recorded from within the dorsal horn, develop in the extracellular space due to a shift of cations into the dorsal horn interneurons that occur during excitatory postsynaptic potentials and action potentials. Extracellular potentials represent the summed activity of many neurons and the distribution of field potentials can be spatially mapped to specific cord regions depending on the input. For example, Aβ primary afferent fibres strongly excite interneurons in laminae IV and V and Aδ primary afferent fibres strongly excite interneurons in lamina I and V-VI.[143] Another important consideration is the magnitude of the field potential, which is a function of the number of interneurons activated and the distance between the activity and the recording electrode. For example, a volley in Group 1 muscle afferent fibers in cats results in only a small negative cord dorsum potential likely due to the fact that a muscle afferent volley excites fewer interneurons than a cutaneous sensory volley.[145] Along this line of reasoning, it has been demonstrated that cord dorsum and field potentials are largest when repetitive stimulation is used, in flexor muscles in particular, due to temporal summation.[146]

To summarize, it is important to remember that the majority of cellular activity in the spinal cord is a result of interneuronal processing of afferent signals. Electrophysiology recording techniques can provide information about individual cellular activity or population based activity, and in the case of the latter, cord dorsum and field potentials can provide information regarding the degree of neuronal activity in response to a particular input.

2.5.1.2 Mechanical stimulation of the skin

When designing an fMRI experiment to investigate the human spinal cord, one must consider both the neurophysiological consequences of a particular stimulus and the ease of delivering such as stimulus within the confines of the imaging environment. The sensation of touch and pressure represent a continuum of stimulus intensity much the same way flutter and vibration represent a continuum of stimulus frequency. The basis of each of these perceptions rests within mechanoreceptors with myelinated afferent fibers projecting to the spinal cord. The glabrous

skin of the human hand contains approximately 17 000 mechanoreceptors, half of which are slowly adapting (SA I and SA II) and half of which are fast adapting (FA I and FA II) receptors.[128] The hairy skin, in addition to slowly adapting (SA I and SA II) and fast adapting (FA I) receptors, also contains hair follicle receptors that respond to dynamic displacement of individual hairs.[147] Thus, by considering the structural components of mechanoreception, a properly designed stimulation paradigm should differentiate between the glabrous and hairy skin; the touch-pressure continuum should consider the area of skin displaced, the force of displacement, the duration of stimulus and the inter-stimulus interval. The flutter-vibration continuum should differentiate the frequency of stimulation (flutter: 5-40 Hz, vibration > 60 Hz), the duration, inter-stimulus interval and the area and force of skin displacement. Finally, brush stimulation of the hairy skin should be considered within the framework of area stimulated and stimulus duration. On a finer scale, one would consider the number of hairs displaced and by how much, but for the purposes of a spinal fMRI study, such considerations are not practical.

It is widely accepted that SAI receptors, and the corresponding Merkel cell complexes, are largely responsible for the sensation of touch-pressure and controversial whether or not SA II receptors also contribute.[148] Using microneurography techniques, it has been established that axons of SA I receptors in human glabrous skin have a conduction velocity of 58.7 +/- 2.3 m/s, an average receptive field size of 44.7 mm^2 (with a range of 2 – 451 mm^2), and an amplitude threshold of 0.51 mm (range 0.15 – 1.35 mm).[149] The receptive field sizes are reported to be smaller on the distal phalanx than on the palm. The sensation evoked by activity in a single SA I unit is that of pressure, and results in continuous firing of afferent fibers; the threshold for sensation occurs at a stimulation frequency of 3-10 Hz, the intensity of the pressure increases with stimulation frequency and the perceived intensity of pressure is a function of afferent fiber discharge rate.[150] It has been demonstrated that the density of SA I receptors in the glabrous skin of the human hand (in addition to that of FA I receptors) corresponds to the gradient of threshold for two-point discrimination[128] Thus, if one were to consider designing a spinal fMRI study and wanted to control for variations in receptor density or function, it would be prudent to use, for example, two-point discrimination or other quantitative sensory assessments as a control between individuals. For example, if one desired to test the sensitivity and specificity of spinal fMRI to detect mechanical stimulation of the skin in the C6 distribution of the glabrous skin of the dominant hand of healthy volunteers, using a 3 mm blunt Von Frey probe, one could control for

the density of peripheral receptors and their function by ensuring the candidate could perceive a two-point discrimination stimulus prior to the fMRI trial. The skin region could be marked and then tested in the MRI environment. In this way, an attempt has been made to account for possible confounding variables such as variations in the number of peripheral receptors or dysfunction of these receptors due to various clinical conditions.

Afferent fibers pertaining to touch-pressure sensation project to the dorsal horn and are distributed in a series of elliptical zones along the rostro-caudal spinal cord through laminae III, IV and the dorsal portion of lamina V.[151] Spinal cord neuron responses to touch-pressure stimulation consist of excitatory, inhibitory and combinations of these responses. It is likely that the response to afferent fiber input is closely tied to the receptor type rather than the peripheral fiber frequency pattern whereby a pressure stimulation (SA I afferent input) resulting in sustained afferent input is reproduced in the dorsal horn and stimulation of rapidly adapting receptors, for example by brushing the hairy skin and stimulating hair follicle receptors, is amplified during a portion of the sensory stimulus (dynamic movement of hair rather than maintaining individual hairs in different positions).[152] This distinction between peripheral afferent fiber spiking trains and spinal cord processing becomes even more amplified when thermal stimuli are considered, as will be discussed below.

The transmission of touch-pressure information occurs in both the dorsal columns and the dorsal lateral funiculus, and to a lesser extent in the spinothalamic tract.[153] Rostral projection of touch-pressure stimulation to the thalamus and cortex result in higher functions such as stereognosis and graphesthesia.

2.5.1.3 Warm thermal stimulation of the skin

As a prelude to the use of warm thermal sensation in a novel spinal fMRI study described in Chatper 5, the literature review presented here will provide key background and context. Other thermal sensations not elaborated on in this thesis include cold sensation and both hot and cold pain sensations.[128] Warm thermal sensation is perceived when skin temperature rises above the ambient range of 32-34°C and is kept below 45°C.[154] The perception threshold for thermal sensation depends on the rate of temperature change, the degree of change, the surface area affected and the original or adapting temperature.[155] A number of transient receptor potential (TRP) ion channels have been characterized whose activity depends on the temperature of their

environment.[128] A total of 28 different TRP receptors have been identified in humans that have been categorized into 6 families, 3 of which are thought to play a role in thermoception: the vanilloid TRP channel (TRPV), the melastatin or long TRP channel (TRPM) and the ankyrin transmembrane protein channel (TRPA).[156] Each ion channel has been found to operate over a specific temperature range, providing a molecular basis for thermosensation. These specialized warm thermal receptors are embedded in the terminals of afferent fibers (mostly C fibers in the case of warm sensation, but also possibly include A-delta fibers), which end as free nerve endings just beneath the surface of the skin.[157] The endings of each fiber form a small, discretely sensitive point, separated from the sensitive receptor endings of neighboring fibers. The total area of skin occupied by a receptor ending is in the range of approximately 1 mm but the density of such thermo-sensitive points varies by body region. For example, warm spots are sparser than cold spots, and relative density decreases from lips to fingertips to trunk.[158] In addition to affecting warm receptors, temperature change can also affect mechanoreceptors.[159] Receptors have been defined as slowly conducting units that exhibit a steady-state discharge at constant skin temperature and a dynamic response to temperature changes.[160] The sensation of warmth increases in parallel to this increase in discharge.[161]

Cutaneous Aδ and C fibers terminate in laminae I, II and V of the spinal cord. A number of studies have been completed that conduct electrophysiological recordings from neurons in these regions.[162] Second order neurons rarely exhibit the same bursting firing pattern as thermoreceptive fibers, perhaps due to the fact that second-order cells receive a convergent input from many receptors that are firing out of phase with each other.[163] Lamina I neurons receive most cutaneous thermal signals.[164] Thermoreceptive neurons of the dorsal horn have been found to project contralaterally to the level of the cervical spinal cord [165] and many reports identify thermoreceptive neurons as spinothalamic neurons.[166] There are three main types of lamina I neurons that have been categorized according to their responses to cutaneous thermal and mechanical stimuli: nociceptive-specific cells responding to noxious mechanical and heat stimuli, polymodal nociceptive cells responding to noxious mechanical, heat and cold stimuli and theroreceptive-specific cells responding linearly to graded, innocuous cooling or warming stimuli and not activated in the noxious temperature range.[128] Many of the spinothalamic neuons also respond to stimuli other than thermoception, but some respond exclusively to thermal

stimuli.[128] Thermoreceptive spinothalamic cells found in cats project to the medial rather than the lateral thalamus.[166]

2.5.2 Blood flow to the spinal cord

2.5.2.1 Vascular architecture

The vascular architecture of the spinal cord is considerably different than the cerebral cortex and given that the fMRI signal is driven by the hemodynamic response to underlying neural activity, it is important to understand this architecture. During an fMRI experiment, the rostral-caudal extent of the spinal cord is positioned roughly inline with the static magnetic field. The paired anterior spinal arteries arise from the vertebral arteries and descend along the anterior surface of the spinal cord, fusing to a common anterior spinal artery usually within 2 cm of their origin but certainly by the fifth cervical vertebral level.[167] The anterior spinal artery (ASA) supplies the anterior two-thirds of the spinal cord. The paired posterior spinal arteries (PSA) also arise from the posterior circulation, usually the vertebral arteries but occasionally from the posterior inferior cerebellar arteries, and supply the posterior one-third of the spinal cord.[168] Both the ASA and PSAs traverse the entire rostral-caudal length of the spinal cord and are supplied by segmental radicular arteries along their extent. Branches of both the ASA and PSA's form an anastomosing pial arterial plexus that encircles the spinal cord.[169] These branches penetrate the spinal cord perpendicular to its surface, resulting in the characteristic centrifugal blood supply. The majority of penetrating branches of the arterial plexus traverse the dorsal midline of the spinal cord and supply the dorsal horns extending to the substantia gelatinosa.[167] Arterial braches arising from the ASA are termed central arteries[170], which penetrate the spinal cord in a posterior direction via the anterior median fissure and supply the white matter bordering the central sulcus, the gray matter of the anterior horn and the deep gray matter of the dorsal horns.[171] The central arteries can divide into short ascending, descending and horizontal branches before transitioning into capillaries.[172] Central arteries have a mean diameter of 0.21 ± 0.05 mm in the cervical region, 0.14 ± 0.04 mm in the thoracic region, 0.23 ± 0.6 mm in the lumbar region and 0.2 ± 0.5 mm in the upper sacral region.[170] Capillary beds of the spinal cord are five times denser in the gray matter than the white matter[173] and more subtle variation exists whereby the lateral horns, anterior horns and superficial dorsal horn (substantia gelatinosa) have the thickest capillary beds and the base of the dorsal horn are less well supplied.[168] Changes in blood flow are under the control of vascular smooth muscle cells in arteries and arterioles, and are probably the main

target of neurovascular coupling pathways.[128] While capillaries themselves are void of smooth muscle cells, they are encircled by pericytes whose functional mechanisms contribute to cerebral blood flow but have an uncertain role in neurovascular coupling mechanisms.[128]

2.5.2.2 Autoregulation

Blood flow to the spinal cord is only 40-60% of that to the brain but tissue oxygen levels are identical, in the range of 35-39 mmHg.[174] The process of autoregulation ensures a constant blood flow to the spinal cord when systemic changes in either blood pressure or $pACO_2$ levels occur. While a detailed review of autoregulation is beyond the scope of this work, a few points are worth mentioning. Spinal cord blood flow (SCBF) has been measured in lambs and results are as follows: in the cervical gray matter: 124-141 mL/100 g / min and cervical white matter: 22-26 mL/100g/min; lumbar gray matter 74-104 mL/100g / min and lumbar white matter 15-24 mL / 100g / min.[128] These values remained constant between a mean arterial blood pressure (MABP) of 40 to 100 mmHg and fell off considerably below a MABP of 40 mmHg. Similar results were found in monkeys.[175] Blood volume perfusing the spinal cord increases when arterial CO_2 tensions increase and decreases when CO_2 tensions decrease.[176] When $PaCO_2$ was between 10-50 mmHg in monkeys, SCBF remained constant.[175] SCBF increases markedly at MAPB greater than 135 mmHg and PaCO2 levels greater than 50 mmHg; in such situations, the capillary endothelium responsible for normal blood-brain barrier can be disrupted resulting in edema and neuronal dysfunction.[177]

To investigate the potential for regional differences in autoregulation between the cerebrum, cerebellum and spinal cord, Sato *et al.* used the hydrogen clearance method to study the effect of changing arterial CO_2 and blood pressure on regional blood flow.[178] The results demonstrate regional differences in the anesthetized cat. Under control conditions, blood flow is lower in the cerebellum and spinal cord relative to the cerebral cortex, consistent with previous work.[174] In the normocapnic range, a rise in $PaCO_2$ by 1 mmHg was accompanied by an average CBF increase of 1.7 ml/100 g/min for the cerebral cortex, 1.1 ml/100 g/min in the cerebellum, and 0.9 ml/100 g/min in the dorsal horn of the lumbar spinal cord. The larger regulatory capacity of the cortex may be due to the greater microvascular density in this region. In fact, comparative morphometric studies of the capillary system of the CNS reveal that the highest capillary length per tissue volume are in the cerebral cortex (1,155 mm/mm3), followed by the cerebellar cortex

(approx. 800 mm/mm3) and spinal gray matter (approx.730 mm/mm3), thus forming the same descending order established for regional response to $PaCO_2$ changes.[179] Using percentage change from baseline flow (to account for subtle differences between animals, the effect of anesthesia and a measurement bias towards lower flow values with the hydrogen clearance technique) as a means to describe the autoregulatory capacity of different CNS regions to changes in blood pressure, Sato *et al.* demonstrated that autoregulatory capacity was greatest in the cerebellum (from 53 to 146% of control MABP), while cerebral and spinal cord blood flow exhibited autoregulation in a significantly narrower MABP range (79-123% and 83-128% of control respectively). Autoregulation entails the adaptation of vascular resistance across changes in MAPB, whereby a higher blood pressure requires a higher vascular resistance to limit flow; at extremely high blood pressures this resistance gives way, autoregulation fails, and hemorrhage results. The spinal cord autoregulatory curve demonstrates that the spinal cord is more susceptible to autoregulatory failure during hypotensive episodes than the corresponding cerebellum. While the implications of this are unlikely to affect the normal functioning spinal cord, the underlying mechanisms should be considered as a clue to the control of blood flow to different regions of the CNS. For example, regional variation in cholinergic innervation of pial arteries exists and this may impact the regional response to systemic variations in blood pressure or $PaCO_2$.[180] Along this line of reasoning, as will be discussed below, there is emerging evidence of regional variation in the signaling pathways responsible for recruiting blood flow in response to spatial-temporally isolated increases in metabolic activity within certain nuclei or CNS regions.

2.5.3 Neurovascular coupling and functional hyperemia

As outlined in the preceding section, the spinal cord is unique in terms of vascular structure, capillary density, vascular innervation, and functional response to changing systemic conditions (autoregulation). How these different pieces of the puzzle fit together to maintain optimal perfusion of the spinal cord in different metabolic states remains to be determined. As others have pointed out, the ratio of fractional changes in CBF to the local cerebral metabolic rate of oxygen consumption ($CMRO_2$) is not only different in different regions of the CNS but also of critical importance to understanding the magnitude of fMRI signal changes in response to specific stimuli.[128] Given that the central nervous system has little capacity to store energy and that it must meet metabolic requirements for complex processing in a matter of seconds, certain

mechanisms are in place to ensure the continual processing of neural signals. While the details of these mechanisms are under intense study in specific regions of the brain (with no studies completed on the spinal cord), two broad terms are generally agreed upon in the literature: **neurovascular coupling** describes the signaling events between neurons and the surrounding milieu of astrocytes, pericytes and microvascular networks and **functional hyperemia** describes the resultant increase in blood flow to meet the increased metabolic requirements of regional neural processing. The reason for the distinction between neurovascular coupling and functional hyperemia rests in the notion that different brain regions may utilize unique signaling mechanisms to call upon increased blood flow to meet the metabolic demands of that specific region. For example, while it is agreed upon that both the cerebral cortex and the cerebellum have the capacity to recruit blood flow to meet increased metabolic requirements (functional hyperemia) there is evidence that these regions have unique neurovascular coupling mechanisms whereby the cerebellum, a phylogenetically older portion of the central nervous system, uses NO as a direct mediator between neurons and blood vessels, and the newer cerebral cortex uses NO as a mediator of neuron-to-vessel signaling by modulating astrocyte signaling pathways that dilate and constrict blood vessels.[181] Furthermore, while neurovascular coupling within the cortex and cerebellum involve NO, there is evidence that brainstem nuclei utilize adenosine.[128] To date, there have been no studies into the mechanisms of either neurovascular coupling or functional hyperemia on spinal cord tissue and the remainder of this literature review will therefore focus on developments that have occurred in the brain.

A number of specific signaling molecules have been proposed to communicate the metabolic requirements of neural tissue and the need for increased or decreased blood flow to meet local oxygen and glucose requirements. Whether such signaling pathways act through a feedback loop (also known as the metabolic hypothesis) whereby changes in neuronal activity drive changes in metabolism which in turn drive vasoconstriction / vasodilation or through a feed-forward loop (also known as the neurogenic hypothesis) whereby neuronal activity directly drives vasocontriction / vasodilation is open for debate.[128] Regardless of where the balance lies, and there is ample evidence for both arguments in the literature, a number of signaling mechanisms have been established. Acting through far reaching projections are neurons of the nucleus basalis magnocellularis (vasodilation effect of acetylcholine), dorsal raphe nucleus (vasocontriction effect of seratonin) and the rostral ventrolateral medulla who's oxygen sensitive neurons

influence cortical blood flow through thalamic intermediates and the modulatory actions of acetylcholine, seratonin and noradrenergic input from the locus coeruleus.[128] On a finite spatio-temporal scale, subclasses of cortical inhibitory interneurons have been found to act directly on smooth muscle of vascular arterioles whereby certain transmitters relax smooth muscle to dilate vessels (NO and vasoactive intestinal peptide) and others constrict smooth muscle (somatostatin and neuropeptide Y) in a concerted effort to regulate blood flow in response to activity within these networks.[128] There is a rather large body of evidence linking the action of excitatory neurons acting through an astrocyte intermediate to regulate blood flow. Commonly referred to as the neurovascular unit, the neuron-astrocyte-arteriole complex acts in the following fashion: excitatory glutamate leads to an increase in intracellular astrocytic calcium levels initiating the conversion of arachidonic acid to either prostaglandin E and epoxyeisoatrienoic acid (EET) or 20-hydroxyeicosatetraenoic acid (20-HETE) resulting in a net vessel dilation or constriction, respectively.[128] The identification and characteristics of these signaling molecules provides a strong foundation to establish how these pathways vary in different regions of the CNS and ultimately how they function to ensure adequate blood supply during times of need.

As evident in the publication dates of references cited in this section, there is a long history of study into the function of the spinal cord and how the neurovascular unit is intricately coordinated to ensure efficient flow of information to and from the brain. Optical imaging methods are perhaps the newest tool available for *in vivo* measurements allowing for visualization of single cells and blood vessels (high spatial resolution) combined with a sampling time fast enough to reconstruct the events of neural processing (high temporal resolution). Given the infancy of such tools, the majority of work into understanding neurovascular and neurometabolic coupling has been conducted in the cerebral cortex of animals and the plethora of imaging tools have been recently summarized in an excellent review paper.[182] The ability to concomitantly measure concentrations of oxygen and quantify blood flow in response to specific patterns of neural activity will provide significant insight into how neural, metabolic and vascular events are coordinated to perform a certain function. While it is generally accepted that both at rest and during states of activation, blood flow exceeds the brains requirement for oxygen delivery, the relationship between O_2 concentration and blood flow is uncertain in different compartments: arterial, venous and cellular (mitochondrial). The brain hemodynamic response to functional activation results in a disproportionate increase in CBF relative to O_2 requirements.

This disproportionate increase in flow has been found to be anywhere from 1.5 to 6 times greater than the required amount of oxygen.[128] As such, detailed microscopic measurements of change in blood flow and oxygen concentration in cerebral (or spinal) microvasculature are needed to better guide the interpretation of macroscopic fMRI signals and better appreciate the link between such signals and underlying CNS function. An elegant piece of work from the Boas group utilized a multimodal microscope system capable of simultaneous CBF and pO2 measurements to demonstrate the effect of somatosensory stimulation on these parameters in different vascular compartments.[128] They were able to demonstrate a constant relationship between total extracted oxygen and CBF in individual arterioles and venules (adding credence to the previous claim of constant O_2 extraction efficiency)[183] and arteriolar oxygen extraction in response to stimulation of the sensory cortex suggesting that arterioles contribute to the fMRI BOLD response.[128] While such studies have not been conducted in the spinal cord, speckle variance optical coherence tomography (SV-OCT) feasibility studies have been completed and an extension of this work to include metabolic parameters is underway.[128] By imaging a three dimensional segment of the spinal cord while simultaneously stimulating a peripheral nerve that corresponds with the rostral-caudal spinal cord segment being imaged, it may be possible establish stimulus specific hemodynamic response functions whereby the intensity, duration and inter-stimulus interval of somatosensory stimuli are expected to affect the magnitude of the neurovascular response. Such data are of utmost importance in the interpretation of human spinal fMRI studies and optical imaging methods will certainly play a role in uncovering the biophysical basis of fMRI signal change.

The brain and spinal cord are constantly perfused with an adequate blood supply to meet the metabolic demands of the resting nervous system. The blood flow required to meet the metabolic requirements varies between regions (for example, the gray and white matter of the spinal cord) and is under regulatory control against changes in systemic conditions such as blood pressure and $pACO_2$ levels. When particular regions of the brain or spinal cord are called upon to perform a certain task, for example movement of the right hand, the neuronal networks involved in this task work beyond their resting baseline and call upon local microvascular networks via specific signaling mechanisms (neurovascular coupling) to provide more energy input (oxygen and glucose) and remove metabolic byproducts (carbon dioxide, lactate, etc.) via a transient increase in blood flow (functional hyperemia). While all regions of the central nervous system exhibit the

ability to call upon excess blood flow to meet increased metabolic demands, the signaling mechanisms involved (neurovascular coupling) differ between regions. There is a lack of understanding of both neurovascular coupling and functional hyperemia in the spinal cord but with improved high spatial-temporal resolution methods, such details will certainly emerge in the near future and be a welcome addition to spinal fMRI experiments whose underlying analyses assume a standard hemodynamic response function regardless of the stimulus, an assumption that may prove to have underlying exceptions based on, for example, the intensity of the delivered stimulus.

2.5.4 Measuring metabolic activity in the spinal cord

Processing of information in the central nervous system is metabolically expensive, requiring approximately 20% of cardiac output.[184] The precise events requiring energy include the restoration of ion movements generated by postsynaptic currents, action potentials and neurotransmitter uptake whereby glutamatergic signaling is thought to be the most metabolically expensive.[128] This energy, in its most fundamental biological form, comes from the oxidation of glucose to form adenosine triphosphate (ATP), water and CO_2. Atwell *et al.* estimated that energy requirements of functioning gray matter is equal or greater than a human leg muscle thrusting its owner through a marathon race.[185] Oxygen, reversibly bound to hemoglobin in the vascular space at concentrations of roughly 90 mmHg in the arterial system and 35 mmHg in the venous system, diffuses down a concentration gradient through the capillary into the extravascular environment (where CNS tissue has a PO_2 of approximately 15-20 mmHg) and into the mitochondria where concentrations of at least 1.5 mmHg are required to maintain aerobic metabolism.[128] The cerebral metabolic rate of oxygen consumption ($CMRO_2$) is a function of mitochondrial activity and is between 1.3 – 1.8 μmol / g / min in the healthy brain.[186]

There have been two methods utilized to measure the metabolic response to neuronal function in the spinal cord: the 2-deoxygluscose method and immuno-staining for immediate-early genes. Both techniques can evaluate the distribution of neurons that respond to specific stimuli. While there are few studies that report on such changes in metabolic activity, those that do provide an important link between the spatial specificity of neuronal activity and the metabolic response required to process the applied stimulus. The technique of immuno-staining for immediate-early

genes has largely been applied to study the expression of the FOS protein via the C-Fos gene (activated by a substance P agonist) in the setting of noxious stimuli.[128]

Injection of radiolabeled 2-deoxyglucose followed by stimulation of the peripheral nervous system allows for detection of regions of the CNS that incorporate the radiolabeled glucose via metabolic pathways through autoradiographic detection. This technique requires slicing of the spinal cord after the experiment to provide a quantifiable measure of metabolic activity with high spatial resolution. This technique has been applied to the cat spinal cord with only two different peripheral stimulation paradigms: low threshold mechanical stimulation to activate the plantar cushion reflex[128] and noxious heat stimulation of the paw.[187] The plantar cushion reflex in cats is a cutaneous-spinal reflex characterized by a brisk phasic plantar flexion of the toes following low threshold mechanical or electrical stimulation of the plantar cushion in cats. The reflex arc involves at least 3 neurons (and possibly 4) that consist of a peripheral afferent limb (SA I afferent fiber) that enters the spinal cord at the L7 level and terminates in the medial dorsal horn; a dorsal horn interneuron that resides in the medial dorsal horn at the L7 level and a connection to the motor neuron pool in the dorsolateral ventral horn at the S1 level.[128] In order to detect metabolic activity within the confines of an experimental design, the authors applied an electrical stimulus to the cat paw between 2 and 5 times the stimulus perception threshold for 45 minutes. In doing so, they detected increased metabolic activity in the ipsilateral dorsal horn, ipsilateral ventral horn and to a lesser extent in the contralateral dorsal and ventral horn of the L7 spinal cord segment. Cats simulated at 5 times the stimulus threshold showed greater activity than those stimulated at 2 times the stimulus threshold. Within the ipsilateral structures, activity was concentrated in Rexed laminae II-IV, V-VI and around the central canal.[128] Similarly, Abram and Kostreva applied a suprathreshold pain stimulus (thermal heat, 40-53°C, intermittent 30 second applications for 1 hour or more) and demonstrated metabolic activity concentrated within the ipsilateral superficial dorsal horn (lamina I and II), the lateral portions of lamina IV and V, the ipsilateral ventral horn (lamina VII and IX) and within the central gray (lamina X).[187] The authors point out that the pattern of metabolic activity with a pain stimulus is considerably more diffuse relative to a mechanical stimulus. Also of note is that the distribution of metabolic activity extended to the medial dorsal horn in response to mechanical but not noxious stimulation. This is consistent with previous studies demonstrating that the PC reflex involves interneurons in the medial dorsal horn in response to activation of mechanoreceptors.[188] Last, no

detectable increases in metabolic activity were observed in dorsal root ganglia, consistent with the notion that majority of metabolic requirements necessary to process peripheral sensory information occur within the spinal gray matter.[189]

2.6 A Systematic Review of Spinal fMRI research: Outlining the elements of experimental design

2.6.1 Spinal fMRI research from 1996 to 2012

Functional MRI of the human spinal cord has undergone considerable development since the first published report in 1996.[128] In a similar manner to fMRI of the human brain, extension of this technology to the spinal cord aims to establish a non-invasive means of investigating how different neuronal populations react to either afferent sensory input, descending motor signals, autonomic output or interneuron integration of afferent and efferent signals. In each of these domains, the research potential is vast and would build upon a strong foundation of invasive animal models utilizing tracer studies to uncover the structural aspects of specific neuronal populations and electrophysiological techniques to uncover how different neurons respond to specific stimuli. Tracer studies, for example, have demonstrated that sensory nerve projections reflect limb position during the embryonic period and this position is maintained in adult organization of the dorsal horn.[190] Specifically, the projection of the tibial nerve, innervating the plantar surface of the foot is represented medially in the spinal cord dorsal horn and the common peroneal nerve, innervating the dorsal surface of the foot is represented laterally in the dorsal horn.[191] An excellent review of these detailed structural studies has been published by Grant.[192] Functional properties of neuronal populations of the spinal cord are reported in the electrophysiology literature. For example, Wall has extensively studied neuronal populations of Rexed lamina II, demonstrating that neurons in this location showed a prolonged discharge, lasting seconds to minutes, following a single brush stimulus or a noxious stimulus.[193] Some cells required a stronger stimulus such as intense pressure or pinch and repeated stimuli often resulted in habituation of the neuronal response.[193] Classic physiological and anatomical techniques used to establish a solid foundation for our understanding of how the spinal cord functions, are not possible in humans. Sensory, motor and autonomic circuits of the human spinal cord are largely unstudied in the context of clinical care for patients. Spinal fMRI has potential to uncover how different neuronal populations function *in situ* in humans. It is of critical importance to remember that spinal fMRI will not be able to replicate results obtained

from invasive animal models using electrophysiological or other techniques. Rather, spinal fMRI is an indirect measure of neuronal activity based on the hemodynamic response to neural activity. Depending on the pulse sequence utilized in the spinal fMRI experimental design, either the BOLD (blood oxygen level dependent) contrast mechanism, dependent on the relative proportions of oxygenated and deoxygenated hemoglobin or the SEEP (signal enhancement of extravascular protons) contrast mechanism, dependent on the relative amount of extravascular protons, act as a surrogate measure of neuronal activity. In order to appreciate what information may be gained from utilizing spinal fMRI, we must understand the many components of a typical spinal fMRI experiment.

Stimulation paradigms:

After the research question has been established, one must consider a specific stimulation option – whether it is a sensory modality, such as light touch, vibration or thermal stimulation or a motor task. Stimulation paradigms are carried out in the form of a block design where periods of activity are interleaved with periods of rest. In terms of the stimulus, one must consider the duration, frequency, inter-stimulus interval, intensity and the number and timing of rest periods. Each of these variables has an impact on the activity of spinal neurons, as established in classical electrophysiology experiments.[193]

Acquisition of the fMRI signal:

Two contrast mechanisms have been established to acquire spinal fMRI data, each with their own advantages and drawbacks. The BOLD (blood oxygen level dependent) contrast mechanism relies on T2* decay and is the basis for the vast majority of all functional MRI studies. The SEEP contrast mechanism (signal enhancement by extravascular protons) relies on the shift of protons to different environments that comes with increased blood flow to regions of activity. Subsequent to the increased blood flow, a number of events occur that results in the SEEP signal, including the shift of water to different cellular compartments, cellular swelling and the production of water through metabolic processes. These mechanisms have been recently summarized and the interested reader is encourage to review this work.[194] The SEEP mechanism was first described by Stroman in 2001 and relies on proton density weighted imaging. The BOLD and SEEP contrast mechanism are grounded in the phenomenon of neurovascular coupling – the relationship between neuronal activity and the glial-blood vessel response.[128] Last,

one must consider how to identify regions of activity along the rostral-caudal axis of the spinal cord and how to process the data in order to accurately interpret the results.

We systematically obtained all spinal fMRI studies conducted to date in healthy individuals, as spinal disease – and spinal cord injury in particular – adds a level of complexity that is just beginning to be understood. We will focus on two different themes: the first will focus on the different methods utilized to date, comparing the contrast mechanism utilized (BOLD vs SEEP), the specific stimulation paradigms (motor versus sensory) and the means by which regions of the spinal cord are identified. The second theme will describe the spatial specificity of activation. That is, how different stimulation paradigms aim to activate either a specific population of neurons (for example, tactile stimulation in the C5 dermatome) or a range of neurons (for example, a finger-tapping experiment). We have intentionally limited this review to the neurobiology of spinal fMRI rather than specific data acquisition parameters, data analysis methods, signal-to-noise characterization and other aspects of both spatial and temporal resolution as these aspects of spinal fMRI have recently been summarized in other review papers.[128] We intend for the reader to gain an appreciation for how spinal fMRI has been applied to date in healthy individuals and what information has been learned with regard to the ability of spinal fMRI to reveal information about the function of the spinal cord. We anticipate that the next decade of spinal fMRI research will build on these results with an increased application to specific states of pathology, spinal cord injury in particular.

2.6.2 Systematic Review Methodology

Electronic Literature Database

A systematic search was conducted using MEDLINE for literature published from 1990 through January 2012 reporting on stimulation paradigms used to assess spinal fMRI in healthy individuals. Results were limited to articles published in the English language. Reference lists of key articles were also systematically checked. Studies were included that evaluated heat, cold, electrical, laser, tactile or motor task stimulation applied peripherally. Studies were excluded if conducted in patients with a disease state, included epidural stimulation, or evaluated noxious stimulation paradigms. Two independently working reviewers reviewed each retrieved citation. Most articles were excluded on the basis of information provided by the title or abstract.

Citations that appeared to be appropriate or those that could not be excluded unequivocally from the title and abstract were identified and the full text was reviwed.

Data Extraction

From the included articles, the following data were extracted: method of stimulation, stimulation parameters, fMRI data acquisition parameters, method of identifying spinal cord segment, study rational, and results.

2.6.3 Spinal fMRI studies from 1996 to 2012

Through a systematic approach, 19 peer-reviewed studies were identified spanning from 1996 to 2012 that utilize a combination of different spinal fMRI methods to investigate the human spinal cord in healthy individuals. Figure 2-6 outlines the flow of the systematic search. 10 of these investigations utilized the BOLD contrast mechanism and 9 utilized the SEEP contrast mechanism. The details of each of these studies and their results are summarized in Table 2-7. The specific motor or sensory paradigms along with the rationale of the studies are summarized in Table 2-8.

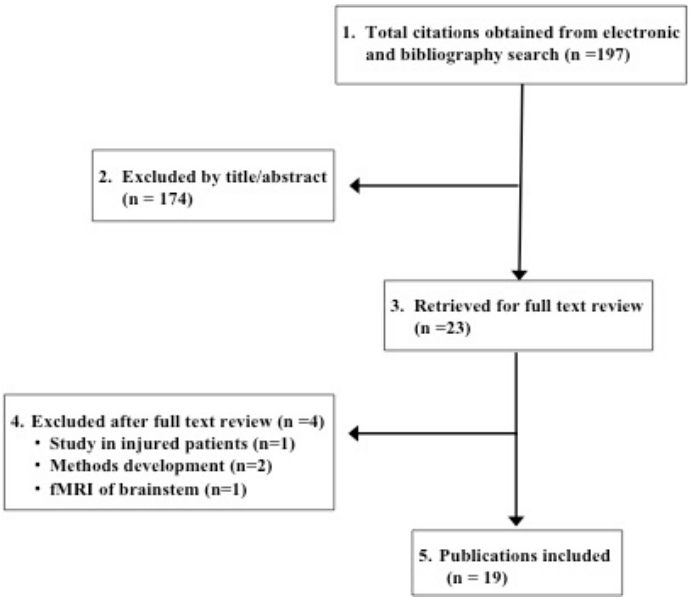

Figure 2-6. A flow diagram illustrating the systematic search results.

Table 2-7. A summary of spinal fMRI studies conducted from 1996 to 2012.

Author (Year)	Method of stimulation	Stimulation parameters	fMRI data acquisition parameters	Method of identifying spinal cord segment	Results
Yoshizawa (1996) n = 4	Motor activation (hand-closing task) (right hand)	• Intensity: self-set • Frequency: 2 Hz • Interval: 6 total examinations per subject; 4 sets of control (rest) images (3 slices each), followed by 4 image sets (3 slices each) during hand-closing task; repeated once for each subject (total of 16 images) • Duration: control and functional image sets: 8-52 min each; total functional time was 34.08 min / subject	• BOLD • A 1.5 T clinical scanner was used with a Siemens neck (C-spine) coil • Slice thickness: 10 mm	• Vertebral bodies C6-7 were used as landmarks for cervical cord nerve segments C7-8 by counting the vertebral bodies and the disc spaces	• Reported individually and as a group • The observed locale of activation was in the ipsilateral intermediate and ventral gray matter of the cervical cord • In all 6 cases, a region of significant signal increase was observed in the right (ipsilateral) ventral quadrant of the cord medial to the central canal and extending slightly ventrolaterally • Positive signal increase areas extended to the contralateral side and to the posterior half of the spinal gray matter, in some cases
Stroman (1999) n = 25	Motor: Squeezing a rubber ball (dominant hand)	• Intensity: self-set • Frequency: squeeze rubber bulb once per second • Interval: 5 condition exercise paradigm with alternating rest and exercise; entire exercise paradigm performed twice • Duration: 5 images were acquired during each condition, which lasted	• BOLD • A 3-T whole body MR system • An oblique transverse slice through the spinal cord at C8 and a sagittal slice through one-half of the spinal cord • Slice thickness: 5 mm	• Cervical segments were selected based on adjacent vertebral bodies • The authors note that vertebral level C7 corresponds to spinal cord segment C8	• Reported individually and as a group • 13/18 subjects showed areas of activation on the same side of the spinal cord as the hand performing the exercise (ipsilateral) • Intensity time courses that correlated with the exercise paradigm were observed within the spinal cord and on the cord surface, within the large vessels of the neck and within the neck and shoulder muscles • Intensity changes observed within the spinal cord and surface vessels had a peak value of 8.5% and averaged 7.0% for the 13 subjects for which both transverse and sagittal views were acquired • Within the spinal cord, the areas

		1.5 min, 1 min rest			that underwent intensity changes between periods of rest and exercise were primarily on the same side of the spinal cord as the hand performing the exercise, and were localized between the C6 and T1 spinal cord segments • Intensity changes were not isolated to the motor areas in the central-ventral region, but were commonly within both central and dorsal regions • Regions undergoing intensity changes between rest and exercise were identified in the central region of the gray matter, on the same side of the spinal cord as the exercising hand in nine subjects • The areas of activation were predominantly on the same side of the spinal cord as the hand performing the exercise, between the levels of C6-T1
Backes (2001) n = 11	Fist clenching (n=11) and median nerve stimulation (n=7) (alternating right and left)	Fist clenching: • Intensity: maximal extension and flexion of fingers • Frequency: 1 Hz • Interval: rest and activation were alternated, repeated 4-5 times • Duration: 30-s epochs Median nerve stimulation: • Intensity: stimulation current of 20-40 mA, with 0.2-ms constant current pulses • Frequency: 1 Hz • Interval: alternating rest and activation repeated 4-5 times	• BOLD • Images were acquired with a 1.5-T MRI system using sagittal and transverse sections • The functional imaging sessions consisted of a multishot single-section T2-sensitive echo-planar imaging sequence • Slice thickness: 8 mm (sagittal) and 5 mm (transverse)	• Cervical segments were selected based on adjacent vertebral bodies	• Reported as a group • In the sagittal view, 5/7 subjects had an fMRI response in the lower cervical cord upon median nerve stimulation • 7/11 subjects showed activation with the fist-clenching task • Within the cord, the measured fMRI response level was 8-15% with respect to the baseline signal level • In the transverse imaging plane, significant fMRI responses could be measured in only 2/6 and 6/9 subjects with median nerve stimulation or fist clenching, respectively • In the sagittal plane, median nerve stimulation at the elbow can evoke an fMRI response in the lower cervical spinal cord (C4-T1), comparable to that obtained by fist clenching • In the transverse plane, reliable fMRI responses were obtained much less frequently, and assignment of distinct areas of the spinal cord to the stimulation methods used was not possible

		• Duration: 30-s epochs			
Madi (2001) n = 6	Motor task, isometric movements: • Biceps (C5,C6) • Wrist extensors (C6,C7) • Hand abductors (C8,T1)	• Intensity: self-set • Frequency: all movements (biceps flexion, wrist extension, and finger abduction) were repeated at a rate of one or two every second • Interval: block design; 16 cycles for isometric activity; 8 cycles of motor activity • Duration: 30 seconds of activity (holding weights) followed by 30 seconds of rest	• BOLD • A 1.5 T clinical scanner was used with ramp sampling (to reduce the motion artifacts) • 6 sagittal slices were used • Slice thickness: 4 mm (isometric) and 5 or 6 mm (for all other trials)	• Cervical segments were selected based on adjacent vertebral bodies	• Reported individually and as a group • The observed location of activity for each task primarily matched expected anatomic locations on the basis of known innervation patterns of the tested muscle groups • Elbow flexion elicited a response in C5 and C6 • Wrist extension elicited a response at C6 and C7 • Finger abduction activity was expected in C7-T1, however it was found in T1 for all 6 subjects; in T2 for 5 subjects; in only half the subjects was C7 involved • Amplitude of observed signal varied widely from 0.5% to 7.5% among subjects • As was the case for activation, deactivation was observed to occur over noncontiguous clusters • The strength of the BOLD signal for both activation and deactivation for a substantial fraction of the active voxels shows a linear relationship with respect to applied force • For all but one subject, a signal was detected at the C5-C6 level during isometric exercise • Additional activity was detected at the C8 through T1 levels • While regions of activity were distributed throughout the spinal cord, concentrated activity was found in the anatomic locations of expected motor innervation
Stroman (2001) n = 15	Motor task: • Squeeze ball with right hand Sensory: • Blowing puffs of air onto the palm	• Intensity: self-set • Frequency: Time between repetitions of the imaging sequence was typically 5 s, but varied from 3-7 s • Interval: block design; alternate conditions of	• BOLD • A 1.5 T clinical MR system was used • Transverse slices • Slice thickness: 7.5 mm	• Cervical segments were selected based on adjacent vertebral bodies	• Reported as a group • A motor-task carried out with the dominant hand yielded intensity changes which averaged 4.3 ± 0.6% during exercise conditions lasting roughly 50 s each • With the non-dominant hand, the intensity changes averaged 4.5 ± 1.0% • When an asymmetric paradigm as used the average values over the initial long exercise condition (~70 s) were 5.6 ± 1.1% and 5.7 ± 1.0% for the dominant and

		rest and stimulation; 5 conditions with 10 images acquired during each; asymmetric paradigm consisted of 12 images at rest, 14 with stim, 10 rest, 8 stim, 10 rest, for a total of 54 time points • Duration: 25 time points for the symmetric paradigm and 27 for the asymmetric paradigm, acquired an average of 10 seconds apart			non-dominant hands, respectively • The average values were lower during the shorter exercise condition in the second half of the paradigm at 4.8 ± 0.7% for the dominant hand and 3.8 ± 0.4% for the non-dominant hand • The time to reach the maximal effect with the motor task appears to be as long as 20 to 30 s • For stimulation of the dominant hand during sensory stim, the magnitude of intensity change was 4.4 ± 0.9% during the initial ~70 s period, and lower at 3.2 ± 0.7% ($p = 0.05$) during the subsequent ~40 s stimulation • Stimulation of the non-dominant hand yielded similar values of 5.5 ± 0.7% and 4.1 ± 0.5% ($p < 0.05$) during the two stimulation periods respectively • The time to reach maximal effect in the spinal cord with sensory stimulation is approximately 15 seconds; while the time to reach the maximal response is faster than with the motor task (20-30 s), it is still considerably longer than the time required for maximal BOLD response in the brain (5-6 s) • With a motor task the activated pixels on the ipsilateral side were mainly in the ventral regions and were spread over 3-4 adjacent slices (~2-3 spinal cord segments) • Activated pixels on the contralateral side were more localized and tended to be grouped into the 7th cervical spinal cord segment • The distribution of activated pixels for sensory stimulation appeared to be slightly more localized over 3 slices centered at the 8th cervical spinal cord segment • The contralateral activation was primarily localized over a small range of 1-2 slices (one spinal cord segment), as observed with the motor stimulus
Stroman,	Sensory	• Intensity: skin	• SEEP	• Cervical	• Reported as a group

Krause (2002) n = 13	(cold) stimulation of the thumb, little-finger, and forearm (right hand and forearm)	temperature (30-32˚C) or cold (5-7˚C) water • Frequency: NR • Interval: 8 equal stimulation periods, alternating "rest" (skin temp) and stimulation (cold) (with only one region being stimulated at a time; each region stimulated twice), repeated 3 times • Duration of intervals: NR (volume of interest in the spinal cord was imaged 64 times during the course of stimulation paradigm)	• A 1.5 T MR system using a phased-array spine coil receiver and a body coil was used to transmit uniform excitation pulses • 8 parallel slices transverse to the spinal cord from C4-5 to T1 • The imaging pulse sequence used was a single-shot fast spin-echo with a 9 second repetition time • Slice thickness: 7.5 mm	segments were selected based on the vertebrae centers or at the intervertebral discs	• Stimulation of the thumb side of the palm resulted in a peak activity at the 6th cervical spinal cord segment whereas stimulation of the little-finger side of the palm peaked a little lower at C7 or C7/C6 • Distribution of activity was noticeably higher in the spinal cord when the forearm was stimulated with most of the activity spreading from C6 across C5 • Number of active pixels is significantly ($p < 0.05$) lower with stimulation of the little-finger side of the palm at the level of C6 and above • Stimulation of the forearm resulted in significantly lower numbers of active pixels at the level of C7/C8 and below • Clustering of active pixels into groups based on their intensity time courses discriminates false activations from true activations • Following clustering, the distribution of activity observed with fMRI matched the expected regions of neuronal activation with the different areas of stimulation on the hand and forearm
Kornelsen (2004) n = 6	Lower limb motor activity – ankle movement (alternating right and left)	• Intensity: self-set • Frequency: NR • Interval: block design with 2 series of active pedaling and 1 series of passive pedaling • Duration of blocks: NR (Images were acquired repeatedly during alternating rest and stimulation periods, resulting in a total of 56 time	• SEEP • A 1.5 T GE MR system was used • Single-shot fast spin-echo imaging with sets of 8 contiguous slices from S3 up to L1 (repetition time of 11 seconds) • Slices were oriented transverse to the spinal cord • Slice	• Lumbar segments were selected based on adjacent intervertebral discs or centers of the vertebrae	• Reported as a group • During active ankle movement, activity was detected in the lumbar spinal cord motor areas and sensory areas bilaterally (ventral and dorsal horns) • During passive ankle movement, activity was detected in the motor and sensory areas in lower lumbar spinal cord segments and motor activity in higher lumbar spinal cord segments • More activity was observed at higher spinal cord segments than in lower spinal cord segments for both active and passive maps

		points recorded)	thickness: 7.0-7.5 mm		
Stracke (2005) n = 9	Mechanical tactile stimulation in either C6, C7 or C8 dermatomes of the right hand	• Intensity: stimulation pulses rate of 2.5 Hz • Frequency: up to 3 Hz • Interval: block design with alternating rest and stimulation conditions completed 6 times (3 runs performed: 1- stimulation at the thumb (dermatome c6); 2- tip of the third finger (c7); and 3- tip of the fifth finger) (c8) • Duration: each phase lasted 24 s, resulting in an overall scanning time of 288 s, or 4 min 48 s	• BOLD • A T-1.5 scanner was used with a standard cervical neck-linear cage coil • Sagittal orientation • Repetition time was 2,000 ms with a total of 144 repetitions • The field of view covered the whole cervical spine including as much as possible of the medulla oblongata • Four slices were acquired • Slice thickness: 4 mm	• Cervical segments were selected based on adjacent vertebrae • Authors note that activity is expected one vertebral body above the dermatome stimulated i.e. C6 activity is expected at the level of the C5 vertebral body	• Reported individually and as a group • The stimuli gave an increase of BOLD signal (activation) in 3 different locations of the spinal cord and brain stem: • First, activations could be seen in the spinal segment corresponding to the stimulated dermatome in 7/9 subjects for c6 stimulation, 2/8 for c7, and 3/8 for c8 (transmission to dorsal horn interneurons) • Second, activation in the medulla oblongata was evident in 4 subjects, most likely corresponding to the location of the nucleus cuneatus • Third location (strongest and most reliable) was in the c3 and c4 segments. Activation at these spinal levels was almost invariably observed independently of the dermatome stimulated (9/9 for c6, 8/8 for c7, and 7/8 for c8 stimulation)
Govers (2007) n = 12	Finger-tapping (right hand)	• Intensity: self-determined force of apposition of the different fingers towards the thumb • Frequency: individually fixed rapid rhythm • Interval: Rest and activation were alternated, repeated 3 times • Duration: 30-s epochs	• BOLD • T2-weighted gradient-echo echo-planar imaging on a 1.5-T clinical unit was used • Cord activation was measured in the transverse imaging plane, between the spinal cord levels	• T1-weighted anatomical images; mid-sagittal section was used to position the fMRI sequence • Cervical segments were selected based on adjacent vertebral bodies • Inferior vertebral notch was used to estimate the location of the cervical nerve root	• Reported individually and as a group • No significant difference between activation at (or adjacent to) the dorsal or ventral horns was found • While regions of activation were distributed throughout the spinal cord, concentrated activity was found at the anatomical location of expected motor innervation, namely nerve root C8, in 6 of the 12 subjects • The location of neuronal activation (spinal cord segment C5 through T1, with a peak on C8) corresponds to the craniocaudal anatomical location of the neurons that activate the muscles in this complex motor task

			C5 and T1 • Slice thickness: 3 mm		
Maieron (2007) n = 13	Motor activity (finger tapping) (both hands – expt 1; dominant (right) hand – expt 2)	Experiment 1: finger opposition (n=11) • Intensity: self-set • Frequency: 0.5 Hz • Interval: block design; 20 s periods of alternating rest and movement (8 movement periods, 9 rest) • Duration: Total of 17 periods over 340 s Experiment 2: 3 conditions sequentially alternating: finger tapping of dominant (right) hand at two rates and alternating in a fixed order (n=12) • Intensity: self-set • Frequency: 0.5 Hz (low) and max ~ 1Hz (high-subject set) • Interval: 6 periods of finger tapping for each rate, each period of movement alternated with 30 s periods of rest • Duration: 25 periods total, 750 s	• BOLD • A 3-T GE scanner was used • 10 oblique slices approximately perpendicular to the longitudinal axis of the spinal cord were positioned from C7-C5 • Slice thickness: 4.5 mm	• fMRI slices were positioned from the 5th to 7th cervical vertebral body	• Reported as a group Experiment 1 – • Right-hand finger tapping was performed at an average rate of 0.6 ± 0.4 Hz, and the average number of errors across the four blocks was 0.7 ± 1.4 • Left-hand finger tapping was performed at an average rate of 0.5 ± 0.3 Hz, and the average number of errors across the four blocks was 1.5 ± 2.3 • Difference in rate and errors between right- and left-hand movements was not significant ($p < 0.1$) Experiment 2- • Motor task was executed with the right hand only • The low-rate finger tapping was performed at an average rate of 0.5 ± 0.1 Hz, and the average number of errors across the six blocks was 0.03 ± 0.08 • The high-rate finger tapping was performed at an average rate of 1 ± 0.1 Hz • Average number of errors across the six blocks was 0.5 ± 0.8 • Differences in rate and errors between the two movement rates were both significant ($p < 0.0001$ and $p < 0.05$, respectively) Spinal cord activity (experiment 1) • In each subject, clusters showing signal increases related to right or left finger movements were present on both sides of the cord (both ipsilateral and contralateral to the moving hand) • Peak percentage increases of fMRI signals were significantly higher on the side of the cord ipsilateral to the moving hand (3.59 ± 0.46 vs 2.80 ± 0.23%; $t = 2.62$; $p < 0.05$) • A trend toward higher increases during movements of the right hand was also observed ($p < 0.06$) • A significant side difference was

					found, with a larger extent of clusters in the hemi-spinal cord ipsilateral to the moving hand ($p < 0.001$) Frequency-dependent activity during right-hand movements (experiment 2) • Significant effect of movement rate ($p < 0.05$) and of side (with higher values on the side of the cord ipsilateral to the moving hand; $p < 0.01$) on the intensity of signal increases • On the ipsilateral side, fMRI signals related to high movement rates were significantly higher than those related to the low movement rates ($p < 0.01$) • A trend toward higher signals during higher movement rates was found on the contralateral side ($p < 0.1$) • The overall spatial extent of movement-related clusters was not significantly different for the two movement rates
Xie (2007) n = 6	Electrical stimulation of the median nerve	• Intensity: 0.2 ms constant current pulses • Frequency: 20 Hz • Interval: 3 cycles of stimulation periods alternated with 4 rest periods • Duration: 35 s stimulation periods, 49 s rest periods; total of 43 time points recorded	• SEEP • A 1.5-T MRGE imaging system equipped with a standard neck coil was used with single shot fast spin echo imaging sequence • 7 slices in the sagittal and 7 in the transverse plane • Slice thickness: sagittal: 2.8 mm, transverse: 7 mm	• Transverse slices were aligned to adjacent vertebral bodies • The authors note that vertebral levels C5-C7 correspond to spinal cord segments C6-T1	• Reported as a group • Activation correlated with the time course of stimulation was consistently detected in both sagittal and transverse imaging planes of the cervical spinal cord • Most functional MR imaging response located between the vertebral levels C5 and C7, corresponding to the spinal cord segments C6-T1 • Dorsal activation localized on the ipsilateral side of the spinal cord in most subjects, but activation of the contralateral side spinal cord observed in 2 subjects • Regions of the spinal cord associated with motor and pain response were observed by 20Hz functional electrical stimulation of the median nerve
Lawrence (2008) n = 7	Vibration stimulation of the biceps (C5), wrist	• Intensity: NR • Frequency: 50 Hz • Interval: paradigm	• SEEP • A 1.5-T clinical MR system with a	• Cervical, lumbar and sacral segments were selected based on	• Reported as a group • The peak number of active pixels was observed at the expected level of the spinal cord with some activity in the adjacent

	(C7), right palm (C8-T1), patella (L4) and Achilles tendon (S1)	consisting of 7 alternating rest and stimulation conditions with 8 volumes acquired during each block (total of 56 volumes) • Duration of intervals: NR	phased array spine coil was used • Spinal fMRI data were acquired from 7 transverse slices • During biceps stimulation, slices were positioned spanning vertebrae C4 to C7; wrist and palm: C6 to T12; lumbar spinal cord studies: T10 to L1 • Slice thickness: 7 mm	adjacent vertebral bodies	segments • Biceps: bilateral activity in the ventral horns at C5 vertebral level, and in the right dorsal horn at C5/C6 disc • Wrist: right dorsal horn at C6/7 disc, left dorsal horn at C7 vertebra, and bilaterally in the ventral horns at T1 vertebra • Palm: left dorsal horn at C6/7 disc and right and left ventral horns at C7 vertebra • Patella: right dorsal horn at T11 vertebra and left dorsal horn at T11/12 disc • Achilles tendon: mainly ventral horns, but also intermediate zone of T11/12 disc • The rostrocaudal distribution of activity was observed to correspond to the dermatome being stimulated • Cross-sectional localization of activity was primarily in dorsal areas but also spread into ventral and intermediate areas of the gray matter
Ng (2008) n = 10	Motor: Finger tapping with either right or left hand; sequential (LS or RS) or interleaved (LI or RI)	• Intensity: self-set • Frequency: rate of 1 Hz in a self-paced manner • Interval: block design; 4 cycles of alternating rest and motor periods, acquiring 10 scans per period • Duration: completed finger-tapping sequences in a self-paced manner	• BOLD • A 3 T MR system was used with a multi-element spine coil from C1-C7 • 13 axial slices were used • Slice thickness: 5 mm	• Cervical segments were selected based on adjacent vertebral body centers or intervertebral discs	• Reported individually and as a group • For the difficulty measurement test, the time for doing 20 cycles of the interleaved tasks (LI and RI) was significantly longer than for the sequential tasks (LS and RS) ($P < 0.001$) • 7/10 subjects exhibited BOLD activation in all four fMRI sessions • Comparison between left and right handed tasks- mean contrast value of the activation areas in the LS task was significantly higher than that in the RS task, while there was no significant difference between the LI and RI tasks • There was a trend toward an increase in the mean contrast value on the ipsilateral side in the LS task, although it did not pass the statistical threshold • Although the percentage signal change showed a trend similar to contrast value, it was not statistically significant

Valsasina (2008) n = 12	Proprioceptive (passive, flex-ex of the wrist) and tactile (tapping palm with wooden spoon) stimulation (right hand)	• Intensity: Force = 2N • Frequency: 1 Hz • Interval: block design, 4 periods of rest alternated with 4 periods of activity (each period consisting of 5 measurements) • Duration of each period: NR	• SEEP • A 1.5 T scanner with a phased-array neck coil was used with a multi-shot turbo sequence • 9 contiguous axial slices covering segments from C5-C8 were acquired • Slice thickness: 7 mm	• Cervical segments were selected based on adjacent vertebral body centers or intervertebral disks	• Reported as a group • Model-based approaches (cross-correlation (CC) and general linear model (GLM)) revealed similar patterns of activity • Independent component analysis (ICA) could identify a component correlated to fMRI stimulation, although with a lower statistical threshold than model-based approaches • Model-based approaches seem to be more robust for estimating task-related activity, whereas ICA seems to be useful for eliminating noise components from the data • Combined use of ICA and GLM might improve the reliability of spinal fMRI results
Agosta (2009) n = 12	Tactile stimulation of the palm, right hand (wooden spoon)	• Intensity: Force = 2N • Frequency: 1 Hz • Interval: Block design with 4 periods of rest alternated with 4 periods of activity (each period of rest and activity consisting of 5 measurements) • Duration of each block: NR	• SEEP • Used a proton density (PD)-weighted spin-echo (SE) fMRI in a 1.5 T clinical MR system to assess cervical cord recruitment • 9 axial slices covering segments from C5-C8 • Slice thickness: 7 mm	• Cervical cord segments C5 to C8 were selected based on adjacent vertebral bodies and discs	• Reported as a group • During tactile stimulation, subjects showed a higher occurrence of fMRI cord activity in the right than in the left cervical cord (odds ratio = 2.25, 95% CI = 1.31-3.87, $P = 0.003$) • No significant difference in the frequency of activity in the anterior versus posterior portions of the cord was detected ($P = 0.41$) • A significant heterogeneity in frequency of fMRI activity between cord levels was observed ($P < 0.001$), with the highest frequencies of fMRI activity detected at C6 and C7
Stroman (2009) n = 15	Thermal sensory stimulation (right hand)	• Intensity: baseline (32˚C), stimulation periods (29, 25, 22, 18, and 15˚C) • Frequency: NA • Interval: 3 stimulation	• SEEP • A 3 T fMRI with a phased-array spine receiver coil, using a half-Fourier, single-shot, fast spin	• Cervical segments were selected based on adjacent inter-vertebral disks	• Reported as a group • Ipsilateral dorsal gray matter (dGM), the primary site of sensory input, also receives inhibitory input from the rostral ventromedial medulla and the locus coeruleus, two components of the brainstem opiate analgesia system • Ipsilateral ventral gray matter (vGM) receives input from the

		periods alternated with 4 baseline periods, carried out 5 times • Duration: baseline: 72 s (8 volumes), except for initial baseline period of 81 s; stimulation: 45 s (5 volumes)	echo sequence was used • 9 contiguous sagittal slices were imaged spanning from above the thalamus to below the C7/T1 intervertebral disc • Slice thickness: 2 mm		ipsilateral dGM and inhibitory input from the pontine reticular formation, which is involved with coordination of movements by modulation of ventral horn cells • Contralateral vGM regions appear to receive input from only the ipsilateral dGM in these studies
Ghazni (2010) n = 8	Touch and brush (mechanical) sensory stimuli (right hand)	• Intensity: manual stimulation by using 2 or 15g von Frey filaments or 2-cm-wide artist brushes (soft or hard) • Frequency = 1 Hz • Interval: block paradigm consisting of 3 stimulation periods interleaved with baseline periods in which no stimuli applied • Duration: 56 seconds of stimulation, 140 seconds of no stimuli, and an initial baseline of 84 seconds for a total of 11 minutes 12 seconds for each experiment	• SEEP • fMRI studies were carried out in a 3T Magnetom Trio by using a phased array spine receiver coil • 14 contiguous sagittal image sections were selected to span from the C7/T1 disk to the superior edge of the thalamus • Slice thickness: 2 mm	• Cervical segments were selected based on adjacent inter-vertebral disks	• Reported as a group • The 2g von Frey filament showed predominant activity in the medulla around the ipsilateral dorsal gracile and cuneate nuclei • The 15g filament elicited significant activity in the ipsilateral dorsal and contralateral ventral gray matter areas of the spinal cord, areas around the olivary nuclei, pontine reticular formation, periaqueductal gray, and raphe nuclei in the rostral pons and midbrain • The brush stimuli elicited more activity in the medulla around the ipsilateral cuneate and gracile nuclei • The 2g filament and brush stimuli activated areas associated with a touch response, while the 15g filament activated areas associated with a pain response
Summers (2010) n = 11	Noxious (laser) and innocuous (brush)	• Intensity: laser energy = 3.5 J; light brush strokes = 200-	• BOLD • A 3T scanner using the	• Cervical segments were selected based on adjacent	• Reported as a group • Averaged peristimulus signals from all voxels within each half of the spinal cord showed

	somatosensory stimuli (left hand)	400 mN • Frequency: heat pulses = 0.45 Hz; brush strokes=2 Hz • Interval: 2 runs (rest and stimulation); stimulation run: 6 laser and 6 brush stimuli were delivered in separate blocks, alternated with blocks of rest; rest run: same time but with no stimulation • Duration: initial and final rest blocks were 40-s, all other blocks 20-s; total of 9 min, during which 135 spinal volumes were acquired	neck and two posterior coil elements of a neurovascular coil array was used with a gradient-echo, echo-planar imaging sequence involving four segments • 15 contiguous para-axial slices C4-C7 • Slice thickness: 4 mm	intervertebral discs and vertebrae	bilateral fMRI responses to both stimuli • These responses were significantly larger during noxious than innocuous stimulation • A voxel population preferentially responding to noxious stimulation extended rostro-caudally over the length (4 cm) of the explored spinal cord region • By contrast, no evidence of voxel populations responding uniquely to innocuous stimuli, or showing decreased activity following either kind of somatosensory stimulus was found • These results provide the first false-positive-controlled comparison of spinal BOLD fMRI responses to noxious and innocuous stimuli
Stroman (2011) n = 25	Thermal sensory stimulation of the hand while looking at "attention state" (right hand)	• Intensity: baseline (32˚C), thermal stimulation (15˚C) • Frequency: NA • Interval: block design, 4 thermal stimulation blocks interleaved with baseline conditions, for each protocol • Duration: baseline- 63 s, stimulation- 45 s -Protocol 1: 2 repeated experiments (4 total), rating discomfort	• SEEP • A 3 T phased-array spine receiver coil, and posterior neck coil, with a half-Fourier single-shot fast spin-echo sequence with the echo time set at minimum (38 ms) • For protocols 1 and 2, data were acquired spanning the T1/C7 disc to the	• Cervical segments were selected based on adjacent vertebral bodies	• Reported as a group • Attention state had a significant influence on the activity detected in the cervical spinal cord, as well as in brainstem regions involved with the descending analgesia system • The subjective ratings obtained during "Rating" tasks, and the responses provided during "Movie," "Detect," or "Challenge" tasks indicate that the participants performed the tasks correctly, and that their attention states and experiences of the thermal stimuli were successfully altered by the tasks • Activity was consistently observed in localized regions of the ipsilateral dorsal gray matter (dGM) and in the ipsilateral ventral gray matter (vGM) in C6-C8 • The direction of the signal changes (positive or negative) was not the same between the "Rating" and cognitive tasks

		from thermal stimulation or actively watch a movie (N=11) -Protocol 2: rating interleaved with detect tasks (characterizing moving dots) (N=5) -Protocol 3: rating interleaved with challenge tasks (mentally-challenging multiple-choice questions) (N=9)	rostral limit of the thalamus • Protocol 3 spanned from the T1/C7 disc to above the cingulated gyrus • All images acquired in thick, contiguous sagittal slices • Slice thickness: 2 mm		• Attention state can modulate neural function in the human spinal cord during thermal sensory stimulation

Table 2-8. A summary of motor and sensory paradigms utilized in spinal fMRI studies.

MOTOR PARADIGMS		
Study	**Paradigm design**	**Rationale**
Yoshizawa (1996)	Hand-clenching task	To demonstrate the first application of BOLD fMRI in the human spinal cord
Stroman (1999)	Squeezing a rubber ball	To investigate the feasibility of spinal fMRI at 3T
Backes (2001)	Fist clenching compared to electric stimulation of the median nerve	To compare the reliability of a user dependent task (fist clenching) with a user independent task (electric stimulation)
Madi (2001)	Isometric movements of upper extremity muscles: biceps, wrist extensors, hand abductors	To determine the feasibility of spinal fMRI at 1.5T; To determine the spatial extent of spinal fMRI signal changes to upper extremity motor tasks; To determine if the force of isometric contraction is related to the strength of fMRI signal change
Stroman (2001)[%]	Squeezing a rubber ball	To investigate spinal fMRI activation patterns with respect to the BOLD response function
Kornelsen (2004)	Ankle dorsi- and plantar flexion	To test the efficacy of spinal fMRI measurements during motor stimulation of the lower limbs
Govers (2007)	Finger-tapping	To demonstrate sensitivity and resolution of spinal cord functional activity at 1.5T.
Maieron (2007)	Finger-tapping task – dominant vs. non-dominant; high frequency vs. low frequency	To investigate the quantitative relationship between the side and repetition rate of willed motor activity and spinal fMRI signal changes
Ng (2008)	Finger tapping – dominant vs. non-dominant hand; sequential vs. interleaved	To determine the effect of dexterity on the spinal fMRI signal change in right handed persons
SENSORY PARADIGMS		
Study	**Paradigm design**	**Rationale**
Stroman (2001)[%]	Pneumatic air puffs	To investigate spinal fMRI activation patterns with respect to the BOLD response function
Stroman, Krause (2002)	Cold stimulation (5-7˚C)	To investigate the spatial distribution of activity detected with spinal fMRI
Stracke (2005)	Tactile stimulation using a pneumatic device	To apply the tactile stimulus to a small region of a specific dermatome in order to determine if activation of few mechanoreceptors and hence few primary afferent fibers could be detected
Xie (2007)	Electric stimulation of the median nerve	To determine the spinal fMRI activation pattern of 20Hz electric stimulation
Lawrence (2008)	Vibration stimulation	To examine the areas of the spinal cord that were activated in response to vibration and to map the spatial extent of active pixels
Valsasina (2008)	Proprioceptive (passive wrist flexions and extension) and tactile (tapping palm with a	To investigate different spinal fMRI data analysis methods

	wooden spoon) stimulation	
Agosta (2009)	Tapping palm of hand with wooden spoon	To investigate the transverse and rostro-caudal distribution of tactile associated activity in the human spinal cord
Stroman (2009)	Cool stimulation (29˚C, 25˚C, 22˚C, 18˚C and 15˚C)	To determine the spatial extent of innocuous thermal stimulation
Ghazni (2010)	Pressure stimulation with von Frey filaments and soft touch with an artists brush	To map areas of neuronal activity associated with touch and brush sensation
Summers (2010)	Noxious laser stimulation and innocuous brush stimulation	To investigate the intensity and spatial extent of spinal fMRI signal changes in noxious vs. innocuous stimulation
Stroman (2011)	Cool stimulation (15˚C) in the presence or absence of cognitive tasks to distract the participant from the thermal stimulus	To determine if a persons attention state influences the spinal fMRI response to thermal stimulation

2.6.3.1 Localizing the fMRI signal to an anatomical region of the spinal cord

The majority of studies use the adjacent spinal column (vertebral bodies and intervertebral discs) to choose either a region of interest (if a limited portion of the spine is imaged as a functional dataset) or to describe the location of active voxels in spinal fMRI datasets. One study used the inferior vertebral notch as an anatomical landmark for the location of the corresponding cervical nerve root.[195] Four studies note that the expected location of functional activation of any particular dermatome or myotome is roughly one vertebral body level above the intervertebral foramen that contains the nerve root supplying that dermatome or myotome.[128]

2.6.3.2 Inducing neural activity in the spinal cord: the choice of a stimulation paradigm

Eight of the studies utilized a motor stimulation paradigm, 10 used a sensory stimulation paradigm and a single study compared a motor and sensory stimulus. The different motor and sensory stimulation paradigms are listed in Table 2 along with the rational for the investigation as declared by the authors of the paper.

Motor stimulation paradigms:

The most common motor paradigm utilized involved the hand by employing either a finger-tapping paradigm or a fist-clenching paradigm.[128] Hand movements are a complex task that involves both sensory (mechanoreceptive and proprioceptive information) and motor activity at multiple levels of the spinal cord. The complexity of the task can vary if individuals recruit forearm muscles in addition to hand intrinsic muscles. As such, there was a range of results reported among these studies. (See Table 1 for full details) The first spinal fMRI experiment conducted in humans[128] acknowledged that a hand-clenching task is expected to activate range of neurons across many spinal segments. In addition, this group actively coached participants to recruit forearm muscles, presumably to generate the most robust change in neuronal activity in order to demonstrate the ability to detect an fMRI signal in the spinal cord. Indeed, they report locales of activation in the ipsilateral intermediate and ventral gray matter across multiple spinal segments. In contrast, using a finger-tapping paradigm, Govers *et al.* noted a wide variation of

activation pattern across subjects, to the point where they failed to show statistically significant differences between adjacent levels of the spinal cord, between the right and left side or between levels of the same side.[195] They do note however that peak activation in individual subjects occurred at the level of the C7 vertebral body, which corresponds to the level where one would expect nerve rootlets from the C8-T1 region. In contrast to these results, Maieron *et al.* provide evidence for both the spatial extent of movement related clusters (also using a finger-tapping paradigm) and peak signal increases ipsilateral to the moving hand. In addition, they demonstrate that the intensity of the signal change was larger during high frequency finger tapping in comparison to low frequency finger tapping but the spatial extent of activity remained constant (see Table 1 for full details).[196] Building on the concept of specificity of activation, one study investigated isometric movements of specific muscle groups of the upper extremity.[197] This is an important contribution as the authors attempt to isolate specific cervical nerve roots for investigation with spinal fMRI. The authors were able to demonstrate that by targeting different muscle groups (biceps, C5/C6; wrist extensors, C6/C7; and hand abductors, C8/T1) they found a corresponding difference in the location of activation whereby the biceps task resulted in activity in a more rostral position along the cord, hand abduction in a more caudal position and wrist extensors in between.

Sensory stimulation paradigms:

Eleven of the 19 studies reviewed utilized a sensory stimulation paradigm.[128] Five studied mechanical stimulation,[128] three studied thermal stimulation,[128] and there were single studies investigating vibration,[198] laser (focused thermal heat)[128] and electrical stimulation.[199] Of the mechanical stimulation studies Agosta *et al.* report that right hand mechanical stimulation resulted in predominantly right-sided functional spinal cord activation at the C6 and C7 vertebral levels.[128] In contrast, Ghazni *et al.* reported an overall higher number of active voxels in the spinal cord when comparing a 2g with a 15g von Frey filament but there was no statistical difference between specific regions of the spinal cord. There was significant difference in the thalamus.[128] Stracke *et al.* took careful consideration of the dermatome stimulated by mechanically stimulating an area of skin approximately 2-3 mm, much smaller than stimulated in other studies.[200] They demonstrated inconsistent results when examining the spinal cord zones corresponding to the dermatome stimulated (C6, C7 or C8) but noted a rather robust finding of stimulation of the upper cervical spine (C3-C4) in 24 of the 25 trial runs reported. The three

thermal spinal fMRI studies reported the effect of cooling the skin to various temperatures as low as 5-7 degrees Celsius. Stroman *et al.* noted that the distribution of active voxels was higher when the forearm was cooled in comparison to the palm of the hand.[201] This same group reported that cooling the skin of the palm resulted in ipsilateral activity in the dorsal and ventral spinal gray mater and the contralateral ventral horn.[202] Figure 2-7 is an example of how thermal stimulation results are displayed on a group level. Important to note is the activation patter both at the level of stimulation and within the brainstem. In addition, one can appreciate the active voxels in the right-left distribution across the spinal cord.

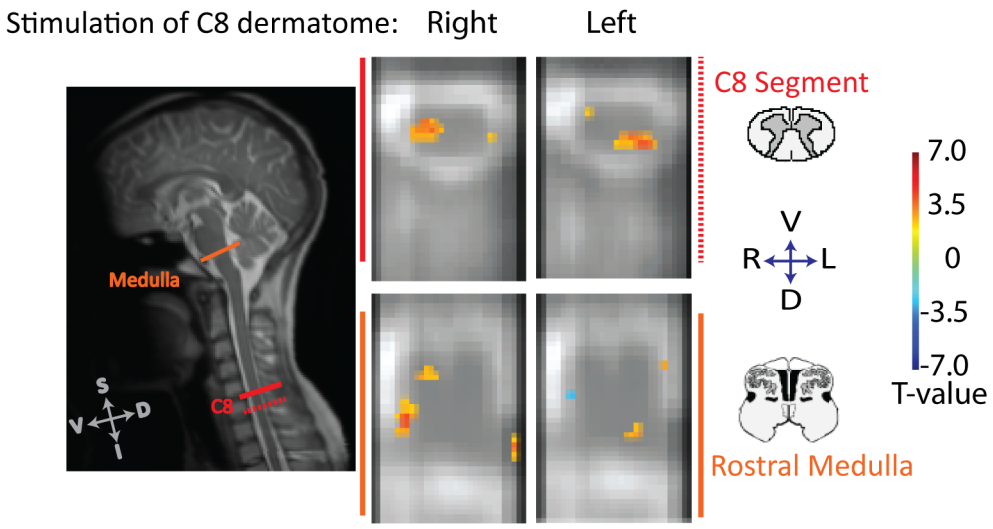

Figure 2-7. Example of spinal fMRI results using SEEP contrast. Thermal sensory stimulation was applied to four different locations (hands and arms, right and left sides), investigating the normal patterns of activity in the spinal cord and brainstem. Selected group results (n = 10) are shown in axial slices (with locations indicated on the sagittal view on the left) for stimulation of the hand on the right and left sides corresponding to the 8th cervical spinal cord segment (C8), with results shown at the level of the C8 segment and the rostral medulla. The correpondence between the side of stimulation and the side of activity within the cord, is clearly visible within the C8 segment. Note that the images are in radiological orientation (dorsal is toward the bottom, the right side of the body is to the left in the image).

Application of a vibration stimulus to different dermatomes of the upper and lower extremity resulted in a rostral-caudal distribution of active voxels that roughly correlated with the stimulated dermatome.[198] The activity present in adjacent segments is of uncertain origin and may be attributed to either methodological limitation of the study or to branching of afferent fibers to adjacent spinal segments. With the detailed hypothesis that nociceptive stimulation induces widespread spinal cord responses including extension to the contralateral side of stimulation (activity that is purported to result from reflex arcs and intraspinal projection systems)[203], Summers *et al.* used a laser to induce a noxious stimulus and compared this to innocuous brushing of the left hand.[128] They demonstrate that noxious stimulation results in a significantly greater spinal fMRI response when compared to innocuous brush stimulus and that the noxious spinal response was bilateral. This study is also unique because the false positive rate of spinal activation was estimated from rest scans; The authors used this information to demonstrate that the magnitude of spinal response to noxious stimulation was above the false positive rate.

As outlined in Table 2-8, the majority of spinal fMRI studies were designed to map the spinal cord response to specific stimuli. Classic radiological tests are usually defined in terms of their sensitivity and specificity. Quantification of a test in this way helps the interpreter decide what signal is due to the entity under study and what may be due to artifact; For example, the detection of a tumor in the case of pathology-anatomical imaging studies or, in our case, the detection of a spinal fMRI signal that corresponds to the activity of neurons. Of the 19 studies reviewed here, we identified 3 that attempted to strengthen the evidence for a neural basis for spinal fMRI signals. The first, by Madi *et al.* demonstrated that the force applied to a particular muscle group (i.e. biceps muscle) demonstrated a linear relationship with the percentage signal change within a voxel.[197] The second study used a rest run to estimate the false positive rate of activation.[128] In this study, the subjects underwent two spinal fMRI runs in the same experiment: an experimental run in which the sensory stimuli were applied and a rest run in which no stimuli were applied. The order of these two runs was balanced among the 11 participants. The authors used the data to estimate the false positive rate to ensure that the data acquired in the functional run was not only above the baseline of the block paradigm design but also above any false

positive activation that might be expected for unknown reasons. The third combined the above mentioned principles together: Maieron *et al.* utilized both a rest run to estimate the false positive rate and studied the effect of frequency of hand movements on the intensity and spatial extent of signal change.[196] They demonstrated that the spinal fMRI signal change was significantly above that of a rest run and while the spatial extent of activity did not change based on the frequency of finger-tapping, the intensity of the signal change did however, thus providing rather strong corroborating evidence for the neural basis of the spinal fMRI signal.

2.6.4 Discussion and Conclusions

The above represents a systematic review of all spinal fMRI studies conducted in healthy humans. Fourteen of 19 spinal fMRI studies reviewed here were designed to demonstrate the feasibility of spinal fMRI, the signal change in response to a specific stimulation paradigm or the spatial distribution of a spinal fMRI signal.[128] The remaining five were designed to investigate the effect of a user dependent task versus a user independent task,[204] to determine the effect of dexterity on hand motor tasks,[205] to investigate the effect of attention state on spinal fMRI signals,[206] to compare different data analysis methods,[207] and to investigate the spinal response to pain.[128] Although there are some differences in the results of various studies, even when similar stimulation paradigms were used, this body of literature supports that spinal fMRI signals can be obtained from the human spinal cord. The different results between studies could stem from a number of sources: slightly different stimulation paradigms, differences in MR systems at different research institutes, and the plethora of data analysis techniques utilized.

Localizing the fMRI signal to an anatomical region of the spinal cord

As alluded to above, hand motor tasksrepresent a complex array of both motor and sensory information that is processed through multiple peripheral nerves that send information to spinal segments C6 through T1 and may involve C5 in some cases. The majority of studies reviewed here use the vertebral bodies as markers for the specific spinal segment of interest. While this is most certainly a reasonable estimate of the spinal segments, for example the C5 vertebral body is a reasonable estimation for the location of entering / emerging C6 spinal nerve rootlets, Lang and Bartram, in an anatomic dissection study, point out that there is variation among individuals with regard to the rostral-caudal location of nerve rootlets as they emerge from the spinal cord to form the cervical nerve roots.[208] This anatomical variation stems from the fact that the spinal column

continues to grow after the spinal cord has attained its greatest length.[209] Furthermore, we know that degenerative changes can occur in the spinal column resulting in population variation in vertebral body and intervertebral disc height.

Inducing neural activity in the spinal cord: linking the stimulation paradigm to the fMRI signal

Neurovascular coupling describes the relationship between neuronal activity and the resultant change in blood flow to that portion of the central nervous system.[181] While the complex details of this relationship are still being unraveled, the fMRI signal obtained from either the BOLD or SEEP contrast mechanism purports to stem from vacular changes that can be traced back to the activity of specific populations of neurons. Several studies reviewed here attempt to strengthen our understanding of the relationship between neuronal activity and the spinal fMRI signal by going beyond the classic block paradigm design of comparing signal change at alternating time points of stimulus and rest. For example, Govers *et al.* designed a study in order to investigate the sensitivity of spinal fMRI to detect spinal cord activity in response to a finger-tapping paradigm by comparing the degree of activation at the expected level and compared it to adjacent levels on the contralateral side; each comparison revealed a negative result and the authors concluded that finger-tapping could not be detected with a reliable degree of sensitivity.[195] Porro's group has twice used the concept of rest-run's to estimate the degree of false positive activation patters whereby the data analysis methods are used in both the experimental run (where the subject completes the specified task) and the rest-run (where the subject simple lies still during the acquisition of functional data).[128] Last, two studies investigated the effect of altering either the intensity[197] or the frequency[196] of the stimulus and its effect on the spinal fMRI signal. In doing so, the authors are suggesting that by making the spinal population of neurons 'work' more, the resultant neurovascular coupling response should be greater and we should see a relationship between the stimulus and the spinal fMRI response. In both cases this result was evident, providing credence to the notion that the spinal fMRI signal is a result of the neurons activated by the isometric muscle activation[197] or the finger-tapping paradigm.[196]

Spinal fMRI as a method to improve our understanding of spinal cord function

Structural (tracer studies) and functional (electrophysiology) studies have formed the basis of our understanding of how the spinal cord functions. Spinal fMRI offers a non-invasive means to investigate the human spinal cord with a unique spatial and temporal resolution that has potential

to build on knowledge obtained from more invasive means. For example, the spinocervicothalamic pathway was first described in 1955[210] as a sensory pathway receiving information from the periphery and transmitting it to the thalamus with a relay nucleus in the cervical spine. This relay nucleus, the lateral cervical nucleus, is a special group of neurons located just lateral to the dorsal horn in the C1-C3 region of the spinal cord. Its existence has been demonstrated in many mammalian species, including monkeys.[211] The presence of a lateral cervical nucleus in humans has been debated with evidence presented both for and against its existence.[128] Using a tactile sensory stimulation paradigm, Stracke *et al.*[200] compared delivery of this stimulus to either the C6, C7 or C8 dermatome of the right hand. (See Table 2-7 for full details) Interestingly, when the spinal cord data was analyzed, the authors conclude that activation occurred in the spinal segment corresponding to the stimulated dermatome occurred in 7/9 subjects for C6 stimulation, 2/8 for C7, and 3/8 for C8, a less robust result than was anticipated. The strongest and most reliable activation in the spinal cord actually occurred in the upper cervical spine, in the region of C3-C4. Here, the authors report significant activation in 9/9 subjects for C6 stimulation, 8/8 for C7, and 7/8 for C8 stimulation. This anatomic location corresponds to the purported location of the lateral cervical nucleus in animal and postmortem human studies. A similar finding was noted in Govers *et al.* study.[195] However, we only speculate that the unexpected results of Stracke *et al.* and Govers *et al.* could be evidence for a controversial sensory pathway in humans. With a properly designed spinal fMRI study in a large enough study population, long outstanding questions in neurobiology may begin to reveal answers. Furthermore, with the application of connectivity analysis techniques it may be possible to investigate how these distinct neuronal populations work together to allow for the transmission of information to and from the brain.

Conclusions

A total of 19 peer-reviewed publications utilizing spinal fMRI to investigate the human spinal cord have been reviewed in detail. There are challenges associated with accurately identifying regions of the spinal cord along its rostral-caudal axis along with the spatial extent of activity that might be expected in different stimulation paradigms. In addition, emphasis was placed on studies that put particular attention on the relationship between neuronal activity and the resultant fMRI signal and outline the different methods that were utilized to demonstrate this. Last, a brief introduction to neurovascular coupling as the mechanism that links neuronal activity

with the glial-blood vessel response is presented, as it is this response that underlies the BOLD signal and is presumed to underlie the SEEP signal but there is no direct evidence of this to date. As spinal fMRI methods and experimental designs improve in the coming years, this technology will provide further insight into both the normal functioning human spinal cord and how motor and sensory circuits adapt in response to pathology, and spinal cord injury in particular.

Chapter 3
Rationale and Specific Aims

3 Rationale and Specific Aims

The general aim of this thesis is to investigate the use of magnetic resonance imaging biomarkers in the context of providing clinical care for spinal cord injury patients. Study I establishes how intramedullary T_1 and T_2 weighted signal changes have been historicially used to infer damage to the spinal cord along a spectrum of injury severity. This builds on an extensive pre-clinical animal literature that establishes a range of pathophysiological events that occurs at the epicenter of traumatic spinal cord injury.[9] Study I answers the research question of whether intramedullary signal characteristics offer an advantage over standard clinical assessments to predicting outcome after traumatic spinal cord injury. Study II uses novel spinal fMRI methods to characterize the effect of traumatic spinal cord injury adjacent to the epicenter of damage, both above and below the level of injury. Completed within the context of chronic injury, the specific aims of this work are centered on capturing changes to the processing of afferent information whereby pre-clinical animal investigations of plasticity after traumatic spinal cord injury support the notion of decreased GABAergic activity in combination with axonal sprouting and regeneration, phenomenon that this work supports in humans for the first time.[128] Study III addressess a specific question raised through the reaserch conducted in study II and aims to characterize the distribution of vertebral and spinal segments across individuals relative to a fixed point in the brainstem. Using novel methods, the work presented in Study III establishes that significant variation exists in the segmental anatomy across individual subjects and that this variability should be considered in the analysis of advanced imaging data to accurately localize specific populaitons of neurons.

Each of the three studies presented herein provide new knowledge with regard to the use of both standard and advanced MRI-based techniques to investigate SCI patients with the ultimate aim of improving our collective understanding of spinal cord injury and patient care. The rationale and specific aims for each of these studies are provided below.

3.1 Study I. Magnetic resonance imaging as a prognostic tool in acute SCI: establishing sensitivity and specificity

With the adoption of magnetic resonance imaging into clinical medicine in the 1980's, clinicians treating patients for spinal cord injury saw immediate benefit in terms of being able to visualize the damaged spine. Clinicians were suddenly able to characterize the pattern of injury and take an inventory of damaged tissues such as the vertebral column, inter-vertebral discs and the posterior ligamentous complex, the benefits of which were immediately applied in terms of surgical planning and decision-making. Traumatic injury involving primarily the posterior elements was approached with surgical decompression and fusion from a dorsal midline surgical approach whereas traumatic injury disrupting the ventral disco-ligamentous complex was more suited with an anterior cervical approach. Slower to be implemented was the use of MRI technology to visualize the spinal cord itself and use the signal characteristics of standard T_1 and T_2 weighted images as a biomarker to reflect the degree of underlying pathology. Several different clinical research groups utilized changes in T_1 and T_2 weighted imaging signal characteristics to advance our understanding of traumatic spinal cord injury. This line of resarech occurred concurrently along pre-clinical animal research investigating eventings occurring at the epicenter of traumatic spinal cord injury and how these events affect patient outcome. As an extreme example, visualization of spinal cord trans-section had not been possible before the advent of MRI; knowledge of this severe injury pattern confirms a poor prognosis. Much less clear was the multitude of other signal characteristics such as a subtle T_2 hyper-intensity with normal T_1 signal or mixed T_1 and T_2 signal. This pattern of signal change in the damaged spinal cord was thought to reflect cavitation and necrosis by one research group and spinal cord edema by another.[128] Despite not being able to agree on the underlying pathological correlates of specific signal characteristics, there was motivation at this time to utilize this information to guide the management of patients, mainly in terms of an additional piece of information to add to the diagnosis of spinal cord injury and hopefully offering the prospect of a more reliable prognosis than clinical examination alone.

The time period from roughly 1980 to 2010 represents the first application of MR-based biomarkers for use in spinal cord injury patients. The pioneers at the time were most assuredly amazed at their ability to visualize the human spinal cord, a feat not possible by their mentors only a few years earlier, and at a loss for how to use this information to best care for their

patients with a debilitating condition. The **primary aim of Study I** is to examine the historical context with which T_1 and T_2 weighted intramedullary signal characteristics were first used as MR-based imaging biomarkers in the setting of traumatic spinal cord injury. This aim was accomplished by systematically reviewing all clinical studies that incorporated the use of MRI into the clinical care of traumatic spinal cord injury patients.

Specific Aims:

1. To characterize the different combinations of intramedullary signal characteristics captured from standard T_1 and T_2 weighted images across the studies obtained by systematic review.

2. To outline how the patterns of signal characteristics identified in aim 1 serve as biomarkers to classify patients along a spectrum of injury severity.

3. To calculate the sensitivity and specificity with which with above stated biomarkers could predict neurological function at follow-up.

4. To determine if standard anatomical T_1 and T_2 weighted intramedullary signal changes offer an advantage over clinical assessments to predict neurological function at follow-up.

3.2 Study II. Plasticity of the injured human spinal cord: insights revealed by spinal cord functional MRI

As evident from the results presented in Study I, characterizing traumatic spinal cord injury with imaging characteristics obtained from the injury epicenter has limited value in patient care. Study II builds on this experience by investigating the effect of injury above and below the epicenter of injury and across the whole spinal cord. Extensive pre-clinical literature exists that documents evidence of plasticity of spinal structure and function after traumatic injury that has, to date, not been investigated in humans. Two examples include reduced inhibitory activity of the spinal cord in response to dysfunctional GABAergic systems of the spinal cord and evidence of axonal regeneration and spouting that coincides with improved neurological function.[128] In this study,

spinal fMRI is used to investigate changes in the processing of afferent sensory information. Based on pathophysiological mechanisms observed in anaimal models, we would expect a more robust response to afferent stimulation in SCI patients relative to healthy controls as a result of diminished GABAergic activity after injury and increased axonal regeneration or sprouting.

Traumatic SCI can disrupt transmission of afferent somatosensory signals and an inability to process motor, autonomic and reflex arcs within the damaged region of the spinal cord. The effect of traumatic injury to the spinal cord is classically considered in two stages, the primary injury, whereby mechanical forces are transmitted through the spinal column resulting in a shear force to axons and blood vessels within the spinal cord and the secondary injury that encompasses a cascade of events whereby the remaining viable neural tissue responds to its new, damaged environment.[9] Aside from secondary destructive mechanisms, the spinal cord has an innate ability to recover partial and sometimes full sensory, autonomic and motor function.[2] This interplay between ongoing destructive forces and an innate regenerative ability eventually reaches a balance that is often described in terms of adaptive or maladaptive plasticity. Currently, there is no way to predict whether a patient will recover along the spectrum of adaptive plasticity and regain sensation, motor or autonomic function or will experience consequences of maladaptive plasticity and suffer from spasticity or neuropathic pain. With non-invasive spinal fMRI, we hope to better characterize both underlying neural activity and how spinal circuits function as a whole to process information in the setting of spinal cord injury. Thus, it may be possible to monitor the effects of different treatment strategies that aim to promote adaptive rather than maladaptive plasticity. In addition, it may be possible to assess rehabilitation strategies and provide feedback with regard to the function of specific neuronal populations and how these spinal neurons function as a concerted network to transmit information to both the brain and the peripheral nervous system. Prior to being able to realize the goal of classifying patients according the response of specific neuronal populations, specific goals have been established to aid in the implementation spinal fMRI for use in SCI patients. The **primary aim of Study II** is to determine whether or not spinal functional MRI can be used to distinguish spinal cord injury subjects from healthy controls. The specific aims of this study are:

Specific aims:

1. To determine whether there is an abnormal neuro-vascular response to afferent stimulation in dermatomes of normal sensation, above the level of injury, in SCI patients relative to controls

2. To determine whether the neuro-vascular response to afferent stimulation in dermatomes of altered sensory perception, below the level of injury, is correlated to the degree of sensory loss.

3. To determine the functional connectivity between regions of the spinal cord that process an afferent stimulus and other regions of the brainstem-spinal cord axis.

Specific Hypotheses:

SCI patients will have:

1. An increased response to afferent stimulation in dermatomes of normal sensation

2. The degree of perceived sensation will correlate with the measured neurovascular response in dermatomes of abonormal sensation.

3. A distributed patter of functional connectivity in SCI patients representing a distributed pattern of neuronal activity that occurs subsequent to mechanisms of plasticity observed after traumatic injury

3.3 Study III. The anatomic variability of the human cervical spinal cord: implications for advanced neuroimaging.

Considerable variation exists among the axial skeleton of adult humans. This variation begins during embryological development and extends into adult life. By the third month of fetal development the spinal cord extends the entire length of the vertebral canal. After this time, mesodermal elements (bones and cartilage) grow more rapidly than the spinal cord such that by birth the caudal extent of the spinal cord lies at the level of the third lumbar vertebrae. The site where nerve rootlets emerge from the spinal cord does not change after fetal development but the nerve root filaments lengthen to reflect the differential growth rate between the vertebral column

and spinal cord. Growth of the axial skeleton continues into adulthood where the caudal extent of the spinal cord terminates in the region of the first or second lumbar vertebrae.[138] During adult life, variation in spinal bones, cartilaginous discs and ligaments can be potentiated by age-dependent vertebral changes, congenital anomalies, neurological disorders, traumatic injury or disorders of the para-spinal musculature. The general aim of this study is to quantify the differences in the position of vertebral and spinal cord segments relative to the arc-length axis of the brainstem – spinal cord. The hypothesis is that these differences are great enough to adversely impact the analysis and interpretation of advanced imaging studies of the spinal cord, should bony landmarks be used to infer the position of specific spinal cord segments. The **primary aim of Study III** is to characterize the segmental anatomy of the human cervical spinal cord for use in advanced imaging studies. To do this, a novel spinal cord segmentation algorithm for use on high-resolution T_2-weighted anatomical images of the human cervical spine was developed and implemented. The specific aims of this study are:

Specific aims:

1. To determine the variation in position of a) vertebral bodies and b) spinal cord segments along the arc length of the spinal cord relative to a fixed point in the brainstem (the ponto-medullary junction).

2. To determine the variation in cross-sectional area of the cervical spinal cord along its longitudinal axis from the level of the third cervical segment through the eighth cervical segment along the arc length of the spinal cord.

3. To determine the reliability with which vertebral bodies are a reliable indicator for the position of spinal cord segments.

4. To determine if patient age, sex, height, neck length and vertebral body position (relative to the ponto-medullary junction) can predict the position of spinal cord segments.

5. To determine if patient positioning within the MR environment exacerbates the difference between vertebral and spinal cord segments.

Chapter 4
Study I: Magnetic resonance imaging as a prognostic tool in acute SCI: establishing sensitivity and specificity

This chapter is modified with permission from the following:

Cadotte DW, Wilson JR, Mikulis D, Stroman PW, Brady S, Fehlings MG. Conventional MRI as a diagnostic and prognostic tool in spinal cord injury: a systematic review of its application to date and an overview on emerging MRI methods. Expert Opin Med Diagn 2011;5(2):121-33.

4 Magnetic resonance imaging as a prognostic tool in acute SCI: establishing sensitivity and specificity.

4.1 Introduction

A central issue in the management of traumatic SCI patients is that of prognosis: Is it possible to determine, at the time of injury, who will improve and who will not. Accurate prognostication has broad implications including but not limited to 1) communicating to patients and families regarding expectations for recovery, 2) planning for in-hospital course and timing of rehabilitation, and 3) targeting specific rehabilitation strategies.

Prognostication in traumatic spinal cord injury is typically conducted by classifying patients along a spectrum of severity, from mild to severe, and declaring that a less damaged spinal cord is more likely to recover neurological and functional ability than is a more severely damaged spinal cord. An assumption of this approach is the simple notion that with greater damage to spinal neurons, axonal tracts and neurovascular relationships, the likelihood that such neuronal circuits are able to recover to their previous level of functioning is diminished. The classification of SCI patients along a spectrum of severity has traditionally been carried out using a clinical scale, where the level of injury is identified and motor and sensory testing is used to describe the neurological abilities of the patient (for example, a C5 level indicates the SCI affects motor and sensory function immediately below the C5 spinal cord level; for more detail see section 2.1.2 Clinical classification of SCI patients). An injury designated as grade A is the most severe with no motor or sensory function below the level of injury whereas grade E represents normal neurological function. The prognostic ability of clinical examination has been assessed by reviewing data collected in the context of large clinical trials.[103] Based on an extensive literature review that captured 69 unique studies of ASIA standards, the authors concluded that the ASIA standards represent an appropriate instrument to discriminate and evaluate SCI patients in a longitudinal fashion with the following caveats: 1) ASIA standards do not reliably assess children less than 4 years of age 2) the use of ASIA upper and lower extremity motor sub-scores instead of a single ASIA motor score is recommended, 3) the notion of a minimally clinically important difference of ASIA standards requires further investigation and 4) the threshold of a functionally meaningful change in ASIA score to document the benefit of a novel therapeutic intervention varies according to the level and severity of SCI.

Magnetic Resonance Imaging (MRI) became a clinically useful tool in the early 1980s. Perhaps the most immediate effect of introducing MRI into clinical practice was the ability to evaluate the overall effect of traumatic injury to the spinal column and assess whether or not the injury had disrupted the anterior, middle or posterior column of the spine and associated disc and ligament complexes. This knowledge allowed surgeons to better plan reconstructive strategies to stabilize the spinal column using different instrumentation techniques. In addition, clinicians and researchers suddenly gained the ability to visualize the damaged spinal cord and make inferences about how changes in T_1 and T_2 weighted signal intensity reflect the pathophysiological mechanisms that underpin loss of motor, sensory and autonomic function. There was often debate concerning the correlation of signal characteristics and underlying pathophysiological events; for example, certain authors suggest that increased T_2 signal implies cavitation and necrosis within the spinal cord[212] while others attribute this signal change to edema.[213] In all likelihood, more than one pathophysiological event could lead to, for example, increased T_2 signal change in the spinal cord after traumatic injury. Nonetheless, authors generally agreed that a spectrum of imaging characteristics of the spinal cord could be identified where 'normal' images sit at one end of the spectrum and complete spinal cord trans-section sits at the other end.

The general aim of this chapter is to determine how T_1 and T_2 signal characteristics have been used as the first imaging biomarker in spinal cord injury patients to describe a spectrum of injury from mild to severe and how this information was used to predict prognosis. To accomplish this goal, a systematic review of the scientific literature was conducted capturing the first 30 years that MRI was used in clinical practice (1980-2010). All studies conducted in this time frame were then used to evaluate the prognostic ability of an MRI-based biomarker relative to standard clinical examination by calculating the sensitivity and specificity of each test to predict clinical outcome at follow-up.

4.2 Methods

4.2.1 Systematic Review

The OVID Medline and EMBASE search engines were queried from 1965 to January 2010. SCI was used as a MeSH heading (human only, English language only). This was cross-referenced with either "magnetic resonance imaging" or "clinical examination" as a keyword. Studies referenced within these publications but not returned with our original search were also included.

Inclusion and exclusion criteria were applied as follows:

Clinical examination studies: We included all studies in which initial ASIA or Frankel scores could be correlated with neurologic outcome at a minimum follow-up of 6 months. Studies with less than 15 patients were excluded. When several different studies used the same dataset at different time points, we utilized the study that displayed the most complete version of the dataset.

MRI studies: Inclusion: the presence of a clear patient history, description of the timing of MRI relative to the spinal cord injury, the MRI sequences obtained, the mode of measurement (i.e. increased T_2-weighted signal intensity, degree of cord compression, etc.), and the time for long term follow up (at least two weeks). Exclusion: a follow-up period of less than 2 weeks, review articles, case reports and meeting abstracts. Review articles that addressed the current topic were examined in full text to ensure that we incorporated all original studies into our analysis. The review articles themselves were not incorporated to avoid duplicate data.

In order to account for the confounding effect of spinal shock (discussed in the literature review, section 2.1.1), clinical examination and MRI studies were divided into those that acquired baseline information either within or after 72 hours of the initial injury.

4.2.2 Review of Methodological Quality

All clinical studies were assessed for methodological quality by the most appropriate means available. Studies with a randomized controlled or similar design were assessed using the criteria of Downs and Black.[214] The quality of non-randomized cohort studies was based on an evolving paradigm of assessment laid out by Cochrane guidelines and the work of Guyatt.[128] Disagreements were resolved by consensus. Articles were not excluded based on the methodological quality.

4.2.3 Meta-analysis

Studies that report individual patient data at both baseline (either within 72 hrs or after 72 hrs) and at follow-up were collated. Initial clinical grade or MRI imaging characteristics was compared to whether or not the patient improved at the time of follow-up. The null hypothesis is that individuals will not recovery from their injury. Alternatively stated, a positive test is defined

as a lack of recovery in order to reflect the clinicians' ability to use either the clinical examination or MRI signal characteristics to inform a patient that recovery is unlikely.

4.2.4 Receiver Operator Characteristics

Data, reported in table 4-2 and 4-3, was then analyzed to create empirical receiver operator characteristic (ROC) curves.[215] Next, we created a fitted curve using the maximum likelihood estimation assuming a binomial distribution. We used the statistical software Rockit (WINDOWS version 1.0.1 BETA 2), available from the University of Chicago (www.radiology.uchicago.edu/sections/roc/software.cgi), to fit the curve and estimate the area under the curve, where 1 represents a perfectly sensitive and specific test.[216] Graphs were created using MS Excel (2008 for Mac).

4.3 Results

4.3.1 Systematic review and methodological quality assessment

A total of 39 studies were identified (10 clinical assessment[128] and 29 MRI[128]). These studies along with their methodological quality assessment are presented in Table 4-1.

Table 4-1. Studies identified in the systematic review along with the methodological quality assessment.

Reference:	§Rep. Sample	¶Defined Sample	⌘Follow-up > 80%	$Blinded outcome	£Outcome data reported	¥Statistical adjustment
Studies that use clinical examination to predict prognosis after traumatic SCI.						
Marino *et al.* (1999)	Y	Y	Y	N	Y	N
Middendorp *et al.* (2009)	Y	Y	Y	N	Y	N
Frankel *et al.* (1969)	N	Y	Y	N	Y	N
Coleman *et al.* (2004)	Downs and Black score: 22/32					
Maynard *et al.* (1979)	N	N	Y	N	Y	N
Sannohe *et al.* (1996)	Y	N	Y	N	Y	N
Katoh S *et al.* (1995)	Y	Y	Y	N	Y	N
Crozier *et al.* (1991)	N	Y	Y	N	Y	N
Folman *et al.* (1989)	N	Y	Y	N	Y	N
Geisler *et al.* (2001)	Downs and Black score: 22/32					
% Yes	50%	75%	100.0%	0.0%	100.0%	0.0%
Studies that use MRI to predict prognosis after traumatic SCI.						
Bondurant *et al.* (1990)	N	Y	Y	Y	Y	N
Yamashita *et al.* (1991)	N	N	Y	N	Y	Y
Nidecker *et al.* (1991)	N	Y	Y	N	Y	N
Silberstein *et al.* (1992)	N	Y	Y	N	Y	N
Schaefer *et al.* (1992)	N	Y	Y	N	Y	N
Silberstein *et al.* (1992)	N	Y	Y	N	Y	N
O'Beirne *et al.* (1993)	N	Y	Y	N	Y	N
Mascalchi *et al.* (1993)	Y	Y	Y	N	Y	N
Takahashi *et al.* (1993)	N	N	Y	N	Y	N
Marciello *et al*. (1993)	N	Y	Y	N	Y	N
Silberstein *et al.* (1993)	N	Y	Y	Y	Y	N
Sato *et al*. (1994)	N	Y	Y	N	Y	N
Flanders *et al.* (1996)	N	Y	Y	Y	Y	Y
Ramon *et al.* (1997)	N	N	Y	N	Y	N
Shepard *et al.* (1999)	N	Y	Y	N	Y	Y
Shimada *et al.* (1999)	N	Y	Y	N	Y	N
Flanders *et al.* (1999)	N	Y	Y	Y	Y	Y
Selden *et al.* (1999)	N	Y	Y	Y	Y	Y
Liyang (2001)	N	Y	Y	N	Y	N
Takahashi *et al.* (2002)	N	Y	Y	N	Y	N
Ishida *et al.* (2002)	N	Y	Y	N	Y	Y
Tewari *et al.* (2005)	N	Y	Y	N	Y	N
Shin *et al.* (2005)	N	Y	Y	Y	Y	N
Andreoli *et al.* (2005)	Y	Y	Y	N	Y	N
Boldin *et al*. (2006)	N	Y	Y	N	Y	N
Tsuchiya *et al.* (2006)	Y	Y	Y	Y	Y	N

Miyanji *et al.* (2007)	Y	Y	Y	Y	Y	Y
Miranda *et al.* (2007)	N	Y	Y	N	Y	N
Mahmood *et al.* (2008)	N	Y	Y	Y	Y	N
% Yes	13.8%	89.7%	100.0%	31.0%	100.0%	24.1%

[§]Representative sample: participants were selected as consecutive or random cases.
[¶]Defined sample: description of participant source and inclusion and exclusion criteria.
[⌘]Follow-up >80%: outcome data were available for at least 80% of participants at one follow-up point.
[$]Blinded outcome assessment: assessor was unaware of prognostic factors at the time of outcome assessment.
[£]Outcome data: reporting of outcome data at follow-up.
[¥]Statistical adjustment: multivariate analyses conducted with adjustment for potentially confounding factors.

Thirty-one of 39 studies (79.5%) reported data on individual patients, as opposed to group analysis, and were further used for analysis. The studies included represent 4804 patients. Table 4-2 summarizes the studies that report clinical examination at baseline (either within or after 72 hours) and at follow-up in those that recover and those that do not. Table 4-3 summarizes studies that report the MRI signal characteristics at baseline (either within or after 72 hours) and clinical examination at follow-up in those that recover and those that do not. Results reported within these tables were subsequently used to construct receiver-operator curves and calculate sensitivity and specificity of each test (clinical examination or MRI) to predict prognosis at follow-up.

Table 4-2. A summary of studies that use clinical examination to predict prognosis after traumatic SCI.

Clinical examination conducted within 72 hours

		Initial clinical grade:				
	Reference:	D	C	B	A	
Recovery	Maynard *et al.* (1979)	7	21	15	12	
	Geisler *et al*. (2001)	44	0	20	20	
	Sannohe *et al*. (1996)	0	2	1	4	
	Katoh *et al*. (1995)	0	0	16	0	
	Crozier *et al*. (1991)	0	17	0	0	
	Folman *et al*. (1989)	9	19	33	0	
No recovery	Maynard *et al*. (1979)	4	2	3	50	
	Geisler *et al*. (2001)	15	0	29	175	
	Sannohe *et al*. (1996)	0	3	0	5	
	Katoh *et al*. (1995)	0	0	5	0	
	Crozier *et al*. (1991)	0	0	10	0	
	Folman *et al*. (1989)	3	3	4	0	
	Total recovery	60	59	85	36	240
	Total no recovery	22	8	51	230	311
	Sum	82	67	136	266	**551**
	% Recovery	73.17%	88.06%	62.50%	13.53%	

Clinical examination conducted after 72 hours

		Initial clinical grade:				
		D	C	B	A	
Recovery	Marino et al (1999)	9	273	225	163	
	Middendorp et al (2009)	5	32	27	42	
	Frankel et al (1969)	11	16	21	42	
	Coleman et al (2004)	0	0	61	62	
	Marino et al (2) (1999)	0	0	0	0	
No recovery	Marino et al (1999)	278	181	146	1127	
	Middendorp et al (2009)	27	11	10	119	
	Frankel et al (1969)	30	5	12	81	
	Coleman et al (2004)	0	0	70	420	
	Marino et al (2) (1999)	0	0	0	0	
	Total recovery	25	321	334	309	989
	Total no recovery	335	197	238	1747	2517
	Sum	360	518	572	2056	**3506**
	% Recovery	6.94%	61.97%	58.39%	15.03%	

Table 4-3. A summary of patient characteristics from studies that use MRI to predict prognosis after traumatic SCI.

MRI conducted within 72 hours

		MR signal characteristics:				
	Reference:	No signal change	T2 hyper-intensity	Cord compression (measured on mid sagittal T1 or T2 image)	T2 hypointensity +/- T2 hyperinensity; T1 hypoinenstiy +/- T2 hyperintensity or T2 hypoinensity; mixed T1 and T2 hyperinensity	
Recovery	Sato *et al*. (1994)	0	0	0	8	
	Shimada *et al.* (1999)	10	33	0	1	
	Selden *et al.* (1999)	0	0	19	7	
	Takahashi *et al.* (2002)	0	24	0	0	
	Ishida *et al.* (2002)	18	4	0	0	
	Tewari *et al.* (2005)	4	18	0	5	
	Andreoli *et al.* (2005)	0	16	0	2	
No recovery	Sato *et al*. (1994)	0	0	0	10	
	Shimada *et al.* (1999)	0	22	0	9	
	Selden *et al.* (1999)	0	0	30	15	
	Takahashi *et al.* (2002)	0	17	0	2	
	Ishida *et al.* (2002)	0	0	0	0	
	Tewari *et al.* (2005)	0	5	0	8	
	Andreoli *et al.* (2005)	0	10	0	10	
	Total recovery	32	95	19	23	169
	Total no recovery	0	54	30	54	138
	Sum	32	149	49	77	**307**
	% Recovery	100.00 %	63.76%	38.78%	29.87%	

MRI conducted after 72 hours

		MR signal characteristics:					
		No signal change	T2 hyper-intensity	Cord compression (measured on mid sagittal T1 or T2 image)	Cord swelling (measured on mid sagittal T1 or T2)	T2 hypointensity +/- T2 hyperinensity; T1 hypoinenstiy +/- T2 hyperintensity or T2 hypoinensity; mixed T1 and T2 hyperinensity	Spinal cord Trans-section
Recovery	Bondurant (1990)	8	10	0	0	3	0
	Yamashita et al. (1991)	0	9	7	2	2	0
	Silberstein *et al.* (1992)	11	9	0	1	4	0
	Schaefer *et al.* (1992)	0	0	0	0	2	0
	Silberstein *et al.* (1992)	12	4	0	0	2	0
	O'Beirne *et al.* (1993)	15	2	0	0	0	0
	Mascalchi *et al.* (1993)	4	9	9	4	0	0
	Takahashi *et al.* (1993)	12	16	0	0	0	0

	Marciello *et al*. (1993)	0	0	0	0	3	0	
	Silberstein *et al.* (1993)	0	4	0	0	4	0	
	Sato *et al*. (1994)	0	7	0	0	1	0	
	Ramon *et al.* (1997)	0	14	2	0	8	0	
	Shin *et al.* (2005)	0	6	0	0	1	0	
	Boldin *et al*. (2006)	0	0	0	0	1	0	
No recovery	Bondurant (1990)	0	6	0	0	10	0	
	Yamashita et al. (1991)	0	11	0	0	6	0	
	Silberstein *et al.* (1992)	0	2	0	0	3	0	
	Schaefer *et al.* (1992)	0	0	0	0	19	0	
	Silberstein *et al.* (1992)	0	0	0	0	1	1	
	O'Beirne *et al.* (1993)	4	3	0	0	11	1	
	Mascalchi *et al.* (1993)	0	5	14	11	10	0	
	Takahashi *et al.* (1993)	1	14	0	0	6	0	
	Marciello *et al*. (1993)	0	0	0	0	12	0	
	Silberstein *et al.* (1993)	2	1	0	0	2	2	
	Sato *et al*. (1994)	0	4	0	0	6	0	
	Ramon *et al.* (1997)	0	1	7	0	16	2	
	Shin *et al.* (2005)	0	9	0	0	13	0	
	Boldin *et al*. (2006)	0	0	0	0	16	0	
	Total recovery	62	90	18	7	31	0	208
	Total no recovery	7	56	21	11	131	6	232
	Sum	69	146	39	18	162	6	**440**
	% Recovery	89.9%	61.64%	46.15%	38.89%	19.14%	0.00%	

4.3.2 Observed T_1 and T_2 weighted signal characteristics after traumatic SCI: a biomarker to indicate injury severity

Studies captured in this systematic review utilized both T_1 and T_2 weighted acquisitions to evaluate the spinal cord after traumatic injury. Authors of individual studies reviewed each of the images and reported patient-specific MRI characteristics as follows: normal (no change in T_1 or T_2 signal intensity within the spinal cord), T_2-weighted signal hyper-intensity, evidence of spinal cord compression, evidence of spinal cord swelling, evidence of intramedullary hemorrhage and spinal cord trans-section.

Utilizing changes in T_1 and T_2 weighted signal characteristics as an imaging biomarker to evaluate the human spinal cord after traumatic injury introduces a certain degree of subjectivity. This is an inherent limitation in such studies and will be elaborated on below. Perhaps the most difficult signal to interpret is that involving hemorrhage within the spinal cord, as the T_1 and T_2 properties of blood change over time as blood products are broken down. An overview of this process is outlined in Figure 4-1.

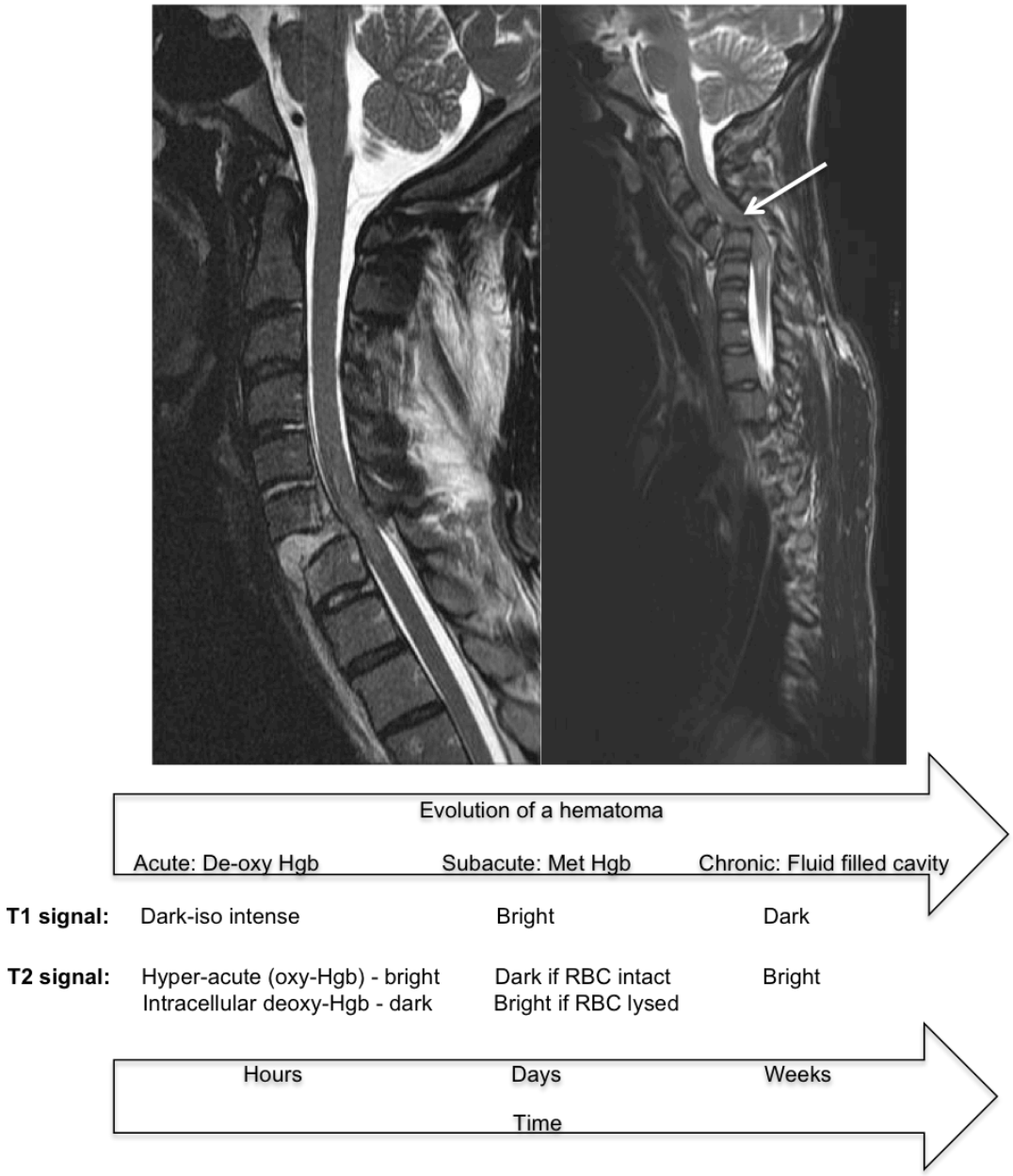

Figure 4-1. A guide to the interpretation of intramedullary signal characteristics along with two case examples. The left image is a mid-sagittal T2 weighted MRI that was obtained within 72 hours of a 32-year-old male sustaining a traumatic spinal cord injury in a motor vehicle collision; note the T2-weighted hyperintensity within the spinal cord. The right image is a mid-sagittal T2 weighted MRI that was obtained within 72 hours of a 26-year-old female sustaining a traumatic spinal cord injury due to a fall from > 10 meters; the white arrow points to mixed T2-weighted hypo- and hyperintensity indicating hemorrhage within the cord. In addition, there is a significant amount of spinal cord compression.

4.3.3 The sensitivity and specificity of an MRI-biomarker to predict neurological outcome at follow-up

In order to determine the sensitivity and specificity with which changes in T_1 and T_2 weighted signal characteristics can predict neurological function at follow-up, data from individual studies were tabulated (see Table 4-3) and receiver-operator characteristic curves were constructed (see Figure 4-2 and Figure 4-3). When performed within 72 hrs, MRI has an area under the curve (AUC) = 0.78 (95% confidence interval: 0.71, 0.83). This result is displayed graphically in Figure 4-2. An MRI with no signal changes (normal) has a sensitivity of 100% and a specificity of 19% to predict prognosis (defined as: no recovery) whereas an MRI revealing evidence of intramedullary hemorrhage has a sensitivity of 39% and a specificity of 86% to predict prognosis (defined as: no recovery).

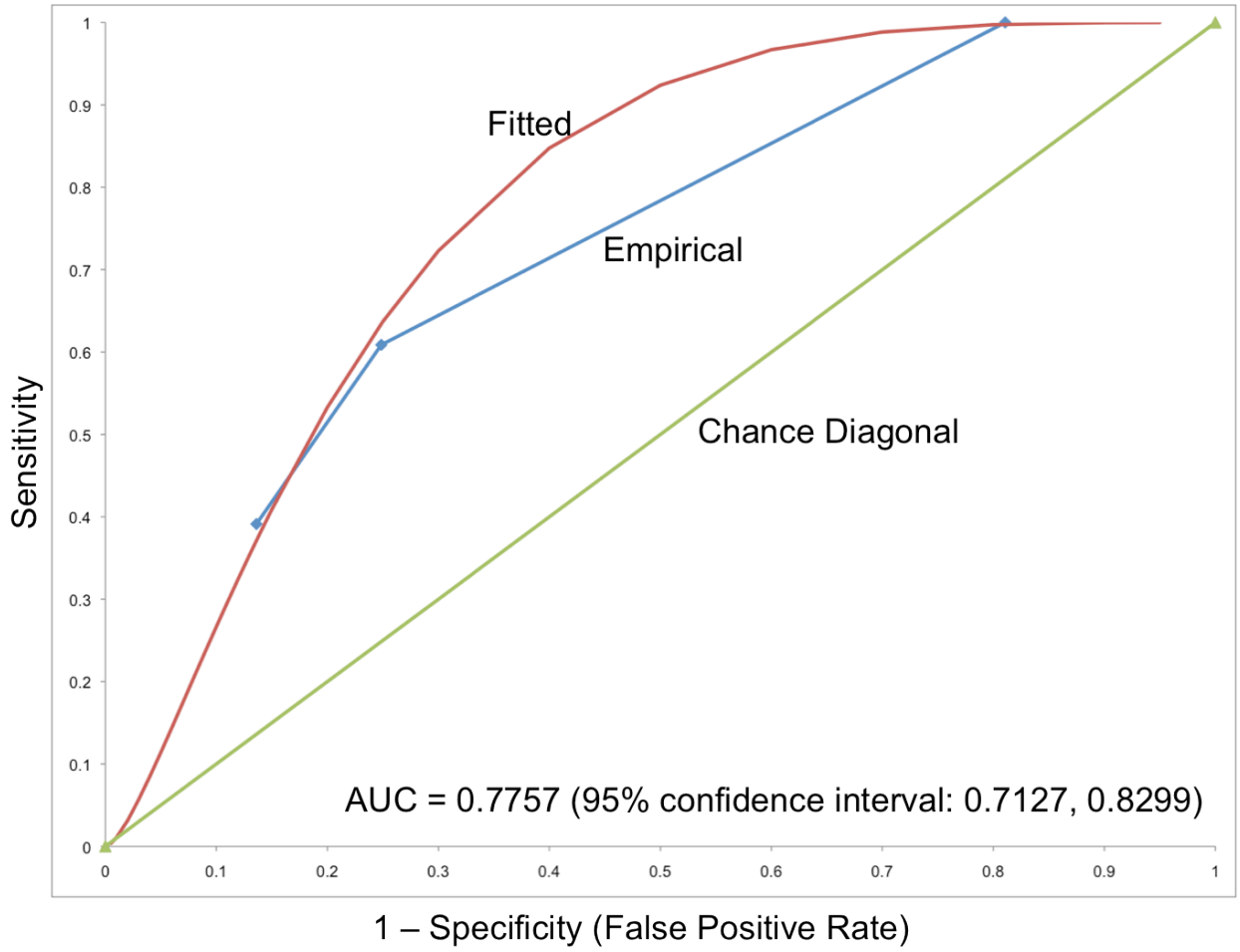

Figure 4-2. Receiver operator characteristics for MRI carried out within 72 hours of SCI. A 'positive test' is defined as no change in clinical examination at follow-up. Shown are the empirical curve (blue line), the fitted curve (red line) and the chance diagonal (green line). The area under the curve (AUC), when the empirical data is fitted to a binomial distribution, is 0.78 (95% confidence interval: 0.71, 0.83) where 1 represents a perfectly sensitive and specific test.

When performed after 72 hours MRI has an AUC = 0.82 (95% confidence interval: 0.77, 0.85). This result is displayed graphically in Figure 4-3. An MRI with no signal changes (normal) has a sensitivity of 97% and a specificity of 30% to predict prognosis (defined as: no recovery) whereas an MRI revealing evidence of intramedullary hemorrhage has a sensitivity of 2.5% and a specificity of 85% to predict prognosis (defined as: no recovery).

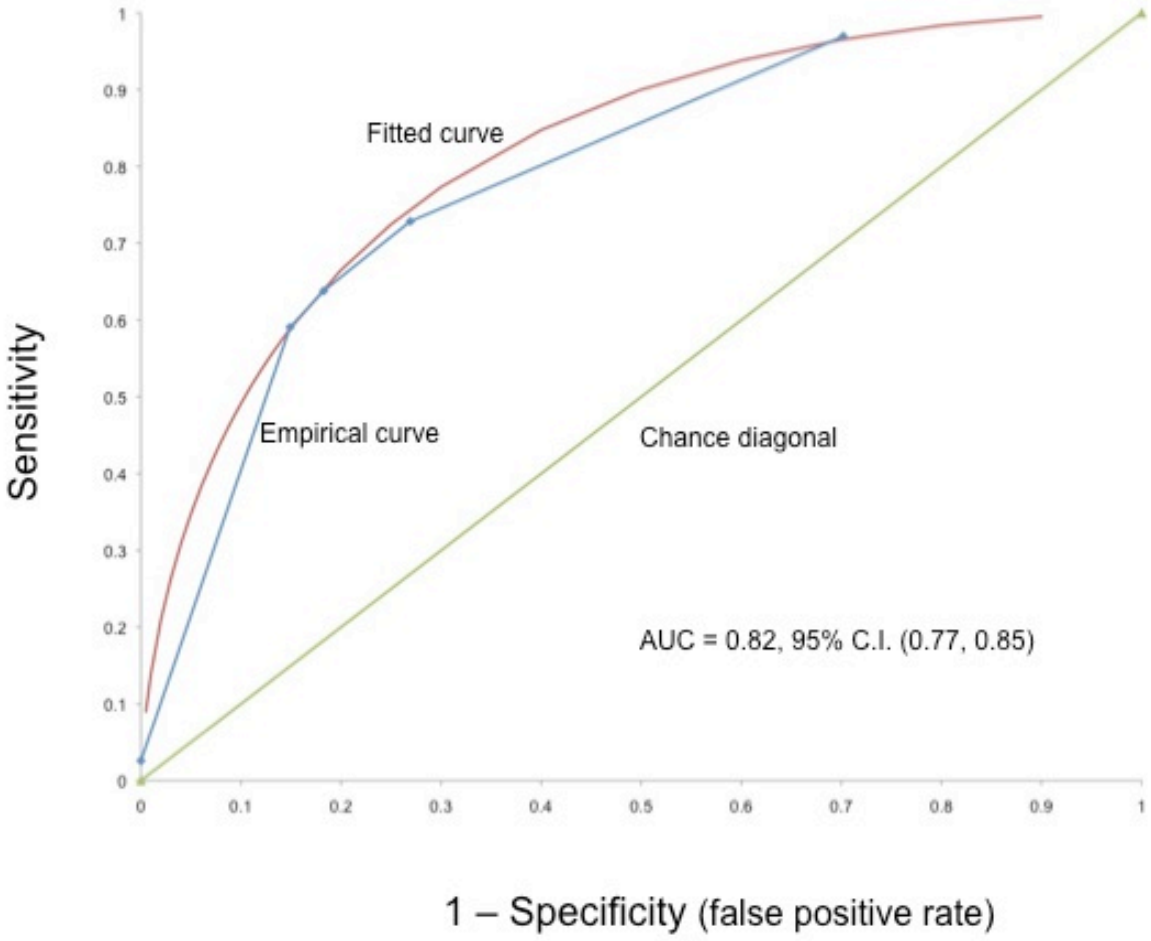

Figure 4-3. Receiver operator characteristics are displayed for MRI carried out after 72 hours of SCI. A 'positive test' is defined as no change in clinical examination at follow-up. Shown are the empirical curve (blue line), the fitted curve (red line) and the chance diagonal (green line). The area under the curve (AUC), when the empirical data is fitted to a binomial distribution, is 0.82 (95% confidence interval: 0.77, 0.85) where 1 represents a perfectly sensitive and specific test.

4.3.4 Does an imaging biomarker offer an advantage over clinical assessment to predict neurological outcome at follow-up?

In order to determine if classifying injury severity with an imaging biomarker offers an advantage to predicting prognosis over the classically used clinical assessment, receiver operator curves were also constructed so as to calculate the sensitivity and specificity of clinical assessment to predict prognosis. In this way, a direct comparison between the use of clinical assessment and an imaging biomarker can be made. As with the MRI-biomarker to classify patients, clinical assessments were also segregated into those conducted within and after 72 hours of injury.

When performed within 72 hrs, clinical examination has an area under the curve (AUC) = 0.86 (95% confidence interval: 0.82, 0.87). This result is displayed graphically in Figure 4-4. Empirical data reveals that an initial clinical assessment of ASIA D has a sensitivity of 93% and a specificity of 25% to predict prognosis (defined as: no recovery) whereas an initial clinical assessment of ASIA A has a sensitivity of 74% and a specificity of 85% to predict prognosis (defined as: no recovery).

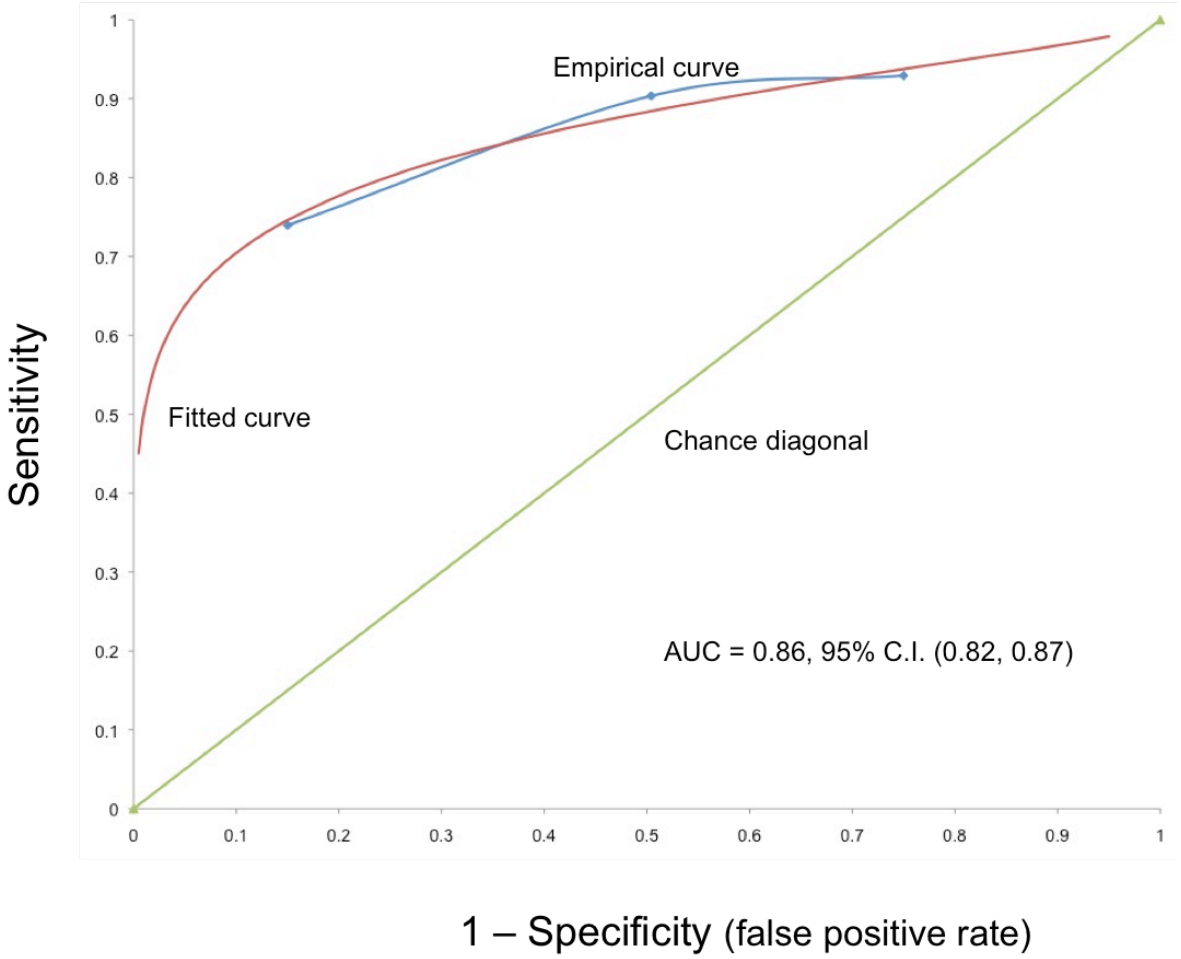

Figure 4-4. Receiver operator characteristics are displayed for clinical examination carried out within 72 hours of SCI. A 'positive test' is defined as no change in clinical examination at follow-up. Shown are the empirical curve (blue line), the fitted curve (red line) and the chance diagonal (green line). The area under the curve (AUC), when the empirical data is fitted to a binomial distribution, is 0.86 (95% confidence interval: 0.82, 0.87) where 1 represents a perfectly sensitive and specific test.

When performed after 72 hours, clinical examination has an AUC = 0.73 (95% confidence interval: 0.72, 0.75). This result is displayed graphically in Figure 4-5. Empirical data reveals that an initial clinical assessment of ASIA D has a sensitivity of 87% and a specificity of 2.5% to predict prognosis (i.e. no recovery) whereas an initial clinical assessment of ASIA A has a sensitivity of 69% and a specificity of 69% to predict prognosis (defined as: no recovery).

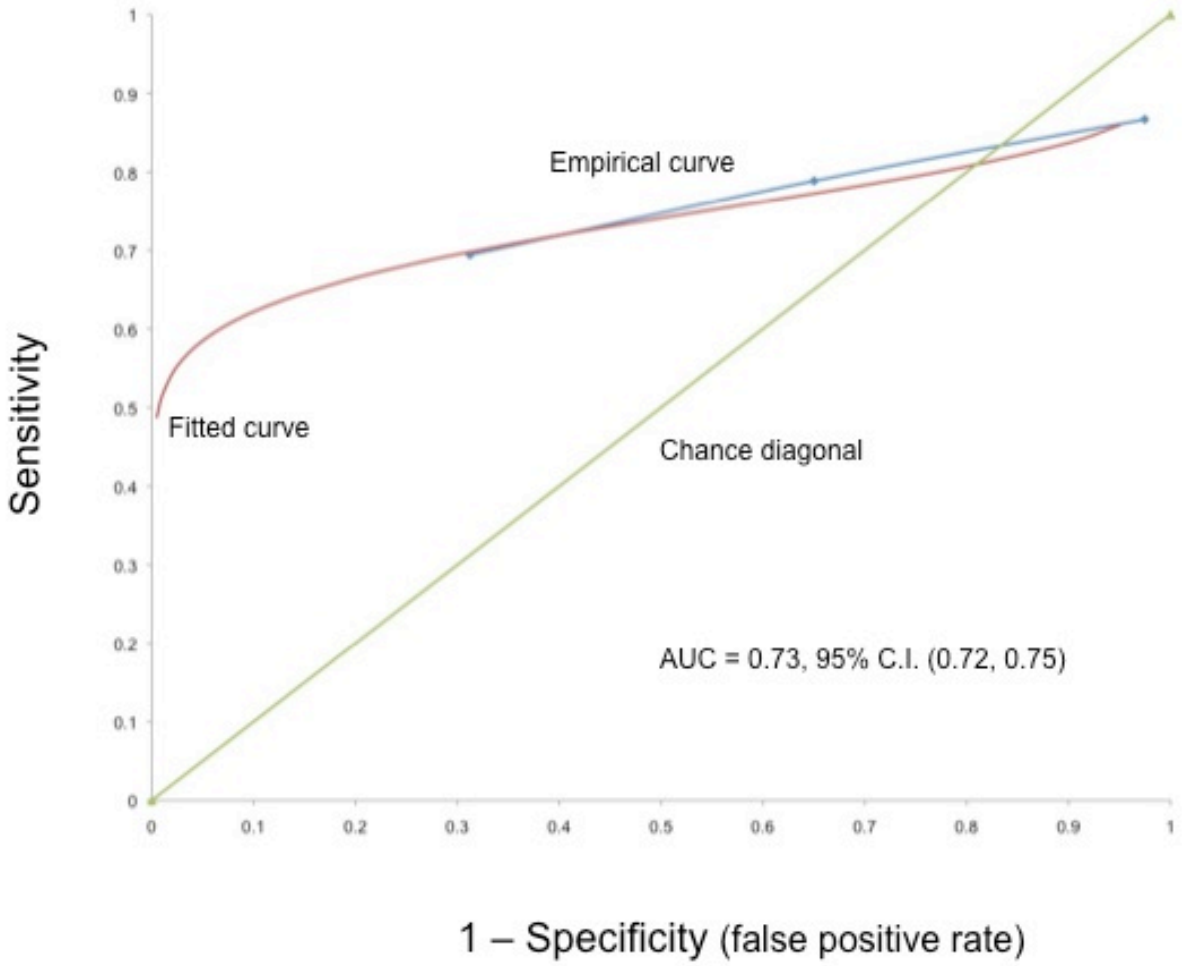

Figure 4-5. Receiver operator characteristics are displayed for clinical examination carried out after 72 hours of SCI. A 'positive test' is defined as no change in clinical examination at follow-up. Shown are the empirical curve (blue line), the fitted curve (red line) and the chance diagonal (green line). The area under the curve (AUC), when the empirical data is fitted to a binomial distribution, is 0.73 (95% confidence interval: 0.72, 0.75) where 1 represents a perfectly sensitive and specific test.

Sensitivity and specificity results for MRI and clinical examination to predict prognosis are summarized in Table 4-4. Each classification measure (MRI or clinical examination) is summarized at the mild and severe end of the spectrum of injury both within and after 72 hours.

Table 4-4. A summary of the sensitivity and specificity of utilizing a spectrum of injury severity based on either an MRI biomarker or clinical examination to predict outcome, defined as no neurological recovery, after traumatic spinal cord injury.

Patients identified as having sustained a **mild SCI** based on:			
MRI		Clinical Examination	
< 72 hrs	> 72 hrs	< 72 hrs	> 72 hrs
High sensitivity Low specificity	High sensitivity Low specificity	High sensitivity Low specificity	High sensitivity Low specificity

Patients identified as having sustained a **severe SCI** based on:			
MRI		Clinical Examination	
< 72 hrs	> 72 hrs	< 72 hrs	> 72 hrs
Low sensitivity High specificity	Low sensitivity High specificity	High sensitivity High specificity	High sensitivity High specificity

When patients are classified as having a **mild injury** according to either MRI or clinical examination, both MRI and clinical examination tests have a high degree of sensitivity and a low degree of specificity to predict prognosis at follow up. Recalling that the null hypothesis is that individuals will not recover, a test with high sensitivity and low specificity indicates low type II error and high type I error, respectively. A type II error means that the null hypothesis is false but falsely fails to be rejected. That is, spinal cord injury patients would make a recovery but our test would not identify this. A low type II error (few false negatives) suggests that both MRI and clinical examination are indeed capable of correctly identifying individuals that will go on to recover. A type I error means that the null hypothesis is true but is falsely rejected. That is, spinal cord injury patients who have a normal MRI or low-grade clinical examination make no recovery but our test indicates that they would indeed recover. A high type I error (many false positives) suggests that both MRI and clinical examination are not capable of identifying patients who will not recover from their injury; stated another way, patients with a normal MRI or low-grade clinical examination, often do not recover from their injury and this lack of recovery cannot be identified with either MRI or clinical examination. Reasons for this might include pathology not captured on standard T_1 and T_2 imaging or the ceiling effect of clinical examination, both of which are elaborated on in the discussion section.

When patients are classified as having a **severe injury** according to either MRI or clinical examination, MRI has a low sensitivity and high specificity whereas clinical examination has a high sensitivity and high specificity to predict prognosis at follow up. Recalling that the null hypothesis is that individuals will not recover, a test with low sensitivity and high specificity indicates a high type II error and low type I error, respectively. A high type II error (many false negatives) suggests that a MRI that indicates hemorrhage in the spinal cord is not capable of determining who will, in fact, recover. A low type I error suggests that an MRI that indicates hemorrhage in the spinal cord is capable of determining individuals who will not recovery. Clinical examination, on the other hand, when indicative of a severe spinal cord injury, has both a high sensitivity and specificity for predicting prognosis (a low type I and type II error).

4.4 Discussion

This study examines the first use of MRI as a biomarker to classify SCI patients along a spectrum of injury severity and to utilize this information to predict prognosis after injury. In order to provide context, the use of a spectrum of MRI characteristics to predict outcome is compared to clinical examination, the *de facto* gold standard means of classifying SCI patients. The sensitivity and specificity of each test to predict prognosis was calculated to determine the performance of each test and to allow for meaningful comparison. When patients are identifies as having a mild SCI, both MRI and clinical examination have a high sensitivity and low specificity to predict prognosis. That is, each test indicates that individuals are likely to recover from their injury, but these tests are not capable of determining which individuals will not recover. When patients are identified as having a severe SCI, clinical examination performs better than MRI to predict prognosis. Individuals who have been identified as having a severe SCI on MRI may in fact go on to recover, but MRI is not able to distinguish whom this will be (high type II error also described as many false negatives). Clinical examination revealing a severe injury has both a low type I and type II error, suggesting that it performs better than MRI at determining prognosis.

Different approaches have been used to predict prognosis after SCI and each one has shown its limitation. Physical examination, electrophysiology, computed tomography and myelography have each been studied.[128] While the neurological examination is paramount to understanding both the immediate clinical situation and gain insight into prognosis following spinal cord injury, two factors make it difficult to use as a tool. The first is that patients who suffer from traumatic spinal cord injury often have other associated injuries, are intoxicated or are medically unstable. The second is that a neurological examination taken immediately after injury is often not a good indicator of prognosis due to the possibility of spinal shock.[128]

4.4.1 T_1 and T_2 weighted signal characteristics as a biomarker

Whether conducted within or outside 72 hours from the initial injury, the use of an MRI-biomarker to first classify patients along a spectrum of injury severity and then use this information to predict prognosis has limited value.

If a SCI patient were to have a normal MRI, and therefore sit on the mild injury end of the severity spectrum, receiver operator characteristic calculations reveal a high sensitivity and low

specificity to predict outcome (defined as no recovery at follow-up). A test with high sensitivity indicates that few false negatives exists (low type II error); in this case it indicates that individuals that demonstrate no recovery do not have a normal MRI. A test with low specificity indicates that many false positives exist (high type I error); in this case it indicates that individuals that demonstrate some degree of recovery have a normal MRI.

If a SCI patient were to have MRI characteristics of intramedullary hemorrhage, and therefore sit on the severe injury end of the severity spectrum, receiver operator characteristic calculations reveal a low sensitivity and high specificity to predict outcome (defined as no recovery at follow-up). A test with low sensitivity indicates that many false negatives exist (high type II error); in this case it indicates that individuals who go on to recover from their injury have no evidence of intramedullary hemorrhage. A test with high specificity indicates that few false positives exist (type I error); in this case it indicates that individuals who recover from their injury rarely show evidence of intramedullary hemorrhage.

By comparing the receiver operator characteristics of an MRI-biomarker to standard clinical assessment to predict prognosis in traumatic SCI, it becomes clear that classifying patients along a spectrum of injury severity by either methodology offers roughly the same prognostic ability.

4.4.2 Study limitations

There are inherent limitations to this study. The meta-analysis presented here represents a total of 4057 patients who underwent clinical examination after SCI and 747 patients who had an MRI after SCI with detailed assessment by a trained radiologist. While these numbers are impressive, conducting both clinical assessments and review of MR images are bound to have variation between clinicians and radiologists that might impact the reliability of the data. Also, we were not able to review the primary MR images of SCI patients and were only able to report the summary findings as detailed by the original authors. In addition, these images were acquired on different MRI machines from different manufacturers at different field strengths, potentially contributing to heterogeneity of results. Last, a number of imaging studies reported only group data rather than patient specific MR characteristics, as a result the MR imaging group reported here (n=747) is much lower than the clinical assessment group (n=4057) potentially introducing a reporting bias.

4.5 Conclusions

This is the only meta-analysis reported in the literature examining the prognostic ability of clinical examination and standard T_1 and T_2-weighted imaging characteristics as a biomarker for injury severity. It is possible to establish a spectrum of injury severity using both clinical examination and standard imaging metrics as a biomarker. Using sensitivity and specificity as a means of evaluating the ability of either clinical examination or MR-based biomarker to predict prognosis, it becomes clear that standard T_1- and T_2-weighted signal characteristics of the injured human spinal cord offer no advantage over clinical assessments. This is likely due to a number of factors, including but not limited to 1) difficulty in reporting spinal cord signal characteristics; 2) a lack of clear correlation between signal characteristics and underlying pathophysiology and 3) confounding effects of the timing of MRI after injury. The use of MRI-based biomarkers will likely be improved by moving away from standard T_1 and T_2-based signal characteristics to imaging metrics that are more reflective of underlying pathophysiological events such as structural imaging (DTI or MT to evaluate white matter pathology) or functional imaging to evaluate the integrity of specific spinal cord circuits.

Chapter 5
Study II: Plasticity of the injured human spinal cord: insights revealed by spinal cord functional MRI

This chapter is modified from the following:

David W. Cadotte, Rachael Bosma, David Mikulis, Natalia Nugaeva, Karen Smith, Ronald Pokrupa, Omar Islam, Patrick W. Stroman and Michael G. Fehlings. Plasticity of the Injured Human Spinal Cord: Insights revealed by spinal cord functional MRI. PLoS ONE 7(9): e45560. doi:10.1371/journal.pone.0045560 Published September 19, 2012.

5 Plasticity of the injured human spinal cord: insights revealed by spinal cord functional MRI

5.1 Introduction

Traumatic spinal cord injury (SCI) results in an acute disruption of afferent somatosensory signals and an inability to process motor, autonomic and reflex arcs within the damaged region of the spinal cord. The effect of traumatic injury to the spinal cord is classically considered in two stages. The primary injury is when mechanical forces are transmitted through the spinal column and this results in a shear force to axons and blood vessels within the spinal cord. The secondary injury encompasses a cascade of events whereby the remaining viable spinal cord tissue responds to its new, damaged environment that might include, for example, reduced blood flow or an increase in inflammatory mediators.[9] For example, traumatic disruption of the microvasculature and increased interstitial pressure can lead to hypoperfusion and subsequent ischemia of the spinal cord.[9-11] The secondary effects of this ischemic insult include cytotoxic cell swelling of both neurons and glial cells, which disrupts action potential transmission.[12] Despite secondary destructive mechanisms, the spinal cord has an innate ability to recover varying degrees of sensory, autonomic and motor function.[2] This interplay between ongoing destructive mechanisms and innate reparative processes eventually reaches a balance that is often described in terms of adaptive or maladaptive plasticity.

There are several distinct mechanisms that underly functional recovery, some of which likely result from specific forms of plascticity. One such mechanism is the regeneration of damaged spinal cord pathways or compensatory collateral axon sprouting that results in increased function.[217] If the time course of positive symptoms, such as pain or autonomic dysreflexia, coincide with the time course of such axonal changes (usually taking weeks to months after the injury, not days) than one can infer maladaptive plasticity. Adaptive changes include the recovery of sensation or motor or autonomic function along a similar time course. In some respects, the disctinction between adaptive and maladaptive plasticity is speculative in human tissue injury (without the advantage of special invasive imaging techniques) as such positive symptoms or functional recovery might result from non-plastic mechanisms, such as the resolution of spinal cord edema. A number of pre-clinical investigations are progressing toward a deeper understanding of the cellular mechanisms underlying plasticity[128] and clinical trials are

underway to mitigate the secondary mechanisms of injury.[218] In fact, a recent international clinical trial demonstrated that early decompressive surgery favors adaptive plasticity in the form of improved motor and sensory function at six months after injury.[128] With non-invasive spinal fMRI methods, we hope to better characterize both the degree of neural activity in specific regions of interest (for example, the dorsal horn) and how spinal circuits function as a whole (connectivity) to process information in the setting of spinal cord injury. In this respect, it may be possible to monitor the effects of different treatment strategies that aim to promote adaptive rather than maladaptive plasticity. In addition, it may be possible to follow rehabilitation strategies and provide feedback with regard to the function of specific neuronal populations and how these spinal neurons function as a concerted network to transmit information to both the brain and the peripheral nervous system.

Evidence for plasticity of the central nervous system after traumatic SCI is abundant in animal models.[128] Characterizing these changes in human patients is more challenging but has been accomplished with modern non-invasive imaging techniques. High-resolution structural magnetic resonance imaging (MRI), in the form of voxel-based morphometry measurements, has been used to demonstrate atrophy of the sensorimotor cortex following traumatic cervical SCI.[219] A brain fMRI study demonstrated a shift of cortical activation corresponding to tongue movements, toward the adjacent disconnected cortical hand area in chronic SCI patients, as compared to healthy controls.[220] Other studies concluded that somatotopic organization is left unchanged after SCI, but movements of muscle groups rostral to the site of injury result in increased activity in the primary motor cortex and associated regions of the cerebellum.[128] Using a longitudinal functional MRI design, temporal changes that occur in both the motor and sensory cortex have been shown that accompany recovery after SCI.[128]

Investigation of the spinal cord after traumatic injury is an inherently more difficult feat. Artifacts arising from magnetic susceptibility differences between bone and soft tissues, and cord motion, present challenges for conducting high quality studies in the spinal cord.[221] Nonetheless, neural activity has been infered using established spinal fMRI methods.[128] In addition, spinal fMRI has been used to study spinal cord injury where activity has been reported caudal to the site of injury.[222] This is an important contribution to the spinal literature as it demonstrates that neuronal populations below the level of injury are engaged. Spinal fMRI studies have also

demonstrated a graded stimulus response pattern across cool – cold noxious stimuli below the level of SCI.[223]

Both animal and human spinal fMRI studies have shown that spinal processing of sensory input is altered after SCI but there remains a significant knowledge gap as to the nature of this plasticity in the human spinal cord.[128] Given the spectrum of clinical symptoms after traumatic SCI, ranging from a complete lack of sensation to altered sensation to normal sensation, we hypothesize that the injured spinal cord processes somatosensory information differently than healthy controls. Unique to this work, we apply a stimulus both above and below the level of the spinal cord injury in dermatomes of normal and abnormal sensation. In doing so, and with the application of a connectivity analysis, we aim to better understand changes that occur to somatosensory processing pathways following spinal cord injury. Specifically, we investigate the spinal cord response to thermal stimulation above the level of injury, below the level of injury and across the whole spinal cord. Based on animal studies of SCI, we hypothesize that the combined mechanisms of reduced GABAergic activity, regeneration of damaged pathways or compensatory collateral axonal sprouting would lead to a more robust response to afferent stimulation than would be observed in healthy controls.[128] This is the first spinal cord imaging study to investigate this in humans, and would build on animal evidence of increased spinal cord excitability after injury.[224]

5.2 Methods

5.2.1 Study Design

All methodological protocols received approval from institutional ethics review boards at both the University of Toronto, University Health Network, and Queens University.

Participants:

All participants provided written, informed consent prior to the initiation of the study and were free to withdraw at any time. If participants were not able to provide written consent due to the nature of their spinal cord injury, verbal consent was given and recorded on the consent form in the presence of a caregiver. Healthy controls were recruited by means of posted information. SCI participants were recruited though the spinal cord injury clinic at the Toronto Western Hospital of the University Health Network and neurosurgery clinics at Kingston General Hospital.

In this study we compared healthy control subjects (n=20, 12 at Toronto and 8 at Kingston) to chronic (> 1year after injury) spinal cord injury patients (n=18, 13 at Toronto and 5 at Kingston). Control and SCI patient characteristics are listed in Table 5-1. We grouped chronic SCI patients according to degree of sensory loss according to the American Spinal Cord Injury Association (ASIA)[225] grade: A (complete injury, no preserved sensation below the level of injury); B,C,D (incomplete injury with some preserved sensation below the level of injury) and E (complete motor and sensory recovery after SCI).

American Spinal Injury Association **I**mpairment **S**cale (AIS) sensory scores were evaluated in all patients in order to compare the degree of spinal fMRI activation to a clinical measure of sensory preservation. Briefly, the AIS sensory score is a measure of light-touch (LT) and pin-prick (PP) sensation that can be applied to each sensory dermatome. For example, the C5 dermatome can be evaluated as normal (AIS=8) through to a complete lack of sensory perception (AIS=0) where each of LT and PP are rated as normal (2 points), abnormal (1 point) or absent (0 points) on both the right and left side of the body. The AIS sensory scale thus evaluates a total of 28 sensory dermatomes (7 cervical, C2-C8, 12 thoracic, 5 lumbar and 4 sacral) with a maximum score of 8 points in each dermatome for an overall maximum of 224 points. This easy-to-use sensory scoring system has become the standard clinical measure to evaluate spinal cord injury patients.[226]

Statistical Power Calculation:

We utilized the method of Murphy[227] to estimate the number of time points necessary in an individual fMRI dataset. Based on a temporal signal-to-noise ratio of >40 (measured), a desired significance of p=0.001 (GLM analysis, see below) and an effect size of approximately ± 2%, it is necessary to collect 48 time points. The GLM analysis yields the number of 'active' voxels whereby we account for multiple comparisons by only considering voxels that cluster in a group of 5 or more (10 mm^3).

Individual person data was grouped as follows: healthy controls (n=20), incomplete SCI (n=9) and recovered SCI (n=6). To compare regions-of-interest (in terms of the number of active voxels), we used a random-effects analysis of the 1st level GLM analysis as previously reported.[228] Based on a two-sample Student's t-test, a sample size of 6 in each group is sufficient

to detect differences of one standard deviation at a significance level of $p < 0.05$ and a sample size of 12 in each group is sufficient to detect differences at a significance level of $p < 0.01$.

5.2.2 Stimulation protocol

Using an automated thermal delivery system, heat (44°C) was applied to both the right and left side of the body, as described previously.[229] Thermal stimulation was applied in an identical fashion to both healthy control and SCI participants although the dermatome stimulated depended on the individual subject (see Table 5-1). A total of 4 heating thermodes were used on each participant. Dermatomes were heated in an interleaved fashion. In control subjects, the C5 and C8 dermatomes were heated on both the right and left side of the body. In SCI participants, we chose a dermatome above the level of SCI and a dermatome below the level of SCI. For three individuals, it was not possible to place one or both thermodes in the prescribed positions. For example, individual number 5 (see Table 5-2) had sustained a C4 ASIA C spinal cord injury and had thermodes placed on the C4 and C8 dermatomes. According to our experimental design, it would have been preferred to place the above level thermode on the C2 or C3 dermatome. However, this individual could not tolerate the thermode being placed on her neck. In such special circumstances, we placed the thermode as close as possible to the desired region, in this case the C4 dermatome. We do not expect that these deviations from protocol would have an impact on statistical comparisons, as the instances in which we had to deviate from protocol (3 in total, individuals 4, 5 and 12) occurred in incomplete SCI patients whereby individuals had normal sensation in the region stimulated (see Table 5-1). As previously reported,[228] thermal stimulation across different sensory dermatomes of normal sensation yield consistent patterns of activity within the spinal cord. The stimulation paradigm was different for each of the four thermodes, and the four paradigms form a linearly independent set. The paradigms spanned 405 seconds, and consisted of 3 warm stimulation periods of 45 seconds duration, separated by rest periods (passive cooling to skin temperature) of 45 seconds or 67 seconds. The paradigms began and ended with rest periods with durations of 67 seconds or more. This stimulation paradigm is expected to elicit activity in the dorsal horn of the spinal cord and project via the spino-thalamic tract to the thalamus and higher cortical centers as follows: Lamina I neurons receive most cutaneous thermal signals, although lamina II and V also receive afferent terminations from cutaneous Aδ and C fibers.[128] Thermoreceptive neurons of the dorsal horn have been found to project contralaterally to the level of the cervical spinal cord [165] and many reports identify

thermoreceptive neurons as spinothalamic neurons.[166] There are three main types of lamina I neurons that have been categorized according to their responses to cutaneous thermal and mechanical stimuli: nociceptive-specific cells responding to noxious mechanical and heat stimuli, polymodal nociceptive cells responding to noxious mechanical, heat and cold stimuli and theroreceptive-specific cells responding linearly to graded, innocuous cooling or warming stimuli and not activated in the noxious temperature range.[128] Many of the spinothalamic neuons also respond to stimuli other than thermoception, but some respond exclusively to thermal stimuli.[128]

5.2.3 fMRI acquisition and data analysis

Spinal fMRI data were collected on a 3T General Electric system (GE Healthcare, Waukesha, WI) at TWH and a 3T Siemens system (Siemens Healthcare, Erlangen, Germany) at Queen's University using previously established methods based on the SEEP (Signal Enhancement by Extravascular Protons) contrast mechanism which takes advantage of changes in tissue water content concomitant to neural activity.[128] A 3D volume that spanned from the T1 vertebra to above the thalamus was imaged repeatedly by means of a half-fourier single shot fast spin-echo (HASTE, Siemens; SSFSE, GE) imaging sequence. This sequence consisted of 79 echoes with a spacing of 5.4 msec, and the 7th echo was acquired at the center of k-space to produce an echo time 38 msec determining the image contrast. Nine sagittal slices were acquired contiguously with repetition time of 9 seconds (1 sec/slice), a 28 x 21 cm field-of-view (FOV) with 1.5 x 1.5 x 2 mm resolution. A total of 48 functional volumes were acquired. The image quality was enhanced by means of spatial suppression pulses anterior to the spine, and motion compensating gradients in the head-foot direction.

Data analysis:

Prior to analysis, lines were manually drawn to demark the anterior, posterior, right and left edges of the spinal cord in each dataset. Furthermore, the pontomedullary junction (PMJ) and the C7/T1 disc was marked as reference points in the image. These reference lines were later used to aid the co-registration and normalization steps. Co-registration was applied to correct for bulk body movements, and a 3-pixel-wide boxcar function smoothing kernel was applied in the direction parallel to the long axis of the spinal cord.

After aligning all fMRI data into a common coordinate system using the ponto-medullary junction as a rostral reference point, it was necessary to determine the location along the spinal cord where the cervical nerve roots enter/emerge from the cord corresponding to the dermatome stimulated. To do this, we used data obtained from a cadaveric dissection study that mapped out the rostral-caudal extent of cervical nerve rootlets and divided the spinal cord into zones.[208] After each zone was established in the common coordinate system, the spinal cord was further divided into four quadrants: right dorsal, right ventral, left dorsal and left ventral. This allowed for a region of interest analysis; **Figure 5-1** outlines this coordinate system. As an example, the dorsal right C5 region of the spinal cord corresponding to nerve rootlets serving the C5 dermatome can be found at the following coordinates: 8, -2.5, 45 whereby 8 is the distance in mm from the anterior edge of the spinal cord, -2.5 is the distance in mm from the midline (negative numbers represent right and positive number represent left) and 45 is the distance along the midline from the fixed reference point, the ponto-medullary junction.

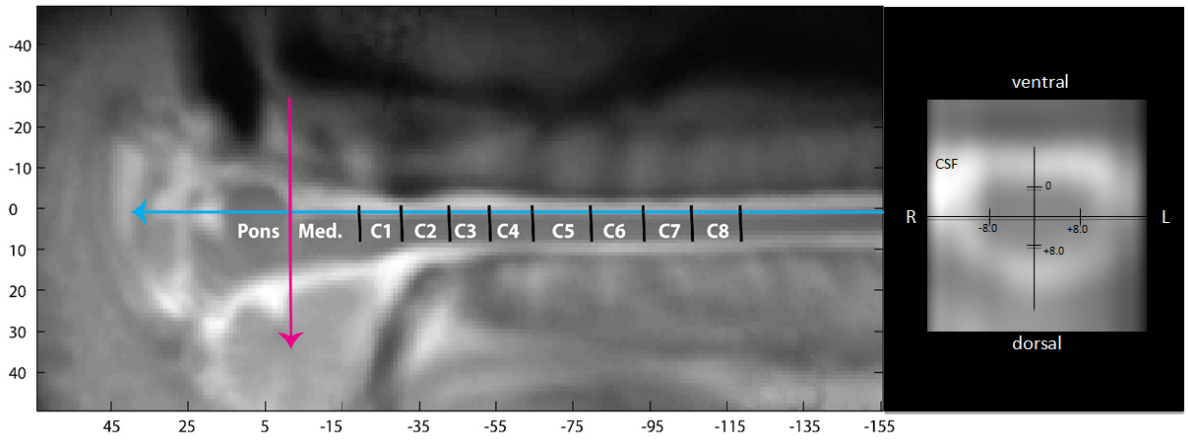

Figure 5-1. Spinal Coordinates. The above coordinate system was used to localize regions of the cervical spinal cord to the associated sensory dermatome. The pink arrow represents a rostral landmark – the ponto-medullary junction. The blue line represents the anterior border of the spinal cord. Shown on the right is an axial view with the white cerebrospinal fluid (CSF) along with the coordinates used to identify the ventral-dorsal and right-left divisions of the spinal cord. Zones of the spinal cord (C1 through C8) are labeled in white lettering and based on anatomic dissection of the cervical nerve rootlets as they emerge from the spinal cord (see text for further details and reference).

Data were analyzed according to the general linear model (GLM).[230] The basis functions for the GLM consisted of the model paradigms which describe the presentation of the thermal stimulation, models of the cardiac-related motion [128], a linear ramp, and a constant function. The stimulation paradigms were then convolved with the hemodynamic response function, as determined in previous studies.[231] Normalization of the data was performed after the GLM was conducted on the data, for purposes of displaying group results. Significance was set at $p < 0.001$. Correction for multiple comparisons was conducted by selecting only clusters of at least 5 active voxels (10 mm^3). Within the GLM analysis, we captured both positive and negative correlations and termed these positive activation (a change in the fMRI signal above the resting baseline) and negative activation (change below the resting baseline) respectively. We did this so as to capture the entire change in spinal tissue consistent with thermal stimulation in the associated dermatome. While the precise biophysical events associated with negative activation remain somewhat elusive, a reduction in neuronal activity (and hence a reduction in the metabolic response) has been proposed.[194] It is important that the resting "baseline" condition involves tonic descending input to the spinal cord. Given the prominent role of inhibition in the spinal cord, the complexity of understanding and distinguishing positive and negative activation increases. While our study was not designed to test for differences between positive and negative activation signals, such work will be important for further characterizing the link between spinal fMRI signal change and the underlying physiology.

Connectivity analyses were applied to both individual and group average time-series data created from spatially normalized data from participants. A "seed" point was identified within each spinal cord region of interest by identifying the active voxel with the time-series with the highest correlation (positive activation), R, to the stimulation paradigm. For example, if the right C5 dermatome was stimulated, the seed point was chosen in the right dorsal quadrant of the C5 zone of the spinal cord. If no active voxels were detected in this region, then no connectivity was inferred. This seed point was grown into a "prime cluster" by identifying all of the contiguous voxels that are correlated with the seed point time-series at $R \geq 0.33$. The average time-series of the cluster was then used for the connectivity analysis. Functional connectivity between the

prime cluster and every other voxel in the brainstem and spinal cord was determined by means of the voxel-by-voxel correlation, with a threshold of $R \geq 0.5$.

Group (healthy control, incomplete SCI, recovered SCI) differences of ROI activation, degree of connectivity (either inter-spinal or supra-spinal) and total number of connected voxels were analyzed by using a one-way ANOVA and post-hoc Tukey test (SPSS, Chicago IL). Differences in ROI activation were compared across a single spinal level. Correlation between clinical AIS sensory scores of the dermatomes stimulated (incomplete SCI) and the degree of ROI activation was carried out using Pearson's correlation coefficient (SPSS, Chicago IL). A value of $p < 0.05$ was assumed as the statistical threshold.

5.3 Results

Patient characteristics & Anatomic localization along the spinal cord

In this study we compared 20 healthy individuals with 18 chronic traumatic spinal cord injury patients who sustained their injury at least 12 months prior to enrolling in our study. SCI patients were further categorized into sub-groups based on the severity of injury: complete (n=3), incomplete (n=9) and those that recovered full function (n=6). Characteristics of this participant group are summarized in Table 5-1.

Table 5-1. Demographic and clinical information of healthy control subjects and chronic spinal cord injury patients. Abbreviations: ASIA: American Spinal Injury Association; Grade A: complete loss of motor and sensory function below the level of injury with no sacral preservation; Grade B: incomplete injury with preservation of sensory but not motor function below the level of injury; Grade C: incomplete injury with preservation of motor and sensory function below the level of injury and motor function is grade 3/5 or less in key muscles below the level of injury; Grade D: incomplete injury with preservation of motor and sensory function below the level of injury and motor function is grade 3/5 or more in at least half of key muscles below the level of injury; Grade E: recovery to normal motor and sensory scores; LT: light touch; PP: pin-prick.

Healthy Control Subjects						
N=20, Average age = 37 years, age range 23-62, M:F = 10:10						
Chronic SCI subjects						
Participant No.	Age	Sex	Level of Injury	Thermode placement	ASIA grade	AIS Sensory Score (LT/PP)
1	39	M	C6	C5/C8	A	108(76/32)
2	31	F	C4	C3/C8	A	12(6/6)
3	36	M	C5	C4/C8	A	22(10/12)
4	27	F	C5	C5/C8	B	81(54/27)
5	24	F	C4	C4/C8	C	78(51/27)
6	60	M	C6	C5/C8	D	223(112/111)
7	29	M	C6	C5/C8	D	214(102/112)
8	19	M	C6	C5/C8	D	150(79/71)
9	74	M	C5	C3/C8	D	215(109/106)
10	41	F	C6	C5/C8	D	218(108/110)
11	56	M	C7	C4/C8	D	207(104/103)
12	50	M	C2	C4/C8	D	115(49/66)
13	63	M	C5	C3/C6	E	224
14	25	F	C7	C5/C8	E	224
15	55	M	C6	C5/C8	E	224
16	60	M	C6	C5/C8	E	224
17	21	F	C6	C5/C8	E	224
18	66	M	C6	C5/C8	E	224

5.3.1 Response to afferent stimulation in dermatomes of normal sensation, above the level of injury

Region of Interest Analysis: Healthy controls

Thermal stimulation was applied to the C5 and C8 dermatomes on the right and left side of the body (a total of four stimulation points) for each of the healthy controls. The corresponding zone of the spinal cord was defined as the dorsal quadrant of that dermatomal segment (i.e. C5 right dermatome corresponds to the right C5 dorsal quadrant of the spinal cord). Spinal fMRI data sets were analyzed on a voxel-by-voxel basis using the general linear model according to the thermal stimulation paradigm for each dermatome. Those voxels showing a change in signal intensity above the baseline (positive activation) are displayed along the red spectrum (axial images, see Figure 5-2) and those showing a change in signal intensity below the baseline (negative activation, see Figure 5-2) are displayed along the blue spectrum. Figure 5-2 demonstrates an individual example whereby active voxels in the region of interest are shown along with the axial reconstructions of functional images. The average number of active voxels in the C5 region is 4.6 ± 1.9 and the C8 region is 4.9 ± 1.9 representing the entire group of healthy controls (n=20). (See Figure 5-3) There was no statistical difference between the average number of active voxels between upper and lower levels.

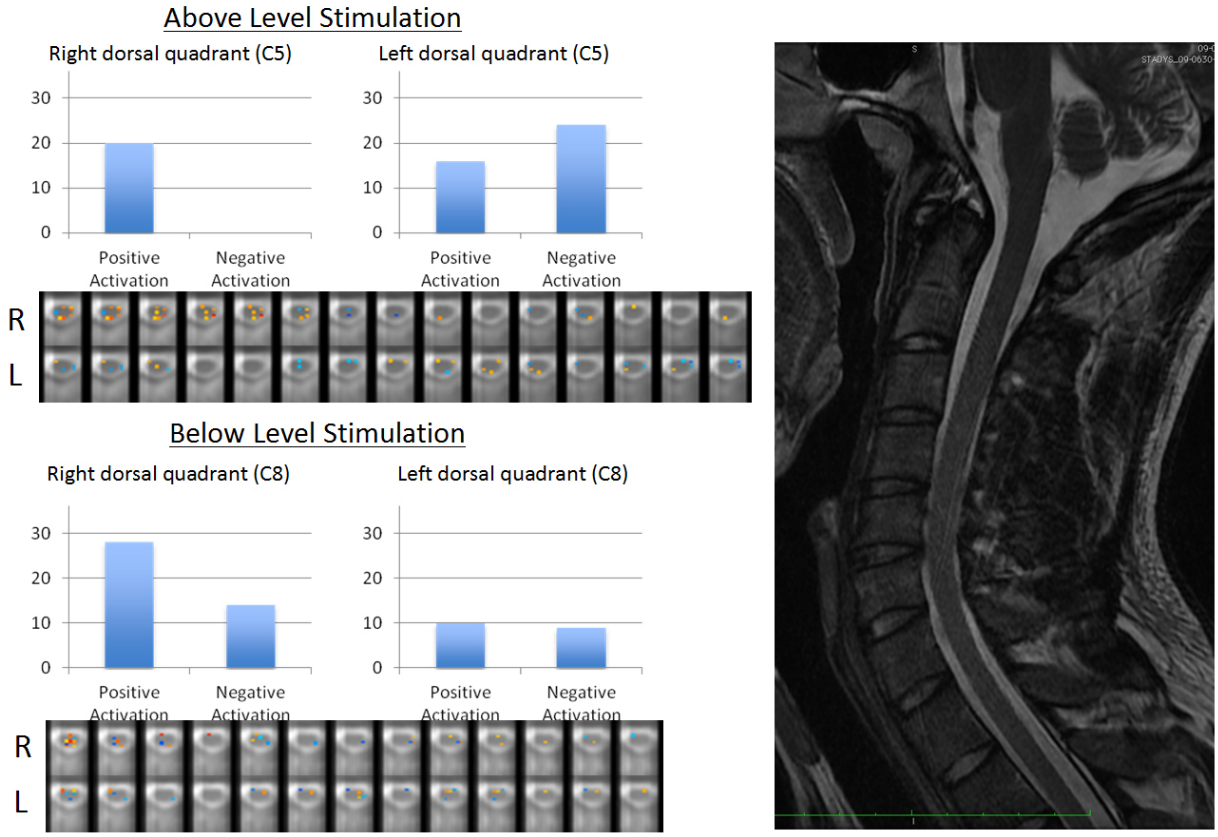

Figure 5-2. Single subject results. Shown is the spinal fMRI region of interest analysis of an uninjured 24-year-old male who underwent thermal stimulation of the C5 and C8 dermatomes on both the right and left side. The blue bar graphs represent the absolute number of active voxels contained within the dorsal quadrant each spinal cord zone. Positive indicates a change in proton density above the resting baseline and negative indicates a change below the resting baseline. Below each bar graph is the activation pattern across the stimulated region in axial cross-section. A T_2 anatomical image is provided to the right for reference.

Region of Interest Analysis: ASIA A Complete SCI

Patient participants consisted of 3 individuals who sustained severe injuries and were left with no motor or sensory function below the level of their injury (ASIA A). When a dermatome of normal sensory perception was stimulated (above the level of injury), the average number of active voxels in the corresponding zone of the spinal cord was 14 ± 9.4, not significantly different than the average number of active voxels in dermatomes of normal sensation in controls. There was a relatively high degree of variability in the ASIA A participant population, as evidenced by the 95% confidence interval. The zone of the cervical spinal cord corresponding to the dermatome stimulated below the level of injury was severely damaged in each of these 3 individuals (images not shown). Based on the extensive tissue damage in the area of interest, isolation of a functional signal change is of questionable significance and was not conducted.

Region of Interest Analysis: Incomplete SCI (ASIA B, C, D) and recovered SCI (ASIA E)

Our patient participants consisted of 9 individuals with an incomplete SCI (ASIA B, C, D) and 6 individuals who recovered completely from their SCI (ASIA E). Thermal stimulation was applied to a dermatome above and below the level of spinal cord injury. On an individual patient basis, the number of active voxels was greater in regions above the level of SCI in comparison to dermatomes below the level of SCI. (Individual patient data not shown; see Table 5-2 for detailed information) On a group level, incomplete SCI patients (ASIA B, C, D), the average number of active voxels above the level of injury, in a dermatome of normal sensation, was 10.1 ± 2.5 voxels and the average number of active voxels below the level of injury was 7.1 ± 3.0 voxels (see Figure 5-3). Table 5-2 summarizes the region of interest, site of thermal stimulation, coordinates of active voxels and the total number of active voxels for each individual. A one-way ANOVA comparing the mean number of active voxels in control participants and the mean number of active voxels in incomplete SCI patients was significant at $p = 0.003$. A post-hoc Tukey test revealed a significant group difference between control participants stimulated on the C5 dermatome and incomplete SCI participants stimulated above the level of their SCI in a dermatome of normal sensation ($p = 0.025$). There was no significant difference between incomplete SCI participants stimulated below the level of injury and that of healthy controls. The

average number of active voxels in participants that recovered completely from their SCI (ASIA E) was 8.2 ± 3.4 voxels above the level of the initial SCI and 10.5 ± 3.8 voxels below the level of the initial SCI, not significantly different from either controls or incomplete SCI participants (data not shown).

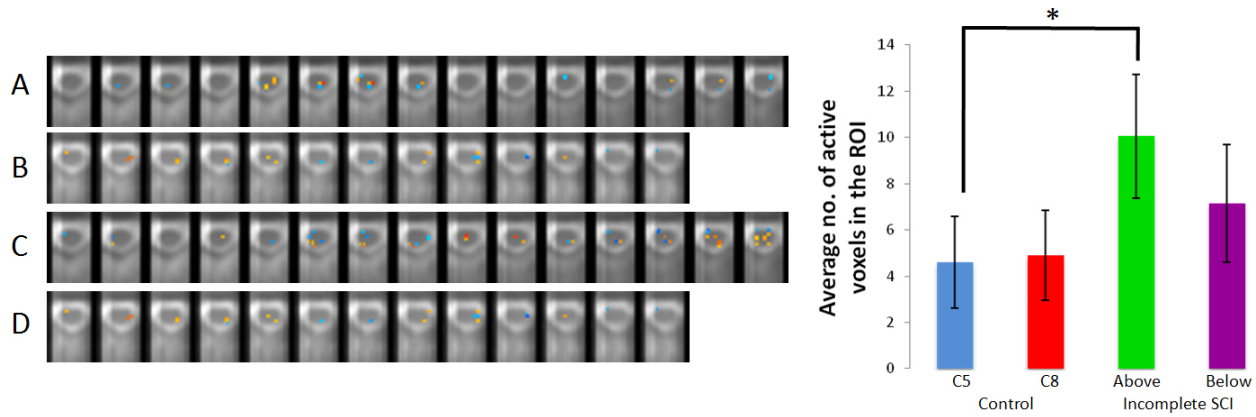

Figure 5-3. Region of interest analysis. Left panel: A region of interest (ROI) analysis conducted in a healthy individual (A and B) and a chronic SCI patient (C and D); axial images through the cervical zone of the spinal cord corresponding to the dermatome stimulated. A: Thermal stimulation of the right C5 dermatome of a 30 year old male. B: Thermal stimulation of the left C8 dermatome of the same individual. C: Thermal stimulation of the right C5 dermatome in a 19 year old male with a chronic C6 ASIA D SCI. D: Thermal stimulation of the left C8 dermatome in the same individual. Right: Quantification of the ROI analysis across all healthy controls (n=20) and incomplete SCI patients (n=9). Bar graph: uninjured controls stimulated at the C5 dermatome (blue) and C8 dermatome (red). Incomplete, chronic SCI patients stimulated above the level of injury (green) and below the level of injury (purple). Error bars are SD. A one way ANOVA was significant at p=0.003. Post hoc tukey test revealed a significant difference between thermal stimulation, evoking a heat senstation, above the level of injury in chronic SCI patients, *p=0.025. There was no significant difference between thermal stimulation of the C5 and C8 regions of control participants. There was no significant difference between thermal stimulation below the level of injury in chronic SCI patients and thermal stimulation of either the C5 or C8 regions in healthy controls.

Table 5-2. The spinal fMRI response of chronic SCI patients.

Region of Interest	Site of stimulation	Location of cluster	Coordinates of active cluster with highest absolute T value (dorsal-ventral, left-right, rostral-caudal)	total number of active voxels: positive (signal change above baseline) negative (signal change below baseline)	
Individual No. 4 27 F, C5 ASIA B					
C5	Right side	Right dorsal horn	4, -5, 66.5	Positive:	22
			6.6, -1.5, 70.2	Negative:	11
	Left side	Left dorsal horn	5, 2.5, 70.5	Positive:	10
			8, 0.5, 67	Negative:	3
C8	Right side	Right dorsal horn	N/A	Positive:	0
			N/A	Negative:	0
	Left side	Left dorsal horn	N/A	Positive:	0
			7, 2.5, 111	Negative:	4
Individual No. 5: 24 F, C4 ASIA C					
C4	Right side	Right dorsal horn	N/A	Positive:	0
			6.6, -3.5, 49.4	Negative:	22
	Left side	Left dorsal horn	N/A	Positive:	0
			5, 6.5, 51.5	Negative:	10
C8	Right side	Right dorsal horn	6.3, -4.3, 105.5	Positive:	23
			3.7, -2.5, 113.7	Negative:	11
	Left side	Left dorsal horn	N/A	Positive:	0
			5.4, 1.4, 109.2	Negative:	11
Individual No. 6: 60 M, C6 ASIA D					
C5	Right side	Right dorsal horn	7, -3.5, 66	Positive:	12
			7, -1.4, 64.2	Negative:	6
	Left side	Left dorsal horn	8, 3, 69.5	Positive:	8
			6, 3.5, 72.5	Negative:	6
C8	Right side	Right dorsal horn	6, -3.3, 112.3	Positive:	3
			4.7, -2.5, 110.3	Negative:	4
	Left side	Left dorsal horn	3.7, 2.5, 117.3	Positive:	7
			N/A	Negative:	0
Individual No. 7: 29 M, C6 ASIA D					
C5	Right side	Right dorsal horn	7.5, -2.3, 72.3	Positive:	12
			N/A	Negative:	0
	Left side	Left dorsal horn	4.6, -0.3, 71.9	Positive:	18
			5.7, 3.6, 75.9	Negative:	7
C8	Right side	Right dorsal horn	N/A	Positive:	0
			N/A	Negative:	0
	Left side	Left dorsal horn	7, 1.4, 107.8	Positive:	10
			3.5, -0.5, 105	Negative:	23
Individual No. 8: 19 M, C6 ASIA D					
C5	Right side	Right dorsal horn	7.8, -2, 69	Positive:	25
			6.5, -3, 68	Negative:	17
	Left side	Left dorsal horn	N/A	Positive:	0
			8, 0.5, 74	Negative:	22
C8	Right side	Right dorsal horn	6, -4.5, 115	Positive:	5
			N/A	Negative:	0
	Left side	Left dorsal horn	5.5, 3.5, 120	Positive:	20

			4, 5.5, 106	Negative:	7
Individual No. 9: 74 M, C5 ASIA D					
C3	Right side	Right dorsal horn	8, -2.5, 45	Positive:	8
			N/A	Negative:	0
	Left side	Left dorsal horn	N/A	Positive:	0
			4.3, 0.9, 45.9	Negative:	18
C8	Right side	Right dorsal horn	5, -2.5, 105.5	Positive:	8
			6.5, -2.5, 109	Negative:	8
	Left side	Left dorsal horn	N/A	Positive:	0
			N/A	Negative:	0
Individual No. 10: 41 F C6 ASIA D					
C5	Right side	Right dorsal horn	7, -1.5, 70	Positive:	6
			8, -1.5, 71	Negative:	10
	Left side	Left dorsal horn	6, 0.5, 70	Positive:	8
			6.7, 0.5, 65.7	Negative:	13
C8	Right side	Right dorsal horn	7, -1.6, 108.8	Positive:	5
			3.6, -4.6, 111.8	Negative:	3
	Left side	Left dorsal horn	6, 0.7, 107.7	Positive:	10
			7, 0.3, 109.3	Negative:	10
Individual No. 11: 56 M, C7 ASIA D					
C4	Right side	Right dorsal horn	N/A	Positive:	0
			N/A	Negative:	0
	Left side	Left dorsal horn	3.6, 5.1, 54.2	Positive:	10
			6, 6, 54	Negative:	13
C8	Right side	Right dorsal horn	7, -2.5, 108	Positive:	12
			N/A	Negative:	0
	Left side	Left dorsal horn	6, 3.5, 105.5	Positive:	4
			6, 5.5, 108.5	Negative:	4
Individual No. 12: 50 M, C2 ASIA D					
C4	Right side	Right dorsal horn	4.7, -4.9, 52.2	Positive:	32
			7.5, -1.5, 58	Negative:	8
	Left side	Left dorsal horn	4, 2.5, 59	Positive:	6
			5.3, 0.5, 59.3	Negative:	19
C8	Right side	Right dorsal horn	N/A	Positive:	0
			6.3, -3.5, 106.7	Negative:	18
	Left side	Left dorsal horn	4.7, 6, 113.7	Positive:	27
			4.6, 0.5, 113.6	Negative:	20

5.3.2 Response to afferent stimulation in dermatomes of altered sensory perception, below the level of injury

Next, we examined the relationship between the degree of spinal fMRI signal change and the degree of sensory impairment in participants with an incomplete SCI (ASIA B, C, D). To do this, we utilized Pearson's correlation coefficient to compare the number of active voxels in the dorsal quadrant of the spinal cord that corresponded to the dermatome of abnormal sensation stimulated. For example, participant number 4 (ASIA B SCI) had a combined AIS sensory score of 3/8 in the C8 dermatome. There is a correlation between the AIS sensory score and the number of active voxels in the corresponding region of the spinal cord, $r = 0.93$, $p < 0.001$ whereby more impaired regions of sensation (a low AIS sensory score) are associated with a higher degree of spinal fMRI activation and a normal region of sensation is associated with a lower degree of activation. The results are shown in Figure 5-4, dermatome sensory scores are reported in Table 5-1.

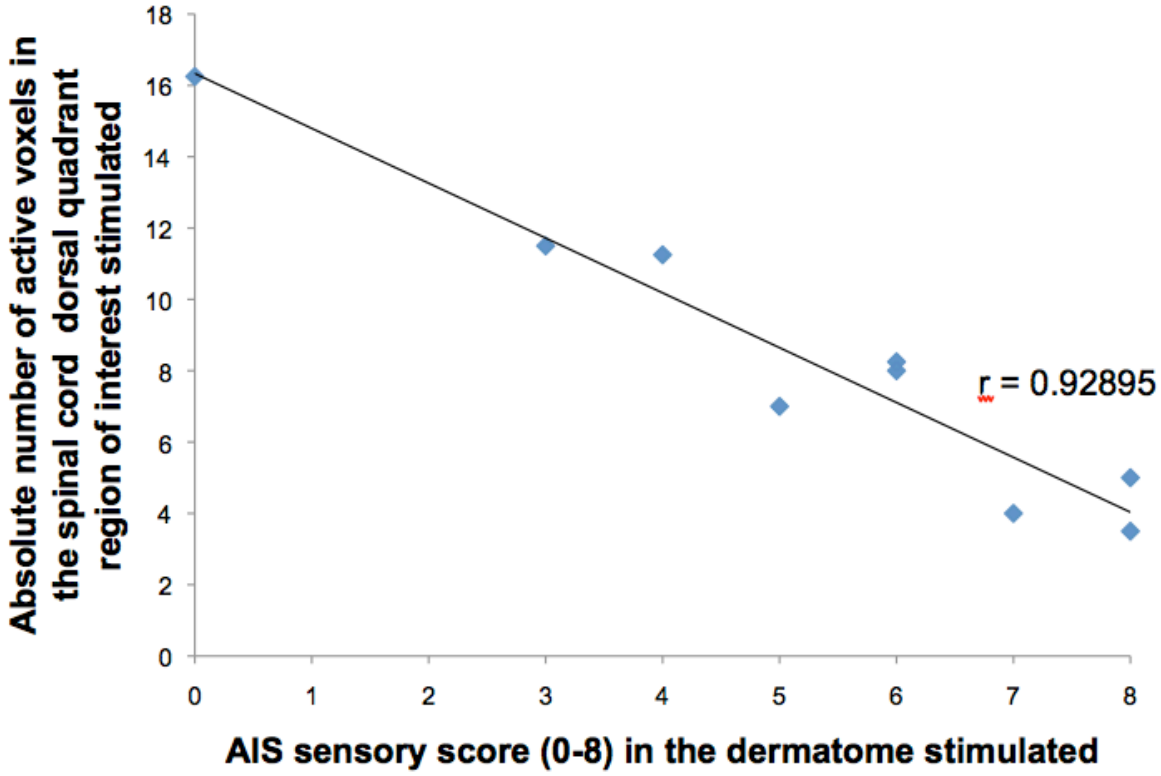

Figure 5-4. Spinal fMRI / sensory deficit relationship. Pearson's correlation analysis between the absolute number of active voxels in the spinal cord dorsal quadrant region of interest (corresponding to the dermatome stimulated) and the AIS clinical sensory score of that same dermatome. All data contained within this analysis was taken from incomplete SCI patients who were stimulated in dermatomes below the level of their SCI. $r = 0.93$, $p < 0.001$. AIS sensory score = 8, normal sensation. AIS sensory score = 0, no sensation. AIS sensory score encompasses both pin-prick and light touch clinical tests.

5.3.3 Functional connectivity between regions of the spinal cord that process an afferent stimulus and other regions of the brainstem-spinal cord axis

In order to determine the relationship between active voxels in the region of the spinal cord corresponding to the dermatome stimulated and the remainder of the spinal cord and brainstem, we applied a connectivity analysis. Functional connectivity was inferred from the temporal correlation between all voxels in a selected region of interest, and all other regions using evoked ata. For example, when the C5 dermatome is stimulated, we examined the relationship between the prime cluster in the C5 region of the spinal cord and other regions of the spinal cord and brainstem. In this analysis we examined three different variables: the number of interspinal connections (within the cervical spinal cord), the number of supra-spinal connections (connections between the region-of-interest and the brainstem) and the total number of connected voxels.

The number of interspinal connections was significantly higher in incomplete SCI patients stimulated above the level of their injury in a dermatome of normal sensation, $p = 0.045$, in comparison to healthy controls (Figure 5-5, left bar graph). Similarly, in persons who recovered from their SCI (ASIA E), the number of interspinal connections is significantly higher in comparison to controls when stimulated above the level of injury ($p = 0.03$) (Figure 5-5, right bar graph). The overall one-way ANOVA for the group comparisons was significant at $p < 0.001$. There was no significant difference between control and SCI participants when stimulated below the level of injury. In addition, there was no significant difference between the controls and SCI participants in terms of supraspinal connections or the total number of connected voxels (data not shown).

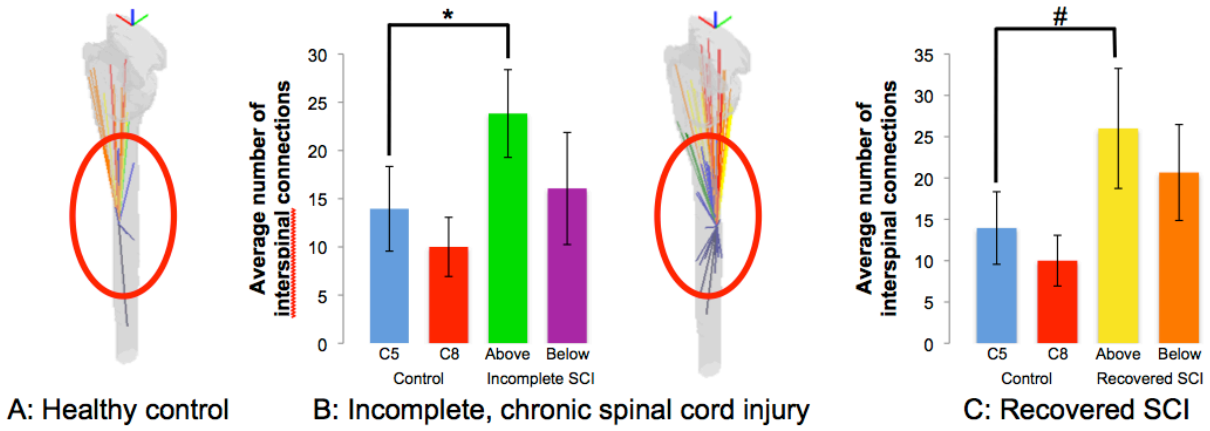

Figure 5-5. Spinal connectivity analysis. From left to right: Interspinal connectivity analysis in healthy controls (projected image), statistical comparison of controls to incomplete SCI patients (bar graph), interspinal connectivity analysis in incomplete SCI patient (projected image) and statistical comparison of controls to recovered SCI patients. The projected images represent a single subject from three angles (oblique left, coronal, obliqe right). The blue lines represent interspinal connections, the orange-yellow lines represent spinal cord-caudal brainstem connections and the red spectrum represents spinal cord-rostral brainstem connections. The number of inter-spinal connections to the prime cluster is shown as a projected image for both uninjured controls (A) and incomplete, chronic SCI patients (B). A one-way ANOVA comparing the mean number of interspinal connections to the prime cluster across healthy control (blue and red bar graph), incomplete SCI (green and purple bar graph) and recovered SCI participants (yellow and orange bar graph) was significant ($p < 0.001$). Significant post-hoc Tukey tests included the difference between control participants stimulated in the C5 dermatome and incomplete SCI patients stimulated above the level of injury (* $p = 0.045$, blue vs. green bar graph) and recovered SCI participants stimulated above the level of injury (# $p = 0.03$, blue vs. yellow bar graph).

5.4 Discussion and Conclusions

Here we present a novel spinal fMRI study whereby we stimulate sensory dermatomes both above and below the level of traumatic spinal cord injury and employ a connectivity analysis to gauge how spinal circuits are altered along with sensory perception. We demonstrate that chronic incomplete SCI patients, when stimulated above the level of their injury, in a dermatome of normal sensation, show a heightened spinal fMRI response to thermal stimulation relative to controls (see Figure 5-3, $p=0.025$). This heightened response to thermal stimulation was not observed in SCI patients who fully recovered from their injury (ASIA E patients).

When we examined the relationship between the number of active voxels in a spinal cord region of interest corresponding to a dermatome of abnormal sensation, we demonstrated an inverse relationship between the degree of sensory impairment and the number of active voxels (see Figure 5-4, $R^2 = 0.93$, $p < 0.001$). That is, thermal stimulation of dermatomes with a complete lack of sensory perception results in a higher number of active voxels in comparison to those with impaired sensation or normal sensation. Together, a significant increase in spinal fMRI response to thermal stimulation in dermatomes of normal sensation in incomplete SCI patients, a lack of this heightened response in persons who completely recover from their injury and a strong inverse correlation between the number of active voxels and the degree of sensory impairment support the notion of plasticity subsequent to traumatic spinal cord injury.

In order to capture the relationship between active voxels in the dorsal quadrant of the spinal cord corresponding to the dermatome stimulated (the prime cluster) and the remainder of active voxels in the spinal cord and brainstem we performed a connectivity analysis. Similar methods have been applied to brain fMRI data in order to understand the relationship between different brain regions that function together to produce complex attributes such as language[232] and how these networks may be disrupted in the presence of language difficulties such as stuttering.[233] To do this in the spinal cord, we employed a connectivity analysis whereby we looked for patterns between the prime cluster and either 1) the total number of connected voxels in the spinal cord and brainstem; 2) the total number of interspinal connections or 3) the total number of supraspinal connections. Our results indicate that the total number of connected voxels is not

significantly different between controls and chronic SCI patients. However, there are a significantly increased number of interspinal connections in incomplete SCI patients relative to controls. Moreover, this increased degree of interspinal connectivity is maintained in patients who fully recover from their injury (Figure 5-5). This is consistent with known mechanisms of spinal cord plasticity after traumatic injury whereby either damaged or spared axons develop novel connections that allows for an alternate route of establishing connections with upper cervical spinal, brainstem or higher CNS centers.[217]

Study limitations

We chose a chronic spinal cord injury population so as to avoid potential ongoing plasticity that often occurs within the first year of injury. However, we cannot be certain that our patient group is uniform with regard to circuit alternations after their respective injuries. Nonetheless, given that the majority of plastic changes subsequent to traumatic SCI are thought to occur in the first 12 months[2], an imaging study at one point in time across a total of 38 subjects does provide sufficient data to support the notion of an altered spinal cord response between groups. To build on these findings, it will be important to apply similar methods in a longitudinal fashion from the acute phase of injury through the chronic phase while conducting concordant clinical examinations to correlate to imaging parameters.

The negative correlation between abnormal sensations in chronic, incomplete SCI patients with the number of active voxels in the corresponding region of the spinal cord ($r = 0.93$, $p < 0.001$) is a rather robust finding in this study. Further characterizing this relationship will be important given that dermatomes of normal sensation above the level of injury in the same patient group show an overall higher average number of active voxels in the ROI analysis. Although this difference is not significant ($p=0.485$) it is contrary to the inverse correlation observed in dermatomes of abnormal sensation whereby one might expect an overall lower number of active voxels in dermatomes of normal sensation. As can be gleaned from the electrophysiology literature, properties of spinal dorsal horn neurons can change dramatically in the setting of disrupted descending input either in experimental animal models[234] or in the setting of traumatic spinal cord injury. The data presented here suggest that with a greater degree of descending fiber disruption (more severe injury) caudal segments of the spinal cord respond in a more robust fashion to thermal stimulation (significantly higher number of active voxels). This finding agrees

with electrophysiology data where it has been demonstrated that spinal cord trans-section in cats results in a higher firing rate of caudal dorsal horn neurons in response to heat stimuli.[234] The relationship between specific spinal cord segment response to stimulation and the degree of disruption of descending input through traumatic injury certainly warrants further investigation, as a graded stimulus-response-degree of injury relationship would further strengthen evidence for the specificity of the spinal fMRI signal.

Conclusions

This work represents the first of its kind to use innocuous heat stimulation across multiple sensory dermatomes in single subjects with a spinal cord injury. We have demonstrated its feasibility and outlined specific metrics that can be used to quantify the spinal cord response. Above the level of injury, SCI patients show a heightened response to thermal stimulation. Below the level of injury, the injured spinal cord responds to thermal stimuli with an inverse relationship to sensory perception. Lastly, SCI patients demonstrate an increased spatial extent of spinal cord response to thermal stimulation. Each of these results is consistent with known mechanisms of plasticity of the human spinal cord: reduced segmental GABAergic activity, axonal sprouting and the establishment of alternate spinal circuits.[128] We have also highlighted particular limitations that with further study will allow for the advancement of this technology as a non-invasive means of determining the function of specific cell populations of the spinal cord (ROI analysis), how these cell populations work as a unit to transmit information to the brain (connectivity analysis) and how these circuits are altered after traumatic injury (spinal plasticity). Chapter 6 addresses how the segmental anatomy of the spinal cord varies across individuals and what this means for the analysis of data across groups of subjects.

Chapter 6
Study III: Characterizing the location of spinal and vertebral levels in the human cervical spinal cord

This chapter has been submitted to NeuroImage for peer-review:

David W. Cadotte, Adam Cadotte, Julien Cohen-Adad, David Fleet, Micha Livne, Jefferson R. Wilson, David Mikulis, Natalia Nugaeva, and Michael G. Fehlings. Characterizing the location of spinal and vertebral levels in the human cervical spinal cord. (under peer-review)

.

6 Characterizing the location of spinal and vertebral levels in the human cervical spinal cord

6.1 Introduction

Advanced imaging techniques of the human spinal cord are capable of visualizing pathophysiological events of conditions such as traumatic injury, degenerative spondylosis or neuroinflammatory conditions such as multiple sclerosis. Advanced imaging techniques provide the opportunity to assess sub-clinical changes in spinal cord structure and function. For example, diffusion tensor imaging (DTI) and magnetization transfer (MT) can be utilized to follow the integrity of white matter tracts in specific regions of the human spinal cord;[128] fMRI can be used to track the spinal response to specific stimuli, reflecting the integrity of specific functional circuits.[133] Recently, the microstructure of the corticospinal motor pathway was mapped; imaging characteristics of this map correlated with clinical function.[235] The ultimate goal of early detection of sub-clinical recovery or deterioration should provide the opportunity to personalize treatment strategies in both the acute and chronic phase of injury.

A prerequisite to accurate interpretation of advanced imaging data is appreciating the neuroanatomical origin of the acquired signal. An imaging atlas serves the purpose of bringing prior spatial knowledge to an imaging dataset. Advanced brain imaging has benefited from the design and improvement of brain atlases that allow for registration of various functional and structural imaging studies.[128] Atlases of the spinal cord are not as developed and have been used by individual research groups to meet the objectives of specific studies. For example, certain spine imaging studies infer neuroanatomical positions within the spinal cord by counting the adjacent vertebral bodies and stating that, for example, the C6 spinal cord segment is adjacent to the C5 vertebral body.[200] Other studies have created manually segmented templates based on specific anatomical information of nerve rootlet position.[133] However, each of these approaches is associated with substantial potential error. The diversity of human anatomy offers two principle sources of variability: 1) inter-subject differences in spinal column anatomy and 2) inter-subject differences in spinal cord segments relative to a fixed point in the brainstem. The

work presented here considers these two sources of diversity across a cohort of healthy individuals and presents a unique solution that can be applied in advanced MR imaging assessment of the human cervical cord.

Considerable variation exists among the axial skeleton of adult humans. This variation begins during embryological development and extends into adult life. By the third month of fetal development the spinal cord extends the entire length of the vertebral canal. After this time, mesodermal elements (bones and cartilage) grow more rapidly than the spinal cord such that by birth the caudal extent of the spinal cord lies at the level of the third lumbar vertebrae. The site where nerve rootlets emerge from the spinal cord does not change after fetal development but the nerve root filaments lengthen to reflect the differential growth rate between the vertebral column and spinal cord. Growth of the axial skeleton continues into adulthood where the caudal extent of the spinal cord terminates in the region of the first or second lumbar vertebrae.[138] During adult life, variation in spinal bones, cartilaginous discs and ligaments can be potentiated by age-dependent vertebral changes, congenital anomalies, neurological disorders, traumatic injury or disorders of the para-spinal musculature. We are not aware of any studies that quantify differences in spinal anatomy across individuals or present a solution to dealing with this neuroanatomical variability.

To do this, computer vision algorithms are used in a novel way to segment the spinal cord from high-resolution magnetic resonance images. This aids in accounting for personalized anatomy of single subjects. Using expert markings as ground truth data, a neuroanatomical context is given to each individual's spinal images by delineating the location of vertebral bodies and spinal cord segments down the central axis of the spinal cord. The distribution of vertebral segments, spinal cord segments and spinal cord area is reported across the cohort of twenty subjects studied. This is the first work to present a quantitative, accurate solution to deal with the anatomical variability of the human cervical cord. We anticipate that this technique will dramatically enhance the accuracy of quantitative MR-based assessment of the normal and diseased spinal cord.

6.2 Methods

6.2.1 Study Design

In this work we investigate 20 healthy volunteers (35% male, mean age = 30.5 years, range = 19 to 52 years) who were recruited through posted signs at the Toronto Western Hospital in order to delineate the segmental structural anatomy of the human cervical spinal cord. We implement a cylindrical coordinate system to describe the spatial relationships of both intra-subject segmental anatomy and inter-subject differences in relative anatomical locations. Informed consent was obtained in all cases and approval to conduct this work was granted by the institutional ethics review board at Toronto Western Hospital.

6.2.2 Overview of Image Processing Methods

Two other methods have been reported that segment the human spinal cord from MR images.[128] The method established by Horsfield *et al.* was attempted but proved difficult in regions of low CSF volume around the spinal cord.[128] The method presented by Coulon *et al.* is computationally intensive and was not explored. The method developed herein aims to improve on previous methods both in terms of segmenting the spinal cord in regions of low CSF volume and in terms of computational efficiency.

The goal of the presented image-processing pipeline is to use an MR image to create a 3D representation of the human spinal cord, from which measurements of various spinal cord parameters can be made. An overview of this process is listed below, while the details of each step are presented throughout the remainder of the methods section.

- Define a co-ordinate system and use it to represent the spinal cord as a generalized cylinder
    1. Implement a Catmull-Rom spline to represent the central axis of the spinal cord. The spline was initialized by a set of user markings and refined after segmenting the spinal cord.
- Identify the spinal cord / CSF boundary and segment the image
    1. This was accomplished by using one-dimensional template matching.
        - A set of “templates” or “training” data was created from manually segmented spinal cord MR images. The templates hold ground-truth

information regarding the spinal cord / CSF boundary and can be used to identify this boundary in un-segmented images.

- The newly determined spinal cord / CSF boundary data was smoothed to remove outlier data points.
- The spline was refined by determining the center of sets of spinal cord / CSF boundary points which transect the spinal cord at various levels.

- Establishing a Neuroanatomical context to spinal imaging
    1. The segmented spinal cord and spline was used to measure distances to various anatomical landmarks, calculate areas and volumes, and compare measurements between subjects.
- Accounting for inter-individual differences in spinal anatomy
    1. Determine if there are ways to predict spinal segment locations and if neck flexion or extension impacts measurements.

Algorithms were composed using a combination of Python and C++, with use of the ITK imaging software package (www.itk.org), Numpy (www.numpy.org), Scipy (www.scipy.org), Matplotlib (matplotlib.org), Sci-kit Learn (scikit-learn.org), and MayaVI (mayavi.sourceforge.net).[128]

6.2.3 Defining a coordinate system and representing the spinal cord as a generalized cylinder

6.2.3.1 MRI Acquisition

All imaging data was acquired on a 3T GE MR system at the Toronto Western Hospital using an 8-channel neurovascular array coil. Subjects were carefully positioned to limit head movement and were requested to not move. A T_2-weighted acquisition was obtained to optimize visualization of cervical nerve rootlets emerging from the spinal cord in a segmental fashion. Specifically, a FIESTA-C sequence (T_2-weighted); 512 x 512, NEX 1.0, FOV 200 mm, Slice thickness 0.3 mm; resulting in a voxel size of (0.3906 mm x 0.3906 mm x 0.3000 mm) was used. Total scan time: approx. 12 min.

In a subset of individuals (n = 6) a total of three volumes were acquired: one in a neutral position, one in neck flexion and one in neck extension. Although neck flexion and extension are limited within the confines of the imaging environment, approximately 6-10 degrees of either

flexion or extension was obtained by placing extra padding under the occiput (neck flexion) or under the shoulders (neck extension). This represents the normal range of position that one might expect in the imaging environment.

6.2.3.2 Definition of a common coordinate system

The co-ordinate system of the MRI scanner will be defined as (X, Y, Z), as shown in Figure 6-1, where Z points in the caudal direction, Y from the center of the scanner towards the floor, and X from the center of the scanner towards the right hand side of a subject that is lying face-up.

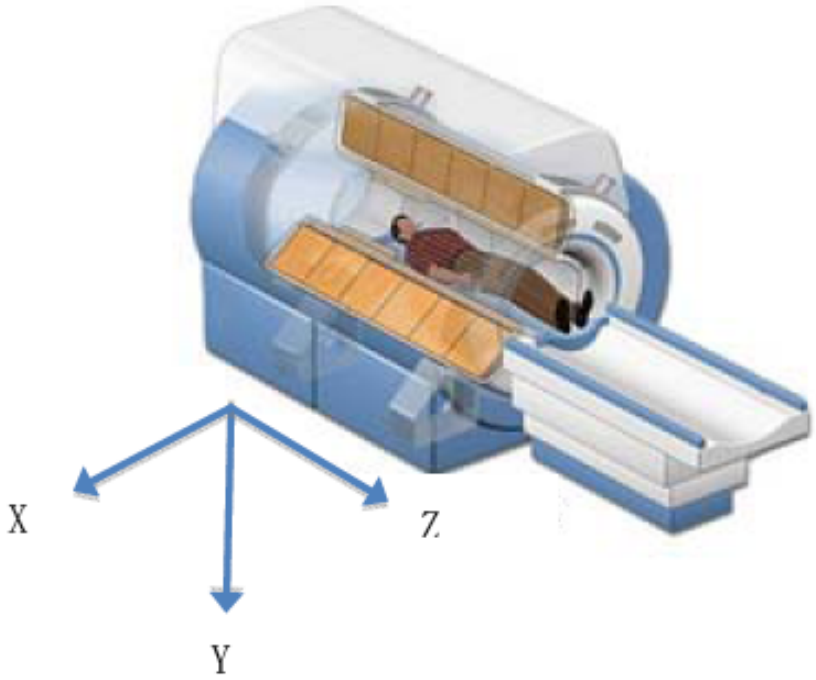

Figure 6-1. Co-ordinate system of the MRI scanner. Source: http://www.slicer.org/slicerWiki/index.php/File:Coordinate_sytems.png

The 3D co-ordinate system of the generalized cylinder, with which the spinal cord is represented, is defined as $\vec{c} = (z, \theta, r)$, where z is the arc length (distance) along the spline (the "spline" is defined in further detail below, but can be thought of as the central axis of a generalized cylinder) from the spline origin, and where θ and r denote a polar representation of the plane perpendicular to the spline at z. We considered angle θ = 0° to point to the patient's anterior direction $\hat{d}_0$.

a) Initialization of the Catmull-Rom Spline

Using 3D Slicer[236] (freely available, http://www.slicer.org), a user manually marks the ponto-medullary junction (PMJ) on a mask layer of the T_2-weighted anatomical image. Next, using an axial view, the user marks several points of the spinal cord, moving from the PMJ in the caudal direction, ensuring the markings are as close to the center of the spinal cord as possible. There is no requirement for the exact number of points, although more points in areas of high curvature will result in a more accurate spline representation. The user-selected points start at the PMJ and end below the C7 vertebrae, the last area of interest for this study. On average, points were marked approximately every 7 mm in areas of high curvature and every 30 mm in areas of low curvature.

The markings along the spinal cord are used to generate a three-dimensional Catmull-Rom spline function (the "spline"), which represents the central axis of the spinal cord from the PMJ to below the C7 vertebrae. The spline is a continuous polynomial function, represented by a set of control points. The Catmull-Rom representation is typically used for numerical interpolation problems where each control point lies on the curve. Interpolations can be made at any point along the curve. The equation for an interpolated spline point is presented below, where $\{P_i\}_{i=1}^{N}$ represents the set of N control points (the control points are the 3D spinal cord markings). We calculate the position $\vec{p}(t)$ with the next equation:

$$\vec{p}(t) = \vec{P}_{i+1} \cdot h_{00}(t') + N\left(\vec{P}_{i+2} - \vec{P}_i\right) \cdot h_{10}(t') + \vec{P}_{i+2} \cdot h_{01}(t') + N\left(\vec{P}_{i+3} - \vec{P}_{i+1}\right) \cdot h_{11}(t'); t \in [0, \dots, 1)$$

where $i = \lfloor t \cdot (N-1) \rfloor$, $t' = N \cdot t - i$ and h_{ij} are Hermite basis functions, t is the control variable, and we assign $t = 0$ to represent the PMJ, and $t = 1$ to represent the last control point in C7 vertebrae. In our formulation we assign the control points to be equidistributed in $t \in [0, \ldots, 1]$. That is a choice of representation, and the control points themselves do not have to be equidistributed along the spine (direction). That does not hold any problem since t is an auxiliary variable and is not used directly. Instead, we use s in our formulation, which can be calculated as the arc length of any interval, as explained below.

Notice that P_0, P_{N+1} are additional control points that are chosen such that the tangent of the spline in the first/last points would be the direction to the next/previous point, respectively.

The tangent of the spline can be calculated at any point, *p(t)*, using the interpolated spline point formula shown above, but replacing h_{ij} with $N\frac{dh_{ij}}{dt'}$.

Arc length, *s*, is measured from the spline origin, the PMJ, to any point along the spline using the following equation: $s(1)$ represents the spline's length in mm, and is referred to as z in our generalized cylindrical coordinates system; the arc length (*z*) can be calculated as follows:

$$s(t) = \int_0^t \sqrt{\vec{p}(t')^2}\, dt'$$

To convert a Euclidean point $\vec{x} = (X, Y, Z)$ to its generalized cylindrical coordinates representation $\vec{c} = (z, \theta, r)$, we search for t*, the closest point on $\vec{p}(t)$ and then calculate the new coordinates

$$\vec{c} = \left(s(t^*), arccos\frac{\left(\vec{x} - \vec{p}(t^*)\right)\hat{d}_0}{|\vec{x} - \vec{p}(t^*)|}, |\vec{x} - \vec{p}(t^*)|\right)$$

Notice that the formulation assumes that the spline's shape is such that $\vec{x}$ lies in the plane perpendicular to $\vec{p}(t^*)$. Conversion from $\vec{c}$ to Euclidean representation $\vec{x}$ can be done by finding t^*, the point where $s(t^*) = c_z$ and then calculate the Euclidean position.

$$\vec{x} = \vec{p}(t^*) + r * R(\theta)\left(\frac{\partial \vec{p}(t^*)}{|\partial \vec{p}(t^*)|} \times \left(\hat{d}_0 \times \frac{\partial \vec{p}(t^*)}{|\partial \vec{p}(t^*)|}\right)\right)$$

Where R is a 2x2 rotation matrix. Notice that we assume that $\vec{q}$ is never parallel to $\hat{d}_0$. That is, the spine never points to the patient's anterior direction. Using a spline function to represent the spinal cord allows us to utilize the generalized cylindrical coordinate system as explained above. The following is a visual representation of the spline function (red curve) in the coronal plane of an MR image, passing through three axial planes. The red curve starts at the PMJ. The image illustrates both the scanner / Cartesian and generalized cylinder coordinate systems.

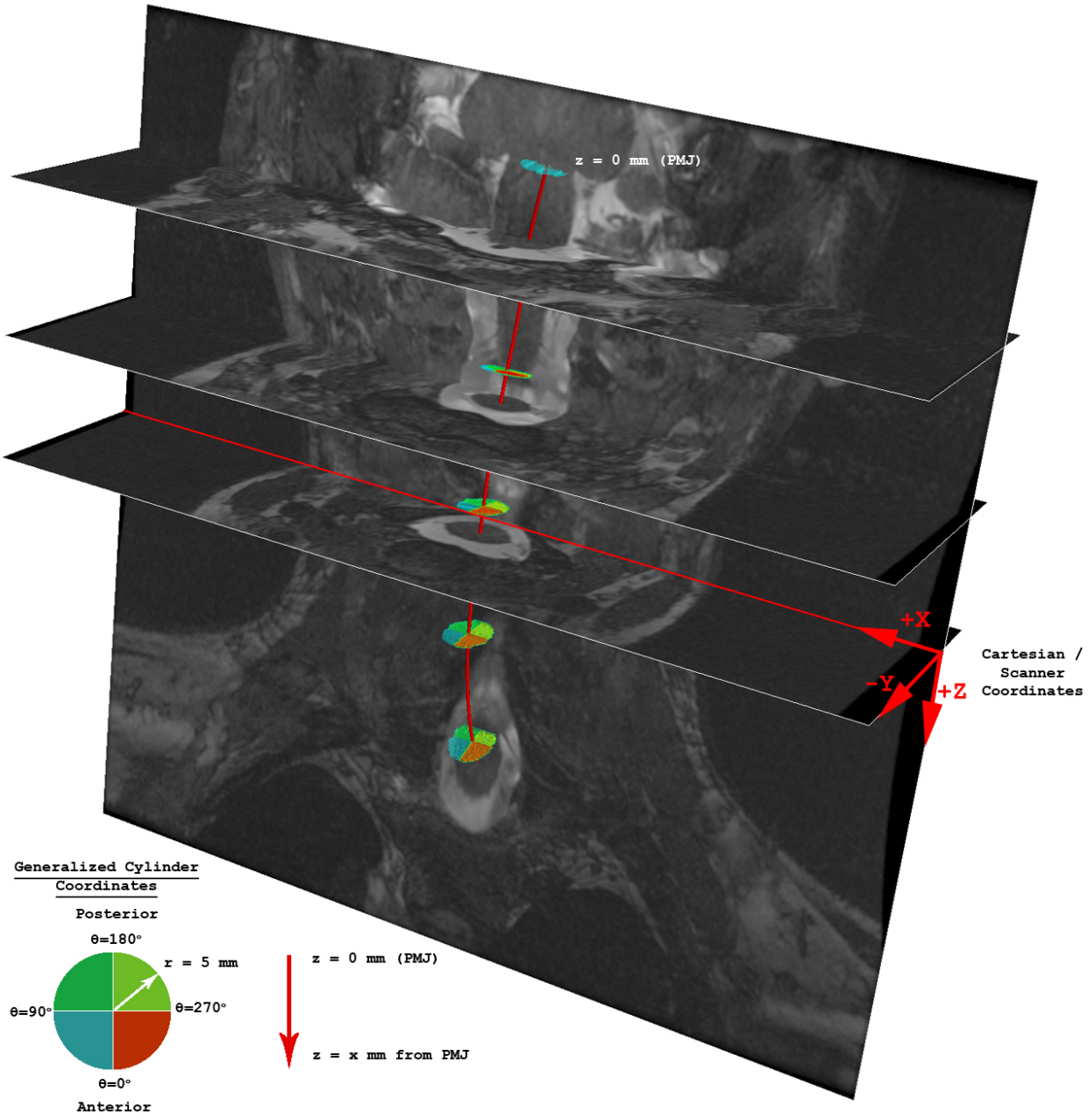

Figure 6-2. Initialized spline function. The red line running down the longitudinal axis (z) of the brainstem and spinal cord is initially created with user-defined points roughly outlining the spinal cord within the 3D high-resolution anatomical volume. In this figure, the spline has already been re-centered as is discussed in further detail below. The Cartesian / scanner coordinate system is shown on the right side of the image.

6.2.4 Identifying the spinal cord / CSF boundary and segmenting the image

To accurately measure distances from the PMJ to any set of nerve rootlets or vertebrae along the spinal cord, the spline created in section 5.2.3 is used. To ensure an accurate distance measurement, it is essential to have a precise estimate of the center of the spinal cord at all arc lengths from the PMJ. The user initially marks the center point, which is refined as follows: the spinal cord / CSF boundary is located at all points along the curve and then the center of the spinal cord is calculated as being the center of these sets of points, or the center of mass, in any given two-dimensional slice that is perpendicular to the spinal cord. Template matching is used to locate the spinal cord / CSF boundary. Template matching uses a set of ground-truth spinal cord / CSF segmentation data to compare against non-segmented spinal cords in order to ascertain the location of the unknown boundaries, as described in more detail below.

a) Building a "template matching database"

One-dimensional normalized template matching is the basis for the spinal cord segmentation to determine a more precise centerline of the spinal cord than the original estimations provided by the user (i.e., a set of refined control points for the spline function). One-dimensional matching was chosen rather than two- or three-dimensional matching, because it is more likely that matching arrays are found in the non-segmented images. It also reduces the complexity of the calculations and thus reduces processing time. As shown in Figure 6-3, one-dimensional template arrays are created from the set of radial lines emanating from the center of the spinal cord of the ground-truth, manually segmented images. The left image shown in Figure 6-3, an axial slice of a Gaussian smoothed MR image, shows the segmented spinal cord (shaded light green) and a single radial line from the approximate center of the spinal cord (as interpolated from the spline initialized by the manual center point markings) to 70 voxels away from the center of the spinal cord. The right image in Figure 6-3 shows the magnitude of the gradient of the image (the "gradient image"), for the same slice.

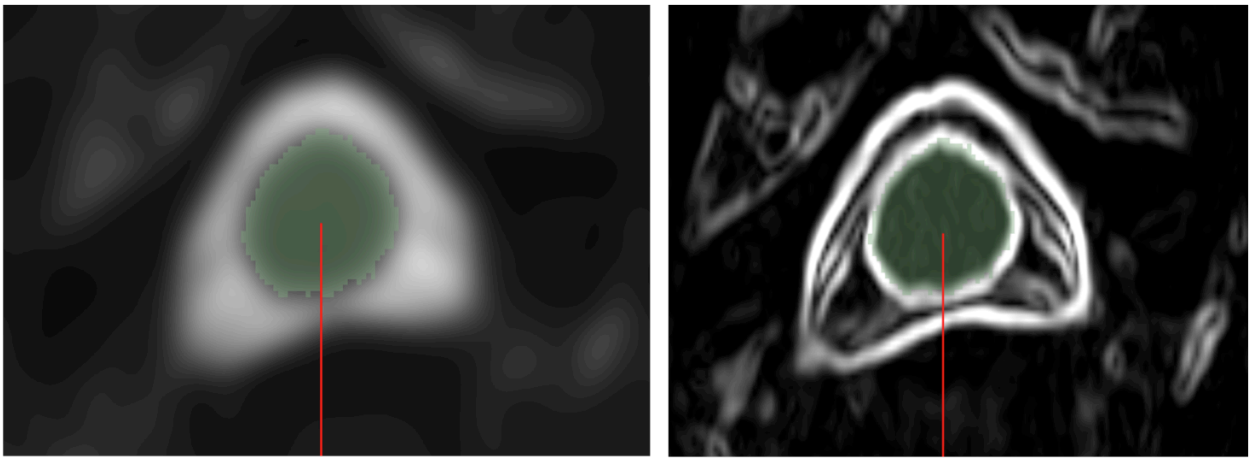

Figure 6-3. An axial slice of the cervical spinal cord. Shown is a red radial line originating from approximately the center of the spinal cord (the exact center point will be improved upon in subsequent processing steps as outlined below) and the light green shading illustrating the manual segmentation overlay. Left: Gaussian smoothed MR image. Right: gradient image.

Following from the center of the spinal cord, along the red, radial line shown in Figure 6-3, the location of the spinal cord / CSF boundary is located where the shaded green area stops. The gradient image is useful for locating edges on an image, or areas of rapid transition between light and dark regions. It is a measure of the magnitude of the slope, or change in voxel value, between regions of the image. This is illustrated graphically in Figure 6-4 below, which shows the values for the gradient image along the radial line shown in Figure 6-3.

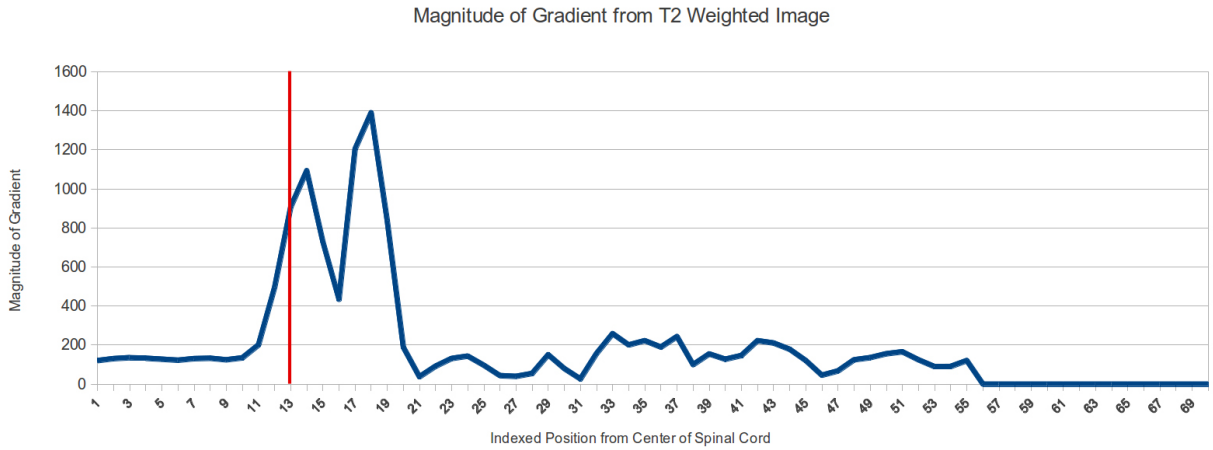

Figure 6-4. Magnitude of gradient of T_2 weighted image voxel intensities plotted against the indexed position from the center of the spinal cord. The red line represents the boundary between the spinal cord (voxel intensities plotted to the left of the red line) and the adjacent CSF (voxel intensities plotted to the right of the red line), as indicated by manually segmenting the spinal cord. Values above indexed positions of 56 are zero because this position marked the border of the image for this subject.

To create these templates, one full T_2-weighted MRI 3D volume was manually segmented using 3D Slicer, and four other 3D volumes were partially segmented, mainly in the brainstem region. The magnitude of the gradient of each image was calculated using ITK. The one-dimensional template arrays were created by using axial slices from each image (a full plane, holding z constant in the scanner co-ordinate system). Within each axial slice, one-dimensional arrays were created in two-degree increments around the z axis. The number of axial slices used from each manually segmented image depended on the size of the segmented region in each image. The size of each array was set at a fixed distance of 70 voxels (~ 27 mm), while the millimeter distance varied based on the direction of the radial, since all three voxel dimensions are not equal. The set of templates from all of the manually segmented images were used to create the "template database". The total number of one-dimensional radials recorded was approximately 90,000. Although the number of templates in the database can be expanded, we found that this set was sufficient for locating the spinal cord / CSF boundary in all 20 subjects presented in this study.

While extracting the one-dimensional templates, the distance from the center of the spinal cord to the CSF boundary was also measured, in millimeters, by using the voxel spacing found along each radial. The "edge distance" calculations yielded another set of 90,000 values that make up the "edge database". Each value in the "template" and "edge" databases correspond to one another, giving each template a unique value where its edge is located and the distance to that edge. Figure 6-5 illustrates a sorted scatter plot showing the distance to the edge of the spinal cord for all 90,000 radial templates. The distances range from roughly 2 mm to 10 mm and there are many templates that correspond to each of these distances, as can be seen by the continuity of the scatter plot in Figure 6-5. The variation in edge distance is large for two reasons: 1) the spinal cord is curved and all distances were measured in the axial plane, as opposed to a plane perpendicular to the tangent of the spline; and 2) there is variation in the diameter of the five spinal cords that were segmented and within different regions of the same spinal cord. As a check of our methods, we quantitatively crosschecked edge distances from several images using the line measurement tool in Osirix[128] to ensure the methodology produced accurate results.

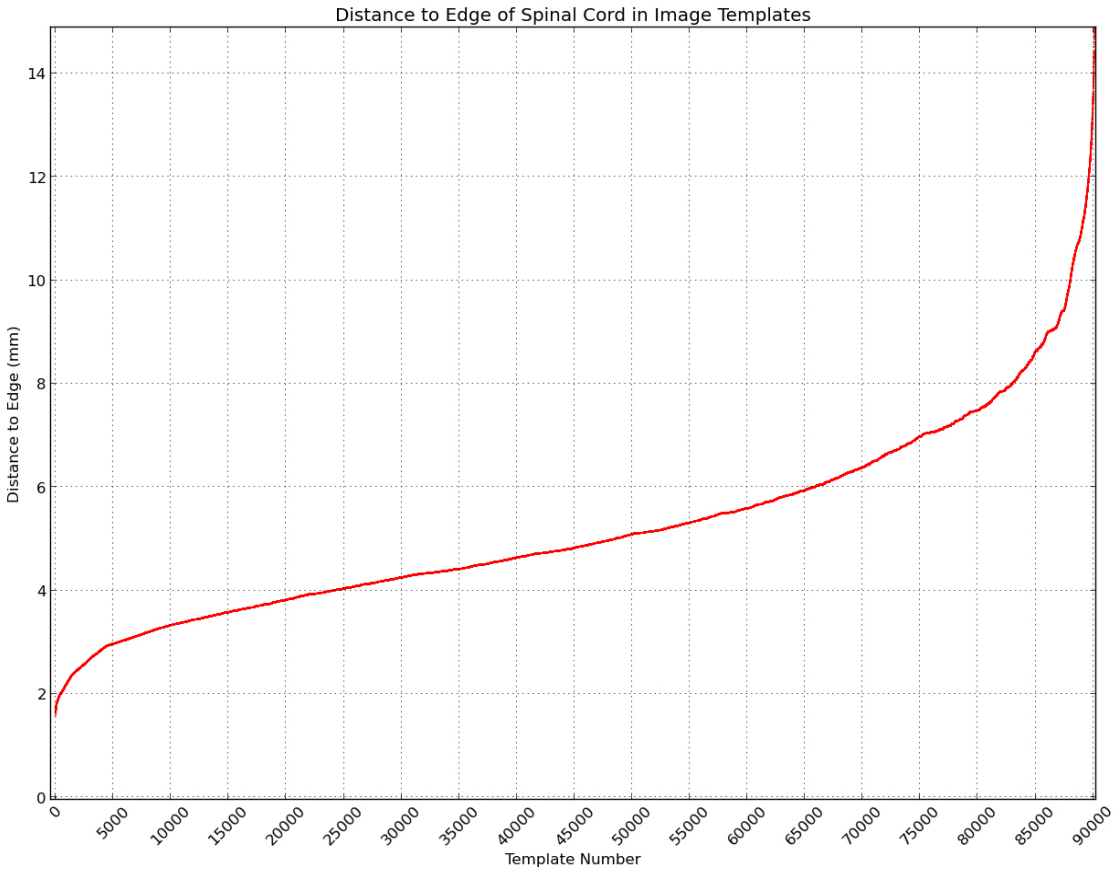

Figure 6-5. A scatter plot showing the distance to the edge of the spinal cord for all 90,000 one-dimensional radial templates recorded from one manually segmented 3D volume. There is no meaningful association between the template number and the longitudinal distance from the PMJ, they are sorted by distance to the edge.

b) Spinal Cord / CSF boundary locating of new images using normalized template matching

The next step is to utilize the spinal cord / CSF boundary location information from the template database to determine the location of the spinal cord / CSF boundary in non-segmented images. This was done using normalized cross-correlation. Non-segmented volumes are initialized as per section 5.2.4a above. The magnitude of the gradient of the image is calculated. 18,000 "test" arrays are taken from the image, consisting of 180 radials from each of 100 axial slices, evenly spaced down the spinal cord from the PMJ to below the C7 vertebrae. Normalized cross-correlation is used to compare the similarity in the shape, not magnitude, of the "template" database arrays and the "test" arrays. For arrays with a certain degree of similarity in shape, we infer that the location of their spinal cord / CSF boundary is located at approximately the same distance from the center of the spinal cord in both the "test" and "template" arrays.

Starting with the "test" arrays located at the PMJ (z = 0 mm) and working caudally, each radial "test" array is compared against all of the "template arrays" in the template database according to the following formulas:

$$Normalized\ Cross\ Correlation = \frac{1}{n}\sum \frac{(f(x) - \bar{f})(t(s) - \bar{t})}{\sigma_f \sigma_t}$$

$$\sigma_f = \sqrt{\frac{1}{n}\sum (f(x) - \bar{f})^2} \quad \text{and} \quad \sigma_t = \sqrt{\frac{1}{n}\sum (t(x) - \bar{t})^2}$$

Where *f* and *t* are the "template" and "test" arrays.

The output of each template comparison is the cross-correlation value, or the percentage similarity between the template and test array. Examples of two matches are shown below in Figure 6-6, the first is a 30% match and the second is a 74% match.

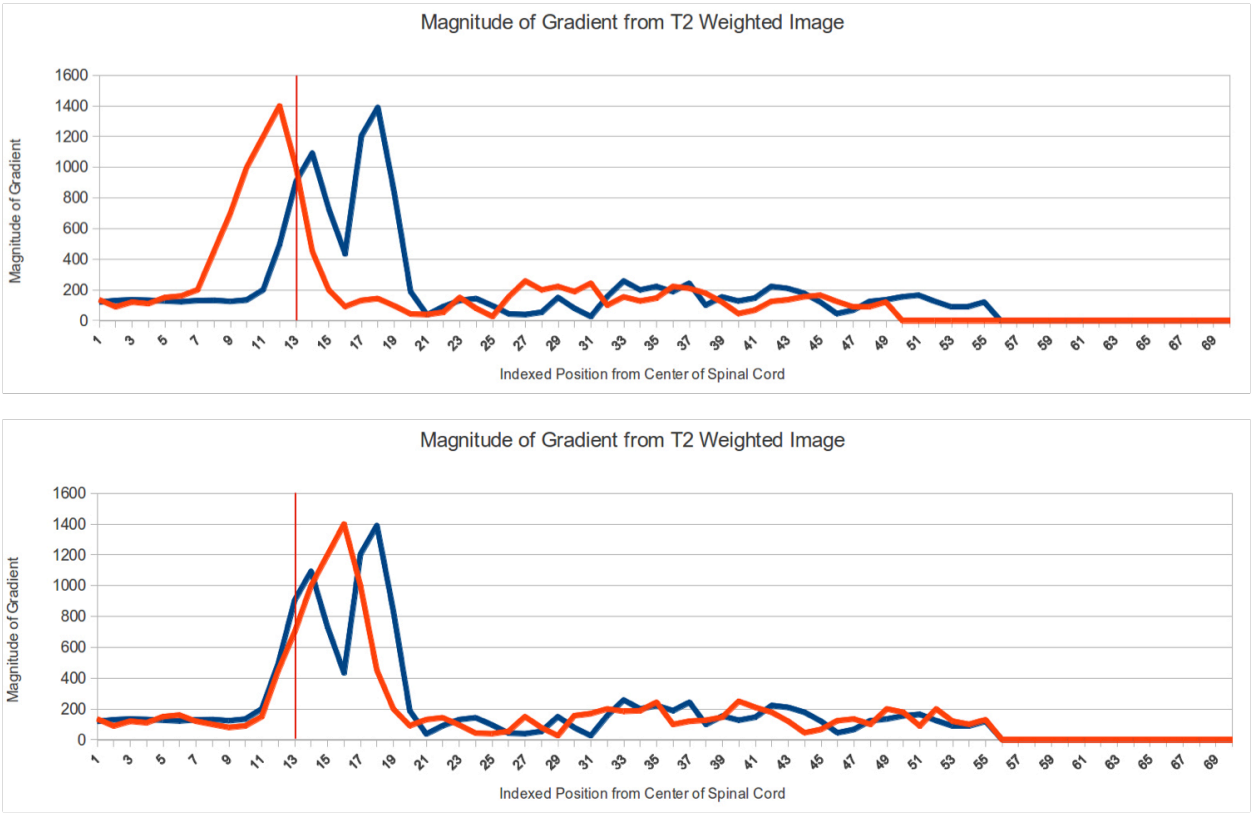

Figure 6-6. An example of normalized cross correlation for two different "test" arrays with the same template array. Shown on the top is a test array with a cross-correlation value of 30% to the template array. Shown on the bottom is a test array with a cross-correlation value of 74% to the template array.

For a single test array, the cross-correlation values between it and each template array are sorted from best match to worst match. The distance to the edge of the "test" array is simply the corresponding edge distance from the template array with the highest cross-correlation value, assuming the highest value was greater than 90% (an arbitrary threshold found to yield suitable matching results). If multiple templates had equal cross-correlation values, the average of the edge distances were taken. In instances where the highest cross-correlation value was less than 90%, the test array was disregarded and that radial location is dealt with in the interpolation and smoothing process discussed below. The more difficult areas to match are those with low CSF volumes, but the smoothing process is able to resolve these difficult areas.

c) Smoothing

When areas of low CSF are encountered, areas where the spinal cord lies directly adjacent to surrounding tissue of the same voxel intensity on the MR image, the template matching algorithm sometimes associates the consistently dark pattern as an area that would normally be found in the brainstem, where the distance from the center of the brainstem to the edge of the brainstem is larger than in the spinal cord. This pattern is observed when the CSF space is either diminished or obliterated as is the case in some normal individuals with a congenitally narrow spinal canal or in cases of pathology such as a disc herniation. To remove these outliers, a series of one-dimensional median smoothing filters are applied in a cascade. The filters are applied to the one-dimensional arrays of newly located edge distances, in two different planes: 1) in the axial plane, holding z constant and 2) along the z direction, holding Θ constant. The filter is applied four times in each of the two planes with different kernel sizes, progressively smoothing the edge distances, in a cascading manner. The kernel size ranges between 3 and 21. The reason for applying the filters in a cascade with varying kernel size is that certain kernel sizes work better in different areas of the spinal cord or brainstem depending on the curvature of the region. The top image in Figure 6-7 shows the distance to the edge for the 180 radial test arrays of a single axial plane (constant z) of an image before and after each filter in the cascade, with the thickest line being the result after all four filters are applied. The second image shows the same smoothing process, but the changes along the length of the spinal cord (variable z), in our area of interest, holding the rotational angle around the center of the spinal cord constant.

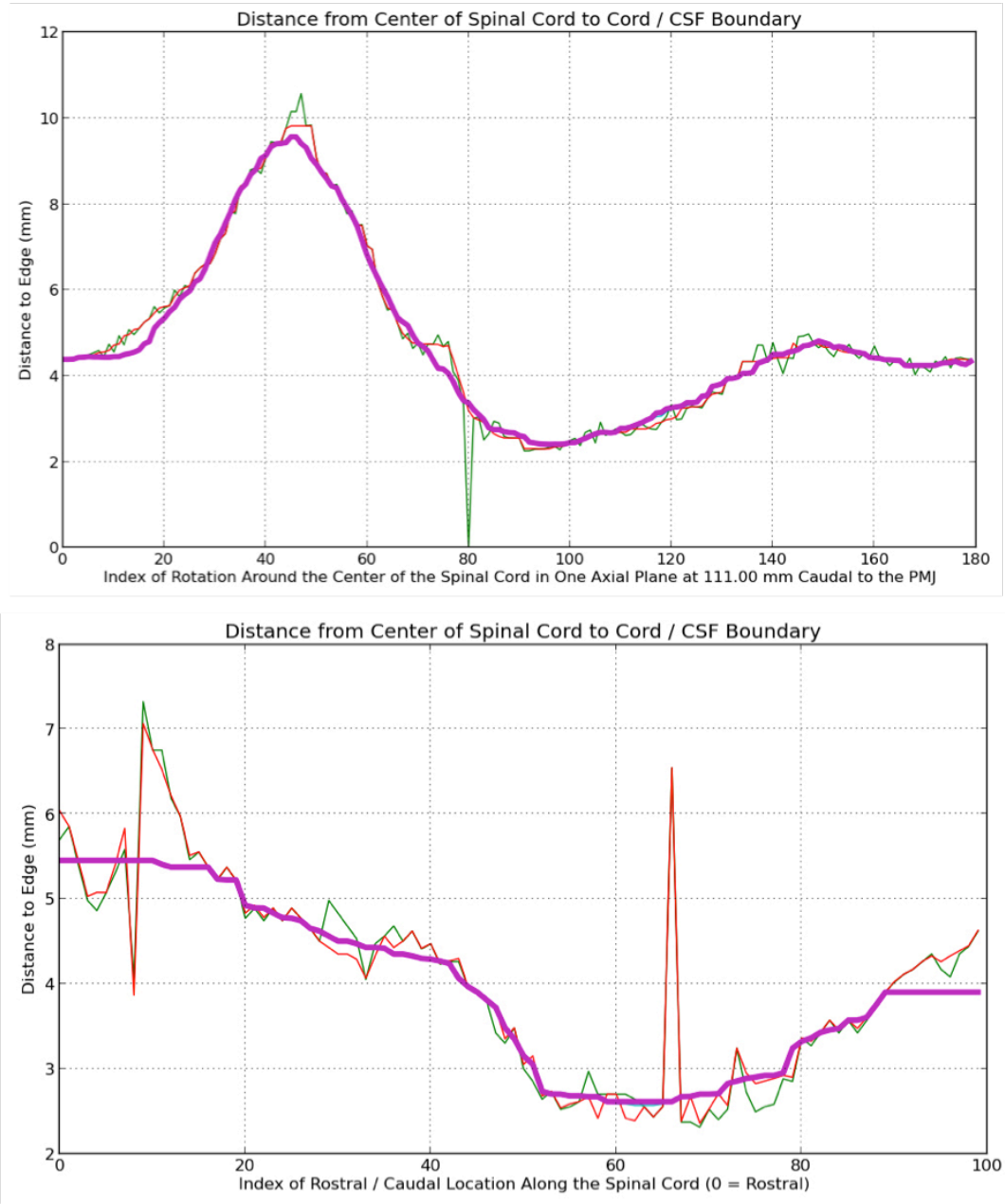

Figure 6-7. An example of smoothing the edge distances. The first image shows the distance to the edge in one axial plane after four cascading one-dimensional smoothing filters are applied and the second image shows the result of the same smoothing but along the entire length of the spinal cord area of interest, holding the rotational angle constant.

The results before and after applying the smoothing filter to a subject with reduced CSF in one area is shown in Figure 6-8. The image on the left is the result of CSF boundary finding of a non-segmented image, with no smoothing or interpolation. The image on the right is the smoothed image. The smoothing process takes only a few seconds.

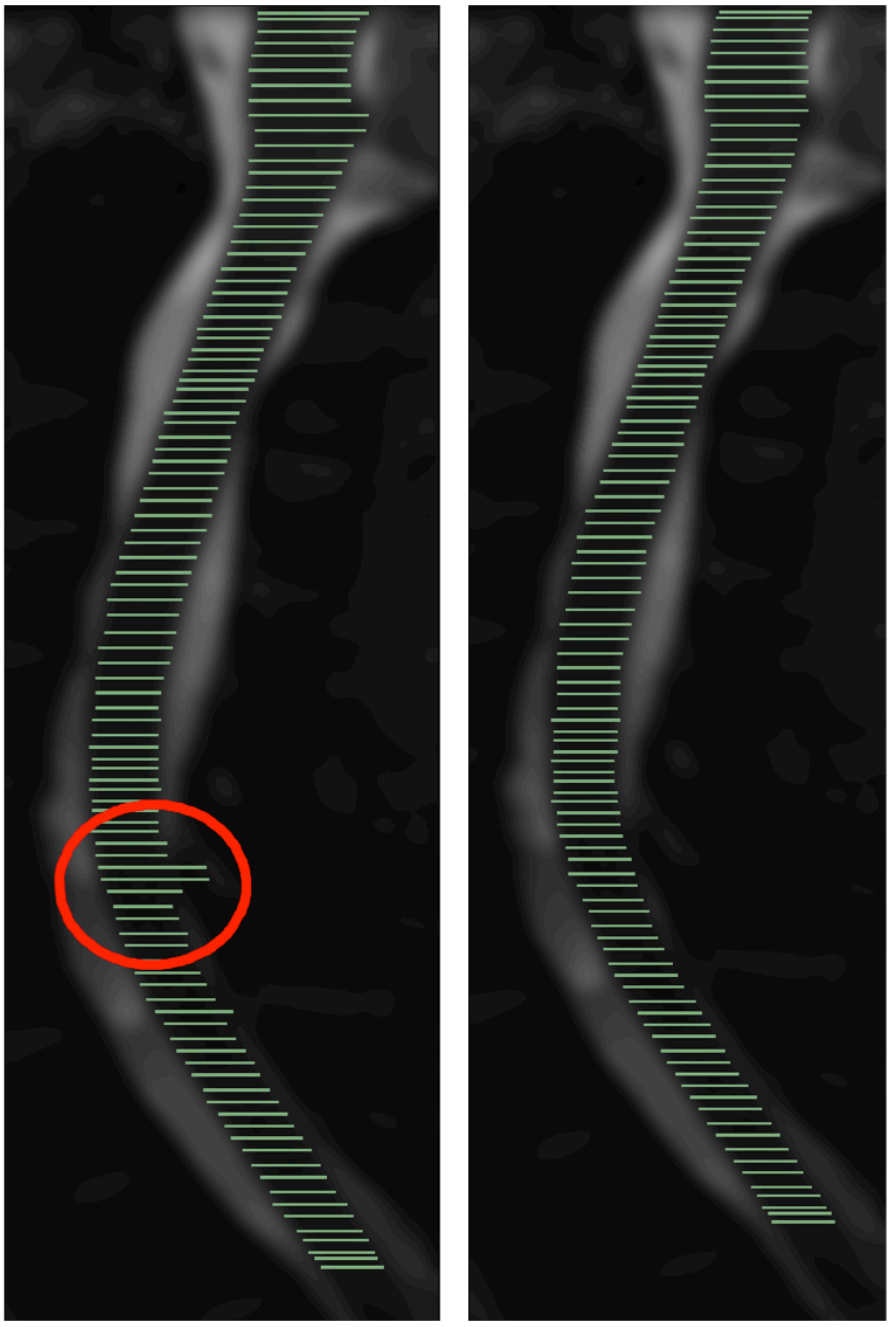

Figure 6-8. A mid-sagittal automatically segmented image. Shown are the results of segmentation at 100 points along the longitudinal axis shown before (left) and after (right) median smoothing filters are applied.

d) Refining the Center Points (Spline Control Points) of the Spinal Cord

To improve the arc distance measurements along the longitudinal, *z*-axis, a set of refined control points is calculated which will be used to re-initialize the spline. These points replace the original control points that were made manually as described above. For each of the 100 axial planes of the spinal cord that were segmented, where all 180 radial "test" arrays in the plane had a corresponding match in the template database, the X and Y coordinates for the maximum and minimum edge distances in the anterior/posterior, Y-axis, and lateral, X-axis, were determined. Since the spinal cord is similar in shape to a circle or ellipse, depending on the region of the spinal cord (for example, the mid-cervical cord is roughly the shape of an ellipse whereas the low-cervical / thoracic spinal cord is roughly circular), by finding the center of the extreme edge distances, one is able to form a better approximation of the center of the spinal cord. This method assumes that the cord is not rotated along its longitudinal axis, i.e., the anterior median fissure is always facing exactly ventral when the subject is lying in the supine position. We postulate this is a fair assumption given the anchoring of the spinal cord to the surrounding dura mater via the dentate ligament and therefore preventing spinal cord rotation.

The re-centering process only occurs on the sub-set of 100 axial planes in which all 180 radial "test" arrays had matches in the template database of greater than 90%. Axial planes in which there were test arrays without a significant match were discarded in the re-centering process.

e) Interpolation

The semi-automatic spinal cord / CSF boundary finding algorithm was applied to 100 axial planes at varying values of z of the MR image, as shown in Figure 6-8. The reason for not applying the CSF boundary finding algorithm to all axial planes in the image is to reduce computation time. To locate the spinal cord / CSF boundary of the remainder of the spinal cord, the edge information was linearly interpolated. Once interpolated, the segmented volume is smoothed once more as described above. The output is a fully segmented image that can be used to make volume calculations and measure distances, as described below. A 2D sagittal slice of a fully segmented spinal cord is shown in Figure 6-9.

Figure 6-9. A fully segmented volume of the human cervical spinal cord shown in the sagittal plane. This is based on the partially segmented image shown in Figure 6-8.

In total, the segmentation process takes approximately 1.5 to 2.0 minutes for a non-segmented "test" volume of the human cervical spinal cord with the same voxel dimensions as the template arrays were created from. The segmentations were performed on a desktop computer with the following specifications: Intel Core i7 (8 core) 3.4 GHz processor, 24 GB of DDR3-1333 RAM, and a 1 TB 7200 RPM Western Digital SATA (3 GB/s) hard drive, running the Ubuntu 12.04 64-bit operating system. No parallel processing optimization was used.

f) Segmentation Error

To estimate the error involved with the semi-automatic template matching and boundary finding process, we compared the automated segmentation pipeline (from spline initialization to interpolation) to a manual segmentation. The process of manually segmenting the whole cervical spinal cord is very time consuming, roughly 5-6 hours per subject using a 0.5 mm brush in 3D Slicer. To measure error associated with the segmentation process we chose to segment the region around the C5 nerve rootlets and compare only that region to the same region calculated from the automated process, for all 20 subjects.

Using 3D Slicer, the region directly above, including, and below the C5 nerve rootlet region was manually segmented. The location of this segment was determined by the initial nerve rootlet markings (see section 5.2.5 below). The area of these manual segmentations was then compared to the area of the automated segmentation. In both cases the exact same spline co-ordinates were used to demarcate the rostral and caudal extents of the volume to be used for the area calculation.

The average area of the C5 segment was calculated by finding the volume of the segment and then dividing by the total length of that segment. The comparison between manual and semi-automatic was made by finding the difference between the average cross-sectional area calculated for each of the semi-automatic and manual segmentations and dividing by the average area of the two: (Area 1 – Area 2) / (Average of Area 1 and Area 2). Finding the percentage difference allows for comparison of cords which have a significant difference in area. Taking the mean and standard deviation of this measure across 20 subjects yields a segmentation difference of 7.0% +/- 9.5% (range of -5.2% to +22.0%). In our subjects which had an average C5 segment

area of ~85 mm^2, this represents a 6 mm^2 average error. We found that the manual segmentation had a larger area in 14 out of 20 subjects. That is, manual segmentation tends to further extend into the CSF zone, or the semi-automatic segmentation tends to be conservative as to the radial distance to the spinal cord / CSF boundary.

6.2.5 Establishing a neuroanatomical context to spinal imaging

After segmenting the cervical spinal cord, as described in sections 5.2.3 and 5.2.4, the information can be used to make inferences about the locations of nerve roots and vertebrae.

6.2.5.1 Nerve rootlet and vertebral body localization

We used the C3 through C8 spinal nerve rootlets as a surrogate marker for the segmental anatomy of the spinal cord in an individual subject. To determine the distance from the PMJ (z = 0 mm) to each set of spinal nerve rootlets, two individuals with specialized knowledge of spinal cord anatomy manually marked the dorsal nerve rootlets of segments C3 to C8 at the edge of the spinal cord where the rootlets meet the CSF using 3D Slicer. To do this, the spinal cord and cervical nerve rootlets were visualized in three planes (axial, sagittal, and coronal) and the rootlets were followed as they transition into cervical nerve roots and traverse the respective intervertebral foramen. For example, the C3 nerve rootlets transition into the C3 nerve root and emerge through the intervertebral foramen between the C2 and C3 vertebrae. After confirming that specific nerve rootlets had transitioned from a specific nerve root, individual dorsal nerve rootlets were marked using a 0.5 mm paintbrush on 3D slicer. An example of these markings is shown in Figure 6-10 in the coronal plane.

Figure 6-10. A coronal plane of the cervical spinal cord showing manual nerve rootlet markings in red.

Using this 3D image overlay of the nerve rootlet markings and the spline function, the distance from the PMJ (z = 0 mm) to each of these markings is determined by calculating the arc length along the spline to each of the user marked points. This method provides both the distance from the PMJ to the nerve rootlet and the rotational angle, Θ, around the *z*-axis, where the rootlets are located. A visual example of the distance and rotational information data is shown in Figure 6-11.

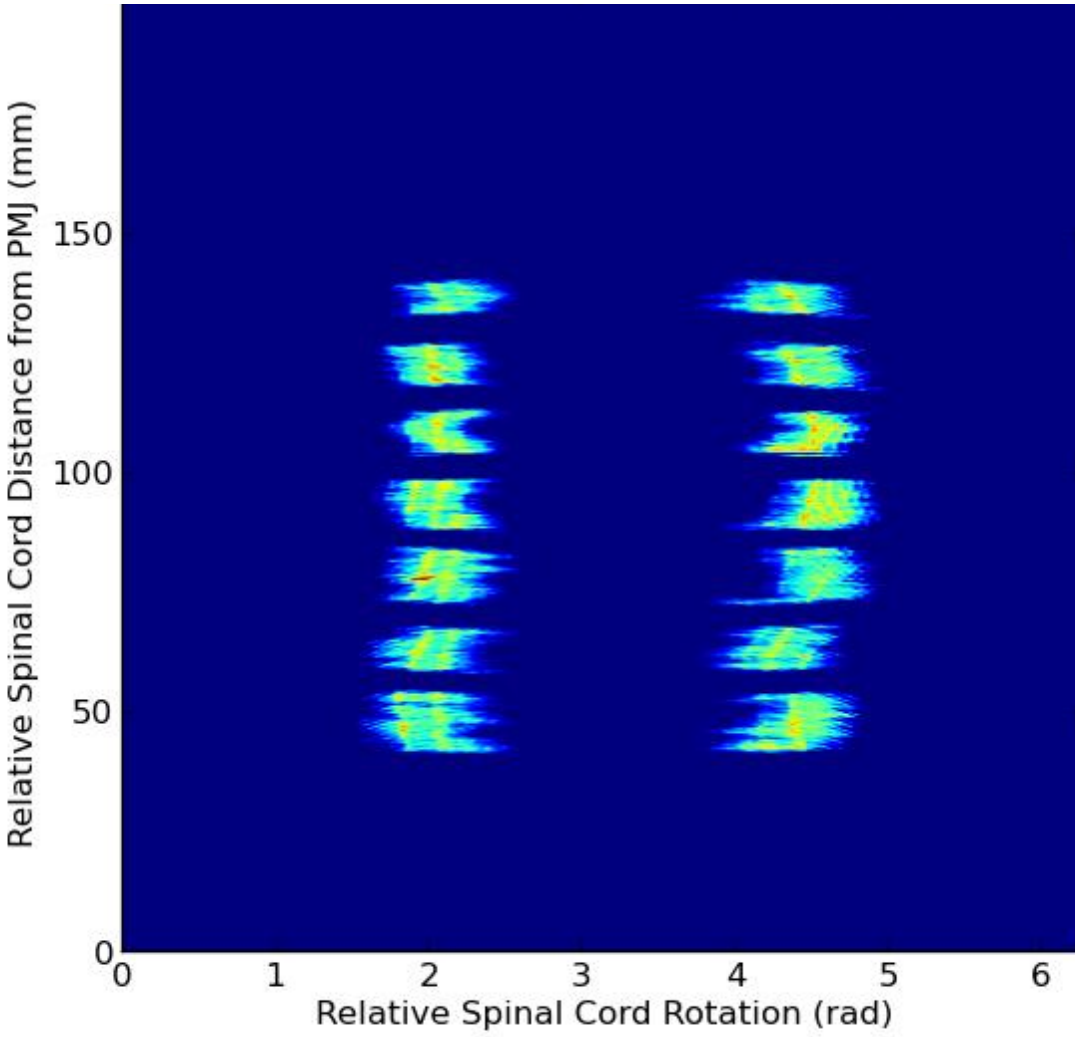

Figure 6-11. Nerve rootlet locations along the spinal cord and rotational angles around the longitudinal axis in a single subject.

Next, K-means clustering was applied (as implemented in the Python Scikit-learn package) to cluster each set of nerve rootlets in order to determine the center and rostral/caudal extents of each cluster. A K value of 6 clusters was used as 6 sets of nerve rootlets were marked, from C3 to C8. The center location of each cluster represents the arc length to that cluster from the PMJ (z = 0 mm).

Vertebral Body Localization

The same two individuals also marked the most rostral and caudal extents of the C3 to C7 vertebral bodies on a mid-sagittal slice of each subject (see Figure 6-15). The arc length from the PMJ to the point at the center of the spinal cord that is perpendicular to the tangent of the spinal cord and intersects the vertebrae was recorded as the distance to each of the vertebral markings. Taking the average of the two arc lengths for each vertebra yields the arc length adjacent to the center of each vertebra.

Inter-observer reproducibility in identifying cervical nerve rootlets and vertebral bodies

The inter-observer reliability of both nerve rootlet and vertebral body measurements were assessed by obtaining the intra-class correlation coefficient values comparing the assessments of two independent observers with specialized training in spinal neurosurgery. These coefficients were obtained using a two-way mixed effects model in IBM SPSS Statistics package Version 21, 2012.

6.2.5.2 Area and volume calculations

Cervical nerve rootlets serve as a surrogate for spinal cord segments. The rostral-caudal extent of any segmental group of rootlets can be used to determine either area (a two-dimensional measurement of the slice perpendicular to the tangential direction of the spinal cord) or volume (a three-dimensional measurement of any length of the spinal cord). The average height of each nerve rootlet-determined spinal cord segment is 9.9 mm with a standard deviation of 1.6 mm and a range of 6.7 mm to 15.6 mm, for all segments across all 20 subjects. To calculate the volume of each spinal cord segment, we add the number of filled voxels in the segmented image in a given

region, as determined by the user inputted nerve rootlet markings or vertebrae markings. Total volume is calculated by multiplying the number of filled voxels by the voxel size (in our case, 0.3906 x 0.3906 x 0.3000 mm). Dividing this amount by the arc length of the segment yields the average area of the spinal cord. Figure 6-12 shows a sagittal image of a subject with only the C5 nerve segment segmented. This is the volume over which the area of the C5 nerve segment would be averaged. It is localized based on the user inputted C5 nerve rootlet markings. The area and volume for this subject in the C5 nerve rootlet region were determined to be 76.9 mm^2 and 627.4 mm^3, respectively.

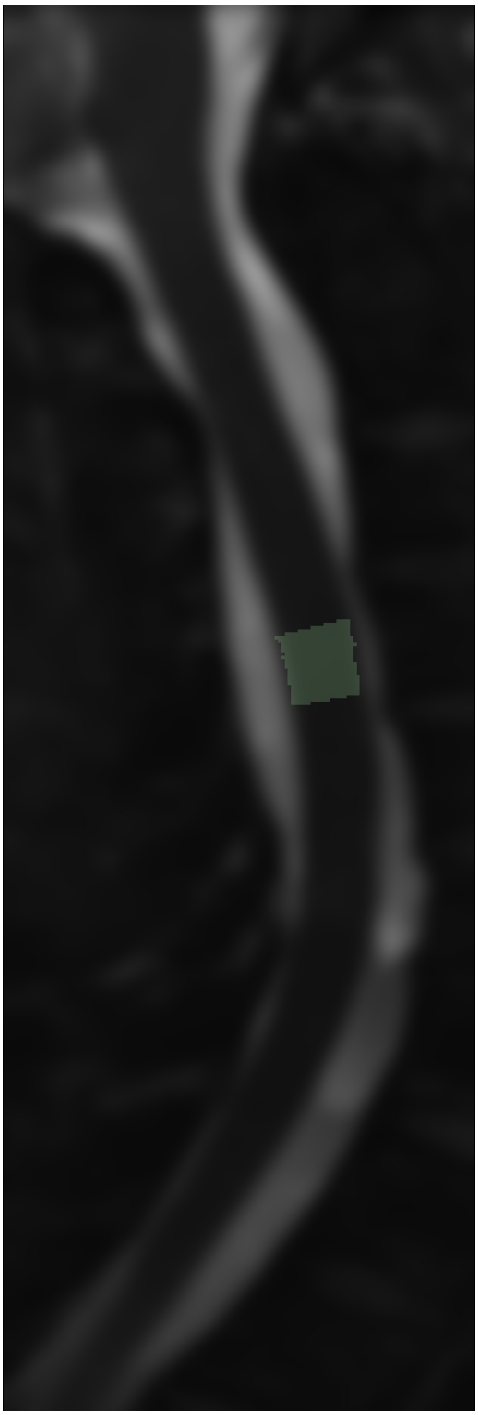

Figure 6-12. A segmented C5 spinal root segment. The area and volume for this subject in the C5 nerve rootlet region were determined to be 76.9 mm^2 and 627.4 mm^3, respectively.

6.2.6 Accounting for inter-individual differences in spinal anatomy

In order to predict the mean position of the nerve rootlets, we used linear regression of 7 measurements. Let x_i be a measurement vector of subject , such that x_i = (vertebrae midpoint position of C3-C7, neck height, subject height). Given $X = \{x^i\}_{S0}^{i=T}$, the measurements of all subjects, a linear regressor is 'learned' to predict the nerve rootlets mean position z_{NR} (is in generalized cylindrical coordinates), such that $z_{NR}^i = w \cdot x_i + w_0$. Learning the linear regression is done by choosing a vector , and a scalar $_0$ that minimize the root mean square error (RMSE) of prediction for all subjects.

Due to relatively small number of subjects (20 subjects), we used a leave-one-out cross validation to calculate the prediction error. In leave-one-out, the model is trained on all subjects but one, and tested on the remaining subject. By averaging that prediction error over all subjects and all nerve rootlets, we get an estimation of the model accuracy when handling new subjects**.**

In addition, we estimated the prediction error of nerve rootlets mean position based on the rostral position of the near-by vertebra (caudal direction). For example, we used the rostral position of C4 to predict the C3 nerve rootlets position. The error was calculated as the distance between the rostral measurement and the mean nerve rootlets position**.**

6.2.6.1 Are vertebral bodies a reliable surrogate marker for spinal cord segments?

To determine if vertebral bodies are a reliable surrogate marker for spinal cord segments, the amount of overlap between the two was determined. This was accomplished by determining the most rostral and caudal distances of the vertebrae and spinal cord segment in question, relative to the PMJ, and calculating the percentage of the spinal cord segment that falls within the vertebral segment area. For example, for one subject, the C6 vertebral body lies at a distance between 116 mm and 128 mm from the PMJ. The C7 spinal cord segment for the same individual lies between 110 mm and 118 mm from the PMJ. The overlap in this case is 2 mm at the rostral end of the vertebrae and caudal end of the spinal cord segment. The percentage overlap is calculated as overlap divided by the total length of the vertebral body, in this case 2 mm / 12 mm, or 17%. This was done on an aggregate basis and shown in Figure 6-18 of the results section.

Since all subjects have slightly different sized vertebrae and spinal cord segments, the sizing of the vertebrae and spinal cord segments were normalized as shown in Figure 6-18. We arbitrarily assumed that the normalized vertebral height was 10 mm (the actual average size for all subjects' vertebrae inclusive of C3-C7 is 11.8 mm). We then scaled the length of the spinal cord segment based on this assumption. For example, using the values from the overlap example above, if a vertebrae was 12 mm in length and the spinal cord segment was 8 mm in length, the scaled spinal cord segment would be ~7 mm (8 mm / 12 mm * 10 mm). The same process was used to scale the relative position of the spinal cord segment to the vertebrae. For example, using the same values as above, the scaled, relative position of the spinal cord segment to the vertebral body would be calculated as (((mid-point of vertebrae – mid-point of nerve segment) / length of vertebrae) * normalized length of the vertebrae). Using the values above (122 mm – 114 mm) / 12 mm * 10 mm, or 7 mm from the center of the normalized vertebrae. On the graph of Figure 6-18, this spinal cord segment would be shown centered at +7 mm, with a total length of 7 mm, therefore ranging from +3.5 mm to +10.5 mm. This process was repeated for all subjects using the same standardized vertebral body length to create Figure 6-18.

6.2.6.2 Does patient positioning within the MR environment exacerbate differences between vertebral and spinal cord segments?

Neck Flexion / Extension

Patient positioning for neck flexion and extension is described in the MRI acquisition section above. To calculate the degree of neck flexion or extension, we compare the tangent of the spinal cord in the sagittal plane at two points along the spinal cord. In previous work the angle is measured as the difference in vertebrae angles at C2 and C7.[128] The angle between these two vertebrae was calculated by drawing a line parallel to the posterior edge of the vertebral body, which runs parallel to the spinal cord, and calculating the angle between those two lines.

Our method utilizes the spline function to measure these angles rather than relying on manually drawing parallel lines. We measure the angle of the tangent of the spline at all locations on the spline function, relative to an imaginary horizontal line that lies across the sagittal plane. By subtracting any of these two points at different locations along the spinal cord, we are able to attain the relative angle with ease. The relative angle, holding the C7 vertebrae as the constant, is shown for one subject in the top half of Figure 6-13. We did not mark the C2 vertebrae in our

subjects, but the angle between the closest vertebral marking, C3, and C7 was determined to be 6.0 degrees, in this case. The top half of Figure 6-13 shows the angle between the tangent of the spinal cord at any point and tangent at the C7 vertebral body for one subject with their neck in flexion (red) and extension (blue). The lower part of the graph shows the difference between the flexion and extension curves, or the maximum extent of curvature of the spinal cord at various locations down the longitudinal axis of the spinal cord.

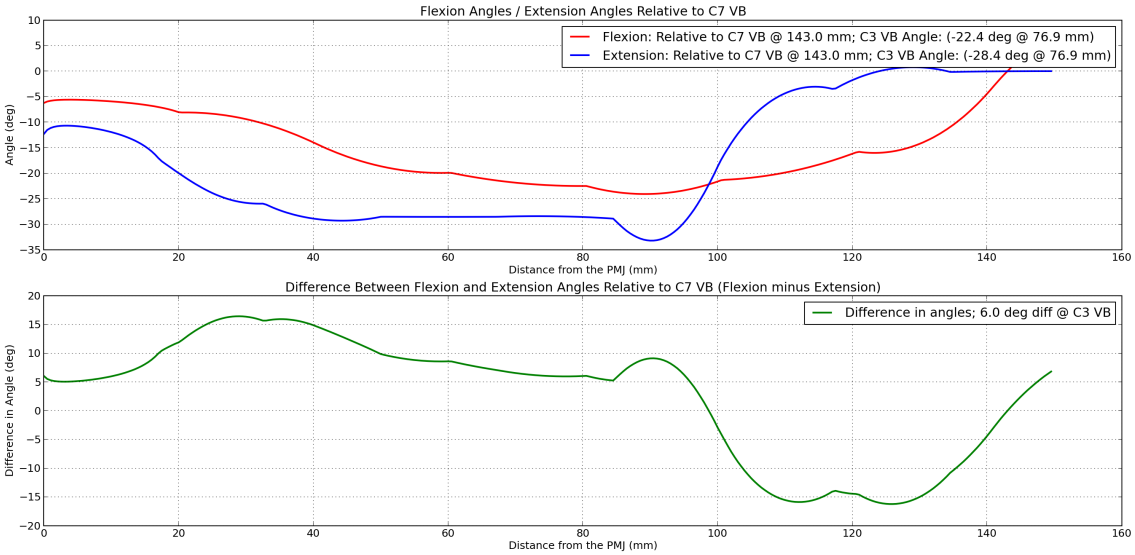

Figure 6-13. Automated analysis of the degree of neck flexion / extension of a subject. Top: the angle between the tangent of the spinal cord at any point and tangent at the C7 vertebral body for one subject with their neck in flexion (red) and extension (blue). Bottom: the difference between the flexion and extension curves, or the maximum extent of curvature of the spinal cord at various locations down the longitudinal axis of the spinal cord (X-Axis). (VB = vertebral body)

To determine whether or not patient positioning within the MR environment (slight neck flexion or extension) has an effect on the discrepancy between vertebral and spinal cord segments, we used the C5 vertebral body as a fixed bony landmark and calculated the position of spinal cord segments relative to this. First, as a control, we utilized the subset of images manually marked by two individuals in the following way: using the midpoint of the C5 vertebral body as a fixed landmark, we calculated the distance to the mid-point of each spinal segment (C3 through C8) and report the range. For example, the C3 spinal cord segment ranged from 20-24 mm from the C5 vertebral body. To determine if slight neck flexion or extension exacerbates this discrepancy between vertebral and spinal segments, we held the mid-point of the C5 vertebral segment constant and calculated the distance to the mid-point of each spinal segment in each position: neutral, flexion and extension.

6.3 Results: a population distribution of segmental spinal cord anatomy

6.3.1 Segmentation of the Spinal Cord

The adult human spinal cord is roughly the shape of a curved cylinder that extends from the cervicomedullary junction at the foramen magnum to approximately the level of the first lumbar vertebral body. The cervical spinal cord typically follows the slight lordotic curvature of the bony spinal column (the convexity of the curve points anteriorly and the concavity points posterior) but this varies significantly between individuals. To account for this variability we measured distances (arc-length, in mm) down the spinal cord from a fixed point in the brainstem, the ponto-medullary junction (PMJ), of 20 healthy volunteers (35% male, mean age = 30.5 years, range = 19 to 52 years, see

Table 6-1). Figure 6-14 illustrates the result of segmenting a T_2-weighted high-resolution (0.4x0.4x0.3 mm^3) 3D volume of the human spinal cord at 3 Tesla on a GE-HDX magnetic resonance system (GE Healthcare, Milwaukee). Spatial information is then available in a cylindrical coordinate frame of reference where the origin of the z-axis is chosen as the PMJ, the orientation around the spinal cord (in degrees) is described as the azimuth, and the radial distance from the central axis of the spinal cord is represented by *r*. For example, the central point of the

C5 segment of the spinal cord is described as z=84mm, an azimuth ranging from 0 to 360° (where, for example, the ventral spinal cord would carry values of 0-90° and 270-360°) and r ranging from 4 to 6 mm (depending on the azimuth, outlined in greater detail below).

Table 6-1. Demographic Information of Study Participants.

Participant No.	Age	Sex	Height (cm)	Neck Length (cm)
1	32	F	163	16.5
2	44	M	181	16.5
3	28	F	168	14.2
4	47	M	170	17.5
5	23	F	171	18.5
6	52	F	170	15.5
7	31	F	157	14.5
8	29	M	182	18
9	21	M	178.5	17.3
10	34	F	163.8	16.7
11	25	F	174.8	16.5
12	22	F	185.5	17.5
13	19	M	180	17.2
14	27	F	173	16.5
15	22	M	162	15.4
16	28	F	158.5	14.5
17	34	F	169	15
18	30	F	168	15.5
19	25	F	176	17
20	36	M	174	16

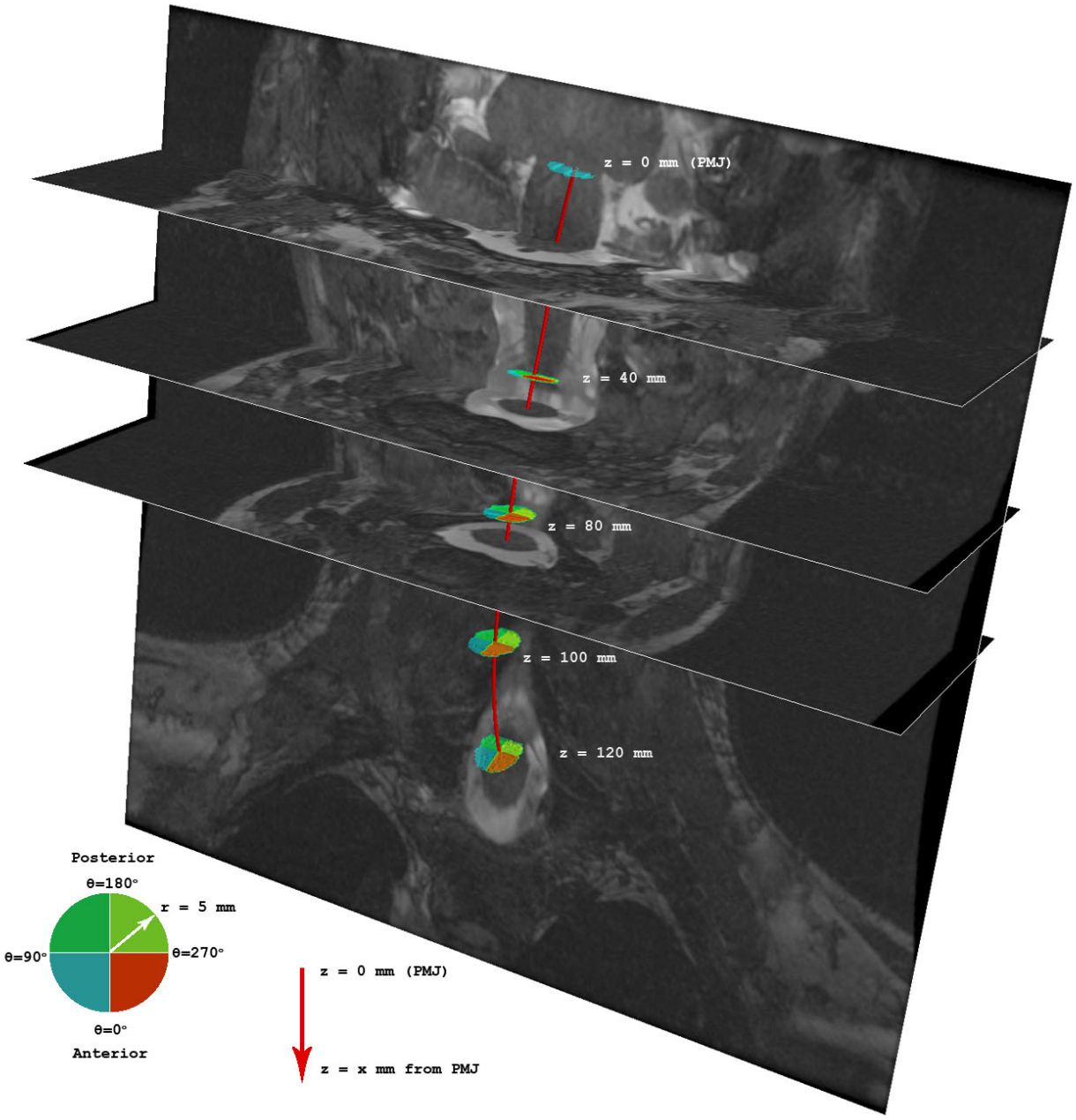

Figure 6-14. A segmented human cervical spinal cord at 3T that illustrates the cylindrical coordinate system used to describe spatial information within the spinal cord. The red line represents longitudinal (z) axis that conforms to the variable curvature of the spinal cord across individuals. The azimuth (Φ) (reported in degrees) ranges from 0 to 360 where values from 0-90 represent the right ventral quadrant, 90-180 represent the right dorsal quadrant, 180-270 represent the left dorsal quadrant and 270-360 represent the left ventral quadrant. The radial distance from the center of the spinal cord (r) is reported in millimeters for any longitudinal distance (z) and any azimuth (Φ, 0-360).

6.3.2 Imparting neuroanatomical context to spinal imaging

In order to provide neuroanatomical context to each individual's spinal images we manually marked the position of vertebral bodies and segmental nerve rootlets as they emerge from the spinal cord. An example of imaging results and the manner in which we marked the vertebral bodies and cervical nerve rootlets, a surrogate for spinal cord segmental anatomy, is illustrated in Figure 6-15.

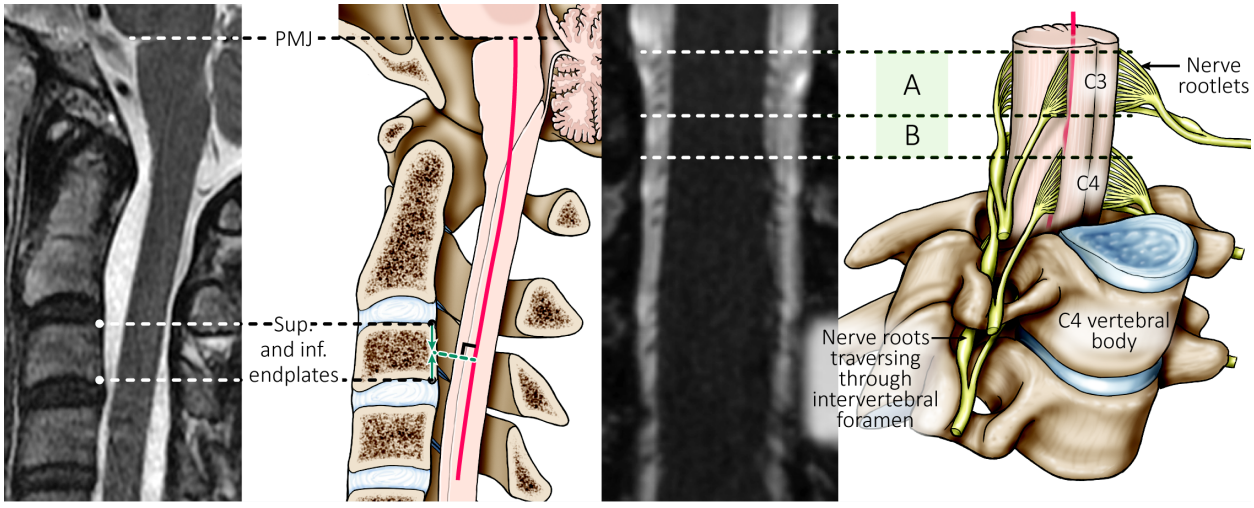

Figure 6-15. MR images and artist illustrations depicting manual segmentation of vertebral bodies and cervical segments of the spinal cord. From left to right: T_2-weighted MR image with the ponto-medullary junction (PMJ) and superior and inferior endplates of the C3 vertebral body marked with dashed white lines. Immediately adjacent to this is an artist's illustration demonstrating how person-specific markings are positioned relative to the individualized arc-length axis of the spinal cord (red line). In this way, distances can be compared across individuals along their personalized spinal cord axis. The T_2-weighted coronal image shown second from right depicts spinal rootlets (A) and the gap that is present between adjacent segmental rootlets (B), delineated by dashed white lines. The far right artist illustration depicts segmental rootlets and the formation of a spinal nerve root that emerges from the intervertebral foramen. In order to accurately localize segmental nerve rootlets, we followed the spinal nerve root that emerges from the intervertebral foramen of the respective vertebral body. Full details are available in the methods.

The common thread between all individual datasets is the personalized spinal cord axis originating at the PMJ and continuing down the spinal cord. By conducting measurements along this personalized axis, we were able to compare the distribution of vertebral body and segmental rootlet position down the rostral-caudal length of an individual persons' spinal cord with others in our cohort. This comparative distribution across twenty individuals is reported in Figure 6-16.

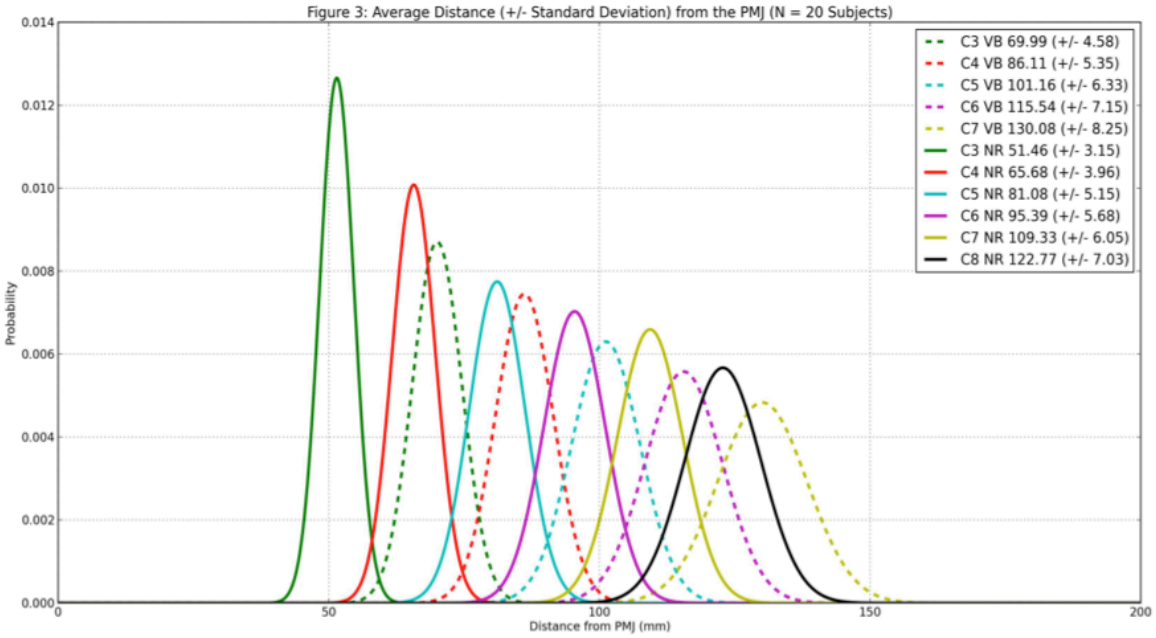

	Distance from the PMJ down the curved axis of the spinal cord	
	Mean distance (mm)	Range (mm)
Spinal Cord Segment (solid lines)		
C3	51.5	41.0 – 62.2
C4	65.7	53.8 – 75.9
C5	81.1	66.9 – 94.6
C6	95.4	79.2 – 109.1
C7	109.3	94.2 – 125.2
C8	122.8	105.8 – 140.3
Vertebral Bodies (dashed lines)		
C3	70.0	55.3 – 84.7
C4	86.1	72.3 – 104.6
C5	101.2	87.1 – 118.6
C6	115.5	99.7 – 133.8
C7	130.1	111.6 – 149.8

Figure 6-16. Nerve rootlet (solid lines) and vertebral body (dashed lines) distribution across our cohort of twenty individuals. The x-axis of this line graph represents the distance from the PMJ along the spinal cord axis, where 0 is the PMJ and the increasing numbers are mm distances down the curved axis of the spinal cord to the midpoint of either the vertebral body (VB) or spinal cord segment as demarcated by nerve rootlets (NR). The y-axis of the line graph represents the probability of finding either NR (solid line) or VB (dashed line) at a given distance down the curved spinal cord. The spinal cord segments and vertebral bodies represented by the colored lines are shown in the graph inset as distances in mm to the midpoint of either the vertebral bodies (VB) or spinal cord segments (as represented by nerve rootlets, NR) and standard deviations. Further details are reported in the table. The rostral-caudal extent of nerve rootlets corresponding to each spinal segment was relatively consistent across all spinal cord segments. The average length of spinal cord segments are: C3 10.5 mm, C4 9.9 mm, C5 10.5 mm, C6 9.7 mm, C7 9.4 mm and C8 9.6 mm.

The distribution of vertebral bodies along the curved longitudinal spinal cord axis is shown as dashed lines and reported within the table of Figure 6-16. A second, independent observer marked a subset of datasets (n=15) yielding an inter-class correlation coefficient of 1.0, $p<0.01$ indicating the high-degree of reproducibility with which a qualified individual can identify the vertebral bodies.

Dorsal and ventral rootlets appear at approximately 5.5 gestational weeks into development and relay segmental information to and from the spinal cord.[237] There are distinct gaps in the position of these rootlets (see MR image and illustration in Figure 6-15), a natural boundary for segmental information prior to the predominant somatotopic representation in the brain. The distribution of the C3 through C8 spinal cord segments along the curved spinal cord axis is shown as solid lines and reported within the table of Figure 6-16. A second, independent observer marked a subset of datasets (n=15) yielding an inter-class correlation coefficient of 1.0, $p<0.01$ indicating the high degree of reproducibility with which a qualified individual can identify segmental nerve rootlets.

The rostral-caudal extent of nerve rootlets corresponding to each spinal segment was relatively consistent across the C3 through C8 spinal levels. The average rostral-caudal length of rootlet groups are: C3 10.5 mm, C4 9.9 mm, C5 10.5 mm, C6 9.7 mm, C7 9.4 mm and C8 9.6 mm.

The cross-sectional area of the spinal cord varies considerably along its rostral-caudal extent. The cervical and lumbar enlargements are larger in area than the thoracic spinal cord as a result of the corresponding brachial and lumbar plexuses. Within the cervical cord, there is also variation both between segmental levels and between healthy individuals. Figure 6-17 outlines the area of C3 through C8 spinal cord segments. Across twenty individuals, the C3 segment was an average of 78.4 mm^2, C4 – 80.7 mm^2, C5 – 84.8 mm^2, C6 – 86.4 mm^2, C7 – 82.3 mm^2, and C8 – 72.6 mm^2.

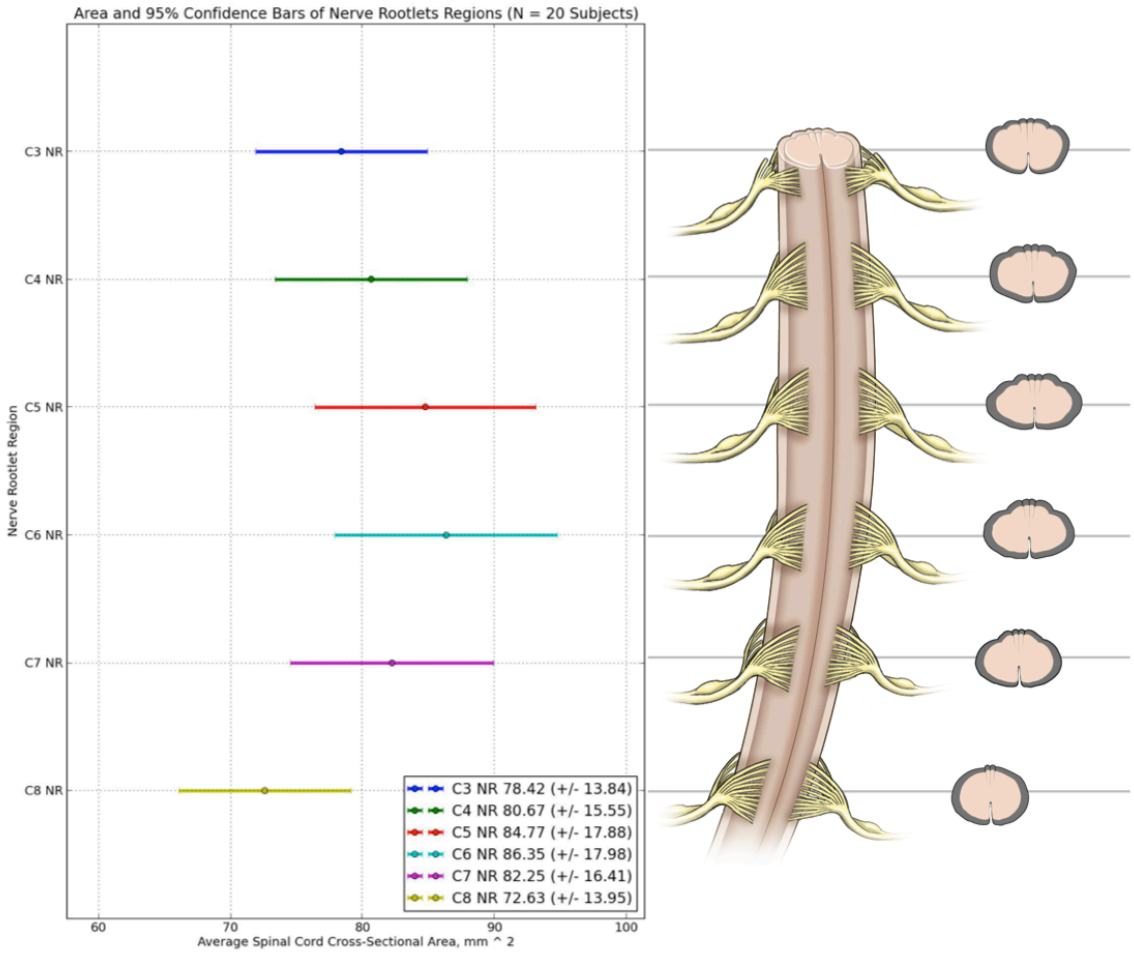

Figure 6-17. The variation of the cross sectional area of the spinal cord across individuals and across spinal cord segments. Using the segmental information obtained from manual markings (described in figure 3) we utilized the segmentation algorithm to determine the spinal cord area for each spinal cord segment (C3-C8). The area was calculated perpendicular to the curved spinal cord axis so as to not over- or under-estimate area in places of spinal cord curvature. Left: A graph showing the cross sectional area of C3 – C8 spinal cord segments with 95% confidence intervals across our cohort of 20 individuals (average segmental area and standard deviation are shown within the inset). Right: An artist illustration showing the variation in spinal cord cross sectional area from the C3-C8 segments. The gray shaded area represents the +/- 95% confidence interval. These results demonstrate that the area of the cervical spinal cord is relatively consistent across the C3 to C8 segments and diminishes at the caudal end of the cervical spinal cord. Comparison with other reported results is elaborated on in the discussion.

6.3.3 Accounting for inter-individual differences in spinal anatomy

The results presented above and illustrated in Figure 6-14 through Figure 6-17 provide a neuroanatomical context to spinal imaging. The differences between individuals have implications for imaging studies conducted across a cohort of subjects; in order to account for these differences and improve the accuracy with which interpretations are drawn from imaging studies, we next consider: 1) the effect of using vertebral bodies as a surrogate for spinal segments; 2) the ability to predict spinal segment position without having to manually identify nerve rootlets; and 3) whether or not patient positioning within the MR environment can exacerbate differences between vertebral and spinal cord segments.

6.3.3.1 Are vertebral bodies a reliable surrogate marker for spinal cord segments?

Given the heterogeneity in spinal column and spinal cord anatomy across even a small sample of the human population, how this might affect the spatial interpretation of imaging data is illustrated by using the vertebral bodies as a rough indication of spinal cord segmental anatomy; this is illustrated in Figure 6-18. In our first example, we illustrate the effect of assuming that a certain vertebral body is immediately adjacent to the corresponding spinal cord segment (e.g., the C7 vertebral body is adjacent to the C7 spinal segment). If we apply this assumption to all 20 subjects in this study then 0% of the C7 spinal cord segment volume is captured in the selected range. The root-mean-squared-error (RMSE) between locations of vertebral bodies and their corresponding spinal cord segments, averaged over 20 subjects 5 groups of nerve rootlets (C3 - C7), is 20.33 mm.

Observation suggests that a more accurate landmark for predicting spinal cord segments is utilizing the vertebral body rostral to the given spinal cord segment. This assumes, for example, that the C7 spinal cord segment lies adjacent to the C6 vertebral body. Using all 20 subjects studied, 44% of the intended spinal cord segment volume would be captured in the targeted volume. The RMSE between locations of spinal cord segments and the rostral end of the vertebral body rostral to the corresponding spinal cord segment in this case is 3.39mm. We also

note that RMSE depends significantly on the subject, ranging from 0.86mm to 6.42mm among the 20 subjects.

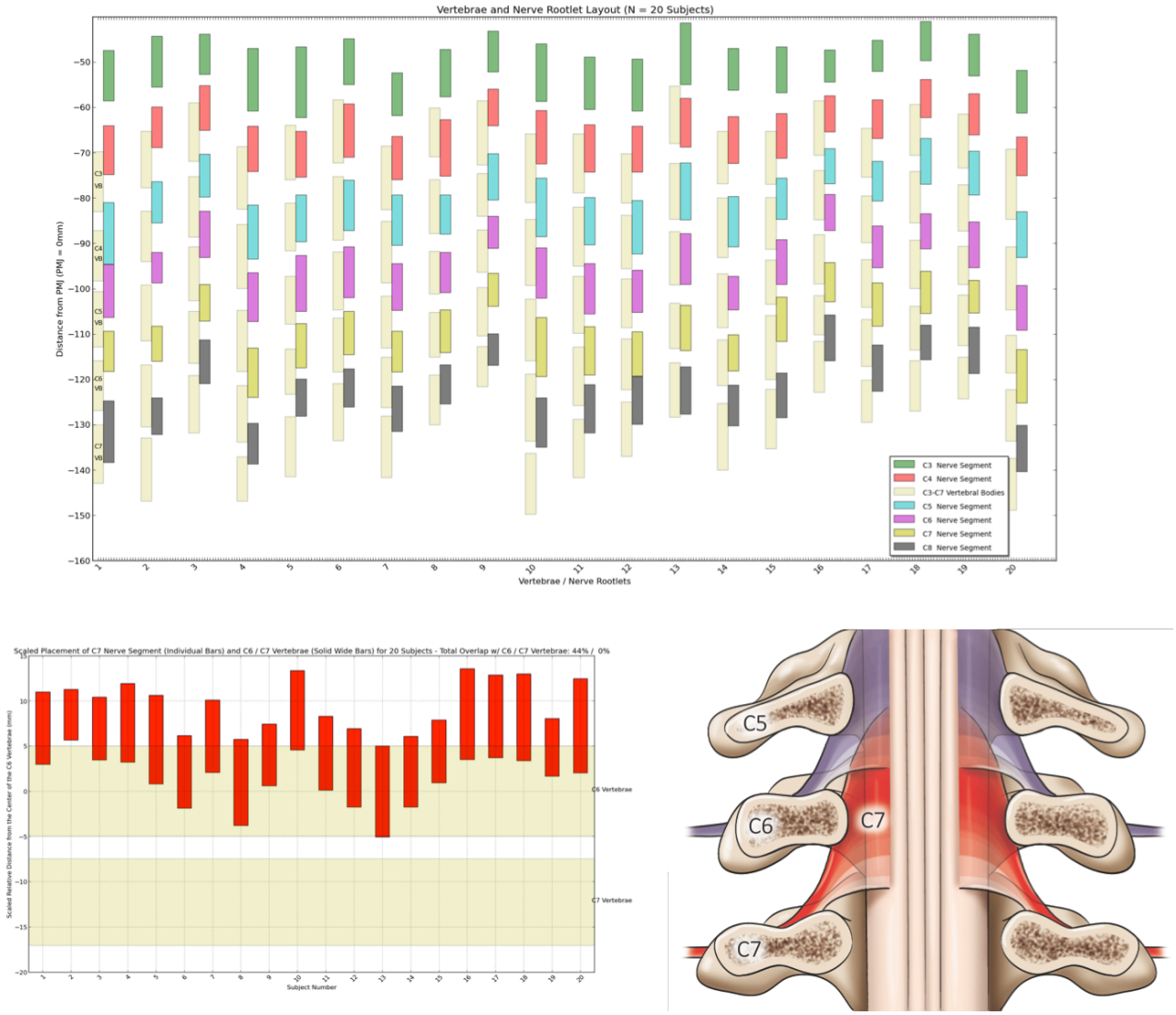

Figure 6-18. Vertebral body and spinal cord segment location across 20 subjects. Top: The distribution of vertebral and spinal cord segments shown for each subject enrolled in this study. Vertebral bodies are represented for each subject by light shaded bars whereas spinal cord segments are represented by colored bars (see graph inset). Bottom left: Scaled relative distance of the C7 spinal cord segments (red bars) from the C6 (upper light brown shaded area) and C7 (lower light brown shaded area) vertebral bodies. When we visualize an individual person's cervical spine MRI, we tend to hold the vertebral bodies constant. This figure illustrates that the position of the 7th cervical spinal cord segment varies relative to the position of the vertebral body across a cohort of individuals. If one were to assume that the C7 spinal segments are immediately adjacent to the C7 vertebral body, then 0% of the actual segments would be captured in such an analysis. Similarly, if one were to assume that the C7 spinal cord segments are 1 vertebral body length rostral to the C7 body, then one would capture 44% of the corresponding spinal segments. Depending on the experimental goals of the imaging experiment, careful attention should be paid to the relative position of spinal segments and vertebral bodies across a cohort of individuals. Assuming spinal segments are constant may lead to false positive or false negative results. Bottom right: An artist depiction showing the range in spinal cord segments relative to the vertebral bodies; light shaded areas represent areas of population level overlap.

6.3.3.2 Prediction of Segmental position relative to PMJ

Given the relatively wide distribution of spinal segments relative to the PMJ reported in Figure 6-16, it would be helpful to be able to predict the position of spinal cord segments to improve efficiency within a data analysis pipeline. One can, for example, use statistical regression to find a predictor for spinal cord segments. To this end we used a linear least-squares (LS) regressor to predict spinal cord segments (C3-C8) from an individuals neck length (straight distance from the external auditory meatus to the clavicle), total body height, and the midpoint location of vertebral bodies C3 to C7 along the spinal cord axis.

To evaluate these predictors we used a simple form of leave-one-out cross-validation. For each subject a regressor is learned from the remaining 19 subjects and then tested on subject not included in the training set. The RMSE in training the 20 regressors was 1.81mm. The RMSE on the held out data was 3.18mm. There was also significant dependence on the spinal cord segment; RMSE for C3 through C8 was, respectively, 2.41, 2.72, 3.20, 3.35, 3.11, and 4.03, all in mm. The RMSE for these predictors show less dependence on subject compared to the methods above, ranging from 0.83mm to 5.32mm over the 20 subjects.

6.3.3.3 Does patient positioning within the MR environment exacerbate differences between vertebral and spinal cord segments?

To determine the effect of patient positioning on the discrepancy between vertebral level and spinal segments, a subset (n=6) of our initial cohort underwent imaging in slight neck flexion (by placing an extra cushion under the occiput) and slight neck extension (by placing an extra cushion under the shoulders). Under conditions of either neck flexion or neck extension (measured at approximately 11 – 15 degrees in either direction from neutral position; details outlined in methods section), the discrepancy between spinal and vertebral segments did not appreciably change as detailed below.

The inter-individual marking differences between the two qualified individuals were used as a control, where each individual manually marked the C3 through C8 spinal segments in 15 subjects. The difference between these two sets of markings for any given subject was defined as the “marking error” associated with each subject. This error was determined to be between -2.0

mm and +1.3 mm, or a total range of 3.3 mm. Under conditions of either neck flexion or extension, the distance from each spinal cord segment to a fixed point of the spinal column (vertebral body) ranged from 0.6 mm to 2.4 mm. The normal / flexion / extension distance range was less than 3.3 mm, suggesting that any subtle change in neck position that is possible within the confines of the MR imaging unit does not exacerbate differences between spinal cord and vertebral segments.

6.4 Discussion

A novel, quantitative solution to resolve the anatomical variability of the human cervical cord is presented. Computer vision algorithms are employed on high-resolution cervical spinal MRI data to identify the longitudinal axis of the brainstem-spinal cord with a polynomial spline function. Based on user-defined markings of segmental nerve rootlets as ground truth data, the position of spinal segments was identified relative to the ponto-medullary junction (PMJ). For the first time, a population distribution of the segmental anatomy of the cervical spine is reported. This has direct implications for the interpretation of advanced imaging studies most often conducted across groups of subjects.

This work demonstrates that significant variation exists in the rostral-caudal position of spinal cord segments between individuals and that a combination of variables (subject neck length, body height and the position of vertebral bodies relative to the PMJ) can be used to predict the position of a given spinal segment. Accounting for this variation will be paramount to accurate interpretation of the neuro-anatomical origin of acquired MR signals in future imaging studies. This especially holds true for functional MRI studies that are challenging due to the low sensitivity for studying single subjects (notably due to low signal-to-noise ratio and high physiological noise), and by the intrinsic variability of spinal rootlet locations that hamper the use of grouped data. This argument is supported by a previous fMRI study on cats, which shows high inter-animal variability on the rostro-caudal location of the BOLD signal relative to the vertebral level, when stimulating the same peripheral nerve.[128]

While other approaches to segmenting the spinal cord from MR images exist, they are fraught by challenges.[128] Initial attempts at utilizing the Horsfield *et al.*[128] approach resulted in difficulty segmenting the spinal cord in regions of low CSF volume around the spinal cord. This limitation was taken into consideration when designing the template matching algorithms presented here.

The method developed by Coulon *et al.*[128] is computationally intensive relative to both the Horsfield approach and the novel methods presented here; as such this method was not studied. The novelty of the work presented here and its potential impact on the neuroimaging community is that we account for neuroanatomical variability rather than the segmentation methods in isolation.

Considerable variation exists within the human cervical spine with little or no reported literature describing these differences and how they might impact advanced neuroimaging studies that incorporate multiple subjects into groups of study participants. As demonstrated from the results herein, there is variation in the rostral-caudal position of emerging nerve rootlets relative to the PMJ and this can impact findings regarding the function of segmental locations along the spinal cord. For example, if one is comparing the sensory function of the C8 dermatomal distribution between two individuals, it is not clear what specific coordinates along the rostra-caudal spinal axis reflects the synaptic connections of sensory neurons and their inter-neurons innervating this dermatome. The results presented here indicate that the natural variation across individuals warrants close attention for neuroimaging studies and that personalized segmentation increases the spatial specificity of attributing an MR signal with its neuroanatomical origin.

In addition to variation in the position of spinal cord segments relative to the PMJ, the cross-sectional area of the spinal cord also varied considerably along its longitudinal axis. Several different methods have been developed to measure the area of the cervical spinal cord in healthy controls and those with spinal cord injury (SCI) and multiple sclerosis.[128] In all cases, the techniques measure area in the upper cervical spinal cord. In cases of pathology such as SCI, studies have reported a decrease in spinal cord area ranging from approximately 10% to 30% of controls.[128] Only a single study to date has made use of a longitudinal design and recorded how spinal cord area changes over time after traumatic SCI.[235] Freund *et al.* highlight (2013) how spinal cord area can be used as an element of an imaging biomarker whereby progressive changes in spinal cord area at a rate of approximately 0.408 mm^2 / month after acute injury correlate to clinical deficit. The rate of spinal cord atrophy in traumatic SCI and other specific disease states deserves further attention as this may provide a means of early detection of response to neuroprotective therapies.[238] The methods proposed in this work allow for documentation of spinal cord area at all levels of the cervical spinal cord.

After providing a neuroanatomical context to spinal imaging data, three important concepts were addressed to account for inter-individual variation in imaging studies conducted across a group of subjects: 1) the effect of using vertebral bodies as a surrogate for spinal segment location; 2) the ability to predict spinal segment location; and 3) the effect of patient positioning on localizing a spinal segment. Subdivision of the spinal cord into discrete segments begins as early as 4.5 gestational weeks in embryological development during which time dorsal nerve rootlets engage the spinal cord from dorsal root ganglia and ventral nerve rootlets emerge from the spinal cord; this process is largely complete by the end of the first trimester after which time the spinal cord white matter develops and is progressively myelinated.[137] Dorsal and ventral nerve rootlets aggregate in clusters, emerge from the spinal cord forming into a spinal nerve and traverse the closest caudal inter-vertebral foramen to innervate the corresponding segment of the body.[137] As such, cervical spinal cord segments are consistently located rostral to the corresponding numbered cervical vertebrae as illustrated in Figure 6-18. However, using vertebral bodies to localize a corresponding spinal cord segment is quite imprecise. The root-mean-squared-error (RMSE) between locations of vertebral bodies and their corresponding spinal cord segments, averaged over 20 subjects and 5 spinal cord segments (C3 - C7), is 20.33 mm. Precision improves somewhat by using the rostral boundary of vertebral body rostral to the given spinal cord segment (for example, the rostral end of the C6 vertebral body sits adjacent to the C7 spinal segment). The RMSE between locations of spinal cord segments and the rostral end of the vertebral body rostral to the corresponding nerve rootlet in this case is 3.39mm. Using a linear regression model along with a leave-on-out cross-validation, the location of spinal cord segments could be predicted with a slightly higher degree of accuracy. The RMSE in training the 20 regressors was 1.81mm. The RMSE on the held out data was 3.18mm, with significant dependence on the spinal cord segment, C3 through C8. Fortunately, patient positioning does not influence the discrepancy between vertebral and spinal cord segments, which has important clinical implications.

6.5 Conclusions

Using novel methods to define the central axis and segment the brainstem – spinal cord, this work demonstrates that significant variation exists in the rostral-caudal position of spinal cord and vertebral segments across individual subjects. This has implications for interpreting advanced imaging studies. The location of a spinal cord segment down the arc-length axis of the

spinal cord can be predicted using a combination of variables offering a means of identifying segmental anatomy without having to perform high resolution imaging to manually identify nerve rootlets, potentially adding efficiency to a data analysis pipeline. Lastly, this work demonstrates that patient positioning within the MR environment does not have an appreciable effect on the spinal-vertebral discrepancy, meaning that one does not have to account for patient positioning when conducting longitudinal studies in single patients.

Remarkable advances have been made over the past decade allowing for improved imaging of the human spinal cord.[128] Imaging acquisitions that take into account magnetic sussceptability gradients of the spinal column and post-proccessing methods to account for cardio-respiratory related motion have allowed for improved applications to detect structural and functional anomalies that occur in relation to traumatic injury of the spinal cord.[128] Other disorders, such as multiple sclerosis, have also benefited from spinal cord imaging.[128] Degenerative spinal disease such as cervical spondylosis is an increasing health burden due to the aging population.[128] Advanced imaging tools stand to play an important role in aiding with decision making such as the optimal time to offer decompressive surgery to maintain neurological function before irreversible neurological deficits are realized. Future work in the realm of spinal segmentation must focus attention on the neuroanatomical context of acquired images and utilizing population based probability data to develop improved methods that aim to identify segmental anatomy. In this way, the user may have to only ensure the accuracy of the segmentation rather than manually identify each region of the spinal cord as we did here. Such advances will improve workflow and reduce post-processing time. Ultimately, this neuroanatomical knowledge may be used for the delivery of targeted therapeutics offering a regenerative strategy toward damaged cell populations.

Chapter 7
General Discussion

This chapter is modified from the following:

Cadotte DW, Cohen-Adad J, Fehlings MG. Visualizing integrative functioning in the human brainstem and spinal cord with spinal functional magnetic resonance imaging. Neurosurgery. 2013 Aug;60 Suppl 1:102-9. doi: 10.1227/01.neu.0000430767.87725.95. PMID: 23839360

7 General Discussion

Traumatic injury to the spinal cord results in specific pathophsyiological events that render an individual with a range of motor, sensory and autonomic deficits. A great deal of pre-clinical animal literature has described the effects of traumatic spinal cord injury both 1) at the epicenter of damage and 2) peri-lesional, including segments of the spinal cord above and below the level of injury and in a more distributed fashion across the brainstem-spinal cord axis. This thesis provides new knowledge with regard to how MR-based imaging characteristics are used in the context of truamtic injury to the human cervical spinal cord.

Chapter 4 details the use of intrameduallary MRI-based signal changes at the epicenter of injury to stratify patients along a spectrum of injury severity whereby T_1 and T_2 signal changes serve as a biomarker to reflect underlying pathophysiology. The following spectrum was established: normal (no change in T_1 or T_2 signal intensity within the spinal cord), T_2-weighted signal hyper-intensity, evidence of spinal cord compression, evidence of spinal cord swelling, evidence of intramedullary hemorrhage and spinal cord trans-section. These signal characteristics can serve as biomarkers to classify patients along a spectrum of injury severity from mild to severe, respectively. When patients are classified as having a **mild injury,** MRI has a high degree of sensitivity and a low degree of specificity to predict prognosis at follow up. When patients are classified as having a **severe injury**, MRI has a low sensitivity and high specificity to predict prognosis at follow up. This is the only meta-analysis reported in the literature examining the prognostic ability of standard T_1 and T_2-weighted imaging characteristics as a biomarker for injury severity. It is possible to establish a spectrum of injury severity using both clinical examination and standard imaging metrics as a biomarker. Using sensitivity and specificity as a means of evaluating the ability of either clinical examination or MR-based biomarker to predict prognosis, it becomes clear that standard T_1- and T_2-weighted signal characteristics of the injured human spinal cord offer no advantage over clinical assessments. This study concludes that 1) T_1 and T_2 signal changes perform worse than standard clinical assessments as a biomarker for injury severity and the ability to prognosticate recovery. 2) Future biomarkers should target specific pathophysiological events (example, myelination) or specific structural or functional elements of the spinal cord rather than rely on non-specific T_1 and T_2 signal changes. Furthermore, imaging the epicenter of injury may preclude capturing biological events that occur in a peri-lesional

fashion such as re-myelination or axonal sprouting that typically occur either rotral, caudal or both to the epicenter of damage.

Chapter 5 uses a spinal functional MRI design to investigate somatosensory afferent stimulation between healthy individuals and chonic spinal cord injury patients, a first of its kind. Afferent thermal stimulation resulted in an increased neurovascular response above the level of injury, consistent with pre-clinical animal models that demonstrate reduced GABAergic activity and regeneration of damaged pathways or compensatory collateral axonal sprouting.[128] In addition, stimulation below the level of injury resulted in a linear inverse relationship between sensory perception and neurovascular reponse below the level of injury. This is in agreement with pre-clinical animal models suggesting that a more severe degree of spinal cord injury results in reduced inhibitory transmitter levels in that region in addition to partial or complete loss of connections with supra-spinal pathways.[224] Spinal cord injury patients, even when they fully recover, demonstrate a more distributed response to afferent stimulation a pattern of activity that is consistent with axonal regeneration and/or an axonal sprouting after injury, potentially forming novel pathways of communication between damaged regions of the spinal cord and supra-spinal circuits.[88-90] This study concludes that patterns of afferent stimulation can be captured with spinal fMRI techniques and that the patterns of spinal cord function revealed are consistent with changes observed in animal models of SCI. A limitaion of this study was the ability to resolve the degree of distributed activity observed relative to spinal cord segments. Chapter 6 addressed this limitation by characterizing the anatomic variability of spinal cord and vertebral levels across a cohort of individuals.

Chapter 6 characterizes the variability in distribution of vertebral and spinal cord segments along the arc-length axis of the brainstem-spinal cord. To do this, computer visions methods were used in a novel way to define the central axis of the brainstem – spinal cord and segment the spinal cord from surrounding structures. The principle finding of this work is that significant variation exists between individuals with regard to the relative positions of both vertebral and spinal cord segments to a common, fixed point in the brainstem – the ponto-medullary junction. This has implications for the interpretation of imaging studies that aim to investigate a specific region of the spinal cord. To build on this finding, a prediction model is presented that might aid in the estimation of specific spinal cord segments given easy to obtain information: the position of vertebral bodies, height and neck length. This study concludes that the natural variation between

individuals is great enough to warrant attention to personal anatomy. For example, if a novel cellular transplant strategy aims to implant stem cells into the C5 and C6 region of the spinal cord in an attempt to regain function in the deltoid muscle, where along the spinal cord axis should one examine for integration of such cells into a spinal cord circuit (functional MRI study) or changes in the structural integrity of the spinal cord (anatomical MRI study)? The results of study II indicate that the precise anatomical position of these spinal cord segments relative to the ponto-medullary junction varies between individuals.

The over-arching aim of this thesis is determine whether magnetic resonance imaging can be used to establish biomarkers that provide guidance for clinical care of patients with SCI. This work also included the development of novel techniques to more accurately resolve the anatomic variability of the human cervical spinal cord, filling a gap in existing MRI methods for use in SCI patients. Relevent aspects of each of these studies will be discussed in further detail, followed by an overview of limitations of this work and future directions.

7.1 Standard T_1 and T_2-weighting as an imaging biomarker

With the widespread adoption of MRI into clinical practice starting around 1980 and reaching most advanced clinical centers 5-10 years thereafter, clinicians and researchers treating spinal cord injury saw both immediate gains in terms of surgical planning and patient management and the opportunity to use this technology to better inform about the extent of injury and prognosis.

The results indicate that MRI, used in this traditional way, offers no benefit to predicting prognosis after spinal cord injury relative to clinical examination. This is likely due to the crude cut-points with which such signal characteristics are able to categorize SCI patients along a spectrum of injury severity, when examined at the epicenter of injury. Along this same line of reasoning, there is a great deal of heterogeneity in signal characteristics that represent, for example, hemorrhage in the spinal cord – one indicator of a severe injury. Going forward, imaging biomarkers should aim to capture specific pathophysiological events so as to reduce heterogeneity among patients undergoing imaging and this should be conducted outside the epicenter of injury, at rostral or caudal positions along the spinal cord where extensive evidence for spinal cord plasticity has been obtained in animal models.

7.2 Spinal cord fMRI to detect disrupted spinal circuits

Investigating the function of the human brainstem and spinal cord is an inherently difficult task, with its proximal region surrounded by the skull base and its longitudinal extent circumscribed by the bony spinal column, cartilaginous discs and ligaments. Invasive animal and tissue-based experiments have formed our understanding of the electrophysiological basis of spinal cord function while the discipline of psychophysics has extended this knowledge to include the perceptual affect of physical stimuli we experience from the environment. The use of spinal functional magnetic resonance imaging (fMRI) aims to investigate how the human brainstem and spinal cord function as a unit to receive and transmit each of motor, sensory and autonomic information as a unit, rather than as individual cells or circuits that is captured with electrophysiological methods. Spinal fMRI is able to capture this information due to its appropriate spatial-temporal profile that allows for simultaneous data collection over the entire brainstem-spinal cord axis. In doing so, the aim will be to build upon our existing knowledge of the structure and function of the human spinal cord with an emphasis on integrative function (or dysfunction).

Imaging science has decisively established functional segregation as a principle of CNS organization and, in recent years, has moved towards improving our understanding of functional integration within the CNS.[239] To state another way, the primary motor cortex is both functionally and spatially discrete from the facial nucleus in the brainstem, yet both work in a concerted effort when one recognizes an old friend and reaches out with a smile to embrace her. How spatially distinct regions are integrated to perform specific functions remains somewhat elusive. Aside from physical axons that might join two distinct nuclei or brain regions, a concept that dates back to invasive tracer methods and is now studied with modern diffusion tensor imaging methods,[240] understanding the integration of distant regions of the central nervous system to perform a common task offers complex challenges. Modern imaging techniques in neuroscience aim to take advantage of the unique spatial-temporal scale offered, for example, by simultaneous fMRI of the brain, brainstem and spinal cord. In doing so, these methods have the ability to capture spatially isolated changes in different regions of the CNS. With advanced post-processing methods we are able to learn how different regions of the CNS function as a unit to perform the functions of life such as respiration, movement and the perception of sensation. With a spatial scale on the order of cubic millimeters, and a temporal scale on the order of seconds,

fMRI experiments should not be thought of as providing low-resolution evidence of neurophysiological events, rather they measure the hemodynamic footprint of neuronal activity. For example, we know from electrophysiology studies that when the skin of an animal is warmed, cells contained in the dorsal horn of the spinal cord at the appropriate segmental level respond by firing action potentials to regions in the brainstem, thalamus and eventually the somatosensory cortex; simultaneously, ongoing activity of cold cells are silenced. Imaging experiments are not required to build on this body of evidence. Rather, such imaging tools should take advantage of their unique spatial-temporal scale to provide novel insights into how different regions of the brainstem and spinal cord function as a unit.

The first twenty years of spinal fMRI research are outlined in the detailed literature review of Chapter 2; by carefully examining the elements of experimental design in healthy control subjects two important concepts are highlighted: the different tasks or stimulation protocols used to elicit spinal cord function and the contrast mechanisms utilized to capture functional changes in the spinal cord (SEEP vs BOLD contrast).[141] Such investigations have provided a platform by which to launch studies aimed at uncovering physiological changes associated with pathological processes, such as spinal cord injury. Equally important in this work in the notion of studying changes to the spinal cord in terms of specific regions of interest including, above and below the level of injury and across the whole brainstem-spinal cord axis. This is in contast to investigating the damaged spinal cord at the epicenter of injury, as was the predominant method used in conventional MR methods upon widespread clinical adoption starting around 1980. The spatially distributed changes in neurovascular response observed in chapter 5 provided a particular impetus to precisely characterize the distribution of segmental anatomy in individual subjects, and was the focus of chapter 6.

7.3 Accounting for population diversity in spinal cord anatomy

Relative to the brain imaging literature, very little effort has been put into accurate anatomical localization of segmental anatomy within the human spinal cord. As outlined in detail in the literature review of Chapter 2, all spinal fMRI studies used to date assume the position of spinal cord segments based on one of two methods: adjacent to the corresponding vertebral body or rostral to the corresponding vertebral body. The work presented in Chapter 6 applies computer vision algorithms in a novel way to accurately segment the human spinal cord from high-

resolution imaging datasets and allows one to conduct measurements along its unique axis. By considering each individuals spinal cord with its own set of spatial coordinates (using a cylindrical coordinate framework), this method allows for the identification of segmental anatomy of one individual and the comparison of many individuals within a common framework. Using this approach, new knowledge is presented in Chapter 6 that describes the population distribution of segmental anatomy of the cervical spinal cord. The data can be used to more accurately identify a specific point in space where a population of neurons resides relative to a fixed position in the brainstem. This has implications for the analysis of advanced imaging studies whereby group data relies on the assumption that signals analyzed from a particular region-of-interest arise from the same neuroanatomical substrate.

A limitation of this approach, when applied to imaging studies involving large numbers of subjects, is that it takes a great deal of time to identify cervical nerve rootlets, the most prominent indicator of the segmental anatomy of the spinal cord. For example, if one were to manually identify each set of cervical nerve rootlets from C3 to C8, it would take several hours to process the imaging data of a single subject. Clearly, this is not feasible for most research studies and is certainly not appropriate for routine clinical use. To address this issue, it would be helpful to have a prediction model that could utilize readily identifiable metrics that could be used to predict the somewhat more elusive position of spinal cord segments. In fact, using the position of vertebral bodies, height and neck length, the position of a spinal cord segment could be predicted to within 3.18 mm accuracy using a linear regression model and a leave-one-out model of validation. This is a dramatic improvement over using vertebral bodies as a surrogate for spinal cord segments, which comes along with an error of greater than 20 mm.

7.4 Limitations of this work

While the limitations of each of the studies presented in this thesis have been discussed in detail in the respective chapters, the general limitations of advancing the use of MRI-based biomarkers in spinal cord injury patient populations are discussed here in the context of two themes: matching an imaging modality to pathophysiological events known to occur after SCI and the longitudinal assessment of a biomarker.

Biomarkers are intended to reflect an underlying structural or physiological event that cannot be directly evaluated. For example, it is not possible to evaluate the degree of myelination of the

human spinal cord. To do so would involve an invasive operation and damaging the white matter itself, a notion that is not acceptable. Rather, one hopes that a surrogate marker can be devised that provides information on the integrity of white matter tracts of the human spinal cord. The limitation of using T_1 and T_2 weighted biomarkers as presented in Chapter 4 of this thesis rests in the fact that such signal changes do not reflect any specific pathophysiological event. Rather, such imaging metrics provide an overall survey of the damaged tissue that might reflect pathophysiological events such as edema, swelling, hemorrhage, cavitation, necrosis, demyelination and others. The work presented in Chapter 5 attempts to develop a biomarker that could be used to assess the integrity of the spino-thalamic tract by applying a thermal stimulus to segmental dermatomes, analyzing the acquired signal and reporting metrics that reflect the integrity of this functional circuit. In a number of ways the results presented in Chapter 5 fulfill the notion of studying a specific pathophysiological event: disruption of spinal cord circuits. The limitation of this work however rests in 1) choosing a spinal cord circuit to investigate and 2) applying an appropriate stimulus during the fMRI experiment to 'activate' this circuit in order to elicit a robust spinal cord neurovascular response that can be measured with the described imaging protocol. The limitations of Chapter 5 can be summarized as 1) investigation of the thermal sensory system of traumatic SCI patients is likely not as clinically relevant as, for example, the cortico-spinal motor pathways that transmit information necessary for upper extremity motor function. Nonetheless, delivery of a thermal stimulus in the confines of the imaging environment is relatively easy to do and provided an excellent platform by which to develop the methods and protocols established in this thesis. 2) The uncertainty with which the delivered stimulus affects a neurovascular response. In choosing a somatosensory stimulus, one has to decide upon the stimulus intensity, duration and inter-stimulus interval. Unfortunately, there are no studies that describe the relationship between different stimulation paradigms and the resultant neurovascular response. Therefore, a significant limitation of the work presented in Chapter 5 is the uncertainty with which the stimulus results in a signal that can be captured with the spinal fMRI protocol prescribed. One means of addressing this limitation is to study the relationship between the delivery of afferent stimuli with the neurovascular response. To do this requires the use of imaging techniques with both a high spatial and temporal profile such the a segment of the spinal cord can be imaged repeatedly during the expected period of hemodynamic response and changes in blood flow or oxygen concentration measured objectively. To this effect, preliminary reports using optical coherence tomography have been put forth. [128]

Imaging biomarkers for use in the SCI patient population are most useful if they are able to provide information over a longitudinal time frame. For example, if a patient sustains a SCI and is offered a novel treatment, clinicians and researchers alike would benefit from knowing if such a strategy is having a positive or negative effect before clinical symptoms materialize. While absolutely necessary before the widespread adoption of biomarkers for use in SCI clinical trials, such an experimental design must be reserved for the next stage of development and lie outside the scope of this thesis representing a limitation of the work presented here.

7.5 Future directions

The most pertinent findings presented in this thesis are as follows: T_1 and T_2 weighted intramedullary signal changes of standard anatomical imaging protcols, captured at the epicenter of traumatic spinal cord injury, offer no advantage to standard clinical assessments to predict outcome after injury. Spinal fMRI can measure the neurovascular response to afferent stimulation in a distributed fashion across the brainstem – spinal cord axis whose signal changes reflect mechanisms of injury and plasticity that have been extensively studied animal models. Characterizing the segmental anatomy of the human spinal cord across individuals is of great importantce to accurately identify the neuroanatomical basis of acquired imaging signals.

Collectively, these findings provide a platform to further advance the use of MRI-based imaging biomarkers to aid in the evaluaiton and management of SCI patients, one such platform is presented here.

Introduction: Study Rationale

Traumatic injury to the human spinal cord results in both immediate primary damage and ongoing secondary mechanisms that disrupt both the structural integrity and functional properties of neuroanatomical circuits.[9] Pre-clinical models of spinal cord injury have provided significant insight into the underlying mechanisms of structural damage such as the loss of oligodendrocyte support via apoptotic mechanisms, the formation of a glial scar and the degeneration of myelinated tracts that transmit neural signals to and from the brainstem and higher cortical centers.[128] This underlying loss of structural integrity results in a disruption of functional circuits that clinically manifest as a loss of sensory perception and the inability to control muscle groups.

A number of specific treatment strategies have either been implemented or are the focus of ongoing investigation to optimize the outcome after traumatic spinal cord injury.[128] For example, safe and prompt transfer to specialized centers and maintenance of adequate blood pressure are two accepted standards to best treat persons afflicted with traumatic spinal cord injury.[128] Other specific surgical options, such as early surgical decompression, have shown to be safe and offer improved neurological outcomes.[49] Neuroprotective strategies are now being tested in multi-center clinical trials.[128]

Clinical outcome in the treatment of spinal cord injury are typically gauged by utilizing the American Spinal Injury Association standards, recorded at intervals of at least 3 months after intervention, and more often than not at 6-month intervals.[128] The reasons for this are clear: recovery after spinal cord injury, whether a result of natural recovery or a result of the tested intervention, typically occurs within the first 12-18 months after injury but may occur beyond this time frame.[2] Thus, recording the standardized clinical examination at intervals of less than 3 months offers little or no information with regard to recovery or lack thereof. It would be naive however, to think that the spinal cord remains quiescent for an extended period of time only to regain sensory and motor capabilities when clinical function becomes apparent. **The work presented here aims to develop an advanced imaging toolbox consisting of both structural and functional modalities that can be used as a surrogate marker for the integrity of white matter tracts and the transmission of functional information through specific spinal circuits.** In utilizing non-invasive markers of spinal cord structure and function, the ultimate aim will be to follow the recovery or deterioration of spinal tracts and functional circuits in response to different treatment strategies. To move in this direction, this proposal focuses on a novel means of processing complex advanced imaging information to make inferences about individual patients with reference to standard clinical examination and electrophysiological studies.

Advances in *structural magnetic resonance imaging* of the human spinal cord, utilizing diffusion and magnetization transfer imaging techniques, have demonstrated the ability to distinguish differences in normal appearing white matter that correlate well with clinical deficits in the setting of spinal cord injury.[128] White matter tracts of the human spinal cord run in a longitudinal direction along the spinal axis with segmental contributions at the first cervical through to the fifth sacral spinal levels; the largest of these in the cervical spine include:

1) The lateral corticospinal tract positioned in the dorsolateral quadrant, carrying motor information from the contralateral cortex to the anterior horn of the spinal cord.

2) The dorsal columns positioned in the dorsal spinal cord spanning from the right posterolateral sulcus to the left posterolateral sulcus, carrying ipsilateral propriceptive information from the segmental spinal cord levels to the nucleus cuneatus in the caudal medulla of the brainstem.

3) The anterolateral system positioned in the anterolateral quadrant, carrying contralateral pain and thermal touch sensations (spinothalamic tract) and contralateral motor information via the rubrospinal tract.

Depending on the degree of spinal cord injury, some or all of these white matter tracts become disrupted and result in a range of clinical findings from complete lack of sensation and motor loss to less severe deficits.

Functional magnetic resonance imaging takes advantage of neurovascular coupling whereby neurons and supporting cells communicate the need for increased energy requirements when functioning at a level above a resting baseline. The functional hyperemia response is then captured as the fMRI signal. Circuits of the human spinal cord can be classified as sensory, motor or autonomic and have been extensively studied and described in the neuroanatomical literature.[128] When a mild electric stimulus is applied in the distribution of a peripheral nerve of the upper extremity, ascending information is transmitted in:

1) The fasciculus cuneatus contained within the dorsal column-medial lemniscal pathway. Synapses are located at the segmental level of the spinal cord and in the nucleus cuneatus of the caudal medulla. Cells of the nucleus cuneatus send projections to the thalamus.[241,242]

2) The spinocervical tract (SCT) located within the dorsal lateral funiculus and contained within the spinocervicothalamic pathway. SCT cells, located in the segmental dorsal horn, receive peripheral input from the skin and send axonal projections to the lateral cervical nucleus, located ventrolateral to the dorsal horn at the C1-3 spinal segmental levels. Projections from the lateral cervical nucleus ascend to the thalamus.[128]

3) The spinothalamic tract (STT), spinoreticular tract (SRT) and spinomesencephalic tract (SMT) located within the ventral quadrant white matter. STT cells project from the segmental dorsal horn to the contralateral thalamus. SRT and SMT cells are considered to be an indirect pathway to the thalamus with synapses in the reticular formation (at the level of the pons and medulla) and in numerous nuclei in the midbrain, respectively.[128]

Disruption of ascending sensory information is captured on clinical assessments by a lack of soft touch sensation (mediated by disruption of the dorsal column-medial lemniscal pathway) and / or a lack of pinprick sensation (mediated mainly by the spinothalamic tract in the ventral quadrant). Here, somatosensory evoked potentials of the upper extremity are utilized to stimulate the dorsal, dorsolateral and anterolateral sensory systems that have synaptic connections in the following regions (from caudal to rostral): the segmental region of the spinal cord, the lateral cervical nucleus of the upper spinal cord, the nucleus cuneatus, the pontomedullary reticular formation, midbrain nuclei, the thalamus and higher cortical centers.

The specific aims of this work are to determine:

1) With what accuracy can our imaging toolbox (DTI, MT, fMRI) predict disruption in ascending somatosensory pathways of chronic SCI patients as measured with standard clinical assessment?

2) With what accuracy can our imaging toolbox predict normal latency dermatomal somatosensory evoked potential's (SSEP's) versus prolonged or abolished latency dermatomal SSEP's in chronic spinal cord injury patients?

To accomplish these aims, a multivoxel pattern analysis (MVPA) is applied to structural and functional MR data (DTI, MT and fMRI). This approach has shown relevance for brain state prediction.[128] MVPA algorithms learn patterns from imaging datasets with an aim to optimally differentiate observations into predetermined categories. This learned pattern analysis of spatially distributed information can then be applied to never-before-seen data. The performance of the learned pattern is then quantified by the prediction error. In applying this analysis to spinal imaging data for the first time, the aim is to establish the accuracy of spinal imaging to draw conclusions about individual patients.

Proposed Methods:

Subjects

Thirty-two subjects will be recruited through the spinal cord injury clinical and by means of posted advertisements at the Toronto Western Research Institute. Sixteen healthy control subjects with no history of neurological disease will be compared with sixteen subjects who sustained a cervical spinal cord injury at least one-year prior to this study. To qualify for inclusion, SCI patients must have a cervical dermatome with abnormal or no sensation below the level of their injury (as assessed by pin prick or soft touch sensation according to the standard American Spinal Injury Association). To qualify for inclusion, all subjects are required to be between the ages of 18 and 70 years old and have no contraindications for MR imaging.

All healthy controls and SCI patients will undergo high-resolution anatomical, diffusion-weighted, magnetization transfer and fMRI studies. In addition, all participants will undergo somatosensory evoked potentials with the same functional stimulus applied in the fMRI study.

MRI data acquisition

All imaging data will be acquired on a 3T GE MR system at the Toronto Western Hospital using an 8-channel neurovascular array coil. Subjects will be carefully positioned to limit head movement and requested to not move.

Structural Spine imaging

An anatomical scan was performed using a FIESTA-C sequence (T_2-weighted); 384 x 384, NEX 2.0, FOV 200 mm, Slice thickness 0.6 mm acquired in the coronal plane. Total scan time: approx. 12 min.

Diffusion-weighted imaging

Diffusion-weighted imaging methods have been previously described and are summarized here.[128] Diffusion-weighted data will be acquired using a single shot EPI sequence with monopolar scheme to achieve low TE.[243] 12 axial slices will be prescribed to cover the C2 to C4 vertebral body levels. Parameters are: FOV=128 mm, TR= ~ 1500 ms, voxel size=$1\times1\times5$ mm^3, phase encoding direction A-P, number of diffusion-weighting directions=25, b-value=700

s/mm^2. Two vertical saturation bands will be used: one positioned ventrally over the trachea to limit flow effects and motion due to swallowing, the other set dorsally and aimed at suppressing signal from the non-spinal cord tissue close to the surface coils and producing high intensity signal.

Magnetization transfer imaging

T1-weighted 3D gradient echo images with slab-selective excitation will be acquired with and without magnetization transfer saturation pulse (Gaussian envelop, duration=9984 μs, frequency offset=1200 Hz). Parameters are: axial orientation, 52 slices (spaced with 20% gap), FOV=230×230 mm^2, TR=28ms, TE=3.2 ms, voxel size=0.9×0.9×2 mm^3, flip angle=23°, phase encoding direction right-left, phase partial Fourier 6/8, bandwidth=400 Hz/Pix, acquisition time ~5 min for each volume (~10 min for both volumes with and without MT pulse).

Functional imaging - acquisition

High-resolution T1-weighted whole brain anatomical scans will be collected using a three-dimensional inversion recovery-prepared fast spoiled gradient recalled (IR-FSPGR) sequence with the following parameters: 160 axial slices, 0.94 x 0.94 – 1.0 mm^3 voxels, 256 x 256 matrix, field of view = 24 x 24 cm, flip angle = 20°, TE = 5 ms, TR = 12 ms, TI = 300 ms.

Acquisition of BOLD functional imaging will be performed using a gradient echo T_2* weighted pulse sequence (TE= 30 ms, matrix 64 x 64, FOV = 200 mm, flip angle = 90°) as previously reported.[128] Briefly, this involves cluster acquisition of 17 coronal slices completed in sequential order within 926 ms with each slice 3 mm thick with 0.6 mm gap (voxel size 3.13 x 3.13 x 3.6 mm) and slightly tilted to be parallel to the brainstem longitudinal axis. This orientation was chosen in order to minimize through-slice brainstem motion.

Functional Paradigm

Each fMRI scan run will be 17min 30sec in duration, during which time the subject will experience either a mild electric somatosensory stimulus or a rest period. Each fMRI run will begin with a 90 second rest block followed by eight 120-second periods of alternating stimulation (60 s) and rest (60 s) as follows: Transcutaneous somatosensory stimulation will be delivered as a repetitive, square wave (0.5 ms) electrical pulse (at 3 Hz) using a Grass nerve

stimulator (model number S88) with a photo-electric stimulus isolation unit (PSIU 6) and standard, MR compatible, surface gel electrodes separated by 2 cm in the ulnar nerve distribution with the cathod proximal (C8 / T1 dermatome). In healthy controls, this represents a dermatome of normal sensation. In SCI patients, this represents a dermatome of abnormal sensation. Before entering the MR environment, subjects will be familiarized with the electrical stimuli. Stimulus intensity will be determined for each individual in order to elicit sensation well above perception threshold but without causing pain. The intensity will not exceed 10 mA. Subjects will be asked to rate the intensity of the stimulus, using a 10-point scale ranging from no sensation (1) to painful sensation (10) with a comfortable sensory stimulus set at 5. This will be done to ensure that participants did not experience a non-painful stimulus. If a subject rated a stimulus as 10 during the familiarization phase, the stimulus intensity will be decreased. If a subject rated a stimulus as 1 during the familiarization phase, the stimulus intensity will be increased. Thus, no subject will enter the study with a rating of either 1 or 10.

Somatosensory Evoked Potential Recordings

SSEPs will be recorded from healthy controls and SCI patients. Each person will undergo stimulation in the ulnar distribution of the right upper extremity (representing the C8 / T1 dermatome). Briefly, the same stimulation equipment will be used in both the fMRI and SSEP recordings. SSEP recording electrodes will be placed in a 10-20 electrode configuration on the contralateral scalp to the dermatomes being stimulated to record averages of 250 to 1200 cortical responses. The impedance of ground and scalp electrodes will be maintained at <5kohms. The first negative (N1) and positive (P1) peak latencies (milliseconds) will be determined based on the mean of the 2 consecutive runs performed. Clinical interpretation of SSEP N1 and P1 markers will be reviewed by a neurologist with special training in the interpretation of SSEP recordings.

Normal latency for SSEP stimulation will be determined based on N1 latency in healthy controls, as previously reported.[128] This is reported to be the most robust component of a cervical SSEP and has been previously demonstrated to demarcate and quantify pathological SSEP recordings in SCI patients.[128] Averaged SSEPs will be visually inspected for waveform configuration to confirm the presence of a SSEP. N1 latency will then be qualified as having 1) a normal N1 latency (within 2 standard deviations of mean values for all control subjects stimulated) or 2) an

abolished N1 latency, defined as the absence of an N1-P1 complex. This binary classification (normal vs. abolished N1 latency) will then used as an endpoint in the MVPA approach described below.

Data processing

Diffusion-weighted data

Motion correction will be completed using FSL FLIRT.[244] Data will first be split along the Z direction and motion correction applied slice-by-slice to account for the non-rigid motion of structures across slices. The motion correction algorithm minimizes the correlation coefficient ratio between each image (including the b=0 image) and the mean DW image using three degrees of freedom (Tx, Ty and Rz), as suggested elsewhere to be optimal for axial spinal cord EPI.[128] The data will then be averaged across repetitions. Diffusion tensor and its related metrics will be estimated voxel-wise using FSL.[128] Of all metrics computed, the fractional anisotropy (FA), the first eigenvalue (axial diffusivity, AD) and the average of the 2nd and 3rd eigenvalues (radial diffusivity, RD) will be further considered for analysis.

For each healthy control or SCI patient, the AD, RD and FA values will be utilized in the SVC algorithm described below.

Magnetization transfer

T_1-weighted volumes with and without MT pulse will be co-registered using the non-linear method available in FSL FNIRT.[128] Magnetization transfer ratio (MTR) will be computed in a voxel-wise fashion following the equation $[(S0-SMT)/S0]\times100$, where S0 and SMT are the T_1-weighted image without and with the MT pre-saturation pulse, respectively. To compare T_1-weighted signal between the two populations, images without MT pulse will be normalized by the signal in the cerebrospinal fluid to account for B_1 inhomogeneities.

For each healthy control or SCI patient, the MTR will be utilized in the SVC algorithm described below.

Functional imaging

Structural data will be co-registered to the MNI152 brain template using the Automated Brainstem Co-registration (ABC) method in order to maximize sensitivity in important brainstem regions.[128] Functional data will be motion corrected using SPM8; briefly, minimal spatial smoothing, FWHM=3mm, will be performed on the fMRI data as some brainstem nuclei are on the order of an image voxel size. The data will also be high-pass filtered in the temporal domain (f_{high} = 0.0083 Hz) to remove baseline signal drifts.[128]

Statistical parametric mapping at the single subject level will be completed via a generalized linear model using SMP 8. The hemodynamic response function utilized in the GLM analysis will be defined by the block design paradigm convolved with a prescribed gamma function (standard deviation = 3 s, mean lag = 6 s). The block paradigm is defined to be "1" during the one-minute ON blocks and "0" during the 1-minute OFF blocks.

Single subject parameter estimates and their variance were then used in the SVC model described below.

Anatomical localization

Given that current MNI and Talairach coordinate systems are not specific for brainstem regions, we utilized a previously validated approach and made appropriate adjustments with the use of brainstem atlases and the neuroanatomical experience of our group.[128] Briefly, the brainstem is divided into 28 parcellation units: 12 midbrain regions, 8 pontine regions and 8 medulla regions using a landmark-based topological methodology. We have outlined these parcellation units in figure 1 along with the topological landmarks. As previously described, we used the obex, a medullary landmark, located roughly at MNI z = -57mm to localize nuclei within the brainstem. Also note that the obex is located approximately 5 mm rostral to the pyramidal decussation, the topological landmark used to differentiate rostral and caudal medullary regions.

Considering nuclei that are known to receive ascending somatosensory stimuli, as outlined in the introduction, we can formulate an anatomical map to describe fMRI regions that show a significant response to the applied stimulus; this is summarized in Table 7-1.

Table 7-1. Brainstem nuclei involved in the processing of somatosensory stimuli. Locations of nuclei are reported relative to the obex along with the parcellation units. See text for further detail.

Somatosensory pathway and brainstem region of interest	Location relative to obex as described in a neuroanatomy atlas.[139] Note that negative numbers imply a caudal direction from the obex and positive numbers imply a rostral direction from the obex.	Parcellation unit
Dorsal column pathway: nucleus cuneatus (caudal medualla)	Obex – 3 mm to Obex + 3 mm	23, 24
Spinoreticular tract: pontomedullary reticular formation	Obex -3mm to Obex + 33mm	Portions of regions 21-24 in the medulla, and portions of regions 13-20 in the pons
Spinomesencehpalic tract: numerous midbrain nuclei including from caudal to rostral: Pontomesencephalic junction: • nucleus cuneiformis • parabrachial nucleus • periaqueductal gray Intercollicular region • nucleus cuneiformis • periaqueductal gray • intercollicular nucleus • deep layers of the superior colliculus Rostral midbrain • periaquedfuctal gray • nucleus of Darkschewitsch • anterior and posterior pretectal nuclei • red nucleus • Edinger Westphal nucleus • Interstital nucleus of Cajal	Obex +33mm to Obex +45 mm	Portions of regions 3-6 and 9-12

Support Vector Classification of fMRI, DTI and MT imaging.

Support vector classification (SVC) is a multi-voxel pattern analysis (MVPA) method that has been demonstrated to have better prediction accuracy and less sensitive to noise than alternative MVPA approaches.[128] SVC has been previously applied to brain fMRI studies using both task-based and resting state designs with the aim of disease state prediction in major depression, drug addiction and attention deficit hyperactivity disorder.[128] SVC will be performed using custom scripts running in MATLAB using the SVM functions from the Bioinformatics Toolbox. Imaging data (Diffusion: FA, GFA, RD; magnetization transfer ratio; and fMRI maps) will be entered into an SVC analysis to discriminate healthy controls from SCI patients. The linear kernel and the box constant was set to 1,000,000 (hard margin) following previous observations that these are sufficient for fMRI data.[128] SVC can be conceptually divided into two steps: feature selection and model selection.

Feature selection is defined as 'the process of selecting a subset of features that are useful for prediction'.[245] In the context of this work, features are the structural and functional imaging data, congruent with the aim of studying disrupted ascending functional circuits of the spinal cord. Feature selection aims to reduce prediction error in order to improve the accuracy with which the MVPA model can distinguish between defined states. The reliability filter (RF) is used as previously reported.[128] Briefly, RF is a multivariate approach, adapted from partial least squares, that retains features most reliably implicated in discrimination.[246] The prediction error and specific features that are most useful in distinguishing healthy controls from SCI patients will be reported.

Model selection is the process by which parameters are selected to minimize the prediction error. Using a cross-validation approach, the data is iteratively split into training and test datasets. A SVC model is 'learned' from the training data and applied to classify the testing data. The 0.632 bootstrap method will be used to estimate prediction error as it has been shown to have low bias and variance compared to other methods.[247,248] This method has been previously applied and well documented.[128]

Model Validation

Leave-one-out cross validation (LOOCV) will be performed to estimate the generalizability of the trained SVC. In this procedure, a single dataset is used as a test sample and the remaining datasets are used for training. The misclassification rate is calculated and averaged over the *N* iterations of the LOOCV procedure to estimate the prediction error. The reproducibility of a feature selection across CV iterations was evaluated by Fleiss' kappa coefficient.[249]

Research Questions:

With what accuracy can our imaging toolbox distinguish between 2 clinical states: normal sensory function and a lack of sensory function in the dermatome of interest.

To address this question, the imaging data from SCI patients and controls (DTI, MT, fMRI) will be utilized. The above described pattern recognition strategy will be applied to distinguish the data obtained from persons with normal sensation in the stimulated dermatome from those with disrupted clinical sensation (as determined by the AIS assessment) in the stimulated region (C8/T1 dermatome).

With what accuracy can our imaging toolbox predict the presence or absence of normal latency in SSEP recordings?

To address this question, the imaging data from healthy controls and SCI patients (DTI, MT, fMRI) will be utilized. The above described pattern recognition strategy will be applied to distinguish the images obtained from persons with a normal SSEP latency time with those of a prolonged or abolished SSEP latency time. (Note: normal SSEP latency times are established in healthy controls)

Both the prediction error and the features of our pattern recognition will be reported that allow for optimal distinction of A) clinical state as determined by standard American Spinal Injury Association standards and B) electrophysiological evidence of disrupted sensory circuits.

Summary:

This proposed next experiment aims to build on the findings presented throughout this thesis. Here, advanced structural and functional imagine techniques are utilized to capture information directly related to the pathophysiology of spinal cord injury. Structural information is captured

that provides data on the macromolecular content of the spinal cord, namely the degree of myelination. Functional information is captured that aims to provide data on the integrity of ascending spinal circuits.

By moving away from collecting standard T_1 and T_2-weighted images as was historically done, and outlined in great detail in Chapter 4, the imaging biomarker presented here captures information directly related to the pathophysiology of spinal cord injury and will therefore allow for assessment and monitoring of the spinal cord in response to novel treatment strategies. Utilizing a high resolution spinal cord acquisition will allow for detailed knowledge of the precise anatomy of an individuals spinal cord, the importance of which was detailed in Chpater 6. The data collection strategy outlined here improves upon the methods presented in Chapter 5 for two principle reasons. First, by collecting functional data within the brainstem, the first relay center for ascending spinal circuits, it becomes possible to image all SCI patients, regardless of whether or not titanium implants are used anteriorly, posteriorly or both. Note that certain cases of spinal fMRI are limited by magnetic succeptibility artefacts caused by instrumentation. Second, there is uncertainty with regard to whether or not the hemodynamic response function is identical in health individuals and across the spectrum of mild to severe SCI patients. By measuring the fMRI signal from the brainstem, any doubt regarding the consistency of neurovascular relationships in the injured spinal cord tissue is eliminated, as all measurements are conducted on healthy brainstem tissue, the only difference being the degree of ascending information affected by the injury itself.

7.6 Conclusions

MRI based imaging biomarkers have made considerable progress since early adaptors first attempted to use T_1 and T_2-weighted signal characteristics to draw inferences from SCI patients and use this information to attempt to inform prognosis. This thesis details this early approach and offers new knowledge based on the shortcomings of this early work – bear in mind the shortcomings were largely due to the technology available at the time and certainly not due to the desire of clinicians and researchers to move the field forward. Imaging biomarkers of traumatic SCI in the future will investigate the spinal cord outside the lesion epicenter and capture both structural and functional metrics that reflect specific pathophysiological mechanisms.

Chapters 5 and 6 embark upon two important factions of advancing imaging biomarkers for use in SCI patients: investigating specific functional circuits and accurately identifying segmental anatomy of the spinal cord. In the first case, novel methods are presented that allow for the imaging description spinal circuit function and how such circuits change over time. In the second, novel methods are presented that allow for accurate segmentation of the spinal cord and provide a means of conducting measurements along the personalized arc-length axis of the brainstem – spinal cord.

Each of the studies presented here offer a novel approach to using imaging biomarkers to better understand and classify spinal cord injury. Future work will have to balance rapidly changing technology with progress in our understanding of the neurobiology underlying spinal cord injury. Advanced imaging biomarkers stand to increase the accuracy of diagnosis, follow sub-clinical changes in spinal cord structure and function and hopefully guide a personalized approach to treating this devastating condition. I envision the next decade of research incorporating these and other methods for use in clinical trials to allow for standardized objective assessments with hypothesis driven research questions that link specific pathophysiological events to imaging biomarker metrics. When this is realized, it will be possible to use such data analysis pipelines to aid in treatment decision-making.

References

1. Bracken MB, Collins WF, Freeman DF, et al. Efficacy of methylprednisolone in acute spinal cord injury. JAMA : the journal of the American Medical Association 1984;251:45-52.

2. Fawcett JW, Curt A, Steeves JD, et al. Guidelines for the conduct of clinical trials for spinal cord injury as developed by the ICCP panel: spontaneous recovery after spinal cord injury and statistical power needed for therapeutic clinical trials. Spinal Cord 2007;45:190-205.

3. Steeves JD, Lammertse D, Curt A, et al. Guidelines for the conduct of clinical trials for spinal cord injury (SCI) as developed by the ICCP panel: clinical trial outcome measures. Spinal cord 2007;45:206-21.

4. Raineteau O, Schwab ME. Plasticity of motor systems after incomplete spinal cord injury. Nature reviews Neuroscience 2001;2:263-73.

5. Sekhon LH, Fehlings MG. Epidemiology, demographics, and pathophysiology of acute spinal cord injury. Spine (Phila Pa 1976) 2001;26:S2-12.

6. Ackery A, Tator C, Krassioukov A. A global perspective on spinal cord injury epidemiology. J Neurotrauma 2004;21:1355-70.

7. Kraus JF, Franti CE, Riggins RS, Richards D, Borhani NO. Incidence of traumatic spinal cord lesions. J Chronic Dis 1975;28:471-92.

8. Priebe MM, Chiodo AE, Scelza WM, Kirshblum SC, Wuermser LA, Ho CH. Spinal cord injury medicine. 6. Economic and societal issues in spinal cord injury. Arch Phys Med Rehabil 2007;88:S84-8.

9. Tator CH, Fehlings MG. Review of the secondary injury theory of acute spinal cord trauma with emphasis on vascular mechanisms. Journal of neurosurgery 1991;75:15-26.

10. Tator CH, Koyanagi I. Vascular mechanisms in the pathophysiology of human spinal cord injury. J Neurosurg 1997;86:483-92.

11. Kwon BK, Tetzlaff W, Grauer JN, Beiner J, Vaccaro AR. Pathophysiology and pharmacologic treatment of acute spinal cord injury. Spine J 2004;4:451-64.

12. Kakulas BA. Neuropathology: the foundation for new treatments in spinal cord injury. Spinal Cord 2004;42:549-63.

13. Schanne FA, Kane AB, Young EE, Farber JL. Calcium dependence of toxic cell death: a final common pathway. Science 1979;206:700-2.

14. Lipton SA, Rosenberg PA. Excitatory amino acids as a final common pathway for neurologic disorders. N Engl J Med 1994;330:613-22.

15. Xiong Y, Rabchevsky AG, Hall ED. Role of peroxynitrite in secondary oxidative damage after spinal cord injury. J Neurochem 2007;100:639-49.

16. Donnelly DJ, Popovich PG. Inflammation and its role in neuroprotection, axonal regeneration and functional recovery after spinal cord injury. Exp Neurol 2008;209:378-88.

17. Bao F, Liu D. Peroxynitrite generated in the rat spinal cord induces apoptotic cell death and activates caspase-3. Neuroscience 2003;116:59-70.

18. Noble LJ, Wrathall JR. Distribution and time course of protein extravasation in the rat spinal cord after contusive injury. Brain Res 1989;482:57-66.

19. Schnell L, Fearn S, Schwab ME, Perry VH, Anthony DC. Cytokine-induced acute inflammation in the brain and spinal cord. J Neuropathol Exp Neurol 1999;58:245-54.

20. Pineau I, Lacroix S. Proinflammatory cytokine synthesis in the injured mouse spinal cord: multiphasic expression pattern and identification of the cell types involved. J Comp Neurol 2007;500:267-85.

21. Fleming JC, Norenberg MD, Ramsay DA, et al. The cellular inflammatory response in human spinal cords after injury. Brain 2006;129:3249-69.

22. Popovich PG, Wei P, Stokes BT. Cellular inflammatory response after spinal cord injury in Sprague-Dawley and Lewis rats. J Comp Neurol 1997;377:443-64.

23. Yan P, Li Q, Kim GM, Xu J, Hsu CY, Xu XM. Cellular localization of tumor necrosis factor-alpha following acute spinal cord injury in adult rats. J Neurotrauma 2001;18:563-8.

24. Bethea JR, Nagashima H, Acosta MC, et al. Systemically administered interleukin-10 reduces tumor necrosis factor-alpha production and significantly improves functional recovery following traumatic spinal cord injury in rats. J Neurotrauma 1999;16:851-63.

25. Kim GM, Xu J, Song SK, et al. Tumor necrosis factor receptor deletion reduces nuclear factor-kappaB activation, cellular inhibitor of apoptosis protein 2 expression, and functional recovery after traumatic spinal cord injury. J Neurosci 2001;21:6617-25.

26. Keane RW, Kraydieh S, Lotocki G, et al. Apoptotic and anti-apoptotic mechanisms following spinal cord injury. J Neuropathol Exp Neurol 2001;60:422-9.

27. Crowe MJ, Bresnahan JC, Shuman SL, Masters JN, Beattie MS. Apoptosis and delayed degeneration after spinal cord injury in rats and monkeys. Nature medicine 1997;3:73-6.

28. Yong C, Arnold PM, Zoubine MN, et al. Apoptosis in cellular compartments of rat spinal cord after severe contusion injury. Journal of neurotrauma 1998;15:459-72.

29. Casha S, Yu WR, Fehlings MG. FAS deficiency reduces apoptosis, spares axons and improves function after spinal cord injury. Exp Neurol 2005;196:390-400.

30. Chu GK, Yu W, Fehlings MG. The p75 neurotrophin receptor is essential for neuronal cell survival and improvement of functional recovery after spinal cord injury. Neuroscience 2007;148:668-82.

31. Quencer RM, Bunge RP. The injured spinal cord: imaging, histopathologic clinical correlates, and basic science approaches to enhancing neural function after spinal cord injury. Spine 1996;21:2064-6.

32. Totoiu MO, Nistor GI, Lane TE, Keirstead HS. Remyelination, axonal sparing, and locomotor recovery following transplantation of glial-committed progenitor cells into the MHV model of multiple sclerosis. Exp Neurol 2004;187:254-65.

33. Norenberg MD, Smith J, Marcillo A. The pathology of human spinal cord injury: defining the problems. J Neurotrauma 2004;21:429-40.

34. Bracken MB, Shepard MJ, Collins WF, Jr., et al. Methylprednisolone or naloxone treatment after acute spinal cord injury: 1-year follow-up data. Results of the second National Acute Spinal Cord Injury Study. Journal of neurosurgery 1992;76:23-31.

35. Bracken MB, Shepard MJ, Collins WF, et al. A randomized, controlled trial of methylprednisolone or naloxone in the treatment of acute spinal-cord injury. Results of the Second National Acute Spinal Cord Injury Study. The New England journal of medicine 1990;322:1405-11.

36. Bracken MB, Shepard MJ, Holford TR, et al. Administration of methylprednisolone for 24 or 48 hours or tirilazad mesylate for 48 hours in the treatment of acute spinal cord injury. Results of the Third National Acute Spinal Cord Injury Randomized Controlled Trial. National Acute Spinal Cord Injury Study. JAMA : the journal of the American Medical Association 1997;277:1597-604.

37. Bracken MB, Shepard MJ, Holford TR, et al. Methylprednisolone or tirilazad mesylate administration after acute spinal cord injury: 1-year follow up. Results of the third National Acute Spinal Cord Injury randomized controlled trial. Journal of neurosurgery 1998;89:699-706.

38. Geisler FH, Coleman WP, Grieco G, Poonian D, Sygen Study G. The Sygen multicenter acute spinal cord injury study. Spine 2001;26:S87-98.

39. TADIE, #160, M., et al. Early care and treatment with a neuroprotective drug, gacyclidine, in patients with acute spinal cord injury. Asnières-sur-Seine, FRANCE: Edimédica; 2003.

40. Walters BC, Hadley MN, Hurlbert RJ, et al. Guidelines for the management of acute cervical spine and spinal cord injuries: 2013 update. Neurosurgery 2013;60 Suppl 1:82-91.

41. Lammertse D, Tuszynski MH, Steeves JD, et al. Guidelines for the conduct of clinical trials for spinal cord injury as developed by the ICCP panel: clinical trial design. Spinal cord 2007;45:232-42.

42. Tuszynski MH, Steeves JD, Fawcett JW, et al. Guidelines for the conduct of clinical trials for spinal cord injury as developed by the ICCP Panel: clinical trial inclusion/exclusion criteria and ethics. Spinal cord 2007;45:222-31.

43. Fehlings MG, Baptiste DC. Current status of clinical trials for acute spinal cord injury. Injury 2005;36 Suppl 2:B113-22.

44. Bracken MB, Shepard MJ, Hellenbrand KG, et al. Methylprednisolone and neurological function 1 year after spinal cord injury. Results of the National Acute Spinal Cord Injury Study. J Neurosurg 1985;63:704-13.

45. Bracken MB. Methylprednisolone and acute spinal cord injury: an update of the randomized evidence. Spine (Phila Pa 1976) 2001;26:S47-54.

46. Furlan JC, Noonan V, Cadotte DW, Fehlings MG. Timing of decompressive surgery of spinal cord after traumatic spinal cord injury: an evidence-based examination of pre-clinical and clinical studies. Journal of neurotrauma 2011;28:1371-99.

47. Bedbrook GM, Sedgley GI. The management of spinal injuries--past and present. International rehabilitation medicine 1980;2:45-61.

48. Fehlings MG, Perrin RG. The timing of surgical intervention in the treatment of spinal cord injury: a systematic review of recent clinical evidence. Spine 2006;31:S28-35; discussion S6.

49. Fehlings MG, Vaccaro A, Wilson JR, et al. Early versus delayed decompression for traumatic cervical spinal cord injury: results of the Surgical Timing in Acute Spinal Cord Injury Study (STASCIS). PloS one 2012;7:e32037.

50. Fehlings MG, Tator CH. An evidence-based review of decompressive surgery in acute spinal cord injury: rationale, indications, and timing based on experimental and clinical studies. J Neurosurg 1999;91:1-11.

51. Gunnarsson T, Fehlings MG. Acute neurosurgical management of traumatic brain injury and spinal cord injury. Curr Opin Neurol 2003;16:717-23.

52. Cengiz SL, Kalkan E, Bayir A, Ilik K, Basefer A. Timing of thoracolomber spine stabilization in trauma patients; impact on neurological outcome and clinical course. A real prospective (rct) randomized controlled study. Arch Orthop Trauma Surg 2008;128:959-66.

53. Vaccaro AR, Daugherty RJ, Sheehan TP, et al. Neurologic outcome of early versus late surgery for cervical spinal cord injury. Spine 1997;22:2609-13.

54. Campagnolo DI, Esquieres RE, Kopacz KJ. Effect of timing of stabilization on length of stay and medical complications following spinal cord injury. J Spinal Cord Med 1997;20:331-4.

55. Chipman JG, Deuser WE, Beilman GJ. Early surgery for thoracolumbar spine injuries decreases complications. J Trauma 2004;56:52-7.

56. Croce MA, Bee TK, Pritchard E, Miller PR, Fabian TC. Does optimal timing for spine fracture fixation exist? Ann Surg 2001;233:851-8.

57. Guest J, Eleraky MA, Apostolides PJ, Dickman CA, Sonntag VK. Traumatic central cord syndrome: results of surgical management. J Neurosurg 2002;97:25-32.

58. Kerwin AJ, Frykberg ER, Schinco MA, Griffen MM, Murphy T, Tepas JJ. The effect of early spine fixation on non-neurologic outcome. J Trauma 2005;58:15-21.

59. Levi L, Wolf A, Rigamonti D, Ragheb J, Mirvis S, Robinson WL. Anterior decompression in cervical spine trauma: does the timing of surgery affect the outcome? Neurosurgery 1991;29:216-22.

60. McKinley W, Meade MA, Kirshblum S, Barnard B. Outcomes of early surgical management versus late or no surgical intervention after acute spinal cord injury. Arch Phys Med Rehabil 2004;85:1818-25.

61. Mirza SK, Krengel WF, 3rd, Chapman JR, et al. Early versus delayed surgery for acute cervical spinal cord injury. Clin Orthop Relat Res 1999:104-14.

62. Schinkel C, Frangen TM, Kmetic A, Andress HJ, Muhr G. Timing of thoracic spine stabilization in trauma patients: impact on clinical course and outcome. J Trauma 2006;61:156-60; discussion 60.

63. Krengel WF, 3rd, Anderson PA, Henley MB. Early stabilization and decompression for incomplete paraplegia due to a thoracic-level spinal cord injury. Spine 1993;18:2080-7.

64. McLain RF, Benson DR. Urgent surgical stabilization of spinal fractures in polytrauma patients. Spine 1999;24:1646-54.

65. Clohisy JC, Akbarnia BA, Bucholz RD, Burkus JK, Backer RJ. Neurologic recovery associated with anterior decompression of spine fractures at the thoracolumbar junction (T12-L1). Spine 1992;17:S325-30.

66. Papadopoulos SM, Selden NR, Quint DJ, Patel N, Gillespie B, Grube S. Immediate spinal cord decompression for cervical spinal cord injury: feasibility and outcome. J Trauma 2002;52:323-32.

67. Chen L, Yang H, Yang T, Xu Y, Bao Z, Tang T. Effectiveness of surgical treatment for traumatic central cord syndrome. J Neurosurg Spine 2009;10:3-8.

68. Pollard ME, Apple DF. Factors associated with improved neurologic outcomes in patients with incomplete tetraplegia. Spine 2003;28:33-9.

69. Sapkas GS, Papadakis SA. Neurological outcome following early versus delayed lower cervical spine surgery. J Orthop Surg (Hong Kong) 2007;15:183-6.

70. Duh MS, Shepard MJ, Wilberger JE, Bracken MB. The effectiveness of surgery on the treatment of acute spinal cord injury and its relation to pharmacological treatment. Neurosurgery 1994;35:240-8; discussion 8-9.

71. Kusiak AN, Selzer ME. Neuroplasticity in the spinal cord. Handbook of clinical neurology 2013;110:23-42.

72. Becerra JL, Puckett WR, Hiester ED, et al. MR-pathologic comparisons of wallerian degeneration in spinal cord injury. AJNR American journal of neuroradiology 1995;16:125-33.

73. Bradbury EJ, Moon LD, Popat RJ, et al. Chondroitinase ABC promotes functional recovery after spinal cord injury. Nature 2002;416:636-40.

74. Bregman BS, Kunkel-Bagden E, Schnell L, Dai HN, Gao D, Schwab ME. Recovery from spinal cord injury mediated by antibodies to neurite growth inhibitors. Nature 1995;378:498-501.

75. GrandPre T, Li S, Strittmatter SM. Nogo-66 receptor antagonist peptide promotes axonal regeneration. Nature 2002;417:547-51.

76. Yick LW, Cheung PT, So KF, Wu W. Axonal regeneration of Clarke's neurons beyond the spinal cord injury scar after treatment with chondroitinase ABC. Experimental neurology 2003;182:160-8.

77. Segal M. Rapid plasticity of dendritic spine: hints to possible functions? Progress in neurobiology 2001;63:61-70.

78. Steward O, Reeves TM. Protein-synthetic machinery beneath postsynaptic sites on CNS neurons: association between polyribosomes and other organelles at the synaptic site. The Journal of neuroscience : the official journal of the Society for Neuroscience 1988;8:176-84.

79. Bradbury EJ, Khemani S, Von R, King, Priestley JV, McMahon SB. NT-3 promotes growth of lesioned adult rat sensory axons ascending in the dorsal columns of the spinal cord. The European journal of neuroscience 1999;11:3873-83.

80. Grill R, Murai K, Blesch A, Gage FH, Tuszynski MH. Cellular delivery of neurotrophin-3 promotes corticospinal axonal growth and partial functional recovery after spinal cord injury. The Journal of neuroscience : the official journal of the Society for Neuroscience 1997;17:5560-72.

81. Neumann S, Woolf CJ. Regeneration of dorsal column fibers into and beyond the lesion site following adult spinal cord injury. Neuron 1999;23:83-91.

82. Oudega M, Hagg T. Nerve growth factor promotes regeneration of sensory axons into adult rat spinal cord. Experimental neurology 1996;140:218-29.

83. Qiu J, Cai D, Dai H, et al. Spinal axon regeneration induced by elevation of cyclic AMP. Neuron 2002;34:895-903.

84. Bunge MB. Transplantation of purified populations of Schwann cells into lesioned adult rat spinal cord. Journal of neurology 1994;242:S36-9.

85. Li Y, Field PM, Raisman G. Repair of adult rat corticospinal tract by transplants of olfactory ensheathing cells. Science 1997;277:2000-2.

86. Liu Y, Kim D, Himes BT, et al. Transplants of fibroblasts genetically modified to express BDNF promote regeneration of adult rat rubrospinal axons and recovery of forelimb function. The Journal of neuroscience : the official journal of the Society for Neuroscience 1999;19:4370-87.

87. Lu P, Jones LL, Snyder EY, Tuszynski MH. Neural stem cells constitutively secrete neurotrophic factors and promote extensive host axonal growth after spinal cord injury. Experimental neurology 2003;181:115-29.

88. Bareyre FM, Kerschensteiner M, Raineteau O, Mettenleiter TC, Weinmann O, Schwab ME. The injured spinal cord spontaneously forms a new intraspinal circuit in adult rats. Nature neuroscience 2004;7:269-77.

89. Thallmair M, Metz GA, Z'Graggen WJ, Raineteau O, Kartje GL, Schwab ME. Neurite growth inhibitors restrict plasticity and functional recovery following corticospinal tract lesions. Nature neuroscience 1998;1:124-31.

90. Z'Graggen WJ, Metz GA, Kartje GL, Thallmair M, Schwab ME. Functional recovery and enhanced corticofugal plasticity after unilateral pyramidal tract lesion and blockade of myelin-associated neurite growth inhibitors in adult rats. The Journal of neuroscience : the official journal of the Society for Neuroscience 1998;18:4744-57.

91. Zhao RR, Andrews MR, Wang D, et al. Combination treatment with anti-Nogo-A and chondroitinase ABC is more effective than single treatments at enhancing functional recovery after spinal cord injury. The European journal of neuroscience 2013;38:2946-61.

92. Guest JD, Hiester ED, Bunge RP. Demyelination and Schwann cell responses adjacent to injury epicenter cavities following chronic human spinal cord injury. Experimental neurology 2005;192:384-93.

93. Waxman SG. Demyelination in spinal cord injury. Journal of the neurological sciences 1989;91:1-14.

94. Cao Q, Zhang YP, Iannotti C, et al. Functional and electrophysiological changes after graded traumatic spinal cord injury in adult rat. Experimental neurology 2005;191 Suppl 1:S3-S16.

95. McTigue DM, Horner PJ, Stokes BT, Gage FH. Neurotrophin-3 and brain-derived neurotrophic factor induce oligodendrocyte proliferation and myelination of regenerating axons in the contused adult rat spinal cord. The Journal of neuroscience : the official journal of the Society for Neuroscience 1998;18:5354-65.

96. Bunge RP, Puckett WR, Hiester ED. Observations on the pathology of several types of human spinal cord injury, with emphasis on the astrocyte response to penetrating injuries. Advances in neurology 1997;72:305-15.

97. Dusart I, Schwab ME. Secondary cell death and the inflammatory reaction after dorsal hemisection of the rat spinal cord. The European journal of neuroscience 1994;6:712-24.

98. Fitch MT, Doller C, Combs CK, Landreth GE, Silver J. Cellular and molecular mechanisms of glial scarring and progressive cavitation: in vivo and in vitro analysis of inflammation-induced secondary injury after CNS trauma. The Journal of neuroscience : the official journal of the Society for Neuroscience 1999;19:8182-98.

99. Liu XZ, Xu XM, Hu R, et al. Neuronal and glial apoptosis after traumatic spinal cord injury. The Journal of neuroscience : the official journal of the Society for Neuroscience 1997;17:5395-406.

100. Oudega M, Vargas CG, Weber AB, Kleitman N, Bunge MB. Long-term effects of methylprednisolone following transection of adult rat spinal cord. The European journal of neuroscience 1999;11:2453-64.

101. Popovich PG, Guan Z, Wei P, Huitinga I, van Rooijen N, Stokes BT. Depletion of hematogenous macrophages promotes partial hindlimb recovery and neuroanatomical repair after experimental spinal cord injury. Experimental neurology 1999;158:351-65.

102. Young W. Methylprednisolone treatment of acute spinal cord injury: an introduction. Journal of neurotrauma 1991;8 Suppl 1:S43-6.

103. Furlan JC, Fehlings MG, Tator CH, Davis AM. Motor and sensory assessment of patients in clinical trials for pharmacological therapy of acute spinal cord injury: psychometric properties of the ASIA Standards. J Neurotrauma 2008;25:1273-301.

104. Platzer P, Jaindl M, Thalhammer G, et al. Clearing the cervical spine in critically injured patients: a comprehensive C-spine protocol to avoid unnecessary delays in diagnosis. European spine journal : official publication of the European Spine Society, the European Spinal Deformity Society, and the European Section of the Cervical Spine Research Society 2006;15:1801-10.

105. Woodring JH, Lee C. Limitations of cervical radiography in the evaluation of acute cervical trauma. The Journal of trauma 1993;34:32-9.

106. Insko EK, Gracias VH, Gupta R, Goettler CE, Gaieski DF, Dalinka MK. Utility of flexion and extension radiographs of the cervical spine in the acute evaluation of blunt trauma. The Journal of trauma 2002;53:426-9.

107. Saini S, Seltzer SE, Bramson RT, et al. Technical cost of radiologic examinations: analysis across imaging modalities. Radiology 2000;216:269-72.

108. Saini S, Sharma R, Levine LA, Barmson RT, Jordan PF, Thrall JH. Technical cost of CT examinations. Radiology 2001;218:172-5.

109. Blackmore CC, Ramsey SD, Mann FA, Deyo RA. Cervical spine screening with CT in trauma patients: a cost-effectiveness analysis. Radiology 1999;212:117-25.

110. Hashemi RH, Bradley WG, Lisanti CJ. MRI the basics. 3rd ed. Philadelphia, PA: Lippincott Williams & Wilkins; 2010:ix, 385 p.

111. Huettel SA, McCarthy G, Song AW. Functional magnetic resonance imaging. 2nd ed. Sunderland, Mass.: Sinauer Associates; 2009.

112. Menon RS, Ogawa S, Tank DW, Ugurbil K. Tesla gradient recalled echo characteristics of photic stimulation-induced signal changes in the human primary visual cortex. Magnetic resonance in medicine : official journal of the Society of Magnetic Resonance in Medicine / Society of Magnetic Resonance in Medicine 1993;30:380-6.

113. Stroman PW, Krause V, Frankenstein UN, Malisza KL, Tomanek B. Spin-echo versus gradient-echo fMRI with short echo times. Magnetic resonance imaging 2001;19:827-31.

114. Stroman PW, Krause V, Malisza KL, Frankenstein UN, Tomanek B. Characterization of contrast changes in functional MRI of the human spinal cord at 1.5 T. Magnetic resonance imaging 2001;19:833-8.

115. Stroman PW, Krause V, Malisza KL, Frankenstein UN, Tomanek B. Extravascular proton-density changes as a non-BOLD component of contrast in fMRI of the human spinal cord. Magnetic resonance in medicine : official journal of the Society of Magnetic Resonance in Medicine / Society of Magnetic Resonance in Medicine 2002;48:122-7.

116. Stroman PW, Lee AS, Pitchers KK, Andrew RD. Magnetic resonance imaging of neuronal and glial swelling as an indicator of function in cerebral tissue slices. Magn Reson Med 2008;59:700-6.

117. Figley CR, Leitch JK, Stroman PW. In contrast to BOLD: signal enhancement by extravascular water protons as an alternative mechanism of endogenous fMRI signal change. Magnetic resonance imaging 2010;28:1234-43.

118. Carusone LM, Srinivasan J, Gitelman DR, Mesulam MM, Parrish TB. Hemodynamic response changes in cerebrovascular disease: implications for functional MR imaging. AJNR American journal of neuroradiology 2002;23:1222-8.

119. Chen Y, Parrish TB. Caffeine dose effect on activation-induced BOLD and CBF responses. NeuroImage 2009;46:577-83.

120. Chen Y, Parrish TB. Caffeine's effects on cerebrovascular reactivity and coupling between cerebral blood flow and oxygen metabolism. NeuroImage 2009;44:647-52.

121. Huettel SA, Singerman JD, McCarthy G. The effects of aging upon the hemodynamic response measured by functional MRI. NeuroImage 2001;13:161-75.

122. Levin JM, Frederick Bde B, Ross MH, et al. Influence of baseline hematocrit and hemodilution on BOLD fMRI activation. Magnetic resonance imaging 2001;19:1055-62.

123. Levin JM, Ross MH, Mendelson JH, et al. Reduction in BOLD fMRI response to primary visual stimulation following alcohol ingestion. Psychiatry research 1998;82:135-46.

124. Aguirre GK, Zarahn E, D'Esposito M. The variability of human, BOLD hemodynamic responses. NeuroImage 1998;8:360-9.

125. Handwerker DA, Ollinger JM, D'Esposito M. Variation of BOLD hemodynamic responses across subjects and brain regions and their effects on statistical analyses. NeuroImage 2004;21:1639-51.

126. Giulietti G, Giove F, Garreffa G, Colonnese C, Mangia S, Maraviglia B. Characterization of the functional response in the human spinal cord: Impulse-response function and linearity. NeuroImage 2008;42:626-34.

127. Figley CR, Stroman PW. Measurement and characterization of the human spinal cord SEEP response using event-related spinal fMRI. Magnetic resonance imaging 2012;30:471-84.

128. Friston KJ. Functional and effective connectivity: a review. Brain Connectivity. 2011; 1(1):13-36.

129. Matsuzaki H, Wakabayashi K, Ishihara K, Ishikawa H, Kawabata H, Onomura T. The origin and significance of spinal cord pulsation. Spinal cord 1996;34:422-6.

130. Mikulis DJ, Wood ML, Zerdoner OA, Poncelet BP. Oscillatory motion of the normal cervical spinal cord. Radiology 1994;192:117-21.

131. Figley CR, Stroman PW. Investigation of human cervical and upper thoracic spinal cord motion: implications for imaging spinal cord structure and function. Magnetic resonance in medicine : official journal of the Society of Magnetic Resonance in Medicine / Society of Magnetic Resonance in Medicine 2007;58:185-9.

132. Fox MD, Raichle ME. Spontaneous fluctuations in brain activity observed with functional magnetic resonance imaging. Nat Rev Neurosci 2007;8:700-11.

133. Cadotte DW, Bosma R, Mikulis D, et al. Plasticity of the injured human spinal cord: insights revealed by spinal cord functional MRI. PloS one 2012;7:e45560.

134. Nimmo WS, Tucker GT. Clinical measurement in drug evaluation. Chichester, West Sussex, England ; New York: J. Wiley; 1995.

135. Smith JJ, Sorensen AG, Thrall JH. Biomarkers in imaging: realizing radiology's future. Radiology 2003;227:633-8.

136. Altman J, Bayer SA. The development of the rat spinal cord. Advances in anatomy, embryology, and cell biology 1984;85:1-164.

137. Altman J, Bayer SA. Development of the human spinal cord : an interpretation based on experimental studies in animals. Oxford ; New York, N.Y.: Oxford University Press; 2001.

138. Parent A, Carpenter MB. Carpenter's human neuroanatomy. 9th ed. Baltimore: Williams & Wilkins; 1996.

139. Paxinos G, Mai JK. The human nervous system. 2nd ed. Amsterdam ; Boston: Elsevier Academic Press; 2004:xvii, 1366 p.

140. Rexed B. Some Aspects of the Cytoarchitectonics and Synaptology of the Spinal Cord. Progress in brain research 1964;11:58-92.

141. Cadotte DW, Stroman PW, Mikulis D, Fehlings MG. A systematic review of spinal fMRI research: outlining the elements of experimental design. Journal of neurosurgery Spine 2012;17:102-18.

142. Chung K, Kevetter GA, Willis WD, Coggeshall RE. An estimate of the ratio of propriospinal to long tract neurons in the sacral spinal cord of the rat. Neurosci Lett 1984;44:173-7.

143. Beall JE, Applebaum AE, Foreman RD, Willis WD. Spinal cord potentials evoked by cutaneous afferents in the monkey. J Neurophysiol 1977;40:199-211.

144. Chung JM, Kenshalo DR, Jr., Gerhart KD, Willis WD. Excitation of primate spinothalamic neurons by cutaneous C-fiber volleys. J Neurophysiol 1979;42:1354-69.

145. Lucas ME, Willis WD. Identification of muscle afferents which activate interneurons in the intermediate nucleus. J Neurophysiol 1974;37:282-93.

146. Eccles JC, Magni F, Willis WD. Depolarization of central terminals of Group I afferent fibres from muscle. J Physiol 1962;160:62-93.

147. Vallbo AB, Hagbarth KE, Torebjork HE, Wallin BG. Somatosensory, proprioceptive, and sympathetic activity in human peripheral nerves. Physiol Rev 1979;59:919-57.

148. Pare M, Smith AM, Rice FL. Distribution and terminal arborizations of cutaneous mechanoreceptors in the glabrous finger pads of the monkey. J Comp Neurol 2002;445:347-59.

149. Knibestol M. Stimulus-response functions of slowly adapting mechanoreceptors in the human glabrous skin area. J Physiol 1975;245:63-80.

150. Ochoa J, Torebjork E. Sensations evoked by intraneural microstimulation of single mechanoreceptor units innervating the human hand. J Physiol 1983;342:633-54.

151. Brown AG, Rose PK, Snow PJ. Morphology and organization of axon collaterals from afferent fibres of slowly adapting type I units in cat spinal cord. J Physiol 1978;277:15-27.

152. Koerber HR, Seymour AW, Mendell LM. Tuning of spinal networks to frequency components of spike trains in individual afferents. J Neurosci 1991;11:3178-87.

153. Willis WD, Trevino DL, Coulter JD, Maunz RA. Responses of primate spinothalamic tract neurons to natural stimulation of hindlimb. J Neurophysiol 1974;37:358-72.

154. Schepers RJ, Ringkamp M. Thermoreceptors and thermosensitive afferents. Neuroscience and biobehavioral reviews 2009;33:205-12.

155. Molinari HH, Greenspan JD, Krenshalo DR. The effects of rate of temperature change and adapting temperature on thermal sensitivity. Sensory processes 1977;1:354-62.

156. Pedersen SF, Owsianik G, Nilius B. TRP channels: an overview. Cell calcium 2005;38:233-52.

157. Hallin RG, Torebjork HE, Wiesenfeld Z. Nociceptors and warm receptors innervated by C fibres in human skin. Journal of neurology, neurosurgery, and psychiatry 1982;45:313-9.

158. McGlone F, Reilly D. The cutaneous sensory system. Neuroscience and biobehavioral reviews 2010;34:148-59.

159. Konietzny F. Peripheral neural correlates of temperature sensations in man. Human neurobiology 1984;3:21-32.

160. Hensel H, Boman KK. Afferent impulses in cutaneous sensory nerves in human subjects. Journal of neurophysiology 1960;23:564-78.

161. Konietzny F, Hensel H. The dynamic response of warm units in human skin nerves. Pflugers Archiv : European journal of physiology 1977;370:111-4.

162. Kanui TI. Receptive field organisation and electrophysiological responses of spinal cord thermoreactive neurones in the rat. Experimental brain research Experimentelle Hirnforschung Experimentation cerebrale 1988;71:508-14.

163. Dostrovsky JO, Hellon RF. The representation of facial temperature in the caudal trigeminal nucleus of the cat. The Journal of physiology 1978;277:29-47.

164. Craig AD. How do you feel? Interoception: the sense of the physiological condition of the body. Nature reviews Neuroscience 2002;3:655-66.

165. Iggo A. Cutaneous thermoreceptors in primates and sub-primates. The Journal of physiology 1969;200:403-30.

166. Craig AD, Kniffki KD. Spinothalamic lumbosacral lamina I cells responsive to skin and muscle stimulation in the cat. The Journal of physiology 1985;365:197-221.

167. Turnbull IM, Brieg A, Hassler O. Blood supply of cervical spinal cord in man. A microangiographic cadaver study. J Neurosurg 1966;24:951-65.

168. Turnbull IM. Chapter 5. Blood supply of the spinal cord: normal and pathological considerations. Clin Neurosurg 1973;20:56-84.

169. Gillilan LA. The arterial blood supply of the human spinal cord. J Comp Neurol 1958;110:75-103.

170. Hassler O. Blood supply to human spinal cord. A microangiographic study. Arch Neurol 1966;15:302-7.

171. Lazorthes G, Gouaze A, Zadeh JO, Santini JJ, Lazorthes Y, Burdin P. Arterial vascularization of the spinal cord. Recent studies of the anastomotic substitution pathways. J Neurosurg 1971;35:253-62.

172. Tveten L. Spinal cord vascularity. III. The spinal cord arteries in man. Acta Radiol Diagn (Stockh) 1976;17:257-73.

173. Turnbull IM. Microvasculature of the human spinal cord. J Neurosurg 1971;35:141-7.

174. Ducker TB, Perot PL, Jr. Spinal cord oxygen and blood flow in trauma. Surg Forum 1971;22:413-5.

175. Kobrine AI, Doyle TF, Martins AN. Autoregulation of spinal cord blood flow. Clin Neurosurg 1975;22:573-81.

176. Smith AL, Pender JW, Alexander SC. Effects of PCO2 on spinal cord blood flow. Am J Physiol 1969;216:1158-63.

177. Kobrine AI, Evans DE, Rizzoli HV. The role of the sympathetic nervous system in spinal cord autoregulation. Acta Neurol Scand Suppl 1977;64:54-5.

178. Sato M, Pawlik G, Heiss WD. Comparative studies of regional CNS blood flow autoregulation and responses to CO2 in the cat. Effects of altering arterial blood pressure and PaCO2 on rCBF of cerebrum, cerebellum, and spinal cord. Stroke 1984;15:91-7.

179. Craigie E. The comparative anatomy and embryology of the capillary bed of the central nervous system. . Res Publ Ass nerv inent Dis 1938;18:3-28.

180. Lavrent'eva NB, McHedlishvili GI, Plechkova EK. [Cholinesterase distribution and activity in the nervous structures of the pial arteries (a histochemical study)]. Biull Eksp Biol Med 1968;66:110-3.

181. Attwell D, Buchan AM, Charpak S, Lauritzen M, Macvicar BA, Newman EA. Glial and neuronal control of brain blood flow. Nature;468:232-43.

182. Devor A, Sakadzic S, Srinivasan VJ, et al. Frontiers in optical imaging of cerebral blood flow and metabolism. J Cereb Blood Flow Metab;32:1259-76.

183. Franceschini MA, Thaker S, Themelis G, et al. Assessment of infant brain development with frequency-domain near-infrared spectroscopy. Pediatr Res 2007;61:546-51.

184. Rolfe DF, Brown GC. Cellular energy utilization and molecular origin of standard metabolic rate in mammals. Physiol Rev 1997;77:731-58.

185. Attwell D, Laughlin SB. An energy budget for signaling in the grey matter of the brain. J Cereb Blood Flow Metab 2001;21:1133-45.

186. Edvinsson L, Krause DN. Cerebral blood flow and metabolism. 2nd ed. Philadelphia: Lippincott Williams & Wilkins; 2002.

187. Abram SE, Kostreva DR. Spinal cord metabolic response to noxious radiant heat stimulation of the cat hind footpad. Brain Res 1986;385:143-7.

188. Egger MD, Freeman NC, Jacquin M, Proshansky E, Semba K. Dorsal horn cells in the cat responding to stimulation of the plantar cushion. Brain Res 1986;383:68-82.

189. Kadekaro M, Crane AM, Sokoloff L. Differential effects of electrical stimulation of sciatic nerve on metabolic activity in spinal cord and dorsal root ganglion in the rat. Proc Natl Acad Sci U S A 1985;82:6010-3.

190. Molander C, Grant G. Laminar distribution and somatotopic organization of primary afferent fibers from hindlimb nerves in the dorsal horn. A study by transganglionic transport of horseradish peroxidase in the rat. Neuroscience 1986;19:297-312.

191. Bryan RN, Trevino DL, Coulter JD, Willis WD. Location and somatotopic organization of the cells of origin of the spino-cervical tract. Exp Brain Res 1973;17:177-89.

192. Grant G. Projection patterns of primary sensory neurons studied by transganglionic methods: somatotopy and target-related organization. Brain Res Bull 1993;30:199-208.

193. Wall PD, Merrill EG, Yaksh TL. Responses of single units in laminae 2 and 3 of cat spinal cord. Brain Res 1979;160:245-60.

194. Figley CR, Stroman PW. The role(s) of astrocytes and astrocyte activity in neurometabolism, neurovascular coupling, and the production of functional neuroimaging signals. Eur J Neurosci;33:577-88.

195. Govers N, Beghin J, Van Goethem JW, et al. Functional MRI of the cervical spinal cord on 1.5 T with fingertapping: to what extent is it feasible? Neuroradiology 2007;49:73-81.

196. Maieron M, Iannetti GD, Bodurka J, Tracey I, Bandettini PA, Porro CA. Functional responses in the human spinal cord during willed motor actions: evidence for side- and rate-dependent activity. J Neurosci 2007;27:4182-90.

197. Madi S, Flanders AE, Vinitski S, Herbison GJ, Nissanov J. Functional MR imaging of the human cervical spinal cord. AJNR Am J Neuroradiol 2001;22:1768-74.

198. Lawrence JM, Stroman PW, Kollias SS. Functional magnetic resonance imaging of the human spinal cord during vibration stimulation of different dermatomes. Neuroradiology 2008;50:273-80.

199. Xie CH, Kong KM, Guan JT, Chen YX, Wu RH. Functional MR imaging of the cervical spinal cord by use of 20Hz functional electrical stimulation to median nerve. Conf Proc IEEE Eng Med Biol Soc 2007;2007:3392-5.

200. Stracke CP, Pettersson LG, Schoth F, Moller-Hartmann W, Krings T. Interneuronal systems of the cervical spinal cord assessed with BOLD imaging at 1.5 T. Neuroradiology 2005;47:127-33.

201. Stroman PW, Krause V, Malisza KL, Frankenstein UN, Tomanek B. Functional magnetic resonance imaging of the human cervical spinal cord with stimulation of different sensory dermatomes. Magn Reson Imaging 2002;20:1-6.

202. Stroman PW. Spinal fMRI investigation of human spinal cord function over a range of innocuous thermal sensory stimuli and study-related emotional influences. Magn Reson Imaging 2009;27:1333-46.

203. Porro CA, Cavazzuti M. Spatial and temporal aspects of spinal cord and brainstem activation in the formalin pain model. Prog Neurobiol 1993;41:565-607.

204. Backes WH, Mess WH, Wilmink JT. Functional MR imaging of the cervical spinal cord by use of median nerve stimulation and fist clenching. AJNR Am J Neuroradiol 2001;22:1854-9.

205. Ng MC, Wu EX, Lau HF, Hu Y, Lam EY, Luk KD. Cervical spinal cord BOLD fMRI study: modulation of functional activation by dexterity of dominant and non-dominant hands. Neuroimage 2008;39:825-31.

206. Stroman PW, Coe BC, Munoz DP. Influence of attention focus on neural activity in the human spinal cord during thermal sensory stimulation. Magn Reson Imaging;29:9-18.

207. Valsasina P, Agosta F, Caputo D, Stroman PW, Filippi M. Spinal fMRI during proprioceptive and tactile tasks in healthy subjects: Activity detected using cross-correlation, general linear model and independent component analysis. Neuroradiology 2008;50:895-902.

208. Lang J, Bartram CT. [Fila radicularia of the ventral and dorsal radices of the human spinal cord]. Gegenbaurs Morphol Jahrb 1982;128:417-62.

209. Sarnat HB, Netsky MG. Evolution of the nervous system. New York: Oxford University Press; 1974.

210. Morin F. A new spinal pathway for cutaneous impulses. Am J Physiol 1955;183:245-52.

211. Mizuno N, Nakano K, Imaizumi M, Okamoto M. The lateral cervical nucleus of the Japanese monkey (Macaca fuscata). J Comp Neurol 1967;129:375-84.

212. Wada E, Ohmura M, Yonenobu K. Intramedullary changes of the spinal cord in cervical spondylotic myelopathy. Spine 1995;20:2226-32.

213. Weirich SD, Cotler HB, Narayana PA, et al. Histopathologic correlation of magnetic resonance imaging signal patterns in a spinal cord injury model. Spine 1990;15:630-8.

214. Downs SH, Black N. The feasibility of creating a checklist for the assessment of the methodological quality both of randomised and non-randomised studies of health care interventions. J Epidemiol Community Health 1998;52:377-84.

215. Obuchowski NA. Receiver operating characteristic curves and their use in radiology. Radiology 2003;229:3-8.

216. Park SH, Goo JM, Jo CH. Receiver operating characteristic (ROC) curve: practical review for radiologists. Korean J Radiol 2004;5:11-8.

217. Bradbury EJ, McMahon SB. Spinal cord repair strategies: why do they work? Nature reviews Neuroscience 2006;7:644-53.

218. Cadotte DW, Fehlings MG. Spinal cord injury: a systematic review of current treatment options. Clin Orthop Relat Res;469:732-41.

219. Jurkiewicz MT, Crawley AP, Verrier MC, Fehlings MG, Mikulis DJ. Somatosensory cortical atrophy after spinal cord injury: a voxel-based morphometry study. Neurology 2006;66:762-4.

220. Mikulis DJ, Jurkiewicz MT, McIlroy WE, et al. Adaptation in the motor cortex following cervical spinal cord injury. Neurology 2002;58:794-801.

221. Leitch JK, Figley CR, Stroman PW. Applying functional MRI to the spinal cord and brainstem. Magn Reson Imaging;28:1225-33.

222. Kornelsen J, Stroman PW. Detection of the neuronal activity occurring caudal to the site of spinal cord injury that is elicited during lower limb movement tasks. Spinal Cord 2007;45:485-90.

223. Stroman PW, Tomanek B, Krause V, Frankenstein UN, Malisza KL. Mapping of neuronal function in the healthy and injured human spinal cord with spinal fMRI. Neuroimage 2002;17:1854-60.

224. Hoheisel U, Scheifer C, Trudrung P, Unger T, Mense S. Pathophysiological activity in rat dorsal horn neurones in segments rostral to a chronic spinal cord injury. Brain research 2003;974:134-45.

225. Kirshblum SC, Waring W, Biering-Sorensen F, et al. Reference for the 2011 revision of the International Standards for Neurological Classification of Spinal Cord Injury. J Spinal Cord Med;34:547-54.

226. DeVivo M, Biering-Sorensen F, Charlifue S, et al. International Spinal Cord Injury Core Data Set. Spinal Cord 2006;44:535-40.

227. Murphy K, Bodurka J, Bandettini PA. How long to scan? The relationship between fMRI temporal signal to noise ratio and necessary scan duration. Neuroimage 2007;34:565-74.

228. Stroman PW, Bosma RL, Tsyben A. Somatotopic arrangement of thermal sensory regions in the healthy human spinal cord determined by means of spinal cord functional MRI. Magn Reson Med.

229. Stroman PW, Bosma RL, Tsyben A. Somatotopic arrangement of thermal sensory regions in the healthy human spinal cord determined by means of spinal cord functional MRI. Magn Reson Med 2011.

230. Worsley KJ, Friston KJ. Analysis of fMRI time-series revisited--again. NeuroImage 1995;2:173-81.

231. Figley CR, Stroman PW. Measurement and characterization of the human spinal cord SEEP response using event-related spinal fMRI. Magn Reson Imaging 2012.

232. Gesierich B, Jovicich J, Riello M, et al. Distinct Neural Substrates for Semantic Knowledge and Naming in the Temporoparietal Network. Cereb Cortex.

233. Xuan Y, Meng C, Yang Y, et al. Resting-state brain activity in adult males who stutter. PLoS One;7:e30570.

234. Handwerker HO, Iggo A, Zimmermann M. Segmental and supraspinal actions on dorsal horn neurons responding to noxious and non-noxious skin stimuli. Pain 1975;1:147-65.

235. Freund P, Weiskopf N, Ashburner J, et al. MRI investigation of the sensorimotor cortex and the corticospinal tract after acute spinal cord injury: a prospective longitudinal study. Lancet neurology 2013;12:873-81.

236. Fedorov A, Beichel R, Kalpathy-Cramer J, et al. 3D Slicer as an image computing platform for the Quantitative Imaging Network. Magnetic resonance imaging 2012;30:1323-41.

237. Okado N. Onset of synapse formation in the human spinal cord. The Journal of comparative neurology 1981;201:211-9.

238. Cadotte DW, Fehlings MG. Will imaging biomarkers transform spinal cord injury trials? Lancet neurology 2013;12:843-4.

239. Friston KJ. Functional and effective connectivity: a review. Brain Connect;1:13-36.

240. Mori S, Zhang J. Principles of diffusion tensor imaging and its applications to basic neuroscience research. Neuron 2006;51:527-39.

241. Ferraro AB, S.E. The nuclei of the posterior funiculi in *Macacus rhesus*: An anatomic and experimental investigation. Arch Neurol Psychiat 1935;33:262-75.

242. Ferraro AB, S.E. Posterior column fibers and their termination in *Macacus shesus.* . Journal of Comparative Neurology 1935;62:507-30.

243. Callot V. DG, Vignaud A., Cozzone P. Toward a better description of the gray matter spinal cord by using highly resolved diffusion-weighted and morphologic T2*-weighted MRI. Proceedings 17th Scientific Meeting, International Society for Magnetic Resonance in Medicine 2009:1302.

244. Jenkinson M, Bannister P, Brady M, Smith S. Improved optimization for the robust and accurate linear registration and motion correction of brain images. NeuroImage 2002;17:825-41.

245. Guyon I EA. An Introduction to Variable and Feature Selection. Journal of Machine Learning Research 2003;3:1157-82.

246. McIntosh AR, Bookstein FL, Haxby JV, Grady CL. Spatial pattern analysis of functional brain images using partial least squares. NeuroImage 1996;3:143-57.

247. Efron B. Estimating the Error Rate of a Prediction Rule: Improvement on Cross-Validation. Journal of the American Statistical Association 1983;78:316-31.

248. Efron B, Tibshirani, R. Improvements on Cross-Validation: The 632+ Bootstrap Method. Journal of the American Statistical Association 1997;92:548-60.

249. Le TH, Hu X. Methods for assessing accuracy and reliability in functional MRI. NMR in biomedicine 1997;10:160-4.

Appendix I: Grants, Awards, Publications and Presentations

Peer-reviewed Research Grants and Salary Awards

2012 Canadian Institutes of Health Research (CIHR) Health Professional Fellowship Award (Salary Award)

2012 Craig H. Neilsen Foundation, Post-doctoral fellowship research grant

2009 Rick Hansen Foundation – Clinical trials funding grant

2009 Cervical Spine Research Society – Post-doctoral fellowship grant for investigation of advanced imaging techniques to evaluate the injured human spinal cord.

2009 Codman Fellowship in Neurotrauma and Critical Care: administered by the American Association of Neurological Surgeons as an unrestricted educational grant

2009 Ontario Neurotrauma Foundation (ONF) - Post-doctoral Fellowship Salary Grant: Spinal Cord Injury Research for the project titled "Functional magnetic resonance imaging evaluation of the injured human spinal cord: an assessment of recovery and functional plasticity"

2009 Congress of Neurological Surgeons/Synthes Spine Post-doctoral Fellowship unrestricted educational grant

Awards and Honors

2013 Patty Rigby and John Wedge Graduate Scholarship in Science and Technology, University of Toronto, School of Graduate Studies and the Province of Ontario.

2013 Queen Elizabeth II Graduate Scholarship in Science and Technology, University of Toronto, Faculty of Medicine

2013 Canadian Neurosurgical Society's 2013 K.G.McKenzie Prize in Clinical Neuroscience Research, "*Visualizing plasticity in the Injured Human Spinal Cord with fMRI*"

2013 American Society of Functional Neuroradiology, 7th Annual Meeting, 3rd place award for the best-submitted abstract. Charleston, South Carolina, March 13, 2013

2012 Congress of Neurological Surgeons – Synthes Award for Resident Research on Spinal Cord and Spinal Column Injury: top paper submitted in the Section on Neurotrauma and Critical Care, 2012 Annual CNS meeting. October 9, 2012 Chicago, IL.

2012 Surgeon Scientist Training Program Fellowship award, administered as an unrestricted

educational grant through the Surgeon Scientist program at the University of Toronto. Donated by Johnson & Johnson Medical Products.

2011 Miriam Neveren Memorial Award – Awarded through the post graduate medical education office at the University of Toronto to the top 20% of MD and non-MD medical research applicants

2011 Chisholm Memorial Fellowship Award – Awarded through the post graduate medical education office at the University of Toronto to the top 20% of MD and non-MD medical research applicants

2011 Edward Christie Stevens Fellowship in Medicine – Awarded through the post graduate medical education office at the University of Toronto to the top 20% of MD and non-MD medical research applicants

2011 Joseph M. West Family Memorial Fund – Awarded through the post graduate medical education office at the University of Toronto to the top 20% of MD and non-MD medical research applicants

2011 Starr Medal – awarded through the University of Toronto.

2010 Miriam Neveren Memorial Award – Awarded through the post graduate medical education office at the University of Toronto to the top 20% of MD and non-MD medical research applicants

2010 Joseph M. West Family Memorial Fund - Awarded through the post graduate medical education office at the University of Toronto to the top 20% of MD and non-MD medical research applicants

2010 Starr Medal – awarded through the University of Toronto

2010 Ontario Graduate Scholarship in Science and Technology – the Patty Rigby & John Wedge Graduate Scholarship

2009 Warren Ho Memorial Scholarship Award - Division of Neurosurgery, University of Toronto; Presented to a research resident demonstrating outstanding leadership and humanitarian qualities.

Publications

Cadotte DW, Fehlings MG. Spinal cord injury: Visualizing plasticity and repair in the injured CNS. Nat Rev Neurol. 2013 Sep 10. doi: 10.1038/nrneurol.2013.190.

Cadotte DW, Cohen-Adad J, Fehlings MG. Visualizing integrative functioning in the human brainstem and spinal cord with functional spinal magnetic resonance imaging. Neurosurgery. 2013 Aug;60 Suppl 1:102-9. doi: 10.1227/01.neu.0000430767.87725.95. PMID: 23839360

Wheeler-Kingshott C, Stroman PW, Schwab JM, Bacon M, Bosma R, Brooks J, **Cadotte DW**, Carlstedt T, Ciccarelli O, Cohen-Adad J, Curt A, Evangelou N, Fehlings MG, Filippi M, Kelley BJ, Kollias S,

Mackay A, Porro CA, Smith S, Strittmatter SM, Summers P, Thompson AJ, Tracey I. The current state-of-the-art of spinal cord imaging - Applications. Neuroimage. 2013 Jul 13. doi:pii: S1053-8119(13)00769-6. 10.1016/j.neuroimage.2013.07.014. PMID: 23859923.

Cadotte DW, Fehlings MG. Will imaging biomarkers transform spinal cord injury trials? Lancet Neurol. 2013 Jul 1. doi:pii: S1474-4422(13)70157-1. 10.1016/S1474-4422(13)70157-1. PMID: 23827393

Stroman PW, Wheeler-Kingshott C, Bacon M, Schwab JM, Bosma R, Brooks J, **Cadotte D**, Carlstedt T, Ciccarelli O, Cohen-Adad J, Curt A, Evangelou N, Fehlings MG, Filippi M, Kelly B, Kollias S, Mackay A, Porro CA, Smith S, Strittmatter SM, Summers P, Tracey I. The current state-of-the-art of spinal cord imaging: Methods. Neuroimage. 2013 May 14. doi:pii: S1053-8119(13)00500-4. 10.1016/j.neuroimage.2013.04.124. [Epub ahead of print] PMID: 23685159

David W. Cadotte, Rachael Bosma, David Mikulis, Natalia Nugaeva, Karen Smith, Ronald Pokrupa, Omar Islam, Patrick W. Stroman and Michael G. Fehlings. Plasticity of the Injured Human Spinal Cord: Insights revealed by spinal cord functional MRI. PLoS ONE 7(9): e45560. doi:10.1371/journal.pone.0045560 Published September 19, 2012.

David W. Cadotte, Patrick W. Stroman, David Mikulis and Michael G. Fehlings. A systematic review of spinal fMRI research: outlining the elements of experimental design. Journal of Neurosurgery *Spine (Suppl) 17:102-118, 2012*. Accepted May 7, 2012. Published September 2012.

David W. Cadotte, Adrian Mariampillai, Adam Cadotte, Kenneth K. C. Lee, Tim-Rasmus Kiehl, Brian C. Wilson, Michael G. Fehlings, and Victor X. D. Yang. Speckle variance optical coherence tomography of the rodent spinal cord: in vivo feasibility. Biomedical Optics Express Vol. 3, Iss. 5, pp. 911–919 (2012).

Stroman PW, Bosma RL, Kornelsen J, Lawrence-Dewar J, Wheeler-Kingshott C, **Cadotte DW**, Fehlings MG**.** Advanced MR imaging techniques and characterization of residual anatomy. Clin Neurol Neurosurg. 2012 Feb 10. [Epub ahead of print] PMID: 22326716. Clin Neurol Neurosurg 2012 Jun;114(5): 460-70.

Cadotte DW, Wilson JR, Mikulis D, Stroman PW, Brady S, Fehlings MG. Conventional MRI as a diagnostic and prognostic tool in spinal cord injury: a systematic review of its application to date and an overview on emerging MRI methods. Expert Opin Med Diagn 2011;5(2):121-33.

David W. Cadotte and Michael G. Fehlings. Spinal Cord Injury – A Review of Current Treatment Options. Clin Orthop Relat Res. 2010 Nov 16. [Epub ahead of print] PMID: 21080129. Mar; 469(3):732-41.

Michael Fehlings MD PhD, Doron Rabin MD, William Sears MD, **David Cadotte MD** and Bizhan Aarabi MD. Current Practice in the Timing of Surgical Intervention in Spine and Spinal Cord Injury. Spine (Phila Pa 1976). 2010 Oct 1;35(21 Suppl):S166-73. PMID: 20881458

Cadotte DW, Singh A, Fehlings MG: The timing of surgical decompression for spinal cord injury. *F1000 Medicine Reports* 2010, September 8; 2:67. PMID: 21173861 URL: http://www.f1000medicine.com/f1000reports/articles/10.3410/m2-**67**/article.html http://f1000.com/reports/m/2/67

Furlan J, Noonan V, **Cadotte DW**, Fehlings MG. Timing of decompressive surgery of spinal cord after traumatic spinal cord injury: An evidence-based examination of pre-clinical and clinical studies. J Neurotrauma. 2010 Mar 4. [Epub ahead of print] PMID: 20001726; 2009 Dec; doi: 10.1089/neu.2009.1147.

Presentations (both poster and platform presentations)

David W. Cadotte, Adam Cadotte, Julien Cohen-Adad, Jefferson R. Wilson, Micha Livne, David Fleet, Michael G. Fehlings. Resolving the anatomic variability of the human cervical spinal cord: a solution to facilitate advanced neural imaging. 82nd Annual Meeting of the American Association of Neurological Surgeons. San Francisco, California, United States of America, April 4-9th, 2014. Poster presentation.

David W. Cadotte, Adam Cadotte, Julien Cohen-Adad, Jefferson R. Wilson, Micha Livne, David Fleet, Michael G. Fehlings. Mapping the Human Cervical Spinal Cord to Visualize Functional Plasticity. 30th Annual Meeting of the AANS / CNS section on Disorders of the Spine and Peripheral Nerves. Orlando, Florida, United States of America, March 5-8th, 2014. Poster presentation.

David W. Cadotte, David Mikulis, Rachael Bosma, Patrick Stroman and Michael G. Fehlings. Visualizing plasticity in the injured human spinal cord with fMRI. 37th European Society of Neuroradiology. Frankfurt, Germany. September 28 to October 1st, 2013. Podium presentation, Tuesday October 1st, 2013 in Section: *Advanced Imaging: Future Techniques in Neuroradiology.*

David W. Cadotte, David Mikulis, Rachael Bosma, Patrick Stroman and Michael G. Fehlings. Visualizing plasticity in the injured human spinal cord with fMRI. 19th Annual Meeting of the Organization for Human Brain Mapping. Seattle, Washington. June 16-20, 2013. Poster presentation, Monday June 17, 2013.

David W. Cadotte, David Mikulis, Rachael Bosma, Patrick Stroman and Michael G. Fehlings. Visualizing plasticity in the injured human spinal cord with fMRI. 48th Annual Congress of the Canadian Neurological Sciences Federation. Award winning podium presentation (Thursday June 13, 2013), McKenzie prize for the top Neuroscience research performed by a Neurosurgical Resident in Canada. Montreal, QC. June 12-14, 2013.
1. Can J Neurol Sci 2013 May;40(3 Suppl 1):S6,S9.

David W. Cadotte and Michael G. Fehlings. Visualizing plasticity in the injured human spinal cord with fMRI. 38th Annual Keith Lectureship in Neurosurgery. Toronto, Canada. June 6th, 2013. Oral presentation.

David W. Cadotte, David Mikulis, Rachael Bosma, Patrick Stroman and Michael G. Fehlings. Visualizing plasticity and altered neuronal signaling in the injured human spinal cord with fMRI. 7th Annual Meeting of the American Society of Functional Neuroradiology. Award winning poster presentation, Charleston, South Carolina, March 11-13, 2013.

David W. Cadotte, David Mikulis, Rachael Bosma, Patrick Stroman and Michael G. Fehlings. Visualizing plasticity and altered neuronal signaling in the injured human spinal cord with fMRI. 13th Annual Meeting of the Canadian Spine Society. Poster presentation, Mont Tremblant, Quebec, February 27-March 2, 2013.

Cadotte DW, Stroman P, Bosma R, Mikulis DJ, Nugaeva N, Fehlings MG. Visualizing plasticity and altered neuronal signaling in the injured human spinal cord with fMRI. Neurosurgery 2012;71(2):E558. Platform presentation at the Congress of Neurological Surgeons, Annual Meeting, October 6-10, 2012. Presented on October 9, 2012, 2:09pm, Chicago, IL. Award winning paper.

David W. Cadotte, David Mikulis, Jefferson R. Wilson, Natalia Nugaeva and Michael G. Fehlings.

Creating an MRI anatomic atlas of the human cervical spine: Implications for spinal fMRI. 18th Annual meeting of the Organization for Human Brain Mapping. Poster presentation. June 10-14, 2012, Beijing, China.

David W. Cadotte, Patrick Stroman, Rachael Bosma, David Mikulis, Natalia Nugaeva and Michael G. Fehlings. Dynamic spinal networks: How incomplete SCI patients process sensory information differently than healthy controls. 9th Annual World Congress of the Society of Brain Mapping and Therapeutics. Oral poster presentation Sunday June 3rd 4:40-4:50pm, Toronto, Canada, June 2-4, 2012.

David W. Cadotte, Patrick Stroman, Rachael Bosma, David Mikulis, Natalia Nugaeva and Michael G. Fehlings. Spinal fMRI: Preliminary results of a novel imaging technique to examine neuroanatomical circuits in the human spinal cord. 9th Annual World Congress of the Society of Brain Mapping and Therapeutics. Poster presentation, Toronto, Canada, June 2-4, 2012.

David W. Cadotte, David Mikulis, Micha Livne, David Fleet and Michael G. Fehlings. Creating an anatomic atlas of Cervical Spinal Intradural Anatomy using FIESTA MRI. iCord: Interdependence 2012. Platform presentation, Vancouver, British Columbia, Wednesday May 16th, 2012.

David W. Cadotte, Patrick Stroman, Rachael Bosma, David Mikulis, and Michael G. Fehlings. Objective spinal fMRI metrics distinguish complete and incomplete clinical grade in chronic spinal cord injury. iCord: Interdependence 2012. Platform presentation, Vancouver, British Columbia, Wednesday May 16th, 2012.

David W. Cadotte, David Mikulis, Jefferson R. Wilson, Natalia D. Nugaeva, and Michael G. Fehlings. Creating an anatomic atlas using MRI and the implications for spinal fMRI. (poster presentation) 38th Gallie Day, University of Toronto, Department of Surgery, May 4, 2012, Toronto.

David W. Cadotte, Rachael Bosma, David Mikulis, Patrick Stroman and Michael G. Fehlings. Objective spinal fMRI metrics distinguish complete and incomplete clinical grade in chronic spinal cord injury. American Association of Neurological Surgeons. Platform presentation, 80th annual meeting. Monday April 16th, 2012 4:30pm.

David W. Cadotte, David Mikulis, Jefferson R. Wilson, Natalia D. Nugaeva, and Michael G. Fehlings. Human cervical spinal cords are distinct: Creating an anatomic atlas using MRI and the implications for spinal fMRI. (poster presentation) American Society of Functional Neuroradiology. 6th Annual meeting. March 6-9th, 2012. Orlando, Florida, USA.

Adrian Miriampillai[#] & **David W. Cadotte[#]**, Adam Cadotte, Kenneth K.C. Lee, Tim-Rasmus Kiehl, Brian C. Wilson, Michael G. Fehlings and Victor X.D. Yang Optical coherence tomography of the spinal cord: optimization of an in vivo model. [#]Co-first author, oral presentation delivered by David W. Cadotte on January 22, 2012 11:50am - 12:10pm. SPIE Photonics West, 21-26 January 2012, San Francisco, CA.

Cadotte DW & Fehlings MG. Plasticity of the Injured Human Cervical Spinal Cord: Insights Revealed by Functional Spinal MRI Using Unique SEEP Imaging. (oral presentation) December 8, 2011. 39th Annual meeting of the Cervical Spine Research Society, Scottsdale, Arizona.

Cadotte D, Stroman P., Mikulis D., Bosma R., and Fehlings M.G. Functional MRI of the human spinal cord: from sensory stimulation to spinal networks. Platform presentation, June 17th, 2011. 46th Congress of the Canadian Neurological Science Federation, Vancouver, British Columbia, Canada.

Cadotte D, Stroman P, Bosma R, Mikulis D, Fehlings M. Recovery after incomplete spinal cord injury is associated with plasticity: Insights revealed by functional MRI of the human spinal cord using unique

SEEP imaging. Can J Surg 2011 Jun; 54(3):S22.

Cadotte D, Bosma R, Mikulis D, Stroman P, Fehlings M. Spinal fMRI: Preliminary results of a novel imaging technique to examine neuroanatomoical circuits in the human spinal cord. Poster presentation, June 8-10, 2011. Annual World Congress of IBMISPS on Brain, Spinal Cord Mapping and Image Guided Therapy, International Brain Mapping and Intraoperative Surgical Planning Society (IBMISPS), San Francisco, CA.

David W. Cadotte, Patrick Stroman, Rachael Bosma, David Mikulis and Michael G. Fehlings. Recovery after incomplete spinal cord injury is associated with evidence of plasticity: insights revealed by functional spinal MRI using unique SEEP contrast. Platform presentation, Monday April 10, 2011. 79th Annual meeting of the American Association of Neurological Surgeons, Denver, CO. USA

David W. Cadotte, Patrick Stroman, Rachael Bosma, David Mikulis and Michael G. Fehlings. Recovery after incomplete spinal cord injury is associated with evidence of plasticity: insights revealed by functional spinal MRI using unique SEEP contrast.

1. (poster presentation) Canadian Spine Society. 11th Annual meeting. March 9-11th, 2011. Quebec City, Canada.
2. (poster presentation) American Society of Functional Neuroradiology. 5th Annual meeting. March 2-4th, 2011. Phoenix, Arizona, USA.

David W. Cadotte and Michael G. Fehlings. Neuropathic pain in the spinal cord injured patient – A systematic review of cases and mechanistic theory. (poster presentation) 4th National Spinal Cord Injury Conference. Niagara Falls, Ontario. October 28-30, 2010.

David W. Cadotte, Jefferson Wilson, Sinead Brady, David Mikulis, Patrick Stroman and Michael G. Fehlings. The sensitivity and specificity of MRI to predict prognosis following traumatic spinal cord injury: Results from a systematic review. (Digital Poster). Congress of Neurological Surgeons Annual Meeting, San Francisco CA, October 16-21, 2010.

David W. Cadotte, Patrick Stroman, David Mikulis and Michael G. Fehlings. The use of heat sensation to detect neuronal activity in the dorsal horn of the human spinal cord at 3T with novel fMRI methods – a proof-of-concept pilot study. Canadian Neurological Sciences Federation, Annual meeting, Quebec City, June 8-12, 2010.

David W. Cadotte and Michael G. Fehlings. A systematic review of neuropathic pain following traumatic spinal cord injury: An instance of aberrant plasticity? Canadian Neurological Sciences Federation, Annual meeting, Quebec City, June 8-12, 2010.

David W. Cadotte and Michael G. Fehlings. Neuropathic pain in the spinal cord injured patient – A systematic review of cases and mechanistic theory. Third International Congress of Neuropathic Pain – Special Interest Group (NeuPSIG) of the International Association for the Study of Pain (IASP), Athens, Greece May 27-30, 2010.

David W. Cadotte, Sinead Brady, David Mikulis, Patrick Stroman and Michael G. Fehlings. Sensitivity and Specificity of structural MRI to predict improvement following spinal cord injury: Receiver operator characteristics. Canadian neuroscience meeting, Ottawa May 15-18, 2010. Abstract available at: http://www.friglobalevents.com/NEUROAbstracts.asp (last accessed August 27, 2010)

David W. Cadotte, David Mikulis, Patrick Stroman and Michael G. Fehlings. Detecting activity in the dorsal horn of the human spinal cord: Results of a proof-of-concept study using novel spinal fMRI techniques. Canadian neuroscience meeting, Ottawa May 15-18, 2010. Abstract available at:

http://www.friglobalevents.com/NEUROAbstracts.asp (last accessed August 27, 2010)

David W. Cadotte, David Mikulis, Patrick Stroman and Michael G. Fehlings. Spinal fMRI: Preliminary results of a novel imaging technique to examine neuroanatomical circuits in the human spinal cord.
1. Gallie Day, University of Toronto, Department of Surgery, May 7, 2010, Toronto.

David W. Cadotte MSc, MD and Michael G. Fehlings MD, PhD. Neuropathic pain in the spinal cord injured patient: a systematic review of animal models. What is our current understanding of its pathophysiology? Treatment strategies for SCI: from biology to clinical reality, 2010 Annual meeting, Banff Conference Center, Alberta, April 20-22, 2010.

David W. Cadotte MSc, MD and Michael G. Fehlings MD, PhD. 44 °C thermal stimulation provides a glimpse into neural activity of the dorsal horn of the human spinal cord – implications for spinal cord injury research.
1. Neurosurgical Society of America, Pebble Beach, California, April 11 – 14, 2010.

D.W. Cadotte, M.G. Fehlings. The evolution of MRI to predict outcome in spinal cord injury–from signal change to functional imaging.
2. The Organization for Human Brain Mapping, San Francisco, CA; June 2009 (poster presentation)
3. Neuroimage Volume 47, Supplement 1, 2009; S68.

D.W. Cadotte, M.G. Fehlings. MRI as a tool to predict outcome in spinal cord injury – a systematic review of the literature. Canadian Congress of Neurological Sciences, Halifax, Nova Scotia; June 2009 (oral presentation) Can J Neurol Sci. 2009 May;36(3)Suppl1;S34.

Copyright Acknowledgements